THE GEOLOGY AND GENESIS OF IRON OXIDE-COPPER-GOLD MINERALISATION ASSOCIATED WITH WERNECKE BRECCIA, YUKON, CANADA

VOLUME I

Thesis submitted by
Julie Hunt B.Sc., M.Sc., PGeo.

in April 2005
for the degree of Doctor of Philosophy
in the School of Earth Sciences,
James Cook University, Queensland, Australia

"It is precisely for this that I love geology. It is infinite and ill defined: like poetry, it immerses itself in mysteries and floats among them without drowning. It does not manage to lay bare the unknown, but it flaps the surrounding veils to and fro; and every so often gleams of light escape and dazzle one's vision."

R. Topfler

Frontispiece: Bonnet Plume River valley, Wernecke Mountains, Yukon, Canada

STATEMENT OF ACCESS

I, the undersigned, author of this work, understand that James Cook University will make this thesis available for use within the University Library and, via the Australian Digital Theses network, for use elsewhere.

I understand that, as an unpublished work, a thesis has significant protection under the Copyright Act and;

I do not wish to place any further restriction on access to this work, with the exception of the following:

All users consulting this thesis are required to sign the following statement:

> "*In consulting this thesis I agree not to copy or closely paraphrase it in whole or in part without the written consent of the author, and to make proper written acknowledgement for any assistance which I have obtained from it.*"

---------- ----------

Julie Hunt 2005

STATEMENT OF SOURCES

DECLARATION

I declare that this thesis is my own work and has not been submitted in any other form for another degree or diploma at any university or other institution of tertiary education. Information derived from the published or unpublished work of others has been acknowledged in the text and a list of references is given.

---------- ----------

Julie Hunt 2005

ABSTRACT

The large scale Wernecke Breccia system occurs throughout the 13 km-thick Early Proterozoic Wernecke Supergroup (WSG) and is spatially associated with regional-scale faults. Breccia emplacement made use of pre-existing crustal weaknesses and permeable zones; metaevaporitic rocks in the lower WSG may be intimately related to breccia formation. The breccia bodies host vein and disseminated iron oxide-copper-gold ± uranium ± cobalt mineralisation and are associated with extensive sodic and/or potassic metasomatic alteration overprinted by pervasive carbonate alteration. Multiple phases of brecciation, alteration and mineralisation are evident. Six widely spaced breccia bodies that occur in different part of the WSG were examined in this study (i.e. Slab, Hoover, Slats-Frosty, Slats-Wallbanger, Igor and Olympic). New information includes geological, paragenetic, geochronological, isotopic, fluid inclusion thermometric and compositional data.

Re-Os analyses of molybdenite from a late-stage vein that cross-cuts breccia gave model ages of 1601 ± 6 and 1609 ± 6 Ma. These ages range from older than to within error of the *ca.* 1594.8 ± 4.6 Ma published U-Pb (titanite) date for breccia in the same area. A second molybdenite sample from a late-stage vein gave a Re-Os model age of 1648 ± 5.97 Ma. This date is considered analytically sound but the significance of it is not clear as it is believed to cut the *ca.* 1595 Ma breccia. Step heating ^{40}Ar-^{39}Ar analyses carried out on muscovite from Wernecke Breccia matrix, a syn-breccia vein and two late-stage veins yielded dates of 1178.0 ± 6.1, 1135.0 ± 5.5, 1052 ± 10 and 996.7 ± 8 Ma respectively. These dates are significantly younger than the minimum age (*ca.* 1380 Ma) of Wernecke Breccia indicated by cross-cutting relationships and must have been reset. Samples submitted for U-Pb and Pb-Pb analyses gave discordant results that cannot be used to constrain the age of Wernecke Breccia or Wernecke Supergroup.

Fluids that formed Wernecke Breccia were hot (185-350 ^{o}C), saline (24-42 wt. % NaCl eq.) NaCl-$CaCl_2$ brines. Isotopic compositions for hydrothermal minerals range from: $\delta^{13}C_{carbonate} \approx$ -7 to +1 ‰ (PDB), $\delta^{18}O_{carbonate} \approx$ -2 and 20 ‰ (SMOW), $\delta^{34}S_{pyrite/chalcopyrite} \approx$ -13 to +14 ‰ (CDT) and $\delta^{34}S_{barite} \approx$ 7 to 18 ‰. Calculated $\delta^{18}O_{fluid} \approx$ -8 to +14 ‰ The isotopic compositions indicate fluids were likely derived from formation/metamorphic water mixed with variable amounts of organic water ± evolved

meteoric and/or evolved seawater. Metals and sulphur were probably derived from host strata and fluids circulated via tectonic (and/or gravity) processes. Magmatic waters are considered less likely as a fluid source because the isotopic data do not have a magmatic signature and mafic to igneous rocks spatially associated with the breccia are significantly older (i.e. *ca*. 1710 vs. 1600 Ma) thus ruling out a genetic connection. This suggests IOCG mineralisation can occur in non-magmatic environments and a division of the broad IOCG class into magmatic and non-magmatic end-members, with hybrid types in between, is suggested that reflects the involvement of magmatic and non-magmatic fluids. Wernecke Breccia and Redbank are representative of non-magmatic end-members, Lightning Creek is a magmatic end-member and hybrid types include Ernest Henry and Olympic Dam.

ACKNOWLEDGEMENTS

Funding for this project was provided in part by the Yukon Geology Program. Additional funding was provided by an Australian International Postgraduate Research Scholarship, a James Cook University scholarship and Merit Research Grant, a Society of Economic Geologists Student Research Grant, and a predictive mineral discovery* Cooperative Research Centre scholarship. Newmont Mines Ltd. and Archer, Cathro and Associates (1981) Inc. kindly allowed us access to their Wernecke Breccia properties and diamond drill core. Tom Setterfield of Monster Copper Resources Ltd gave an informative tour of the Monster Cu property. Al Doherty, on behalf of Blackstone Resources Ltd, gave a tour of the Hem claims. Thanks are due to Dave Caulfield, Henry Awmak and Mark Baknes of Equity Engineering Ltd and Mike Stammers of Pamicon Developments Limited for access to data at the beginning of the project that got the whole process underway. Melanie Brookes and David Gillen braved Yukon summers to provide assistance in the field. Curtis Freeman and Joel Clarkson of TransNorth Helicopters provided exceptional service.

Huge thanks are due to Grant Abbott and the Yukon Geological Survey for support throughout this project and to Tim Baker for his never failing support and encouragement. This project has also benefited greatly from collaboration and discussion with many people, including Derek Thorkelson, Gary Davidson, James Cleverly, Geordie Mark, Robert Creaser, Dave Selby, Mike Villeneuve, Tony Fallick, Chris Clarkson, Martin Hand and Roland Maas and they are thanked for their participation. Thanks to all at JCU who helped and encouraged me throughout this project especially Lucy, James, Kylie, Karen, Damien and Nicole and finally, thanks to Grant for his help and support in the Yukon and Australia.

TABLE OF CONTENTS - VOLUME I

SECTION C: Stable isotope (C,O,S,D) and fluid inclusion constraints on the origin of Wernecke Breccia and associated iron oxide-copper-gold mineralisation

SECTION D: Wernecke Breccias, Yukon, Canada: an example of a non-magmatic end-member IOCG system and implications for IOCG genesis and classification

TABLE OF CONTENTS - VOLUME II

LIST OF FIGURES

SECTION A

9. Igor area showing location of 'Igor ridge', fold axial trace in 'Igor creek', Wernecke Breccia, Quartet Group and Cambrian strata.
10. Examples of alteration and mineralization: a) grey sodic-altered breccia, b) red potassic-altered breccia, c) biotite-scapolite alteration in FLG metasiltstone cut by albite veins, cross-cut by calcite vein, d) potassic-altered Quartet Group metasiltstone cut by dolomite-chalcopyrite vein, e) ankerite-magnetite vein cutting FLG, Slab prospect, f) massive chalcopyrite-pyrite vein cutting FLG, Slab prospect, g) clast of massive sulphide in breccia, Slab prospect, h) calcite-chalcopyrite vein cutting FLG, Slab prospect and i) chalcopyrite forming matrix to breccia, Hoover prospect.
11. Composition of a) feldspar and b) carbonate in Wernecke samples, based on microprobe data. Analyses were obtained with the James Cook University electron microprobe in wavelength dispersive mode, at an accelerating voltage of 15 kV and a current of 20 nA.
12. Examples of mineralization and deformation: a) massive magnetite-coarsely crystalline hematite-ankerite-quartz vein, Slats-Frosty area, b) euhedral magnetite replaced by hematite (rl), Igor prospect, c) euhedral magnetite overgrown by pyrite (rl), Igor prospect, d) hematite overgrown by pyrite with chalcopyrite filling fractures (rl), Olympic prospect, e) clasts of foliated metasiltstone in Wernecke Breccia, f) foliated FLG cut by ankerite vein, both have been kinked during Racklan deformation and g) flattened clasts in foliated breccia. rl = reflected light.
13. Simplified paragenesis for prospects in the Wernecke Mountains: a) Slab, b) Hoover, c) Slats-Frosty, d) Slats-Wallbanger, e) Igor and f) Olympic prospects. NB: paragenetic stages apply only to a specific area, e.g. Slab stage 3 ≠ Hoover stage 3 ≠ Igor stage 3.
14. Cartoon depicting evolution of Wernecke Basin and structural controls on location of Wernecke Breccia. Stage I: deposition of FLG. Stage II: deposition of Quartet Group and GLG. Stage III: emplacement of Wernecke Breccia into pre-existing weak zones in deformed and metamorphosed WSG. Breccia bodies are widespread at the top of FLG in metaevaporite-bearing stratigraphy. See text for detailed description of stages.

SECTION B

1. Location of study area, distribution of WSG and Wernecke Breccia (modified from Thorkelson, 2000) plus simplified geology map of the study area (for details see Thorkelson, 2000 and Thorkelson *et al.*, 2002). Legend shows approximate stratigraphic position of IOCG prospects included in this study.
2. Time stratigraphic column of the Wernecke area showing major depositional, intrusive and deformational events (modified from Thorkelson, 2000).
3. Release spectra for ^{40}Ar-^{39}Ar ages for muscovite from four Wernecke Breccia-related samples.
4. $^{207}Pb/^{235}U$ versus $^{206}Pb/^{238}U$ plot for three fractions of titanite from a Wernecke Breccia-related vein. Error for Pb/Pb age is quoted at the 2σ level.
5. $^{206}Pb/^{204}Pb$ versus $^{207}Pb/^{204}Pb$ plot for 5 analyses of a sample of GLG dolostone.

SECTION C

1. Location of study area, distribution of WSG and Wernecke Breccia plus location of breccia-associated IOCG prospects included in this study (modified from Thorkelson, 2000).
2. Simplified geology map of the study area (for details see Thorkelson, 2000 and Thorkelson *et al.*, 2002). Legend shows approximate stratigraphic position of IOCG prospects included in this study. Slats-F = Slats-Frosty, Slats-W = Slats Wallbanger.
3. Simplified paragenesis for prospects in the Wernecke Mountains: a) Slab, b) Hoover, c) Slats-Frosty, d) Slats-Wallbanger, e) Igor and f) Olympic prospects. NB: paragenetic stages apply only to a specific area, e.g. Slab stage 3 ≠ Hoover stage 3 ≠ Igor stage 3.
4. Photographs of fluid inclusion samples: Slab area - a) large crystals of quartz, calcite and fluorite locally make up the matrix of Wernecke Breccia, b) fluid inclusions in quartz crystal, c) fluid inclusions containing L + V + H and d) fluid inclusion containing L + V + H + h. L=liquid, V=vapour, H=halite, h=hematite; Hoover area – e) metasedimentary clast in Wernecke Breccia, f) trails of secondary fluid inclusions parallel to fractures within quartz in the clast; g) closer view of inclusions in f; Slats-Frosty area - h) ferroan dolomite-pyrite-fluorite vein cutting hematite-altered metasiltstone; the fluorite contains pseudosecondary fluid inclusions, i) fluorite in h), note fluid inclusion trails parallel to fractures that do not

extend beyond the fluorite crystal, j) and k) liquid + vapour fluid inclusions in fluorite; Igor area – l) Wernecke Breccia sample with large barite and magnetite crystals, m) barite crystal in area shown in l); and Olympic area – n) Wernecke Breccia sample used for fluid inclusion analysis, o) quartz grain from breccia matrix with fluid inclusions in the outer rim, p) ferroan dolomite-quartz-chalcopyrite±pyrite vein and q) dolomite with primary fluid inclusions.

5. Summary of fluid inclusion data for samples from the Wernecke Mountains area. Th = final homogenisation temperature; NaCl eq wt % = equivalent weight % NaCl. See Table 1 caption for details of salinity calculations.
6. Comparison of fluid composition for inclusions from the Slab, Hoover, Slats-Frosty, Igor and Olympic areas using the $NaCl\text{-}CaCl_2\text{-}H_2O$ system.
7. $\delta^{18}O$ versus $\delta^{13}C$ results for samples of hydrothermal carbonate from the Slab, Hoover, Slats-Frosty, Slats-Wallbanger, Igor and Olympic areas. Also shown are results for samples of host WSG limestone/dolostone from FLG, Quartet Group and GLG.
8. Overall $\delta^{18}O$ versus $\delta^{13}C$ results for carbonate samples from the Wernecke Mountains. Also shown are fields for common large earth reservoirs that are important in hydrothermal systems. Fields are from Taylor (1974), Sheppard (1977), Graham and Harman (1983), and Hoefs (1987) as compiled in Rollinson (1993). Mean values for Paleoproterozoic carbonates are from Shields and Veizer (2002). FLG = Fairchild Lake Group, Quartet Group = Quartet Group, GLG = Gillespie Lake Group.
9. $\delta^{34}S$ results for samples from the Slab, Hoover, Slats-Frosty, Slats-Wallbanger, Igor and Olympic areas. See text for discussion.
10. Overall $\delta^{34}S$ results for samples from the Wernecke Mountains. Also shown are fields for common large earth reservoirs that are important in hydrothermal systems. Fields are from Chambers (1982), Kerridge *et al.* (1983) and Chaussidon *et al.* (1989) as compiled in Rollinson (1993).
11. Plot of calculated $\delta^{18}O_{water}$ versus δD_{water} values for mineral separates of biotite, muscovite and actinolite from Wernecke samples. See Appendix VII for sample descriptions. $\delta^{18}O_{water}$ values for biotite and muscovite were calculated using the fractionation equations of Zheng (1993). δD_{water} values for biotite and muscovite were calculated using the fractionation equations of Suzuoki and Epstein (1976).

$\delta^{18}O_{water}$ and δD_{water} values for actinolite were calculated using the fractionation equations of Zheng (1993) and Graham *et al.* (1984) respectively for Tremolite. Magmatic water and formation waters fields are from Taylor (1974). Meteoric water line is from Epstein *et al.* (1965) and Epstein (1970). The metamorphic waters field is from values in Taylor (1974) and Sheppard (1981) as compiled by Rollinson (1993). The fields for felsic magma and high temperature volcanic vapour are from Taylor (1992) and Giggenbach (1992) as shown in Hedenquist *et al.* (1998). Composition of ancient seawater from Sheppard (1986). Isotopic trends are given for: 1) seawater undergoing evaporation (Knauth and Beeunas, 1986), 2) meteoric waters undergoing exchange with ^{18}O in minerals, 3) evaporation of meteoric water and 4) isotopic compositions of Salton Sea and Lanzarote geothermal waters compared to their local meteoric waters (Sheppard, 1986). Black bars beneath the main figure are calculated $\delta^{18}O_{water}$ values for calcite, dolomite and siderite from the Slab, Hoover and Igor areas using the fractionation factors of Zheng (1999).

12. Examples of isochores from the Slab and Igor prospects. Diagrams were constructed using the programme Flinc-Calc that is based on the equations of Zhang and Fratz(1987) and Brown (1998).
13. Log fO_2 – log fS_2 plot for Slab area fluids. The following equations were used to define the mineral stability fields. Log K values were calculated for temperature = 300 ^oC and pressure = 2500 bars using the programme "The Geochemists Workbench"® release 4.0.2 (GWB uses information from many sources, these are compiled for e.g. in Johnson *et al.*, 1992).

Reaction used	**Equation**	**Log K**
Pyrite-Magnetite:	$3\ FeS_2 + 2\ O_{2(g)} = Fe_3O_4 + 3\ S_{2(g)}$	-4.6
Pyrite-Hematite:	$4\ FeS_2 + 3\ O_{2(g)} = 2\ Fe_2O_3 + 4\ S_{2\ (g)}$	33.88
Pyrrhotite-Magnetite:	$6\ FeS + 4\ O_{2(g)} = 2\ Fe_3O_4 + 3\ S_2$	55.34
Bornite-Chalcopyrite:	$Cu_5FeS_4 + 4\ FeS_2 = 5\ CuFeS_2 + S_2$	83.64
Graphite-CO2(g):	$C + O_{2(g)} = CO_{2(g)}$	-6.93
Calcite-gypsum:	$2\ CaCO_3 + S_{2(g)} + 3\ O_{2(g)} + 4\ H_2O = 2\ CaSO_4 + 2\ CO_{2(g)}$	36.13

14. Plots of pH versus log fO_2 for the Slab area. a) using a medium value for log aH_2S of -2.6, b) using a low value for log aH_2S of -3.23 and c) using a high value for log aH_2S of -1.97. The positions of δS^{34}_i contours are also shown in a); Numbers in boxes on contours are δS^{34}_{pyrite} values calculated using $\delta S^{34}_{\Sigma S} = 0$ ‰(right side) and

$\delta S^{34}_{\Sigma S}$ = 18 ‰(left side). The shaded oval shows approximate fluid conditions at Slab. The position of sulphur isotope contours were calculated using the method of Ohmoto (1972) and the following conditions: temperature = 300 °C, pressure = 2.5 kb, ionic strength = 3.2 (based on fluid inclusion data). Molality of species was calculated using the programme "The Geochemists Workbench"® release 4.0.2; the following species were most abundant.

Species	Molality	Mole Fraction
$NaSO_4^-$	0.6985	0.497
$CaSO_4$(aq)	0.3741	0.266
KSO_4^-	0.165	0.117
SO_4^{--}	0.1623	0.115
H_2S(aq)	2.51E-03	0.002
HSO_4^-	1.54E-03	0.001
HS^-	1.30E-03	0.001

SECTION D

1. Location of selected IOCG districts. Modified from Hitzman (2000).
2. Location of Wernecke belt, distribution of Wernecke Breccia and location of breccia-associated IOCG prospects included in this study (modified from Thorkelson, 2000) plus simplified bedrock geology map of the study area (for details see Thorkelson, 2000 and Thorkelson *et al.*, 2002, 2003). Legend shows approximate stratigraphic position of IOCG prospects studied.
3. Typical examples of Wernecke Breccia and associated IOCG mineralisation and alteration: **a)** grey sodic-altered breccia, **b)** red potassic-altered breccia, **c)** breccia with abundant clasts of earlier breccia, Slab area, **d)** photomicrograph of Wernecke Breccia matrix (crossed polars) made up dominantly of sedimentary rock fragments, carbonate, feldspar, lesser quartz and minor hematite and magnetite, **e)** calcite-chalcopyrite vein cutting FLG, Slab prospect, **f)** massive chalcopyrite-pyrite vein cutting FLG, Slab prospect, **g)** chalcopyrite forming matrix to breccia, Hoover prospect, **h)** massive magnetite-coarsely crystalline hematite-ankerite-quartz vein, Slats-Frosty area and **i)** photomicrograph of hematite overgrown by pyrite with chalcopyrite filling fractures (reflected light), Olympic prospect.
4. Fluid temperature and salinity for selected IOCG deposits and prospects. References and abbreviations as in Table 1.

5. Measured sulphur isotope compositions for mineralisation and calculated oxygen isotope compositions for mineralising fluid from selected IOCG deposits. Legend shows mineral(s) used for sulphur isotope analysis and mineral used to calculated oxygen isotopic composition of fluid. References and abbreviations as in Table 1. * Values calculated from actinolite are 5.4 if temperature of 200 ^{o}C is used or 9.5 if temperature of 450 ^{o}C is used (see text for details). For δ^{18}O values for magmatic, metamorphic, formation and meteoric waters and modern seawater – *cf.* Sheppard, 1986; Rollinson, 1993. For δ^{34}S values for mantle and evaporite sources –*cf.* Ohmoto and Goldhaber, 1997.
6. Suggested classification of IOCG systems into magmatic and non-magmatic end-members with hybrid IOCG systems in between. Placement in the classification indicates the degree of involvement of magmatic and/or non-magmatic fluids in the formation of the IOCG system. Placement is also affected by the environment of formation of the IOCG system, i.e., magmatic or non-magmatic, which is determined by whether or not there is a **temporal** association with igneous rocks. At the non-magmatic end of the IOCG spectrum it is possible for an IOCG system to have formed from non-magmatic fluids but to have a temporal relationship with a magmatic system, e.g. Salton Sea. See text for discussion and references.
7. Schematic model showing examples of hydrothermal alteration and mineralisation produced by the circulation of non-magmatic fluids (adapted from Barton and Johnson, 2000). Voluminous metal-depleted, sodic(-calcic) ± shallow K feldspar-hematite alteration forms in inflow zones and along the fluid pathway(s) (*cf.* Barton and Johnson, 1996, 2000). Fluids are heated and as they rise and cool they produce intense sodic and/or potassic alteration (depends on host rock composition) plus overprinting and shallow hydrolytic alteration. Metals are leached along the flow path and precipitate due to cooling and/or fluid mixing.

LIST OF TABLES

SECTION A

2. Representative results of scapolite and biotite microprobe analyses. % meionite = 100 (Ca+Mg+Fe+Mn+Ti) / (Na+K+Ca+Mg+Fe+Mn+Ti); marialite = 100 - meionite (after Deer *et al*., 1992). Analyses were obtained with the James Cook University JEOL electron microprobe in wavelength dispersive mode, at an accelerating voltage of 15 kV and a current of 20 nA, ZAF corrections were used. [1] average of 70 analyses, [2] average of 10 analyses.
3. Main characteristics of IOCG prospects included in this study, see text for details. In mineralization column: V = vein, D = disseminated, B = forms breccia matrix. [1]Yukon MINFILE (2003) database number. Information from: [2](Thorkelson *et al.*, 2003), [3](Yukon MINFILE, 2003), [4](Stammers, 1995), [5](Eaton & Archer, 1981) and [6](Caulfield, 1994).

SECTION B

1. Summary of published age dates for Wernecke Breccia-related samples, WSG and Slab volcanics.
2. Summary of sample characteristics and new age dates obtained during this study.

SECTION C

1. Summary of fluid inclusion data for samples from the Wernecke Mountains area. Tfm = temperature of first melting, Tm_{ice} = ice melting temperature, Tm_{hh} = hydrohalite melting temperature, Thv = vapour homogenisation temperature, Ths = halite dissolution temperature, Th = final homogenisation temperature. Temperatures in ^{o}C. NaCl eq wt % = equivalent weight % NaCl. NaCl eq wt % values for Slab were approximated using the graphical methods of Vanko *et al.* (1988) and Zwart & Touret (1994). Values for other areas were calculated from Tm_{ice}, $Tm_{hydrohalite}$, Th_{halite} using the programme FlinCalc (J. Cleverley, written communication) which uses information from Zhang and Frantz (1987) and Brown (1998). In the paragenesis column P = primary, S = secondary and PS = pseudo secondary. In the FI (fluid inclusion) Type column L = liquid, V = vapour, H = halite and Op = opaque.
2. Summary of carbon and oxygen isotope results. * mean value for *ca*. 1.8 to 1.7 Ba carbonates is from Shields and Veizer (2002).

3. $\delta^{18}O_{water}$ values calculated from measured $\delta^{18}O$ values of syn-breccia carbonate samples.
4. Summary of sulphur isotope results
5. Summary of hydrogen and oxygen isotope results. Also shown are calculated δD and $\delta^{18}O$ values for co-existing water. #duplicate analysis. See figure 11 caption for calculation details.
6. Estimates of fluid temperature from fluid inclusion and stable isotope data. *All direct fluid inclusion analyses are minimum temperatures, i.e. not trapped during phase separation. ** Using fractionation factors of Sheppard and Schwarcz (1970) and Golyshev *et al.* (1981). *** Using fractionation factors of Ohmoto and Lasaga (1982).
7. Estimates of: 1) thickness of strata overlying the IOCG prospects based on stratigraphic measurements (Delaney, 1981); 2) depth of the prospects based on pressure estimates; 3) pressure from fluid inclusion data; and 4) trapping temperature of fluid (see text for discussion).

SECTION D

1. Size and grade of selected IOCG deposits. References: **Lightning Creek** – Perring *et al.*, 2000; Williams *et al.*, 1999; **Osborne** – Adshead, 1995; Perkins and Wyborn, 1996, 1998; Adshead *et al.*, 1998; Rubenach *et al.*, 2001; **Eloise** – Baker, 1998; Baker and Laing, 1998; Baker *et al.*, 2001; **Olympic Dam** – Roberts and Hudson, 1983, 1984; Creaser, 1989; Reeve *et al.*, 1990; Johnson and Cross, 1991; Oreskes and Einaudi, 1992; Oreskes and Hitzman, 1993; Eldridge and Danti, 1994; Haynes *et al.*, 1995; Reynolds, 2000; **Aitik** – Frietsch *et al.*, 1995, 1997; Carlon, 2000; Wanhainen *et al.*, 2003; **Candelaria** – Ullrich and Clark, 1999; Marschik and Fontboté, 1996, 2001; Marschik *et al.*, 2000; **Salobo** – Requia and Fontboté, 2000; Souza and Vieira, 2000; **Ernest Henry** – Twyerould, 1997; Ryan, 1998; Mark and Crookes, 1999; Mark *et al.*, 2000; Williams *et al.*, in progress; **Wernecke Breccia (Slab)** – Hunt *et al.*, 2004, 2005; **Tennant Creek (West Peko, Eldorado)** – Ahmad *et al.*, 1999; Skirrow and Walshe, 2002; **Redbank** – Orridge and Mason (1975); Knutson *et al.* (1979).
2. Fluid temperature, salinity, composition and source plus precipitation mechanisms for selected IOCG deposits. References and abbreviations as in Table 1.

3. Tectonic setting, main host rocks, confining structure(s) and age of mineralisation for selected IOCG deposits. References and abbreviations as in Table 1.
4. Regional and ore-related alteration types for selected IOCG deposits. References and abbreviations as in Table 1.

LIST OF APPENDICES

I: Results of microprobe analyses.

II: Analytical Protocols for Ar-Ar, U-Pb, Pb-Pb and Re-Os analyses

III: Thermometric data for fluid inclusions.

IV: Results of stable isotope analyses.

V: Calculations for log fO_2 versus log fS_2 plots.

VI: Calculations for pH versus log fO_2 plots.

VII: Rock sample locations and descriptions

THESIS INTRODUCTION

This thesis investigates structural, stratigraphic and fluid controls on the location and formation of Wernecke Breccia and associated iron oxide-copper-gold (IOCG) mineralisation. The thesis consists of four sections (A to D) written in journal format that are intended for future publication (Section A has been accepted for publication by Mineralium Deposita). Volume I contains text and Volume II contains figures, tables and appendices. The sections are arranged in a logical progression and each follows on from the previous section. The first three sections present new geological, geochronological and fluid characteristic information for six IOCG prospects in the Wernecke Mountains. The final section compares Wernecke Breccia-related IOCG prospects to other districts and discusses the variability between IOCG systems.

Section A

The first section of the thesis presents a geological introduction to the Wernecke Breccias. This includes a brief summary of major geological units in the region. Descriptions of geology and mineralisation for six IOCG prospects are presented along with evidence for the existence of metaevaporites in Early Proterozoic Wernecke Supergroup strata that are host to the breccia bodies. The section concludes with discussion of the timing and mechanisms of breccia formation.

Section B

The second section focuses on geochronology and constraints on the timing of Wernecke Breccia and associated IOCG mineralisation. New Ar-Ar, U-Pb, Pb-Pb and Re-Os date are presented for samples associated with Wernecke Breccia and mineralisation.

Section C

The third section focuses on fluids that formed Wernecke Breccia and IOCG mineralisation and new fluid inclusion and stable isotope data are presented. The section concludes with a discussion of potential sources for breccia forming and mineralising fluids.

Section D

The final section of the thesis examines the characteristics of IOCG systems and discusses variations between them. Evidence for the non-magmatic genesis of Wernecke Breccia is summarised and modifications to the classification of IOCG deposits that reflect the involvement of magmatic and non-magmatic fluids are suggested. Similarities of end-member magmatic and non-magmatic IOCG types to other types of intrusive- and sediment-related deposits are also discussed.

SECTION A

Regional-scale Proterozoic iron oxide-copper-gold-mineralised breccia systems: examples from the Wernecke Mountains, Yukon, Canada

A.1 Abstract

A large scale Proterozoic breccia system consisting of numerous individual breccia bodies, collectively known as Wernecke Breccia, occurs in north-central Yukon Territory, Canada. Breccias cut Early Proterozoic Wernecke Supergroup sedimentary rocks and occur throughout the approximately 13 km-thick deformed and weakly metamorphosed sequence. Iron oxide-copper-gold ± uranium ± cobalt mineralisation is associated with the breccia bodies and occurs as veins and disseminations within breccia and surrounding rocks and locally forms the breccia matrix. Extensive sodic and potassic metasomatic alteration occurs within and around breccia bodies and is overprinted by pervasive calcite and dolomite/ankerite, and locally siderite, alteration, respectively. Multiple phases of brecciation, alteration and mineralisation are evident. Breccia bodies are spatially associated with regional-scale faults and breccia emplacement made use of pre-existing crustal weaknesses and permeable zones. New evidence indicates the presence of metaevaporitic rocks in lower WSG that may be intimately related to breccia formation. No evidence of breccia-age magmatism has been found to date.

A.2 Introduction

Numerous Proterozoic breccia bodies, collectively known as Wernecke Breccia, occur over large areas in the north-central Yukon Territory of northern Canada (Fig. 1; *cf.* Bell, 1986a,b, Thorkelson, 2000). They are associated with extensive metasomatic alteration and potentially economically significant, but little studied, iron oxide-copper-gold ± uranium ± cobalt (IOCG) mineralisation (*cf.* Bell and Delaney, 1977; Bell, 1978; Archer *et al.*, 1977; Yukon MINFILE, 2003) and represent some of the best preserved examples of Proterozoic-age IOCG mineralisation in North America due to the relatively low grade of metamorphism. The scale of brecciation and alteration is similar to that in other large-scale Proterozoic breccia provinces including those in Australia that host the Ernest Henry (167 Mt @ 1.1% Cu, 0.54 g/t Au; Ryan, 1998) and giant Olympic Dam (2320 Mt @ 1.3% Cu, 0.5 kg/t U_3O_8, 0.5 g/t Au, 2.9 g/t Ag; Reynolds, 2000) deposits. Several authors have drawn connections between the two areas based on similar ages and physical characteristics of the breccias and the possible proximity of ancestral North America to Australia in Proterozoic time (*cf.* Thorkelson *et al.*, 2001a). However, unlike many IOCG districts where brecciation and mineralisation are related

to magmatism that acted as a source of fluid(s) (*cf.* Hitzman, 2000; Sillitoe, 2003), and/or provided heat to drive fluid circulation (*cf.* Barton and Johnson, 1996; 2000) a clear relationship with magmatic rocks is not evident for Wernecke Breccias.

New mapping, petrographic and microprobe studies of several Wernecke Breccia-associated IOCG prospects have identified multiple brecciation, alteration and mineralising events. In addition, the studies provide information on structural and stratigraphic features that control the location of breccia and associated alteration and mineralisation and offer clues to the mechanism(s) of large-scale breccia formation.

A.3 Regional geologic setting

Wernecke Breccia bodies and associated IOCG mineralisation occur in Early Proterozoic strata made up of Wernecke Supergroup (WSG), Bonnet Plume River Intrusions (BPRI), and "Slab volcanics[1]" (Figs. 2, 3; *cf.* Gabrielse, 1967; Delaney, 1981, Thorkelson, 2000). The Early Proterozoic rocks are unconformably overlain by Middle Proterozoic Pinguicula Group carbonate and siliciclastic rocks (Fig. 3). The base of WSG is not exposed but is interpreted to sit on ≥ 1.84 Ga crystalline basement that is the westward continuation of the Canadian shield (*cf.* Norris, 1997; Thorkelson, 2000).

A.3.1 Wernecke Supergroup

The Fairchild Lake, Quartet and Gillespie Lake groups make up the WSG and together form an approximately 13 km-thick package of fine-grained marine sedimentary rocks and carbonates (Delaney, 1981) that were deposited pre *ca.* 1710 Ma as two clastic to carbonate grand cycles (*cf.* Thorkelson, 2000). The Fairchild Lake Group (FLG) represents initial subsidence followed by infilling, and the Quartet and Gillespie Lake Groups (GLG) represent subsequent subsidence followed by infilling. The grand cycles may reflect continental rifting and equate to two stages of lithospheric stretching, subsidence and thermal deepening of the basin (Thorkelson, 2000).

Fairchild Lake Group

The Fairchild Lake Group forms the basal part of the WSG and, in the study area, outcrops in a corridor which parallels the Bonnet Plume River valley (Fig. 2; Delaney,

[1] Many of the names used in this paper are informal at present and are initially shown in quotation marks.

1981; Gordey and Makepeace, 1999; Thorkelson, 2000). It consists of at least 4 km of shallow marine sedimentary rocks that have been divided into five formations named, from base to top, F-1 to F-4 and F-Tr (Fig. 4; Table 1; Delaney, 1981). Contacts between formations are conformable with the exception of F-4 which is considered to be facies equivalent to F-3; the contact between F-3 and F-Tr may, in part, be transitional (Delaney, 1981). The formations are made up of variable amounts of grey-weathering, generally thin-bedded, commonly laminated, siltstone, mudstone, claystone and fine-grained sandstone; minor intercalated carbonate rocks occur in F-2 and F-Tr (*ibid.*).

Metaevaporites

Previously unrecognised metaevaporites were identified in the Slab mountain area in strata that Bell and Delaney (1977) correlate with upper FLG. In general, evaporites dissolve during metamorphism and deformation, however they leave behind indirect evidence that they were once part of the stratigraphy (*cf.* Warren, 1999). This evidence includes metamorphic minerals that are enriched in sodium (e.g. marialitic scapolite and albite) or magnesium (tourmaline and magnesium-rich biotite; *cf.* Kwak, 1977; Warren, 1999). The sodium comes from dissolution of salts such as halite and the magnesium from diagenetic minerals such as dolomite and clays (*cf.* Warren, 1999). However, the presence of a likely metaevaporitic mineral assemblage does not, by itself, indicate an undeniable evaporite protolith because, for example, the NaCl in scapolite could have been derived from an outside source such as hydrothermal or sedimentary brines rather than halite. Further evidence is required from the distribution of the metaevaporitic mineral assemblage. Scapolites derived from hydrothermal or basinal brines tend to form haloes or replacement fronts associated with fluid conduits (Warren, 1999). However, scapolite that is distributed as fine-scale interbedded scapolite-bearing and scapolite free layers is representative of an *in situ* salt precursor (*ibid.*). As evaporite dissolution occurs (during deposition, compaction, and/or during uplift associated with collision and basin inversion) strata overlying or intercalated with the evaporites settle and become fragmented leading to the formation of dissolution breccias. These breccias are commonly preserved in the rock record and are another indication of the former presence of evaporites (*ibid.*). Widespread sodic alteration haloes can also be an indication that evaporites were once part of the stratigraphy. The haloes form in fine-grained sediments adjacent to evaporites during burial, diagenesis and metamorphism

due to progressive dissolution of evaporites by circulating fluids (*ibid.*). Resulting fluids are typically saline and chlorine-rich and lead to the growth of metamorphic minerals dominated by sodic phases, thus creating zones of albitisation or scapolitisation as scapolite replaces albite[2].

In the Slab area abundant (< 1 to 5 mm) scapolite occurs in discrete layers < 1 to 30 cm thick, in a sequence of fine-grained metasedimentary rocks at least 100 m thick (Figs. 4c,5). The scapolite is sodium and chlorine-rich with a composition of 69.6 - 77.9 % marialite ($Na_4[Al_3Si_9O_{24}]Cl$) and 22.1 - 30.4 % meionite ($Ca_4[Al_6Si_6O_{24}]CO_3$); Na_2O content ranges from 7.94 - 10.24 weight % (average 9.68 wt.%) and Cl content ranges from 2.90 - 3.55 weight % (average 3.29 wt.%; Table 2). Biotite in this area is magnesium rich with MgO contents from 12.76 – 14.59 weight % (average 13.75 wt. %; Table 2). The occurrence of scapolite within discrete layers and its marialitic composition are consistent with derivation from a protolith that contained abundant halite (*cf.* Warren, 1999). The magnesium-rich nature of biotite associated with the scapolite is also consistent with this interpretation. Probable solution breccia made up of contorted, broken siltstone layers in a carbonate matrix occurs above the scapolite-rich horizon that underlies Slab ridge (Fig. 5). Large zones of sodic metasomatic alteration, typified by albite and marialitic scapolite, occur in fine-grained FLG sedimentary rocks in the Slab area consistent with expected alteration proximal to evaporite-bearing rocks. Taken together, the above indicate *in situ* (halite-facies) evaporites were once present in upper FLG strata.

Quartet Group

The Quartet Group gradationally overlies the FLG and occurs throughout the study area (Fig. 2). It is at least 5 km thick and consists of a monotonous succession of dark grey-weathering clastic rocks that have been divided into basal black carbonaceous shale (Q-1) and conformably overlying, coarsening-upwards, interlayered, shale, siltstone and sandstone (Q-2; Fig. 4 a,d; Table 1; Delaney, 1978, 1981). Q-1 is interpreted to have accumulated in a sediment-starved basin (Delaney, 1981). Q-2 was deposited in a shallow marine (subtidal to intertidal) environment and records a gradually increasing influx of sediment into the basin (*ibid.*).

[2] 3 Albite + NaCl <—> Marialite i.e. 3 Na(AlSi3O8) + NaCl <—> $Na_4(Al_3Si_9O_{24})Cl$

Gillespie Lake Group

The Gillespie Lake Group gradationally overlies the Quartet Group and forms the upper part of the WSG. It occurs throughout the study area (Fig. 2) and consists of at least 4 km of shallow marine, buff-, orange- and locally grey-weathering dolostone, limestone, claystone, mudstone, and sandstone divided into seven conformable formations named, from base to top, G-Tr and G-2 to G-7 (Fig. 4a; Table 1; Delaney, 1978, 1981). G-Tr consists of siliciclastic sediments that gradually increase in carbonate content up sequence (Delaney, 1981). G-2 to G-4 are made up of fine-grained siliciclastic-dolostone admixtures. G-5 is similar to G-2 to G-4 but contains stromatolitic conglomerate and breccia. G-6 is made up of thick sequences of carbonate and terrigenous-carbonate admixtures. G-7 consists of platformal carbonates some of which are stromatolitic (Fig. 4e).

A.3.2 Igneous rocks

Numerous small Early Proterozoic (*ca*. 1715 to 1705 Ma) igneous bodies, known as Bonnet Plume River Intrusions (BPRI), crosscut the WSG and occur as clasts in Wernecke Breccia (Fig. 3; Thorkelson, 2000; Thorkelson *et al.,* 2001a,b). The intrusions are generally fine- to medium-grained and composed of rift-related tholeiitic diorite or gabbro and lesser syenite and anorthosite (Thorkelson *et al.*, 2001b).

Slab volcanics are preserved as clasts within Wernecke Breccia (*cf*. Thorkelson, 2000). The main exposure is a 160 x 380 m block comprising about 34 steeply dipping, 0.8 to 14 m thick, mafic to intermediate, subaerial flows and minor intercalated volcaniclastic and epiclastic units (*cf.* Laughton *et al*., 2002; Laughton, 2004). The age of the volcanic rocks is not known. They are geochemically similar to BPRI and may have been comagmatic with them, thus Slab volcanics could be younger than WSG (*cf.* Thorkelson, 2000). Alternatively, Slab volcanics may be part of lower WSG. They have only been observed in Wernecke Breccia emplaced into upper FLG strata in several localities along the Bonnet Plume River valley (Thorkelson, 2000; Laughton *et al.*, 2002; Laughton, 2004; this study). Clasts within Wernecke Breccia appear to be locally derived from proximal host rocks (WSG or BPRI - see below), thus it seems reasonable to assume clasts of Slab volcanics were also locally derived. Therefore, the eruption of Slab volcanics may have been a localized event during lower WSG deposition. The WSG is a dominantly marine succession and Slab volcanics are subaerial however, the

presence of metaevaporites within lower WSG rocks indicates very shallow marine to emergent conditions were present at least periodically, thus sub-aerial volcanism could have occurred during deposition of lower WSG strata.

A.4 Metamorphism, deformation, and timing

The Racklan Orogeny produced lower to middle greenschist grade regional metamorphism in WSG rocks (*cf.* Delaney, 1981; Thorkelson, 2000, Brideau *et al.*, 2002). Typical metamorphic mineral assemblages include chlorite-muscovite-chloritoid-quartz±garnet indicating peak metamorphic conditions of 450-550 ^{o}C and approximate pressure of 3-6 kbars (Brideau *et al.*, 2002). Three phases of deformation are ascribed to the Racklan Orogeny (Thorkelson, 2000; Brideau *et al.*, 2002). The first phase occurred during peak metamorphism and produced foliations (ranging from slaty cleavage to schistosity) and north- to east-trending folds (*ibid.*). The second phase produced crenulations and local crenulation cleavage and the third phase led to the formation of kink-bands. During Racklan orogenesis some units, especially those in the upper FLG and Quartet Group, were converted to schist, slate and phyllite in regions of high strain, commonly in the cores, or overturned parts, of tight folds (*cf.* Thorkelson *et al.*, 2003). The age of the Racklan Orogeny is not known, however, it is constrained by the age of Wernecke Breccia that contains clasts of deformed WSG (Fig. 3). In the Slab area, hydrothermal titanite from the matrix of Wernecke Breccia that contains clasts of foliated, kinked metasiltstone returned a U-Pb age of *ca.* 1600 Ma (Thorkelson *et al.,* 2001a), thus, the Racklan Orogeny must be older than *ca.* 1600 Ma.

Cross-cutting relationships indicate both the BPRI and the Slab volcanics are older than Wernecke Breccia, i.e. the breccia contains clasts of these lithologies (Thorkelson, 2000). The difference in age between the igneous rocks and the breccia is poorly constrained due to the unknown age of the Slab volcanics and minimal reliable age information for Wernecke Breccia. However, available data for the breccias indicates they are significantly younger than BPRI, i.e. *ca.* 1600 Ma versus *ca.* 1710 Ma (Thorkelson, 2000; Thorkelson *et al.*, 2001a,b). The timing of magmatism relative to Racklan deformation remains uncertain as there are no documented outcrops of BPRI or Slab volcanics that contain Racklan deformation fabrics (*ibid.*). Both the BPRI and the Slab volcanics have been affected by low grade metamorphism - for example in the BPRI, pyroxene has altered to chlorite or actinolite and plagioclase is replaced by

sericite, albite, potassium feldspar or scapolite (Thorkelson *et al.*, 2001b) and in the Slab volcanics plagioclase is commonly replaced by scapolite (Thorkelson, 2000; Laughton *et al.*, 2002; Laughton, 2004). However, some (or all) of this alteration may be due to metasomatism associated with Wernecke Breccia emplacement.

Several post-Racklan orogenic events also affected the study area (Fig. 3). The Middle Proterozoic Corn Creek Orogeny produced west- to southwest-verging folds and thrust faults mainly in the Pinguicula and Hematite Creek groups (Fig. 3; Thorkelson, 2000). The Late Proterozoic Hayhook extensional event produced generally west-trending normal faults some of which truncate folds and faults related to the Corn Creek Orogeny (*ibid*.). Contractional deformation associated with the Cretaceous to Early Tertiary Laramide Orogeny produced large-wavelength, west-northwest-trending folds and reverse faults in WSG and younger strata (Fig. 2; Norris, 1997; Thorkelson *et al.*, 2003). Laramide-age structures are cut by Tertiary normal faults (Thorkelson 2000).

A.5 Geology of Wernecke Breccia

Six widely spaced IOCG prospects were examined in this study (Figs. 1,2): Slab, Hoover, Igor, Slats-Frosty, Slats-Wallbanger and Olympic. The prospects were chosen based on: differences in metasomatic alteration [M. Stammers pers comm. (2000); R. Gorton pers comm. (2000)]; stratigraphic location within host WSG strata (Eaton and Archer, 1981; Thorkelson, 2000); and the availability of diamond drill core. Mapping was carried out at 1:5,000-scale at Slab, Hoover and Igor (Hunt *et al.*, 2002; Thorkelson *et al.*, 2002, 2003); reconnaissance mapping was carried out at the remaining prospects. Diamond drill core from each of the prospects was logged in detail[3] and samples collected for petrographic, microprobe, stable isotope and fluid inclusion analyses. Mapping and core logging were carried out in order to characterize the structural and stratigraphic settings of the breccias and associated alteration and mineralisation, and to provide paragenetic information. This paper presents the results of field, petrographic and microprobe studies. Stable isotope and fluid inclusion data is presented in Section C; a summary is given here. The main characteristics of the prospects are summarised in

[3] The following number of diamond drill holes were logged in detail at Slab, Hoover, Slats-Frosty, Slats-Wallbanger, Igor and Olympic respectively: 5, 2, 2, 3, 2 and 3. An additional 8 holes were examined in less detail at Slab.

Table 3 and described below beginning with a general description of Wernecke Breccia based on combined observations from the prospects studied.

Wernecke Breccia varies from clast to matrix supported (Fig. 6a,b; *cf*. Bell, 1986a,b; Thorkelson, 2000; Hunt *et al*, 2002). Clasts are generally sub-angular to sub-rounded and range from < 1 cm to metres to several hundred metres across (e.g. Slab Fig.7). Clasts are locally derived, dominantly from proximal WSG strata, however, clasts of BPRI (e.g. at Slab, Hoover, Olympic) and Slab volcanics (e.g. at Slab) are abundant where breccia cuts those lithologies. Early phases of Wernecke Breccia are preserved in some locations as clasts within later breccia (Fig. 6c). Breccia matrix is made up of rock fragments and hydrothermal precipitates consisting mainly of feldspar (albite and/or potassium feldspar), carbonate (calcite, or dolomite/ankerite, locally siderite) and quartz (Fig. 6d). Locally, the breccia matrix contains abundant hematite, magnetite, chalcopyrite (see mineralisation section), biotite, muscovite barite and fluorite and lesser tourmaline and actinolite, and rare titanite and monazite. In some places the matrix is coarsely crystalline and is made up of quartz, calcite and fluorite crystals up to 2 cm across. Locally, biotite, muscovite and magnetite crystals up to 1 cm across occur within finer grained matrix.

Wernecke Breccia complexes vary greatly in shape and size. In plan view they are elliptical, elongate, or irregular in shape. In vertical section they can be discordant or parallel to layering with no or numerous offshoots. The size of breccia bodies varies from a few centimetres to several hundred metres to several kilometres across. Contacts between country rock and breccia vary from sharp to diffuse/gradational (Fig. 6 e,f). Gradational boundaries with the WSG extend for a few centimetres to several tens of metres and the degree of brecciation gradually decreases outwards from strongly disrupted sedimentary rocks to layers that appear simply “pushed apart” to fractured country rock.

A.6 Wernecke Breccia: structural & stratigraphic controls

A.6.1 Regional scale

Wernecke Breccias are spatially associated with regional-scale faults (*cf*. Bell, 1986a,b; Thorkelson, 2000). In the study area, breccia bodies lie on the southwestern edge of the Richardson Fault array (Fig. 1). This is a series of deep-seated, long-lived structures that developed in a dilational tectonic regime and are traceable for approximately 600 km in

an area that marks the transition from relatively undeformed rocks of the Northern Interior Platform to those of the Cordilleran Orogenic System (Delaney, 1981; Norris, 1997; Thorkelson, 2000).

A.6.2 Local scale

Breccia emplacement appears to have exploited pre-existing crustal weaknesses (*cf.* Bell, 1986a,b; Thorkelson, 2000) at all scales including the faulted cores of folds, high strain zones, pathways previously used by the BPRI, jointing/fractures and permeable sedimentary layers. Breccia occurs throughout the WSG but is most widespread in the upper FLG (Delaney, 1981).

The Slab prospect is underlain by upper FLG strata (Bell and Delaney, 1977) that are, in part, made up of metaevaporites (Fig. 5; Table 3). It occurs on the eastern limb of a large northwest-trending anticlinal structure proximal to a flexure in the trend of the fold (Fig. 2) and is cut by a northwest-trending zone of schist and phyllite interpreted to a be a high strain zone (Fig. 7; Thorkelson, 2000; Brideau *et al.* 2002). Minor outcrops of BPRI occur within the strain zone. Extensive Wernecke Breccia occurs as large, elongate, irregular-shaped bodies proximal to the high strain zone, as elliptical pipe-like bodies a few metres in diameter within the strain zone and as narrow bodies parallel to layering in metasedimentary rocks. Cross-cutting relationships indicate there are at least three phases of breccia (Hunt *et al.*, 2002). Breccias in this area contain the largest clasts observed with some up to several hundred metres across and it is one of few locations where breccia contains clasts of Slab volcanics (Fig. 7; *cf.* Thorkelson, 2000; Hunt *et al.*, 2002; Laughton *et al.* 2002; Laughton, 2004). A detailed description of part of the Slab area (Slab creek) is given in Brooks *et al.* (2002) and Brooks (2002).

The Hoover prospect is located about 20 km north of Slab and is underlain dominantly by FLG to Quartet Group transitional rocks including a 4 to 10 m-thick regional marker carbonate unit (Figs. 2, 8; Thorkelson *et al.*, 2002, 2003). Like Slab, Hoover occurs on the eastern limb of the antiform whose axis underlies the Bonnet Plume River valley (*ibid.*). Wernecke Breccia occurs in two locations (Fig. 8; *ibid.*): 1) an irregular-shaped breccia body at least 100 m thick occurs at the base of the slope in strongly folded FLG metasiltstone and phyllite and 2) small, discontinuous breccia

bodies 1-20 m thick occur about 500 m upslope in Quartet Group at the contact between slate and metasiltstone. Large (up to 12 x 10 m) clasts of BPRI diorite are abundant locally in the lower breccia. Rare clasts of earlier breccia indicate there have been multiple episodes of brecciation.

The Igor prospect, located about 28 km west of Slab, is underlain by Quartet Group metasedimentary rocks (unit Q-2 of Delaney, 1981) that are faulted against and unconformably overlain by Paleozoic clastic sedimentary rocks and limestone (Figs. 2,9; *cf.* Norris, 1997). Quartet Group rocks have been folded into a north-trending anticline. The core of the anticline is coincident with schistose rocks that likely represent a high strain zone. Abundant Wernecke Breccia occurs in the core of the anticline and cross-cutting relationships indicate several phases of breccia are present. In addition, narrow zones of breccia (< 2 m wide) occur in Quartet Group adjacent to the main breccia complex.

Slats-Frosty is located about 15 km west of Slab and is underlain by the FLG and abundant BPRI dykes and sills (Fig. 2; Thorkelson *et al.*, 2002, 2003). It is located on the east side of a large northeast-trending overturned antiform (Thorkelson, 2000; Thorkelson *et al.*, 2002, 2003). Breccia occurs dominantly as numerous discontinuous narrow bands up to 1.5 m thick emplaced parallel to layering in the FLG, and less commonly as narrow zones (up to 0.8 m) parallel to prominent jointing. The Slats-Wallbanger prospect is located approximately 4 km south of Slats-Frosty and is underlain by Quartet Group-GLG transitional strata (units Q-2 and G-Tr of Delaney, 1981) and abundant BPRI (Thorkelson, 2000). Breccia occurs throughout the Wallbanger area as narrow bands (2 m across) and larger irregular bodies proximal to BPRI rocks. The Olympic prospect, located approximately 15 km southeast of Slab, occurs in the upper part of the WSG and is underlain by GLG dolostone and BPRI (Fig. 2; *cf.* Thorkelson, 2000). The dolostone is in part stromatolitic (Fig. 4e, unit G-5 or G-7 of Delaney, 1981) and intraformational dolostone breccia is locally abundant. Wernecke Breccia occurs as irregular-shaped bodies in the Olympic area that locally contain abundant clasts of BPRI anorthosite, from < 1 cm to tens of metres across (Thorkelson, 2000; this study). Sparse clasts of earlier breccia indicate multiple phases of brecciation have occurred.

A.7 Alteration

Extensive metasomatic alteration occurs within Wernecke Breccia and extends into host WSG and/or BPRI rocks for a few metres to tens of metres (*cf.* Thorkelson, 2000, Hunt *et al.* 2002, 2003a,b). There are two major alteration types, sodic and potassic whose abundance appears to depend on host rock lithology. Sodic alteration generally occurs in breccia hosted by lower WSG rocks where there is evidence for metaevaporites. Breccia and WSG rocks affected by sodic alteration are dominantly grey in colour (Fig. 10a) and contain abundant albite and lesser scapolite. This type of alteration is dominant, for example, at Slab and Hoover where feldspar from breccia clasts, breccia matrix, veins and sedimentary rocks is dominantly albite (Fig. 11a); feldspar at Slab is composed of $albite_{96-100}$, $orthoclase_{0-1}$ and $anorthite_{0-4}$ and at Hoover is composed of $albite_{98-100}$, $orthoclase_{0-1}$ and $anorthite_{0-2}$. Minor orthoclase occurs in both areas (Fig. 11a) and has a narrow compositional range of $orthoclase_{86-99}$, $albite_{0-16}$, and $anorthite_{0-14}$.

Potassic alteration is dominant in breccias hosted by fine-grained clastic rocks i.e. in the Quartet Group, in the FLG where no evidence for metaevaporites was observed, and in the GLG where dolostone is interlayered with fine-grained clastic rocks. Rocks affected by potassic alteration are largely pink to red in colour and contain abundant orthoclase ± sericite (Fig 10b). This type of alteration occurs, for example, at Slats-Frosty and Olympic where feldspar is dominantly orthoclase (Fig. 11a); feldspar at Slats-Frosty is composed of $orthoclase_{94-99}$, $albite_{0-6}$, $anorthite_{0-1}$ and at Olympic is composed of $orthoclase_{88-100}$, $albite_{0-9}$, $anorthite_{0-6}$. Metasomatic alteration at Igor is dominantly potassic consisting of orthoclase and sericite; minor albite is present (Fig. 11a). Feldspar at Igor is composed of $orthoclase_{82-96}$, $albite_{3-18}$, $anorthite_{0-1}$ and $albite_{99-100}$, $orthoclase_{0-1}$, $anorthite_{0-1}$.

At all of the prospects examined, sodic or potassic alteration is overprinted by carbonate that forms the dominant phase in breccia matrix and cross-cutting veins (Fig. 10c,d). The composition of the carbonate also varies. Calcite is dominant in breccias with sodic alteration, for example at Slab and Hoover (Fig. 11b); dolomite occurs in minor amounts. Dolomite and ankerite are dominant in potassically-altered breccias, for example at Slats-Frosty and Olympic. The Igor prospect differs from others in the study in that siderite, in addition to dolomite/ankerite, is locally abundant in breccia matrix and narrow cross-cutting veins (Fig. 11b). Igor is also the only prospect studied where

barite is abundant. It occurs as veins, lenses or pods (locally coarsely crystalline) up to 3 x 15 m that cross-cut breccia, and as disseminations within breccia matrix and zones of massive magnetite-hematite (Archer, 1980; Eaton and Archer, 1981; this study).

A.8 Mineralisation

Sixty five Wernecke Breccia-associated prospects are known from the Wernecke and Ogilvie Mountains and all are associated with IOCG mineralisation (Fig. 1, Archer and Schmidt, 1978; Yukon MINFILE, 2003). Mineralisation is similar at each prospect and occurs as veins and disseminations in breccia and surrounding rocks and locally as breccia matrix; multiple episodes of mineralisation are evident (Figs. 1, 10,12; *cf.* Archer and Schmidt, 1978; Yukon MINFILE, 2003; Hunt *et al.*, 2002, 2003a; Brooks *et al.*, 2002). IOCG minerals include magnetite, hematite, chalcopyrite and lesser pitchblende, brannerite and cobaltite; gold was not observed but reports with copper in assay results (*cf.* Archer and Schmidt, 1978; Yukon MINFILE, 2003; Brooks, 2002). General descriptions of mineralisation at the prospects studied are given below. The characteristics of each prospect, including main mineral assemblage and resource or best intersection, are summarised in Table 3.

Multiple phases of oxide and sulphide mineralisation occur at Slab which has a resource of 20 million tons of 0.35 % Cu and 0.17 g/t Au (Thorkelson *et al.*, 2003). Magnetite is dominant in the early stages of brecciation and locally occurs as massive ankerite-magnetite veins up to 1 m across (Fig. 10e; Hunt *et al.*, 2002). These are cross-cut by and occur as clasts in later breccia. Lesser amounts of magnetite occur in later paragenetic stages as disseminated fine-grained blebs and euhedral crystals. Hematite, chalcopyrite and pyrite occur throughout the paragenesis but are most abundant during brecciation following ankerite-magnetite alteration when they occur mainly as breccia matrix and syn-breccia veins (Figs. 10f). Breccia locally contains clasts of massive pyrite-chalcopyrite up to 20 cm across indicating multiple phases of sulphide mineralisation (Fig. 10g). All breccia is cut by veins up to 1 m thick composed dominantly of calcite ± quartz-albite-hematite-magnetite-muscovite-biotite-fluorite. These veins locally contain chalcopyrite (Fig. 10h) and pyrite and rarely molybdenite.

Breccia-associated mineralisation at Hoover is similar to that at Slab and occurs along the northeast side of the Bonnet Plume River valley for over 6 km (Fig. 2); best intersections returned 0.32 g/t Au and 0.42 % Cu over 73 m and 3.6 % Cu over 3.1 m

(Thorkelson *et al.*, 2003, Yukon MINFILE, 2003). Mineralisation is dominantly copper-gold with minor uranium and cobalt and occurs: 1) as disseminations in albite-quartz-pyrite-chalcopyrite veinlets/replacement layers within siltstone clasts in the breccia and as rare massive sulphide clasts, 2) as disseminations and blebs in breccia matrix, locally forming the entire matrix (Fig. 10i), 3) as blebs up to 5 cm across and disseminations in calcite-chlorite-muscovite-pyrite-chalcopyrite-hematite ± magnetite, quartz-hematite-pyrite-chalcopyrite and calcite ± chalcopyrite veins that crosscut breccia and WSG and 4) as blebs and disseminations in quartz-chalcopyrite ± feldspar ± muscovite ± hematite veins that are parallel to and crosscut calcareous layers in siltstone. In general mineralisation occurs as large zones of low-grade copper-gold that contain higher grade pockets (Table 3).

At the Igor prospect, mineralisation occurs largely as pods up to 4 x 15 m of massive hematite-magnetite-pyrite-chalcopyrite and minor pitchblende with dolomite, ankerite, siderite, barite, quartz and chlorite (Archer, 1976, 1980; Eaton and Archer, 1981; Eaton, 1982; this study). The pods occur within breccia in east-trending fractures that are approximately orthogonal to the axis of the large anticline in Igor creek, and in narrow bands parallel to foliation in breccia. Within the pods, hematite, pyrite and/or chalcopyrite locally form/?replace breccia matrix. Less abundant mineralisation occurs as disseminations in breccia and Quartet Group rocks and in quartz ± siderite ± chalcopyrite ± hematite ± pyrite ± magnetite veins, barite veins and dolomite veins that cut the massive mineralisation. Drilling produced encouraging results including a 19.7 m intersection of 4.74% Cu, 0.088% U_3O_8 and 325 ppm Co and a separate 10.6 m intersection of 6.14% Cu, 0.89% U_3O_8 and 358 ppm Co (Eaton and Archer, 1981). Cobalt is associated with pyrite and is unevenly distributed between pyrite grains (Eaton and Archer, 1981). In some instances a cobalt-bearing pyrite grain is surrounded by barren pyrite grains. Uranium mineralisation appears to be related to chalcopyrite and occurs mainly as pitchblende: 1) associated with barite and minor chalcopyrite that discontinuously fills fractures/joints in breccia, 2) as disseminations in zones of chalcopyrite-rich massive magnetite-hematite and 3) as rims on breccia clasts and disseminations in breccia matrix (Archer, 1980). Thorium is a minor constituent; U:Th is 47:1. Uranium is also found in rare brannerite that occurs in fractures in metasedimentary rocks adjacent to breccia (Eaton and Archer, 1981).

At the Slats prospects (Frosty and Wallbanger) copper ± gold ± cobalt mineralisation is widely distributed and low grade with sporadic higher grade

occurrences (Table 3). In general, at Frosty, chalcopyrite occurs as disseminations in breccia and in veins and fractures. Pods/veins of massive hematite or massive magnetite-coarsely crystalline hematite-ankerite-quartz up to 2 x 4 m occur locally in breccia zones (Fig. 12a); samples returned low values of copper and gold with the best results (1380 ppb Au and 9650 ppm Cu) being returned by a grab sample (Thorkelson *et al.*, 2003). Quartz vein material containing visible gold and brannerite also occurs in the Frosty area (Yukon MINFILE, 2003). Selected samples returned values of 686 to 10,285 g/t Au (*ibid*), however the source of this material has not been found and it is not known if it is related to Wernecke Breccia. Mineralisation at Wallbanger is similar to that in other areas (Table 3); pyrite locally forms the breccia matrix and a pod of massive magnetite occurs at a contact between breccia and shale; the best intersection returned 450 ppb Au, 1115 ppm Cu and 5800 Co over 1 m (Stammers, 1995). IOCG mineralisation at the Olympic prospect is generally low grade and not abundant; the best intersection returned 1593 ppm Cu, 40 ppm Co and 23 ppb Au over 11 m (Table 3; Caulfield, 1994). The observed mineralisation consists of chalcopyrite and pyrite on fractures at siltstone-breccia contacts, euhedral pyrite + chalcopyrite ± erythrite in ankerite-quartz veins in crackle brecciated siltstone, and sparse chalcopyrite porphyroblasts that overprint breccia matrix and clasts.

A.9 Paragenesis

Broad paragenetic sequences were established for the breccia occurrences based on cross-cutting relationships in outcrop and drill core (Fig. 13; Hunt *et al.*, 2002, 2004). Paragenetic stages are unique to each prospect and not equivalent to those of other areas; for example Slab stage 3 ≠ Hoover stage 3 ≠ Olympic stage 3. Each phase in the development of a breccia complex was probably multistage and overlapped other stages (Delaney, 1981). However, there is an overall general trend of: 1) metasomatic alteration (sodic or potassic) that overprints greenschist facies metamorphic mineral assemblages; 2) early stage brecciation accompanied by abundant magnetite ± hematite alteration; 3) main phase of brecciation accompanied by hematite and chalcopyrite-pyrite ± magnetite mineralisation; and 4) syn to post breccia carbonitization (calcite, ankerite/dolomite, siderite) ± pyrite, chalcopyrite, hematite, magnetite. Locally barite veins are abundant during stage 4 (e.g. at Igor). During the main phase of brecciation early euhedral magnetite is commonly replaced by hematite (Fig 12b) and/or pyrite

(Fig. 12c) and, in general, where chalcopyrite is present with other metallic minerals it is usually the latest mineralisation phase (Fig. 12d).

A.10 Discussion

A.10.1 Timing of breccia emplacement: Cross-cutting relationships demonstrate Wernecke Breccia was emplaced syn- to post-Racklan orogenesis, after peak metamorphism. Sodic and potassic metasomatic alteration associated with Wernecke Breccia overprints greenschist facies metamorphic assemblages and all breccia bodies examined contain clasts of foliated metasedimentary rocks (Fig. 12e) thus indicating that Wernecke Breccia was emplaced after commencement of Racklan orogenesis. Syn-deformation breccia emplacement is indicated by foliated breccia at the Igor prospect that occurs as clasts within cross-cutting breccia that does not contain a fabric (Eaton and Archer, 1981) and by kinked breccia-related ankerite-magnetite and magnetite veins at Slab (Fig. 12f). Post-deformation breccia emplacement is demonstrated by the presence of phyllite clasts in the breccia that contain all three phases of deformation, e.g. Slab (Thorkelson, 2000). Locally, Wernecke Breccia contains clasts of foliated metasiltstone and is itself foliated (Fig. 12g), e.g. at Slats-Wallbanger, however, it is not clear if this deformation is related to Racklan orogenesis or to later deformation.

The absolute age of Wernecke Breccia is constrained by a U-Pb age of *ca*. 1600 Ma that was returned by hydrothermal titanite from a sample of breccia matrix at Slab (Thorkelson, 2000; Thorkelson *et al.*, 2001a); this breccia contains foliated, crenulated, kinked clasts of WSG rocks (*ibid*). Additional age dating including Ar-Ar, Re-Os and U-Pb analyses is presented in Section B.

A.10.2 Mechanism of breccia emplacement: Several hypotheses have been suggested for the mechanism of breccia emplacement including mud diapirs (Lane, 1990), phreatomagmatic explosions (Laznicka and Edwards, 1979), diatremes (Tempelman-Kluit, 1981; Bell and Delaney, 1977), modified evaporite diapirs (Bell, 1989) and explosive expansion of volatile-rich fluids associated with deeply buried intrusions (Thorkelson, 2000; Thorkelson *et al.*, 2001a). Recent studies place constraints on these possible mechanisms (*cf.* Thorkelson 2000 for a review). For example: 1) mud diapirism is ruled out because Wernecke Breccia contains clasts of deformed WSG rocks indicating that the sediments were lithified and deformed prior to brecciation; 2) a

diatreme origin seems unlikely because breccia clasts are locally derived; 3) age dating shows that breccia is considerably younger than BPRI (*ca*. 1710 versus *ca*. 1600 Ma) making BPRI magmatism an unlikely mechanism of brecciation; and 4) brecciation caused by the explosive expansion of volatile-rich fluids derived from deeply buried intrusive rocks appears unlikely because stable isotope data do not indicate input from magmatic fluids (see below and Section C).

Any model for the formation of Wernecke Breccia must take into account the following observations: 1) the large-scale of the brecciation and metasomatic alteration; 2) multiple phases of cross-cutting breccia and mineralisation; 3) the spatial association of breccia with regional-scale faults and the occurrence of breccia bodies in weak zones such as cores of folds and faults; 4) the spatial association of breccia with BPRI and the age difference between breccia and BPRI; 5) the emplacement of breccia syn- to post-Racklan deformation and after peak metamorphism; 6) the widespread occurrence of breccia in the upper FLG; 7) the presence of metaevaporites in the upper FLG; 8) the preservation of Slab volcanics as clasts in breccia emplaced into the FLG; 9) the derivation of breccia clasts from proximal host rocks; and 10) the distribution of sodic and potassic metasomatic alteration. Any proposed brecciation mechanism must also take into account characteristics of the breccia-forming fluid. Information available to date is provided by fluid inclusion and stable isotope data (Section C) and is summarised below. Syn-breccia fluids were low to moderate temperature (185 – 350 ^{o}C), high salinity (24-42 wt. % NaCl eq.) NaCl-$CaCl_2$-H_2O brines. Carbon, oxygen and sulphur isotope results for each of the IOCG prospects studied are similar and, in general, do not vary systematically with paragenetic stage: $\delta^{13}C \approx$ -7 to +1 ‰ (V-PDB), $\delta^{18}O \approx$ 9 to 20 ‰ (V-SMOW), $\delta^{34}S_{sulphide} \approx$ -12 to +13 ‰ (CDT) and $\delta^{34}S_{sulphate} \approx$ 8 to 17 ‰ (CDT). The fluid composition and isotopic ratios appear to be rock buffered (*ibid*). The $\delta^{13}C$ values of hydrothermal carbonates indicate the carbon was derived in large part from the host WSG. The $\delta^{34}S$ values of hydrothermal pyrite, chalcopyrite and barite point to a seawater (or sediments/evaporites deposited from seawater) source for sulphur. These data combined with limited hydrogen isotope data indicate the source of fluids was likely formation/metamorphic water mixed with variable amounts of low δD (e.g. organic) water ± evolved meteoric and/or evolved seawater (*ibid.*). Fluid inclusion data also enable the depth of breccia emplacement to be estimated. This was calculated for Slab to be 7.4 to 9.0 km (2.4-3.0 kbars; *ibid.*), thus indicating that breccia at Slab

was emplaced at considerable depth and not close to surface as previously suggested (*cf.* Thorkelson, *et al.*, 2001a; Laughton, 2004).

The following proposed brecciation mechanism takes into account the above constraints and relates breccia emplacement to evolution of the Wernecke Basin, as shown in Figure 14.

Stage I: Deposition of the lower WSG in a region underlain by attenuated continental crust (Thorkelson, 2000). This is represented by the FLG calcareous sedimentary rocks and minor limestone that make up the first WSG clastic to carbonate grand cycle (Delaney, 1981; Thorkelson, 2000). Evaporites (halite facies) were deposited in (at least) the upper part of the FLG. Slab volcanics may also have been deposited at this time.

Stage II: Subsidence and thermal deepening of the basin due to rifting, and the subsequent deposition of the middle and upper parts of the WSG (Thorkelson, 2000). The transition is marked by an abrupt change from dolostone to carbonaceous shale at the top of the FLG (Delaney, 1981). Quartet Group fine-grained clastic rocks and the overlying GLG dolostone were deposited at this time and form a second clastic to carbonate grand cycle (Delaney, 1981; Thorkelson; 2000). The accumulation of thick shallow-water carbonates in the upper part of the WSG indicates protracted subsidence of the basin during this time; abrupt facies changes within the GLG indicate normal faulting was coincident with deposition (Thorkelson, 2000). The suite of BPRI were emplaced *ca.* 1710 Ma, after deposition of the WSG. However, their timing with respect to deformation is poorly constrained and they could be pre- or syn-Racklan orogenesis (Thorkelson, 2000; Thorkelson *et al.*, 2001b).

Stage III: Racklan Orogenesis caused greenschist facies metamorphism and three phases of deformation in WSG rocks (Thorkelson, 2000; Brideau *et al.*, 2002). Peak metamorphic conditions (450-550 ^{o}C and 3-6 kbars), folds and foliations were produced during the first phase. The second and third phases produced crenulations/crenulation cleavage and kink bands respectively (*ibid.*). Cross-cutting relationships indicate that Wernecke Breccias were produced syn- to post-deformation, but post peak metamorphism. The length of time occupied by Racklan orogenesis is poorly constrained. If the *ca.* 1710 Ma. BPRI were emplaced before orogenesis then

deformation and breccia emplacement could have occurred over a geologically short period of time prior to (close to) *ca.*1600 Ma. However, if BPRI were emplaced syn-orogenesis this implies a period of deformation and breccia production that spanned over 100 Ma years (i.e. *ca.* 1710-1600 Ma).

During stages I and II, as the WSG sediments were undergoing diagenesis and compaction, evaporites within the sedimentary pile would have begun to dissolve. Dissolution would have caused disruption of intercalated and overlying sediments and led to the formation of solution breccias (Fig. 5), and strata overlying evaporites would have been extensively tilted and faulted (*cf.* Warren, 1999). Temperatures would have become elevated in deeper parts of the basin due to the increasing weight of overlying sediments as deposition continued. For example, assuming a geothermal gradient of 25 ^{o}C/km (average geothermal gradient of the earth, *cf.* Raymond (1995) and a surface temperature of 25 ^{o}C the temperature at the top of the FLG (~9 km depth) would have been 250^{o}C (Fig. 14). Greenschist facies metamorphism with temperatures of at least 450 ^{o}C was superimposed on the above scenario along with contractional deformation (Brideau *et al.*, 2002). Wernecke Breccia was therefore produced within WSG rocks that had already been affected by syn-depositional faulting, likely contained zones of disrupted and brecciated strata associated with evaporites, had been intruded by BPRI, had reached elevated temperatures due to burial and metamorphism and had been affected by at least one phase of deformation.

The brecciation mechanism that produced Wernecke Breccia was probably not violently explosive, i.e. not diatreme- or volcanic-like. Clasts are derived from proximal host strata and do not show evidence of transport. Clasts of country rocks are commonly angular to subangular and locally, have clear jigsaw-fit texture (e.g. Fig. 10i); this is especially apparent where breccia cross-cuts BPRI or well-laminated sedimentary rocks. Subrounded to rounded clasts (e.g. Figs. 6c, 10a) and intense zones of alteration also occur, generally in areas where cross-cutting relationships demonstrate that multiple brecciation events have occurred. The amount of fluid was probably not voluminous, as evidenced by the rock buffered nature of alteration and isotopic ratios, except in areas of cross-cutting breccia which likely mark zones of more abundant fluid flow.

This evidence best fits a scenario in which breccias were created by the relatively non-violent expansion of over-pressured basinal fluids. These fluids were locally focussed along permeable pathways, such as faults or shear zones, which led to

multiple brecciation events in the same location as pressure repeatedly built up and was released. Basinal fluid would likely have become over-pressured during burial and compaction of sediments, especially in deeper parts of the basin where plastic deformation would be likely to decrease permeability and close porosity leading to an increase in pore fluid pressure (McCaig *et al.*, 2000). It seems probable that pressure within basinal fluids would have been released during initial phases of Racklan deformation. However, in situ evaporites were still present during metamorphism and could have acted as a local seal to fluid flow. In addition, at least at Slab, breccia was emplaced at considerable depth (7-9 km) and strata may have been deforming plastically which would cause over-pressuring of the pore fluid if no permeable pathways such as faults were available. Periodic release of pressure, perhaps by breaking of seals on permeable pathways during continuing deformation, would lead to rapid expansion of fluid and the formation of breccia, particularly in weak, fractured zones such as the cores of folds. In order to maintain repeated brecciation events fluid would have to be added to the system. This may explain why Wernecke Breccia is spatially related to the large-scale Richardson Fault array. These crustal-scale faults could have allowed fluids to enter the basin and recharge the system. The occurrence of widespread breccia bodies in upper FLG strata compared to the rest of the WSG (Delaney, 1981) may be due to the presence of metaevaporites in this part of the stratigraphy. Dissolution of evaporites during diagenesis, compaction and metamorphism would have caused disruption of intercalated and overlying sediments and led to the formation of solution breccias (Warren, 1999) thus providing widespread weak zones that could be utilized by over pressured fluids to produce brecciation. Wernecke Breccias that occur at this stratigraphic level contain the largest clasts observed (100's of metres across) and this also may be related to the presence of evaporites. Large blocks could initially have formed during evaporite dissolution due to foundering of strata overlying evaporite layers. These blocks could then have become entrained in Wernecke Breccia as fluid utilized the pre-existing weak, and probably permeable zone during breccia emplacement.

A.11 Summary

In summary, zones of Wernecke Breccia occur over a large part of north-central Yukon in areas of regional-scale faulting. They occur throughout host WSG strata but

are most widespread in lower WSG where metaevaporites make up part of the stratigraphy. WSG strata and breccia proximal to metaevaporites have been affected by dominantly sodic metasomatism. WSG rocks and breccias distal to evaporites have undergone mainly potassic metasomatism. Sodic and potassic alteration are overprinted by carbonate alteration. IOCG mineralisation is associated with the breccia bodies and occurs as disseminations, veins and breccia matrix. Cross-cutting relationships indicate multiple alteration, brecciation and mineralising events. Breccia emplacement occurred in weak zones of the crust and was probably caused by the expansion of over pressured basinal fluids. Fluids that formed the breccias were low to moderate temperature, high salinity NaCl-$CaCl_2$-H_2O brines likely derived from dominantly basinal sources. There is no evidence for the input of magmatic fluids and the high salinity of the fluid is interpreted to be due to interaction with (halite facies) evaporites (Hunt *et al.*.2004; Section C). Thus, the fluids involved are similar to those proposed by Barton and Johnson (1996, 2000) for the formation of some IOCG deposits.

Wernecke Breccias were emplaced into a thick, dominantly marine sedimentary sequence that was likely deposited in an intra-continental rift basin setting (*cf.* Thorkelson, 2000). Other IOCG districts that formed in a similar tectonic environment and also have large-scale brecciation and metasomatic alteration include those of the Cloncurry district in Australia and the Lufilian arc in central Africa (Hitzman, 2000). Little is known about the IOCG mineralisation in central Africa however the Cloncurry district, has received much exploration attention and several deposits have been discovered including the large Ernest Henry (167 Mt @ 1.1% Cu, 0.54 g/t Au) deposit (*cf.* Ryan, 1998; Williams and Skirrow, 2000; Mark *et al.*, 2000). Breccia-associated IOCG prospects in the Wernecke Mountains contain evidence for multiple cross-cutting brecciation and mineralising events (*cf.* Yukon MINFILE, 2003) but they have received little exploration to date and their full potential remains unknown.

A.12 References:

Archer AR (1976) Report on soil geochemistry, geology and radiometric survey Igor 1-26 claims. Yukon Assessment Report 090083, 8pp.

Archer AR (1980) Drill report Igor 1-26 claims. Yukon Assessment Report 090562, 12pp.

Archer AR and Schmidt U (1978) Mineralised breccias of Early Proterozoic age, Bonnet Plume River District, Yukon Territory. CIM Bulletin, 71:53-58.

Archer A, Bell RT, Delaney GD and Godwin CI (1977).Mineralised breccias of Wernecke Mountains Yukon. Geological Association of Canada Program with Abstracts, 2:5.

Barton MD and Johnson DA (2000) Alternative brine sources for Fe-Oxide(-Cu-Au) systems: implications for hydrothermal alteration and metals. In: Porter TM (ed.) Hydrothermal Iron Oxide Copper-Gold & Related Deposits: A Global Perspective, Volume 1, PGC Publishing, Adelaide, pp. 43-60.

Barton MD and Johnson DA (1996) Evaporitic-source model for igneous-related Fe oxide-(REE-Cu-Au-U) mineralization. Geology vol. 24, 3:259-262.

Bell RT (1989) A conceptual model for development of megabreccias and associated mineral deposits in Wernecke Mountains, Canada, Copperbelt, Zaire, and Flinders Range, Australia. In: Uranium resources and geology of North America: proceedings of a technical committee meeting, organized by the Internal Atomic Energy Agency held in Saskatoon, Canada, 1987, pp.149-169.

Bell RT (1986a) Megabreccias in northeastern Wernecke Mountains, Yukon Territory. Current Research, Part A, Geological Survey of Canada, Paper 86-1A, pp 375-384.

Bell RT (1986b) Geological map of north-eastern Wernecke Mountains, Yukon Territory. Geological Survey of Canada, Open File 1027.

Bell RT (1978) Breccias and uranium mineralisation in the Wernecke Mountains, Yukon Territory – a progress report. Current Research, Part A, Geological Survey of Canada, Paper 78-1A, pp317-322.

Bell RT and Delaney GD (1977) Geology of some uranium occurrences in Yukon Territory. Report of Activities, Part A, Geological Survey of Canada, Paper 77-1A, pp 33-37.

*Brideau M-A, Thorkelson DJ, Godin, L and Laughton JR (2002) Paleoproterozoic deformation of the Racklan Orogeny, Slats Creek (106D/16) and Fairchild Lake (106C/13) map areas, Wernecke Mountains, Yukon. In: Emond DS, Weston LH and Lewis LL (eds) Yukon Exploration and Geology 2001, Exploration and Geological Services Division, Yukon Region, Indian and Northern Affairs Canada, pp 65-72.

Brooks M (2002) Alteration, brecciation and Fe oxide-Cu (-Au) mineralisation at Slab creek, Yukon Territory, Canada. Honours thesis, James Cook University, Australia, 113p.

*Brooks M, Baker T and Hunt J (2002) Alteration zonation, veining and mineralisation associated with the Wernecke Breccias at Slab creek, Yukon Territory, Canada. In: Emond DS, Weston LH and Lewis LL (eds) Yukon Exploration and Geology 2001, Exploration and Geological Services Division, Yukon Region, Indian and Northern Affairs Canada, pp 249-258.

Caulfield DA (1994) Olympic property diamond drilling logs. Yukon Assessment Report 093222, 40pp.

Deer WA, Howie RA and Zussman J (1992) An introduction to rock forming minerals (second edition), Longman Scientific & Technical, 696pp.

*Delaney GD (1978) A progress report on stratigraphic investigations of the lowermost succession of Proterozoic rocks, northern Wernecke Mountains, Yukon Territory. Exploration and Geological Services Division, Yukon Region, Indian and Northern Affairs Canada, Open File Report EGS 1978-10, 12pp.

Delaney GD (1981) The Mid-Proterozoic Wernecke Supergroup, Wernecke Mountains, Yukon Territory; In: Proterozoic Basins of Canada, Geological Survey of Canada, Paper 81-10, pp 1-23.

Eastoe CJ, Long A and Knauth LP (1999) Stable chlorine isotopes in the Palo Duro Basin, Texas: evidence for preservation of Permian evaporite brines. Geochimica Cosmochimica Acta 63:1375-1382.

Eaton WD (1982) Wernecke Joint Venture diamond drill report Igor 1-26 claims. Yukon Assessment Report 091445, 17pp.

Eaton WD and Archer AR (1981) Wernecke Joint Venture drill report Igor 1-26 claims. Yukon Assessment Report 090756, 13pp.

Gabrielse H (1967) Tectonic evolution of the northern Canadian Cordillera. Canadian Journal of Earth Sciences, 4:271-298.

*Gordey SP and Makepeace AJ (1999) Yukon digital geology. , Exploration and Geological Services Division, Yukon Region, Indian and Northern Affairs Canada, Open File 1999-1 (D). Also available as Geological Survey of Canada Open File D3826.

Hitzman MW (2000) Iron oxide-Cu-Au deposits: what, where, when, and why? In: Porter TM (ed) Hydrothermal iron oxide copper-gold & related deposits: a global perspective, volume 1, pp. 9-25.

*Hunt JA, Laughton JR, Brideau M-A, Thorkelson DJ, Brookes ML and Baker T (2002). New mapping around the Slab iron oxide-copper-gold occurrence, Wernecke Mountains. In: Emond DS, Weston LH and Lewis LL (eds) Yukon Exploration and Geology 2001, Exploration and Geological Services Division, Yukon Region, Indian and Northern Affairs Canada, pp 125-138.

Hunt JA, Baker T and Thorkelson DJ (2003a) Basin-scale breccia processes associated with proterozoic iron oxide-copper-gold mineralisation: an example from the Wernecke Mountains, Canada. In: The Geological Society 2003 Fermor Flagship Meeting, World Class Mineral Deposits and Earth Evolution, extended abstracts. Applied Earth Science, Transactions of the Institutions of Mining and Metallurgy: Section B, volume 112, number 2, pp 204-206.

Hunt JA and Baker T (2003b) Wernecke Breccia-associated iron oxide-Cu-Au mineralization, Yukon, Canada. In: Eliopoulos DG *et al.* (eds) Mineral Exploration and Sustainable Development, Proceedings of the seventh biennial SGA meeting, Athens, Greece, volume 2, pp 985-987.

Hunt JA, Baker T, Davidson G, Fallick AE, and Thorkelson DJ (2004) Origin of Wernecke Breccia: results of fluid inclusion and stable isotope analyses. Abstract, GSA Convention, Hobart, Tasmania, February 2004.

Kwak TAP (1977) Scapolite compositional change in metamorphic gradient and its bearing on the identification of metaevaporite sequences. Geological Magazine, 114:343-354.

Lane RA (1990) Geologic setting and petrology of the Proterozoic Ogilvie Mountains Breccia of the Coal Creek inlier, southern Ogilvie Mountains, Yukon Territory. Unpublished MSc thesis, University of British Columbia, Vancouver, Canada, 223p.

Laughton JR (2004) The Proterozoic Slab volcanics of northern Yukon, Canada: megaclasts of a volcanic succession in Proterozoic Wernecke Breccia, and implications for the evolution of northwestern Laurentia. PhD Thesis, Simon Fraser University, Burnaby, British Columbia, Canada.

*Laughton JR, Thorkelson DJ, Brideau M-A and Hunt JA (2002). Paleoproterozoic volcanism and plutonism in the Wernecke Mountains, Yukon. In: Emond DS, Weston LH and Lewis LL (eds) Yukon Exploration and Geology 2001, Exploration and Geological Services Division, Yukon Region, Indian and Northern Affairs Canada, pp 139-145.

Laznicka P and Edwards RJ, 1979. Dolores Creek, Yukon – a disseminated copper mineralization in sodic metasomatites. Economic Geology, 74:1352-1370.

Mark G, Oliver NHS, Williams PJ, Valenta RK and Crookes RA (2000) The evolution of the Ernest Henry Fe-oxide-(Cu-Au) hydrothermal system. In: Porter TM (ed) Hydrothermal iron oxide copper-gold & related deposits: a global perspective, volume 1, pp. 123-136.

McCaig AM, Tritlla J and Banks DA (2000) Fluid mixing and recycling during Pyrenean thrusting: evidence from fluid inclusion halogen ratios. Geochimica Cosmochimica Acta 64:19:3395-3412.

Norris DK (1997) Geology and mineral and hydrocarbon potential of northern Yukon Territory and northwestern district of Mackenzie. Geological Survey of Canada, Bulletin 422, 401pp.

Raymond, J. (1995) Petrology: The study of igneous, metamorphic and sedimentary rocks. McGraw-Hill Higher Education, New York, 742p.

Reynolds LJ (2000) Geology of the Olympic Dam Cu-U-Au-Ag-REE deposit. In: Porter TM (ed) Hydrothermal Iron Oxide-Copper-Gold & Related Deposits: A Global Perspective, volume 1, PGC Publishing, Adelaide, pp. 93-104.

Ryan (1998) Ernest Henry copper-gold deposit. In: Australasian Institute of Mining and Metallurgy Monograph 22, pp. 759-768.

Sillitoe RH (2003) Iron oxide copper-gold deposits: an Andean view. Mineralium Deposita, 38:787-812.

Stammers MA (1995) 1995 drilling report on the Slats mineral claims. Yukon Assessment Report 093436, 19pp.

*Tempelman-Kluit DJ (1981) Nor, summary of assessment work and description of mineral properties. In: Yukon Geology and Exploration, 1979-1980, Exploration and Geological Services Division, Yukon, Indian and Northern Affairs Canada, pp. 300-301.

*Thorkelson DJ (2000) Geology and mineral occurrences of the Slats Creek, Fairchild Lake and "Dolores Creek" areas, Wernecke Mountains, Yukon Territory. Exploration and Geological Services Division, Yukon Region, Indian and Northern Affairs Canada, Bulletin 10, 73pp.

*Thorkelson DJ, Laughton JR, Hunt JA and Baker T (2003) Geology and mineral occurrences of the Quartet Lakes map area (NTS 106E/1), Wernecke and Mackenzie mountains, Yukon. In: Emond DS and Lewis LL (eds) Yukon Exploration and Geology 2002, Exploration and Geological Services Division, Yukon Region, Indian and Northern Affairs Canada, pp 223-239.

Thorkelson DJ, Laughton JR and Hunt JA (2002) Geological map of Quartet Lakes area (106E/1), Wernecke Mountains, Yukon (1:50,000 scale). Exploration and Geological Services Division, Yukon Region, Indian and Northern Affairs Canada, Geoscience map 2002-2.

Thorkelson DJ, Mortensen JK, Davidson GJ, Creaser RA, Perez WA and Abbott JG (2001a) Early Mesoproterozoic intrusive breccias in Yukon, Canada: The role of hydrothermal systems in reconstructions of North America and Australia. Precambrian Research 111:31-55.

Thorkelson DJ, Mortensen JK, Creaser RA, Davidson GJ and Abbott JG (2001b) Early Proterozoic magmatism in Yukon, Canada: constraints on the evolution of northwestern Laurentia. Canadian Journal of Earth Science 38:1479-1494.

Warren J (1999) Evaporites, their evolution and economics. Blackwell Science Ltd, 438p.

Williams, PJ and Skirrow RG (2000) Overview of iron oxide-copper-gold deposits in the Curnamona Province and Cloncurry District (Eastern Mount Isa block), Australia. In: Porter TM (ed) Hydrothermal iron oxide copper-gold & related deposits: a global perspective, volume 1, pp. 105-122.

*Yukon MINFILE, 2003. Database of Yukon mineral occurrences. Exploration and Geological Services Division, Yukon Region, Indian and Northern Affairs Canada, CD-ROM (2).

* These items can be downloaded from the Yukon Geological Survey website www.geology.gov.yk.ca

SECTION B

Constraints on the age of Wernecke Breccia and associated iron oxide-copper-gold mineralisation: new Ar-Ar, U-Pb, Pb-Pb and Re-Os dates

B.1 Abstract

Muscovite, molybdenite and titanite from Wernecke Breccia matrix and/or associated veins were dated using Ar-Ar, Re-Os and U-Pb analytical techniques in order to better constrain the age of Wernecke Breccia and associated IOCG mineralisation. Dolostone from the upper unit of the Wernecke Supergroup (Gillespie Lake Group) was dated using the Pb-Pb method in an attempt to obtain an absolute age for the supergroup. Step heating ^{40}Ar-^{39}Ar analyses carried out on muscovite from Wernecke Breccia matrix, a syn-breccia vein and two late-stage veins yielded dates of 1178.0 ± 6.1, 1135.0 ± 5.5, 1052 ± 10 and 996.7 ± 8 Ma respectively. These dates are significantly younger than the minimum age (*ca*. 1380 Ma) of Wernecke Breccia indicated by cross-cutting relationships and must have been reset. Resetting is interpreted to be due to thermal heating associated with igneous events at *ca*. 1380 Ma and 1270 Ma and burial beneath Middle Proterozoic strata. The Ar-Ar dates probably reflect cooling ages that were set during uplift, some of which is attributed to the Corn Creek Orogeny. Samples submitted for U-Pb and Pb-Pb analyses gave discordant results that cannot be used to constrain the age of Wernecke Breccia or Wernecke Supergroup. Re-Os analyses of molybdenite from a late-stage vein that cross-cuts breccia gave model ages of 1601 ± 6 and 1609 ± 6 Ma. These ages range from older than to within error of the *ca*. 1594.8 ± 4.6 Ma published U-Pb (titanite) date for breccia in the same area. The late-stage vein also cross-cuts mineralisation, thus, the Re-Os dates also indicate that at least some IOCG mineralisation is ≤ *ca*. 1600 Ma. A second molybdenite sample from a late-stage vein gave a Re-Os model age of 1648 ± 5.97 Ma. This date is considered analytically sound but the significance of it is not clear as it is believed to cut the *ca*. 1595 Ma breccia. The age of breccia emplacement is still considered to be best reflected by the published U-Pb date of *ca*. 1595 Ma and is supported by the *ca*. 1600 Ma Re-Os dates from this study. This is considered a reasonable age for breccia emplacement as it is at least consistent with the broad age range (*ca*. 1710-1380 Ma) defined by cross-cutting relationships. However, in detail the age of the breccia and IOCG mineralisation remains poorly constrained; this may be a reflection of the multi-phase nature of the breccia events.

B.2 Introduction

Numerous breccia bodies, collectively known as Wernecke Breccia, are located in the

northern Yukon Territory, Canada (Fig. 1; *cf.* Bell, 1986a,b, Thorkelson, 2000). Extensive iron oxide-copper-gold ± uranium ± cobalt (IOCG) mineralisation occurs within the breccia zones and adjacent host rocks and has been the focus of periodic mineral exploration over the past 50 years (*cf.* Yukon MINFILE, 2003). The Wernecke Breccias are similar to breccia-associated IOCG occurrences elsewhere in the world and they have been compared to those in the Cloncurry and Gawler districts of Australia which host the large Ernest Henry and Olympic Dam deposits (*cf.* Bell and Delaney, 1977; Bell, 1978; Archer *et al.*, 1977; Hitzman *et al.*, 1992). The similarity of Wernecke Breccias and their host Early Proterozoic strata to those of comparable age in Australia has been used in arguments to support plate reconstructions for the Proterozoic (*cf.* Thorkelson *et al.*, 2001a,b). One of the ties used in this argument is the parallel between the *ca.* 1595 Ma age proposed for Wernecke Breccia (Thorkelson *et al.*, 2001a) and the *ca*. 1590 Ma age (Reeve *et al.*, 1990; Johnson and Cross, 1995) of the Olympic Dam deposit. However, the age of Wernecke Breccia is not well constrained. Cross-cutting relationships indicate an age between *ca.* 1710 and 1380 Ma and a U-Pb (titanite) date indicates breccia was emplaced into the lower part of the host Wernecke Supergroup (WSG) *ca.*1595 Ma (Thorkelson, 2000; Thorkelson *et al.*, 2001a,b). No reliable age dates are available for breccia bodies hosted in the upper parts of the WSG and the age of the IOCG mineralisation is not known.

This paper reports new geochronological data for Wernecke Breccia and associated IOCG mineralisation. Ar-Ar dates were obtained from: a) muscovite in the matrix of Wernecke Breccia which is hosted in the middle part of WSG; b) muscovite associated with the main stage of mineralisation; and c) muscovite associated with late-stage carbonate veins and alteration that contain minor mineralisation. U-Pb (titanite) and Re-Os (molybdenite) dates were also obtained for the late-stage veins. A Pb-Pb date was obtained from dolostone in the Gillespie Lake Group (GLG) which forms the upper part of the WSG.

B.3 Geologic framework

Wernecke Breccia occurs in areas underlain by Early Proterozoic rocks (Fig. 1) made up of the WSG, Bonnet Plume River Intrusions (BPRI), and "Slab volcanics[1]" (*cf.* Gabrielse, 1967; Delaney, 1981; Bell, 1986b; Thorkelson, 2000). The WSG is an

approximately 13 km-thick package of marine sedimentary rocks that has been divided into the Fairchild Lake, Quartet and Gillespie Lake Groups (Figs. 1 & 2; *cf.* Delaney, 1981; Thorkelson, 2000). WSG strata are cut by *ca.* 1710 Ma mafic to intermediate dykes and sills that are part of the BPRI suite (Fig. 2; Thorkelson, 2000; Thorkelson *et al.*, 2001b). Intermediate composition Slab volcanics also occur locally in this region but their timing is uncertain as they have been observed only as clasts within Wernecke Breccia (*cf.* Thorkelson, 2000; Thorkelson *et al.*, 2001b). Strata of the WSG were metamorphosed to greenschist facies and multiply deformed during the Racklan Orogeny (*cf.* Thorkelson, 2000; Brideau *et al.*, 2002). The orogeny is Early Proterozoic but its exact age is unknown. Multiply deformed clasts occur in the breccia body that was dated at *ca.* 1595 Ma, therefore the age of the Racklan Orogeny is constrained to pre (to syn) *ca.* 1595 Ma (Thorkelson, 2000; Thorkelson *et al.*, 2001a,b).

Bodies of Wernecke Breccia, from 0.1 to 10 km^2 in size, occur throughout the WSG and are most abundant in the lower part of the stratigraphy (*cf.* Delaney, 1981; Lane, 1990). The breccia is made up largely of clasts of the supergroup in a matrix of rock flour and hydrothermal precipitates (*cf.* Hunt *et al.*, 2005). Where the breccia bodies cross-cut BPRI or Slab volcanics they contain abundant clasts of these lithologies (*cf.* Thorkelson, 2000).

At least 65 bodies of Wernecke Breccia are known and all are associated with IOCG mineralisation (*cf.* Yukon MINFILE, 2003). Mineralisation occurs as disseminations and veins within the breccia and surrounding WSG rocks and is largely made up of early magnetite and/or hematite and later chalcopyrite and pyrite (*cf.* Brookes *et al.*, 2002; Hunt *et al.*, 2002, 2005; Thorkelson *et al.*, 2003; Yukon MINFILE, 2003). Minor uranium (pitchblende, brannerite) and cobalt (cobaltian pyrite, erythrite) mineralisation occurs locally. Gangue is dominantly composed of carbonate (calcite, dolomite, siderite), quartz, albite and K-feldspar with lesser biotite, muscovite, chlorite and fluorite (*cf.* Brookes *et al.*, 2002; Hunt *et al.*, 2002, 2005). Extensive sodic or potassic metasomatic alteration is spatially associated with the breccia bodies and cross-cutting relationships demonstrate that multiple phases of brecciation and mineralisation have occurred. The alteration and breccia zones are cut by late-stage carbonate veins that contain minor pyrite and chalcopyrite and trace molybdenite (Hunt *et al.*, 2002, 2005).

[1] Many of the names used in this paper are informal and are initially shown in quotation marks.

B.3.1 Age constraints on Wernecke Breccia

Cross-cutting relationships

Cross-cutting relationships provide constraints on the age of Wernecke Breccia and limit it to between 1710 and 1380 Ma (*cf.* Thorkelson, 2000; Thorkelson *et al.* 2001a,b). Breccia zones cross-cut WSG, BPRI and Slab volcanics. Attempts at dating the WSG and Slab volcanics have not been successful and their ages are poorly constrained (*cf.* Thorkelson, 2000). However, BPRI have been dated via the U-Pb (zircon) method; ages of *ca*. 1710 Ma were obtained (Thorkelson *et al.*, 2001b). Wernecke Breccia bodies locally contain abundant clasts of Bonnet Plume River Intrusions and must therefore be younger than *ca*. 1710 Ma (Thorkelson, 2000; Thorkelson *et al.*, 2001b). The WSG, BPRI, Slab volcanics and Wernecke Breccia are unconformably overlain by the Pinguicula Group (Fig. 2; *cf.* Thorkelson, 2000). The age of the Pinguicula Group is poorly defined however, the base of this group is cut by a diorite stock that yielded a U-Pb (zircon) date of *ca*. 1380 Ma (Thorkelson, 2000). Hence, Wernecke Breccia must be older than 1380 Ma.

Radiometric dates

A U-Pb date of 1594.8 ± 4.6 Ma was obtained from hydrothermal titanite in the matrix of Wernecke Breccia hosted by the Fairchild Lake Group (FLG) in the lower part of the WSG at the Slab prospect (Thorkelson, 2000; Thorkelson *et al.*, 2001a). This date is considered to be a reliable estimate of the age of breccia emplacement at this stratigraphic level (Fig. 1; Thorkelson, 2000; Thorkelson *et al.*, 2001a). Archer *et al.* (1977) report a K-Ar age of 1500 Ma for biotite from a breccia complex at Quartet Mountain which cuts strata at a similar stratigraphic level (Fig. 1). There are a limited number of other published radiometric dates for Wernecke Breccia (Table 1) but most do not appear to represent the time of breccia emplacement. Archer and Schmidt (1978) and Archer *et al.* (1986) report U-Pb dates ranging from approximately 1250 to 400 Ma determined from U-bearing minerals (brannerite, pitchblende) and whole rock samples. These dates are highly discordant which renders them difficult to interpret and they are considered unreliable estimates of the ages of brecciation and hydrothermal activity (Parrish and Bell, 1987). A U-Pb date of 1270 ± 40 Ma was calculated for monazite from a sample of brannerite-hematite-monazite from the Nor breccia body (Parrish and

Bell, 1987). The uranium concentrations in the monazite were unusually low (*ibid*) and it is not clear what effect this had on the analysis. In addition, the Nor property is located about 130 km north of the main belt of Wernecke Breccia occurrences (Fig. 1) and its relationship to the majority of Wernecke Breccia is not known.

B.4 Radiometric Dating

Samples were selected for geochronology (Table 2) with the aims of dating: 1) emplacement of Wernecke Breccia (Ar-Ar), 2) the deposition of main stage mineralisation (Ar-Ar), 3) the formation of late-stage carbonate alteration that hosts minor mineralisation (Ar-Ar, U-Pb, Re-Os) and 4) upper WSG strata (Pb-Pb).

B.4.1 $^{40}Ar/^{39}Ar$ (Muscovite)

Samples for Ar-Ar analysis were chosen from the Igor and Slab prospects (Fig. 1) because these two areas host rocks that contain abundant muscovite. At the Igor prospect hydrothermal muscovite occurs in the matrix of Wernecke Breccia that was emplaced into the Quartet Group, the middle part of the WSG. Thus, dating the muscovite would provide an age for breccia emplacement into middle WSG strata. At the Slab prospect muscovite occurs in the selvages of a 10 cm-thick vein of massive pyrite-chalcopyrite that cross-cuts FLG strata adjacent to Wernecke Breccia (Section A, Fig. 10f). Dating this muscovite would constrain the age of mineralisation. Muscovite also occurs in late-stage calcite-quartz-albite-molybdenite-chalcopyrite veins at the Slab prospect (e.g. Section A, Fig. 10h). Dating this muscovite would provide an age for the late-stage carbonate alteration.

Ar-Ar analysis was carried out at the Geochronology Section of the Geological Survey of Canada in Ottawa. Dating was done using the $^{40}Ar/^{39}Ar$ step heating technique. Analytical protocols and mineral sample preparation methods are provided in Appendix II. Plateau ages are presented for three of the samples and an inverse isochron diagram for the remaining one (M. Villeneuve, pers. comm., 2004).

Muscovite from Wernecke Breccia matrix at the Igor prospect (sample JH02-12-1) yielded a somewhat noisy spectrum. However, degassing did produce an internally consistent plateau that gives an age of 1078 ± 6.1 Ma (Fig. 3a, Table 2). Excess noise is likely the result of slight under-irradiation of the sample which resulted in increased sensitivity to applied corrections (M. Villeneuve, pers. comm., 2004). Muscovite from

the selvages of the pyrite-chalcopyrite vein at the Slab prospect (JH02-14-1a) produced a well defined multi-step plateau that gives an age determination of 1135 ± 5.5 Ma (Fig. 3b, Table 2). Muscovite from a late-stage calcite-quartz-albite-molybdenite-chalcopyrite vein that cross-cuts breccia at the Slab prospect (sample SB94-1-345.1 m) yielded a complex Ar-Ar spectrum (Fig. 3c, Table 2). Low temperature steps suggest Ar-loss and possible degassing of a contaminating phase (M. Villeneuve, pers. comm., 2004). Mid-temperature steps produced a weakly defined plateau and an age of 996.7 ± 8.0 Ma was interpreted from these steps (Fig. 3c). The fusion step appears to give an older age and may be a second contaminating phase containing excess ^{40}Ar. Muscovite from a second late-stage vein at the Slab prospect (sample JH01-27-3D, Table 2) also yielded complex results and the plot shown in Figure 3d represents mid-temperature steps from replicate analyses on two aliquots with a clear excess ^{40}Ar component (^{40}Ar/^{36}Ar = 4244 ± 894, MSWD = 3.5). However, the sample appears to give a reasonable and reproducible age of 1052 ± 10 Ma from the key heating steps (M. Villeneuve, pers. comm., 2004). Low temperature steps for this sample appear to have variable Ar-loss. The highest temperature steps (of both aliquots) showed distinctly older ages suggesting contamination by a phase that does not degas until high temperatures (M. Villeneuve, pers. comm., 2004).

B.4.2 U-Pb (Titanite)

A calcite-biotite-titanite vein at the Slab prospect (drill core sample SB94-1-6.9 m; Fig. 1, Table 2) was chosen for U-Pb dating. The vein cuts biotite-altered FLG metasiltstone proximal to Wernecke Breccia and is probably related to late-stage carbonate alteration of the breccia. Thus, dating hydrothermal titanite in the vein will provide a date for the carbonate alteration and place a constraint of the timing of breccia formation.

U-Pb dating of the sample was carried out in the Geochronology Laboratory at The University of British Columbia by isotope dilution thermal ionization mass spectrometry. Sample preparation methods and analytical protocols followed those outlined in Friedman *et al.* (2001) and Mortensen *et al.* (1995), as summarised in Appendix II. Three titanite fractions were analysed and all gave discordant results, which may be due to Pb loss (Fig. 4; J.K. Mortenson pers. comm., 2004). Fraction T1 is from the coarsest, turbid, straw coloured grains. Results from this fraction have relatively poor precision due to very low U (~2 ppm) and Pb (~0.4 ppm) contents.

Fractions T2 and T3 consist of yellow, clear subhedral grains. T2 is coarser than T3 and has a U content of 8 ppm. Fraction T3 has 30 ppm U and gave the most precise results. A $^{207}Pb/^{206}Pb$ date of 1113 ± 5 Ma was calculated for this fraction and is considered a minimum age for the titanite (J.K. Mortenson pers. comm., 2004).

B.4.3 Pb-Pb (Carbonate)

A sample of stromatolitic GLG dolostone was chosen for Pb-Pb analysis to try and better constrain the age of the WSG. Pb-Pb analysis was carried out at the University of Melbourne using the sample preparation and mass spectrometry procedures outlined in Woodhead and Hergt (1997), as summarised in Appendix II.

Five samples from a hand specimen of dolostone (sample JH02-21-1, Table 2; Section A, Fig. 4e) were analysed and the results are shown in Figure 5. Two dissolution residues were also analysed, however, the residue data do not appear to be in equilibrium with the samples, i.e. they do not fall on the same isochron, and may be a detrital component (J Woodhead, pers. comm., 2003). They have been discarded from the calculations. A conventional isochron calculation gives an age of 1368 ± 160 Ma.

B.4.4 Re-Os (Molybdenite)

Two molybdenum-bearing late stage calcite-quartz-albite-chalcopyrite-muscovite veins that cross-cut breccia at the Slab prospect were chosen for Re-Os analysis (samples SB94-1-345.1 m & JH01-27-3D; Fig. 1). Dates from the molybdenite would provide an age for the carbonate alteration and an upper limit on the timing of breccia formation (Table 2). These samples were also submitted for Ar-Ar analysis (see Ar-Ar section above).

Re-Os isotope analyses were carried out in collaboration with Robert Creaser and Dave Selby at the Radiogenic Isotope Facility of the Department of Earth and Atmospheric Sciences, University of Alberta, Canada. Molybdenite was analysed using analytical procedures for chemical separation of Re and Os modified from methods described by Shirey and Walker (1995), Cohen and Waters (1996) and Birck *et al.* (1997) as described by Selby and Creaser (2001; Appendix II). Re and Os isotope ratios were measured using negative thermal ionization mass spectrometry (Creaser *et al.*, 1991; Völkening *et al.*, 1991) on a Micromass Sector 54 mass spectrometer using Faraday collectors.

Two analyses of molybdenite in sample SB94-1-345.1 m yielded model ages of 1601 ± 6 Ma and 1609 ± 6 Ma (R. Creaser, pers. comm, 2003). Analysis of molybdenite in sample JH01-27-3D gave a date of 1648.1 ± 5.97 Ma (R Creaser, pers. comm., 2002).

B.5 Discussion

The timing of breccia emplacement into the lower WSG (FLG) is constrained by a U-Pb date of 1594.8 ± 4.6 Ma yielded by titanite obtained from the matrix of breccia at the Slab prospect (Thorkelson, 2000; Thorkelson *et al.*, 2001a). Molybdenite from late-stage calcite veins, also from the Slab prospect, yielded Re-Os model ages of 1609 ± 6 and 1601 ± 6 Ma. The veins cross-cut breccia and were expected to have ages younger than the *ca*. 1595 Ma date, instead they range from older than to within error of the above U-Pb date. One explanation for this discrepancy may be the multiphase nature of the breccia. It is possible that the breccia body that was observed to be cut by the late-stage veins is an older phase of breccia and not the same as the breccia body that was dated using U-Pb techniques. The Re-Os dates also provide constraints on the age of IOCG mineralisation associated with Wernecke Breccia. The main phase of mineralisation occurs within breccia and is cross-cut by the late-stage calcite veins, thus, the mineralisation must be ≤ *ca.* 1600 Ma. However, like the breccia, the mineralisation is multi-phase and there may be more than one age of mineralisation. A sample of molybdenite from a second late-stage vein that cross-cuts breccia gave a Re-Os model age of 1648 ± 5.97 Ma. This date is considered analytically sound (D Selby, pers. comm., 2003) but the significance of it is not clear as the host vein is believed to cut the breccia that was dated at *ca*. 1595 Ma. As mentioned above, one explanation for this discrepancy may be the multiphase nature of the breccia, i.e. the breccia body that was observed to be cut by the late-stage veins may be an older phase of breccia.

As mentioned earlier, cross-cutting relationships constrain the age of Wernecke Breccia to lie between *ca.* 1710 and *ca.* 1380 Ma (Thorkelson, 2000). Breccia-related muscovite samples in this study yielded dates of 1178.0 ± 6.1, 1135.0 ± 5.5, 1052 ± 10 and 996.7 ± 8.0 Ma (Table 2), all of which are considerably younger than 1380 Ma (Table 2). The muscovite-bearing rocks are paragenetically well constrained by cross-cutting relationships and are clearly related to Wernecke Breccia, thus the Ar-Ar dates must have been reset. These results are similar to reset $^{40}Ar/^{39}Ar$ dates of 980 ± 4 and

788 ± 8 Ma yielded by the step heating of white mica from schist in the Early Proterozoic FLG that is cross-cut by Wernecke Breccia (Thorkelson, 2000; Thorkelson *et al.*, in review).

Resetting of the isotope systematics is interpreted to result from reheating of the rocks by igneous events and burial of the strata during the deposition of Middle Proterozoic rocks (Thorkelson, 2000; Thorkelson *et al.*, in review). The geological history of the Wernecke area is incompletely known and several gaps of 200 to 300 Ma exist for which no rock record has been observed (Fig. 2). There are documented igneous events at *ca.* 1380 and *ca.*1270 Ma (*cf.* Thorkelson, 2000; Thorkelson *et al.*, 2001a,b) which could have been responsible for resetting the Ar isotopic systematics. The event at *ca.* 1380 produced the Hart River mafic intrusions 25 to 50 km south of the study area (*cf.* Green, 1972; Abbott, 1997). Rutile in pre *ca.* 1595 Ma Slab volcanics yielded a U-Pb age of *ca.* 1383 Ma and is considered to have crystallised at this time (Thorkelson, 2000; Thorkelson *et al.*, 2001a). Igneous activity at *ca.* 1270 Ma produced the mafic to intermediate composition Bear River dykes in the Wernecke area (*ibid.*) These dykes may be part of the large *ca.* 1270 Ma igneous event that includes the Mackenzie dyke swarm, the Muskox intrusion and the Coppermine lavas in the Northwest Territories and adjacent parts of the Canadian Shield (*cf.* Thorkelson *et al.*, 2001a; in review). Increased temperatures caused by the burial of WSG and Wernecke Breccia beneath Middle Proterozoic strata could also have disturbed the isotope systematics (*ibid*). Middle Proterozoic strata include the approximately 3 km-thick Pinguicula Group made up of marine sedimentary rocks and the up to 1 km-thick carbonate and clastic rocks of the Hematite Creek Group (Fig. 2).

The Ar-Ar dates of *ca.* 980 ± 4 and 788 ± 8 Ma calculated for white mica in FLG were interpreted to reflect cooling ages that were set during uplift caused by the Corn Creek orogeny (<1000 & > 750 Ma), a contractional deformational event characterised by west- to southwest-verging thrust faults (Fig. 2; Thorkelson, 2000; Thorkelson *et al.*, 2001a; in review). Ar-Ar dates of *ca.* 1180 to 1000 Ma calculated for muscovite from breccia related samples in this study are also interpreted to reflect cooling ages. Two of the dates (996.7 ± 8 and 1052 ± 10 Ma) are close to the older age limit of the Corn Creek orogeny and may reflect uplift related to this deformation event. The other two dates are considerably older (1135.0 ± 5.5 and 1178.0 ± 6.1 Ma) and do not correlate to a known orogenic event. However, there is some evidence of uplift during this period in the Wernecke area (*cf.* Thorkelson, 2000) and they may reflect a

more localised deformational event or possibly a more significant, but presently unrecognised event.

Lead isotopic analyses were carried out on a breccia-related vein sample and on GLG dolostone. The calculated minimum U-Pb age for titanite from a breccia-related late-stage vein at the Slab prospect (Fig. 4) is 1113 ± 5 Ma. This date, like the Ar-Ar (muscovite) dates discussed above, is considerably younger than the minimum age of 1380 Ma indicated for Wernecke Breccia. The results for the titanite fractions were all discordant and the calculated age is based on the most precise fraction (T3 in Fig. 4). It is considered a minimum age only as this fraction is quite discordant and has likely undergone Pb loss (J.K. Mortensen pers. comm., 2004). Therefore, this date cannot be used to constrain the age of Wernecke Breccia. A conventional isochron calculated for Pb-Pb data yielded by the sample of GLG stromatolitic dolostone gives a date of 1368 ± 160 Ma (Fig. 5). However, BPRI dykes which cut WSG have reported U-Pb (zircon) dates of 1705.9 ± 0.7, 1709.4 ± 1.4, 1711.1 ± 5.1 and 1713.6 ± 12.7 Ma (Thorkelson *et al.*, 2001a) therefore, 1368 ± 160 Ma cannot represent the age of deposition of GLG and may reflect a later diagenetic/metamorphic event.

B.6 Conclusions

New Re-Os (molybdenite) analyses from a late-stage calcite vein that cross-cuts Wernecke Breccia gave model ages of *ca*. 1601 and 1609 Ma. These ages are slightly older than to within error of the published U-Pb (titanite) date of *ca*. 1595 Ma for breccia emplacement and may be a reflection of the multi-phase nature of breccia emplacement. The dates do confirm that at least some breccia and IOCG mineralisation was emplaced at or before *ca*. 1600 Ma.

Step heating ^{40}Ar-^{39}Ar analyses carried out on muscovite from Wernecke Breccia matrix and associated veins yielded dates of *ca*. 1178 to 997 Ma. These dates are significantly younger than the lower limit of the age range (*ca*. 1710-1380 Ma) for Wernecke Breccia indicated by cross cutting relationships, and must have been reset. The Ar-Ar dates are similar to those calculated for white mica in Early Proterozoic FLG that have also been reset. Resetting is interpreted to be due to thermal heating associated with igneous events at *ca*. 1380 Ma and 1270 Ma that produced the Hart River sills and Bear River intrusions respectively (*cf.* Thorkelson *et al.*, in review). Burial of WSG and Wernecke Breccia by Middle Proterozoic strata may also have added to the thermal

heating. The Ar-Ar dates probably reflect cooling ages that were set during uplift, some of which is attributed to the Corn Creek Orogeny. Samples submitted for U-Pb and Pb-Pb analyses gave discordant results that cannot be used to constrain the age of Wernecke Breccia or WSG.

This study was unable to further constrain the age of Wernecke Breccia and the age of breccia emplacement is still considered to be best reflected by the published U-Pb date of *ca.* 1595 Ma (Thorkelson, 2001a). Support for this date was provided by the *ca.*1600 Ma Re-Os dates obtained in this study. This is believed to be a reasonable age for breccia emplacement as it is at least consistent with the broad age range (*ca.* 1710-1380 Ma) defined by cross-cutting relationships. The exact age of the breccia and IOCG mineralisation remains poorly constrained and may be a reflection of the multiple nature of the breccia events.

B.7 References:

*Abbott JG (1997) Geology of the upper Hart River area, eastern Ogilvie Mountains, Yukon Territory (116A/10, 116A/11). Exploration and Geological Services Division, Yukon Region, Indian and Northern Affairs Canada, Bulletin 9, 73pp.

Archer A and Schmidt U (1978) Mineralised breccias of early Proterozoic age, Bonnet Plume River district, Yukon Territory, Canadian Mining and Metallurgy Bulletin 71:53-58.

Archer A, Bell RT, Delaney GD and Godwin CI (1977).Mineralized breccias of Wernecke Mountains Yukon. Geological Association of Canada Program with Abstracts, 2:5.

Archer A, Bell RT and Thorpe RI (1986). Age relationships from U-Th-Pb isotope studies of uranium mineralisation in Wernecke Breccias, Yukon Territory. Current Research, Part A, Geological Survey of Canada Paper 86-1A:385-391.

Bell RT (1986a) Megabreccias in northeastern Wernecke Mountains, Yukon Territory. Current Research, Part A, Geological Survey of Canada, Paper 86-1A, pp 375-384.

Bell RT (1986b) Geological map of north-eastern Wernecke Mountains, Yukon Territory. Geological Survey of Canada, Open File 1027.

Bell RT (1978) Breccias and uranium mineralisation in the Wernecke Mountains, Yukon Territory – a progress report. Current Research, Part A, Geological Survey of Canada, Paper 78-1A, pp317-322.

Bell RT and Delaney GD (1977) Geology of some uranium occurrences in Yukon Territory. Report of Activities, Part A, Geological Survey of Canada, Paper 77-1A, pp 33-37.

Birck JL, Roy Barman M and Capmas F (1997) Re-Os isotopic measurements at the femtomole level in natural samples. Geostandards Newsletter – Journal of Geostandards and Geoanalysis, 20:19-27.

*Brideau M-A, Thorkelson DJ, Godin, L and Laughton JR (2002) Paleoproterozoic deformation of the Racklan Orogeny, Slats Creek (106D/16) and Fairchild Lake (106C/13) map areas, Wernecke Mountains, Yukon. In: Emond DS, Weston LH and Lewis LL (eds) Yukon Exploration and Geology 2001, Exploration and Geological Services Division, Yukon Region, Indian and Northern Affairs Canada, pp 65-72.

*Brooks M, Baker T and Hunt J (2002) Alteration zonation, veining and mineralisation associated with the Wernecke Breccias at Slab creek, Yukon Territory, Canada. In: Emond DS, Weston LH and Lewis LL (eds) Yukon Exploration and Geology 2001, Exploration and Geological Services Division, Yukon Region, Indian and Northern Affairs Canada, pp 249-258.

Cohen As and Waters FG (1996) Separation of osmium from geological materials by solvent extraction for analysis by thermal ionization mass spectrometry. Analytica Chimica Acta 332:269-275.

Creaser RA, Papanastassiou DA and Wasserburg GJ (1991) Negative thermal ion mass spectrometry of osmium, rhenium and iridium. Geochimica et Cosmochimica Acta 55:397-404.

Delaney GD (1981) The Mid-Proterozoic Wernecke Supergroup, Wernecke Mountains, Yukon Territory; In: Proterozoic Basins of Canada, Geological Survey of Canada, Paper 81-10, pp 1-23.

Gabrielse H (1967) Tectonic evolution of the northern Canadian Cordillera. Canadian Journal of Earth Sciences, 4:271-298.

Green H (1972) Geology of Nash Creek, Larsen Creek and Dawson Creek map areas, Yukon Territory. Geological Survey of Canada, Memoir 364, 157pp.

*Hunt JA, Laughton JR, Brideau M-A, Thorkelson DJ, Brookes ML and Baker T (2002) New mapping around the Slab iron oxide-copper-gold occurrence, Wernecke Mountains. In: Emond DS, Weston LH and Lewis LL (eds) Yukon Exploration and Geology 2001, Exploration and Geological Services Division, Yukon Region, Indian and Northern Affairs Canada, pp 125-138.

Hunt, JA, Baker, T and Thorkelson, DJ (2005, in press). Regional-scale Proterozoic IOCG-mineralised breccia systems: examples from the Wernecke Mountains, Yukon, Canada. Mineralium Deposita, X:x:-x.

Johnson JP and Cross KC (1995) U-Pb geochronological constraints on the genesis of the Olympic Dam Cu-U-Au-Ag deposit, South Australia. Economic Geology 90:1046-1063.

Lane RA (1990) Geologic setting and petrology of the Proterozoic Ogilvie Mountains breccia of the Coal Creek Inlier, southern Ogilvie Mountains, Yukon Territory. MSc. Thesis, University of British Columbia, pp. 223.

Mortensen JK, Ghosh D and Ferri F (1995) U-Pb age constraints of intrusive rocks associated with copper-gold porphyry deposits in the Canadian Cordillera. In: Schroeter TG (ed.) Porphyry deposits of the northwestern Cordillera of North America. Canadian Institute of Mining and Metallurgy, Special volume 46:142-158.

Parrish RR and Bell RT (1987) Age of the Nor breccia pipe, Wernecke Supergroup, Yukon Territory. In: Radiogenic Age and Isotopic Studies: Report 1. Geological Survey of Canada, Paper 87-2, pp. 39-42.

Reeve JS, Cross KC, Smith RN and Oreskes N (1990) Olympic Dam copper-uranium-gold-silver deposit. In: Hughes FE (ed.) Geology of the Mineral Deposits of Australian and Papua New Guinea, Australasian Institute of Mining and Metallurgy, Monograph 14, pp. 1009-1035.

Selby D and Creaser RA (2001) Re-Os geochronology and systematics in molybdenite from the Endako porphyry molybdenum deposit, British Columbia, Canada. Economic Geology 96:197-204.

Shirey SB and Walker RJ (1995) Carius tube digestion for low blank Re-Os analysis. Analytical Chemistry 67:2136-2141.

*Thorkelson DJ (2000) Geology and mineral occurrences of the Slats Creek, Fairchild Lake and "Dolores Creek" areas, Wernecke Mountains, Yukon Territory. Exploration and Geological Services Division, Yukon Region, Indian and Northern Affairs Canada, Bulletin 10, 73pp.

Thorkelson DJ, Mortensen JK, Davidson GJ, Creaser RA, Perez WA and Abbott JG (2001a) Early Mesoproterozoic intrusive breccias in Yukon, Canada: the role of hydrothermal systems in reconstructions of North America and Australia. Precambrian Research 111:31-55.

Thorkelson DJ, Mortensen JK, Creaser RA, Davidson GJ and Abbott JG (2001b) Early Proterozoic magmatism in Yukon, Canada: constraints on the evolution of northwestern Laurentia. Canadian Journal of Earth Science 38:1479-1494.

Thorkelson DJ, Laughton JR and Hunt JA (2002) Geological map of Quartet Lakes area (106E/1), Wernecke Mountains, Yukon (1:50,000 scale). Exploration and Geological Services Division, Yukon Region, Indian and Northern Affairs Canada, Geoscience map 2002-2.

*Thorkelson DJ, Laughton JR, Hunt JA and Baker T (2003) Geology and mineral occurrences of the Quartet Lakes map area (NTS 106E/1), Wernecke and Mackenzie mountains, Yukon. In: Emond DS and Lewis LL (eds) Yukon Exploration and Geology 2002, Exploration and Geological Services Division, Yukon Region, Indian and Northern Affairs Canada, pp 223-239.

Thorkelson DJ, Abbott JG, Mortensen JK, Creaser RA, Villeneuve ME, McNicoll VJ and Layer PW (in review). Early and Middle Proterozoic evolution of Yukon, Canada. Canadian Journal of Earth Science: SNORCLE Special Issue.

Völkening J, Walczyk T and Heumann KG (1991) Osmium isotope ratio determinations by negative thermal ion mass spectrometry. International Journal of Mass Spectrometry Ion Processes 105:147-159.

Woodhead JD and Hergt JM (1997) Application of the "double spike" technique to Pb-isotope geochronology. Chemical Geology (Isotope Geoscience):138:311-321.

Woodhead JD, Hergt JM and Simonson BM (1998) Isotopic dating of an Archean bolide impact horizon, Hamersley basin, Western Australia. Geology, 26:1:47-50.

Yukon MINFILE, 2003. Database of Yukon mineral occurrences. Exploration and Geological Services Division, Yukon Region, Indian and Northern Affairs Canada, CD-ROM (2).

* Can be downloaded from www.geology.gov.yk.ca

SECTION C

Stable isotope (C,O,S,H) and fluid inclusion constraints on the origin of Wernecke Breccia and associated iron oxide-copper-gold mineralisation

C.1 Abstract

Numerous Proterozoic breccia bodies, collectively known as Wernecke Breccia, occur in the north-central Yukon Territory, Canada. The breccias cut Early Proterozoic Wernecke Supergroup (WSG) sedimentary rocks, Bonnet Plume River Intrusions and Slab volcanics. The breccia zones are associated with widespread albite and/or potassium feldspar alteration and are cross-cut by carbonate veins and alteration. Iron oxide (Cu-U-Au-REE) (IOCG) mineralisation occurs within breccia zones and adjacent rocks as disseminations and veins. Multiple phases of brecciation and alteration are evident. Six widely spaced IOCG prospects (Slab, Hoover, Slats-Frosty, Slats-Wallbanger, Igor & Olympic) that occur in different parts of WSG were studied. Fluid inclusion data indicate syn-breccia fluids were high salinity (24-42 wt. % NaCl eq.) NaCl-$CaCl_2$-H_2O brines with low to moderate temperatures (185 – 350^oC). Fluid composition appears to echo that of the host strata, e.g. at the Slab prospect which is hosted by evaporite-bearing Fairchild Lake Group (FLG) strata the fluids are dominated by Na and at the Olympic prospect which is hosted by Gillespie Lake Group (GLG) dolostone the fluids are dominated by Ca. Estimates of fluid pressure determined from fluid inclusion data vary from 0.4 to 2.4 kb and are in reasonable agreement with those based on the approximate thickness of overlying strata. Carbon and oxygen isotope data for hydrothermal carbonates from the prospects range from $\delta^{13}C \approx$ -11 to +1.5 ‰ (PDB) and $\delta^{18}O \approx$ -2 to 20 ‰ (V-SMOW). Results for host WSG limestone/dolostone range from: FLG $\delta^{13}C \approx$ -2 to 0.5 ‰, $\delta^{18}O \approx$ 12 to 14 ‰; Quartet Group $\delta^{13}C \approx$ -2 to -0.3 ‰, $\delta^{18}O \approx$ 14 to 16 ‰; and GLG $\delta^{13}C \approx$ -2 to 1.6 ‰, $\delta^{18}O \approx$ 16 to 25 ‰. Sulphur isotope date for hydrothermal sulphides (pyrite and chalcopyrite) and barite from the prospects vary from $\delta^{34}S_{sulphide} \approx$ -12 to +13 ‰(CD T) and $\delta^{34}S_{sulphate} \approx$ 8 to 17 ‰. Deuterium and oxygen isotope data for syn-breccia hydrothermal biotite, muscovite and actinolite range from δD = -141 to -18 ‰(V -SMOW) and $\delta^{18}O \approx$ 7 to 12 ‰ (V-SMOW). $\delta^{18}O$ values for hydrothermal carbonates appear to reflect those of the host limestone/dolostone. $\delta^{13}C$ values indicate the carbon in hydrothermal carbonates was derived in large part from the host WSG. The $\delta^{34}S$ values of hydrothermal pyrite, chalcopyrite and barite point to a largely seawater (or sediments/evaporites deposited from seawater) source for sulphur. These data combined with the limited deuterium isotope data indicate the source of fluids was likely formation/metamorphic water mixed with variable amounts of organic water ± evolved meteoric and/or evolved

seawater. Fluid flow may have been driven by tectonic and/or gravity processes and metals may have been scavenged from host strata.

C.2 Introduction

Numerous Proterozoic breccia bodies, collectively known as Wernecke Breccia, occur over large areas in the north-central Yukon Territory, Canada (Fig. 1; *cf.* Bell, 1986a,b, Thorkelson, 2000). They are associated with extensive metasomatic alteration and significant, but little studied, iron oxide-copper-gold ± uranium ± cobalt (IOCG) mineralisation (*cf.* Bell and Delaney, 1977; Bell, 1978; Archer *et al.*, 1977; Yukon MINFILE, 2003) that due to the low grade of metamorphism represents some of the best preserved examples of Proterozoic-age IOCG mineralisation in North America. The scale of brecciation and alteration is similar to that in other large scale Proterozoic breccia provinces, including those in Australia that host the Ernest Henry (167 Mt @ 1.1% Cu, 0.54 g/t Au; Ryan, 1998) and giant Olympic Dam (2320 Mt @ 1.3% Cu, 0.4g/t U_3O_8, 0.5 g/t Au, 2.9 g/t Ag; Reynolds, 2000) deposits. However, although many IOCG districts display brecciation and mineralisation that is intimately related to magmatism (*cf.* Hitzman, 2000; Sillitoe, 2003), a clear relationship with magmatic rocks is not evident in the Wernecke Mountains.

One of the key aims of this study was to determine if magmatic fluids were responsible for forming IOCG mineralisation and related breccias in the Wernecke Mountains. Six IOCG prospects (Slab, Hoover, Slats-Frosty, Slats-Wallbanger, Igor & Olympic) were selected for analysis to test this hypothesis. The prospects were chosen based on their varied stratigraphic locations within host Wernecke Supergroup (WSG) strata, their association with extensive sodic or potassic metasomatic alteration, and the accessibility of drill core for study (Fig. 2). This paper presents the results of stable isotope (C, O, S and D) and fluid inclusion analyses for the six prospects and discusses how these results constrain possible fluid sources.

C.3 Regional geologic setting

Bodies of Proterozoic Wernecke Breccia, from 0.1 to 10 km^2 in size, occur over large areas of the north-central Yukon Territory that are underlain by Early Proterozoic rocks

made up of WSG, Bonnet Plume River Intrusions, and "Slab volcanics[1]" (Figs. 1, 2; *cf.* Gabrielse, 1967; Delaney, 1981; Bell, 1986b; Thorkelson, 2000). The WSG is a thick package of marine sedimentary rocks that have been divided, from base to top, into the Fairchild Lake, Quartet and Gillespie Lake Groups (Fig. 2; *cf.* Delaney, 1981; Thorkelson, 2000). The Fairchild Lake Group (FLG) is at least 4 km thick and made up dominantly of fine-grained sandstone and siltstone, and minor limestone (Delaney, 1981; Thorkelson, 2000). These rocks are overlain by the Quartet Group, an approximately 5 km-thick package of carbonaceous to calcareous fine-grained siltstone and sandstone. Transitionally overlying the Quartet Group, and forming the upper part of the WSG, is the approximately 4 km-thick Gillespie Lake Group (GLG) made up largely of dolostone. Mafic to intermediate dykes and sills of the Bonnet Plume River Intrusions (BPRI), *ca.* 1710 Ma., cut WSG (Thorkelson, 2000; Thorkelson *et al.*, 2001a). Intermediate composition Slab volcanics were erupted prior to emplacement of Wernecke Breccia; however, they are preserved only as clasts within the breccia and it is not clear if they are a local unit within WSG or a separate unit that overlies it (Thorkelson, 2000; Section A). Host rocks to Wernecke Breccia underwent deformation and greenschist facies metamorphism during the Early Proterozoic Racklan Orogeny (Thorkelson, 2000).

Wernecke Breccia is confined to areas of WSG and is made up largely of clasts of the supergroup in a matrix of rock flour and hydrothermal precipitates; locally the breccia contains abundant clasts of BPRI and Slab volcanics (Thorkelson, 2000; Hunt *et al.*, 2002, 2005; Section A). Iron oxide-copper-gold (IOCG) mineralisation occurs as disseminations and veins within the breccia and surrounding WSG rocks (*cf.* Yukon MINFILE, 2003; Hunt *et al.*, 2002, 2005). Extensive sodic and potassic metasomatic alteration is spatially associated with the breccias (*cf.* Yukon MINFILE, 2003; Thorkelson, 2000; Section A). Multiple phases of brecciation and mineralisation are evident (*cf.* Hunt *et al.*, 2002, 2005). Cross-cutting relationships indicate syn- to post-deformational emplacement of the breccias (*cf.* Thorkelson, 2000; Hunt *et al.*, 2005).

Wernecke Breccia bodies examined in this study were emplaced into various parts of the WSG stratigraphy (Fig. 2). In the Slab area, breccia occurs in the upper part of the FLG within a sequence of calcareous metasiltstone, minor limestone and probable metaevaporites, cut by BPRI; numerous and large clasts of Slab volcanics occur locally

[1] Many of the names used in this paper are informal and are initially shown in quotation marks.

in the breccia (*cf.* Delaney, 1981; Thorkelson, 2000; Hunt *et al.*, 2005). In the Hoover area, breccia bodies are in calcareous metasiltstone and carbonaceous shale/slate at the transition from FLG to Quartet Group; minor BPRI dykes cut the WSG stratigraphy (*ibid.*). In the Slats region, breccia occurs in two areas known informally as 'Frosty' and 'Wallbanger'. Wallbanger is located about 4 km south-southeast of Frosty (Fig. 2). Breccia occurs within upper FLG calcareous metasiltstone and phyllite in the Frosty area and within transitional Quartet to GLG interlayered calcareous metasiltstone, shale and dolostone in the Wallbanger area (*ibid*). Abundant BPRI dykes cut the WSG in both areas. At Igor, breccia occurs within calcareous to carbonaceous metasiltstone and shale of the Quartet Group (*cf.* Norris, 1997). Breccias in the Olympic area were emplaced into locally stromatolitic GLG dolostone in the upper part of the WSG (*cf.* Thorkelson, 2000). In this area minor BPRI diorite dykes cut the GLG and abundant clasts of BPRI anorthosite occur locally in the breccia (*ibid.*). The age of brecciation is considered by Thorkelson (2000) and Thorkelson *et al.* (2001b) to be *ca*. 1595 Ma based on a U-Pb date of 1595 +8/-5 Ma for hydrothermal titanite from the matrix of breccia in the Slab area.

Each phase in the development of a breccia complex was probably multistage and overlapped other stages (Delaney, 1981). However, broad paragenetic sequences, summarized in Figure 3, were established for the breccia occurrences based on cross-cutting relationships. Paragenetic stages are unique to each prospect and not equivalent to those of other areas; for example Slab stage 3 ≠ Hoover stage 3 ≠ Olympic stage 3. In general there is an overall trend of: 1) metasomatic alteration (sodic or potassic) that overprints greenschist facies metamorphic mineral assemblages; 2) early stage brecciation accompanied by abundant magnetite ± hematite alteration; 3) main phase of brecciation accompanied by hematite and chalcopyrite-pyrite ± magnetite mineralisation; and 4) syn to post breccia carbonitization (calcite, ankerite/dolomite, siderite) ± pyrite, chalcopyrite, hematite, magnetite. Locally barite veins are abundant during stage 4 (e.g. at Igor).

C.4 Fluid inclusion studies

Very limited published fluid inclusion data (Hitzman *et al.*, 1992 – Igor prospect) exist for Wernecke Breccia and a preliminary study was undertaken in order to evaluate fluid processes and conditions during the formation of breccia and mineralisation. Further

work on Wernecke Breccia fluid inclusions is underway (*cf.* Gillen *et al*., 2004) at James Cook University, Australia.

Fluid inclusion petrography was carried out on quartz-, calcite-, fluorite- or barite-bearing samples from Wernecke breccia or associated veins at each prospect to identify well preserved inclusions that likely represent syn-breccia fluid. Fluid inclusion paragenesis was established using the criteria for primary, pseudosecondary, and secondary inclusions outlined in Roedder (1984). Three types of inclusions were identified on the basis of phases present at room temperature: 1) liquid plus vapour ± opaque (L+V); 2) L+V plus halite (L+V+H); and 3) L+V+H plus opaque. Fluid inclusion microthermometry was performed on a Linkam, gas-flow heating/freezing stage at James Cook University. The stage was regularly calibrated using synthetic fluid inclusion standards having known phase transitions at -56.6^{o}C and 0.0^{o}C. During calibrations, the temperatures indicated by the thermocouple were within 0.2^{o}C of the standards. Paired heating-freezing microthermometry was carried out on the same inclusions. In each sample all freezing experiments were carried out before the sample was heated. Results of the fluid inclusion analyses are summarized in Table 1 and Figures 4, 5 and 6; complete results are in Appendix III.

C.4.1 Results

Slab: A 1.5 cm-diameter euhedral quartz crystal from the matrix of Wernecke Breccia was selected for microthermometry in the Slab area (Fig. 4a). The quartz contains clusters of fluid inclusions that are probably primary and therefore syn-breccia, i.e. Slab paragenetic stage 3 (Fig. 3a). At room temperature the inclusions contain liquid (70-90%), vapour (5-10%) and halite (Fig. 4b,c). Rarely, they contain a red mineral that is probably hematite (Fig. 4d). During freezing experiments the formation of brown ice was observed in all inclusions and initial melting temperatures (Tfm) were below -50 ^{o}C (Table 1). Final ice melting temperatures (Tm_{ice}) ranged from -50 to -36 ^{o}C. In heating experiments homogenization occurred via halite dissolution (Th = Ths) between 226 and 245 ^{o}C; homogenization of the vapour bubble (Thv) occurred between 154 and 175 ^{o}C (Fig. 5, Table 1). The estimated salinity of fluid in the inclusions is about 42 weight % NaCl equivalent and the Na:Ca ratio is approximately 1.4 (Table 1, Figs. 5, 6).

Hoover: A metasedimentary clast from Wernecke Breccia that contains 1 mm diameter quartz grains was selected for microthermometry in the Hoover area (Fig. 4e). The

quartz contains trails of secondary fluid inclusions that probably relate to syn-breccia fluids, i.e. Hoover paragenetic stage 3 (Figs. 3b, 4f,g). At room temperature most of the inclusions contain liquid (80-90%) and vapour (10-20%); one inclusion contains liquid (90-95%), vapour (5-10%) and halite. In freezing experiments the formation of ice was observed in all inclusions, Tfm was below -50 ^{o}C and Tm_{ice} ranged from -34 to -25 ^{o}C (Table 1). Hydrohalite ($NaCl.2H_2O$) was observed in two L+V inclusions and melted at -1 and +1 ^{o}C (Tm_{hh} Table 1). Na:Ca ratios for these two inclusions are 0.4 and 0.7 (Table 1, Figs. 5, 6). Estimates of salinity for L+V inclusions range from 26 to 32 weight % NaCl equivalent (Table 1). The salinity of the L+V+H inclusion is estimated to be 38 weight % NaCl equivalent and the Na:Ca ratio is approximately 1.2 (Table 1, Figs. 5, 6). During heating experiments L+V inclusions homogenized via vapour bubble disappearance between 153 and 172 ^{o}C (Fig. 5, Table 1). In the L+V+H inclusion final homogenization occurred via halite dissolution at 188 ^{o}C (Fig. 5, Table 1).

Slats-Frosty: A syn-breccia ferroan dolomite-fluorite-pyrite-chalcopyrite vein was selected for microthermometry in the Slats-Frosty area (Fig. 4h,i). Fluorite within the vein contains fracture-parallel trails of pseudo-secondary fluid inclusions that probably relate to syn-breccia fluid, i.e. Slats-Frosty paragenetic stage 3 (Figs. 3c, 4j). At room temperature the inclusions contain liquid (90-98%) and vapour (2-10%; Fig. 4k) ± solid. Solids are halite, hematite and black opaques. The formation of brown ice was observed in all fluid inclusions during freezing, Tfm ranged from -103 to -72 ^{o}C and Tm_{ice} was between -35 and -23 ^{o}C (Table 1). Hydrohalite was observed in two L+V inclusions and in most L+V+solid inclusions; Tm_{hh} ranged from -22 to 3 ^{o}C. Salinity estimates are between 24 and 32 weight % NaCl equivalent and Na:Ca ratios vary from 0.8 to 1.6 (Table 1, Figs. 5, 6). Daughter phases homogenized at higher temperatures than vapour in all inclusions (i.e. Th = Ths); however, homogenization temperatures were not obtained for the solid phases due to cracking of the polished section during heating and subsequent mass decrepitation of the fluid inclusions. Homogenization of the vapour bubble occurred between 68 and 160 ^{o}C (Table 1).

Igor: Barite from Wernecke Breccia matrix was selected for microthermometry in the Igor area (Figs. 4l, m). The barite contains clusters of small fluid inclusions that are probably primary and therefore syn-breccia, i.e. Igor paragenetic stage 3 (Fig. 3e). At room temperature the inclusions contain liquid (90-95%) plus vapour (5-10%). Phase changes were difficult to observe in this sample due to the small size of inclusions and the cloudiness of the barite. Only one initial melting temperature of -77 ^{o}C was recorded

(Table 1). Tm_{ice} ranged from -54 to -50 ^{o}C. Hydrohalite was observed in one inclusion and melted at -26 ^{o}C. This inclusion has an estimated salinity of 34 weight % NaCl equivalent and a Na:Ca ratio of 0.1 (Table 1, Figs. 5, 6). Thv was between 220 and 250 ^{o}C, somewhat higher than the range of Thv values (70 to 200 ^{o}C) reported by Gillen *et al.* (2004) for quartz from Wernecke Breccia matrix in the Igor area but similar to the upper range of homogenization temperatures (80 to 300 ^{o}C) for inclusions in dolomite, calcite, fluorite and quartz in magnetite-rich assemblages reported by Hitzman *et al.* (1992).

Olympic: Two samples were selected for microthermometry from the Olympic area: a zoned quartz crystal from the matrix of Wernecke Breccia (Fig. 4n,o) and dolomite from a ferroan dolomite-quartz-chalcopyrite±pyrite vein that cross-cuts Wernecke Breccia (Fig. 4p,q). Phase changes were difficult to observe in both samples due to the small size of inclusions. The outer rim of the zoned quartz contains small clusters of fluid inclusions that are probably primary and therefore syn-breccia, i.e. Olympic paragenetic stage 2 (Figs. 3f, 4o). At room temperature the inclusions contain liquid (~80%) plus vapour (~20%). During freezing experiments Tm_{ice} ranged from -29 to -26 ^{o}C; salinity is estimated to be 26 to 28 weight % NaCl equivalent (Table 1). On heating, homogenization occurred via vapour bubble disappearance between 158 and 170 ^{o}C (Table 1, Fig. 5). Dolomite within the vein, in the second sample, contains small clusters of inclusions that are probably primary and therefore representative of post-breccia fluids, i.e. Olympic paragenetic stage 5 (Fig. 3f). At room temperature the inclusions contain liquid (70 to 98%) plus vapour (2 to 30%). During freezing experiments Tm_{ice} ranged from -56 to -25 ^{o}C; salinity is estimated to be 26 to 35 weight % NaCl equivalent (Table 1, Fig. 5). Hydrohalite was observed in one inclusion and melted at -13 ^{o}C. This inclusion has a Na:Ca ratio of 0.1 (Table 1, Fig. 5, 6). Homogenization occurred via vapour bubble disappearance with Thv between 188 and 223 ^{o}C.

C.4.2 Summary of fluid inclusion results

Fluid inclusion data collected during this study is limited but gives an indication of fluid conditions at the time of Wernecke Breccia formation. In the Slab area quartz from breccia matrix contains primary fluid inclusions that indicate syn-breccia fluids were high salinity (~ 42 eq. wt. % NaCl) and Na-dominant with minimum temperatures of

226 to 245°C (based on Th which is < trapping temperature). Quartz from the Hoover prospect contains secondary fluid inclusions that indicate syn-breccia fluids were moderate salinity (26-38 eq. wt. % NaCl), varied from Na-dominant to Ca-dominant and had temperatures of at least 153 to 188°C. At the Slats-Frosty prospect fluorite in a syn-breccia vein contains pseudo-secondary fluid inclusions that indicate syn-breccia fluids were moderate salinity (24-32 eq. wt. % NaCl), ranged from Na-dominant to equal amounts of Na and Ca and had minimum temperatures of 112 to >160°C. Barite from breccia matrix at the Igor prospect contains primary fluid inclusions that indicate syn-breccia fluids had minimum temperatures of 220 to 250°C, were moderately saline (34 eq. wt. % NaCl) and Ca-dominant (based on limited data). Quartz from breccia matrix at the Olympic prospect contains primary fluid inclusions that indicate syn-breccia fluids were moderately saline (26-28 eq. wt. % NaCl) and at least 158 to 170°C.

C.5 Isotope chemistry (C, O, S & H)

Mineral separates from Wernecke Breccia and associated veins were analyzed for carbon-oxygen (94), sulphur (49) and hydrogen (14) isotopes in order to characterize the fluids that produced the breccia and associated IOCG mineralisation. Samples were chosen from various paragenetic stages (Fig. 3) at each prospect in order to document changes in the fluids that may have occurred through time and to compare fluids from prospects hosted in different parts of WSG stratigraphy. In addition, twenty three samples of limestone/dolostone and three samples of carbonaceous shale were analyzed for carbon-oxygen and carbon isotopes, respectively, to provide regional host rock background values. Results are summarized in Tables 2 to 4 and presented in Figures 7 to 11; complete results are in Appendix IV

C.5.1 Methods: carbon – oxygen isotopes

Carbonates were extracted by crushing and handpicking under a binocular microscope and identified using GADDS (general area detector diffraction system) at the James Cook University Advanced Analytical Centre. Whole rock samples were crushed and powdered. Isotopic analyses of mineral separates and whole rock samples were carried out at the University of Tasmania Central Science Laboratory using a modification of the method of McRea (1950). Samples were reacted with H_3PO_4 at 50°C for a 24 hour period, and then CO_2 was separated in a chemical separation line. Gas was analysed on

a Micromass Optima Stable Isotope mass spectrometer. Results were corrected for machine error and are expressed relative to Vienna Standard Mean Ocean Water (V-SMOW) and PeeDee belemnite (PDB). Previous analyses of the Biggenden calcite, used as the international standard, have a standard error of ± 0.06 ‰ for $\delta^{13}C$ and ± 0.1 ‰ for $\delta^{18}O$.

C.5.2 Methods: sulphur isotopes

Sulphides and sulphates were extracted by crushing and handpicking under a binocular microscope after the preparation of cut slabs and inspection of sulphide/sulphate phases in thin section for contaminant inclusions. Isotopic analyses were carried out at the University of Tasmania Central Science Laboratory using the method of Robinson and Kusabe (1978). Powdered samples were reacted with cuprous oxide at high temperatures, and then SO_2 was separated from H_2O, CO_2 and non-condensable gases in a chemical separation line. Gas was analysed on a Sira VG Series 2 mass spectrometer. Results were corrected for machine error and are expressed relative to Cañon Diablo Troilite (CDT). Results were calibrated against a secondary gas standard, and results were reproducible to within 0.2 ‰

C.5.3 Methods: hydrogen – oxygen isotopes

Muscovite, biotite and actinolite were extracted by crushing and handpicking under a binocular microscope after the preparation of polished thin sections and petrographic and microprobe inspection of the phases for alteration and/or contaminant inclusions. Fourteen mineral separates from three of the prospects (Slab, Hoover & Igor) were submitted for hydrogen and oxygen isotope analysis. Unfortunately the other study areas did not yield suitable material for analysis. Analyses were carried out at the Scottish Universities Environmental Research Centre, East Kilbride, Scotland. Oxygen was extracted using a laser fluorination system based on that of Sharp (1990), converted to CO_2, and analysed on a VG PRISM III mass spectrometer. Hydrogen was extracted by the method described in Fallick *et al.* (1993) except that hot chromium rather than uranium was used (see Donnelly *et al.*, 2001). Reproducibility for isotopically homogeneous material is ± 5 ‰ (at 1σ) and NBS 30 gives δD = -65 ‰ All data are reported relative to V-SMOW.

No indications of alteration were found during petrographic and microprobe analyses of the samples. However, two biotite samples gave abnormally high yields of hydrogen and may be chloritized; in addition, three samples of muscovite failed to generate sufficient hydrogen for isotopic assay. These five samples have been omitted from the following discussion.

C.5.4 Results: carbon – oxygen isotopes

WSG: Calcite from limestone layers in FLG returned values of $\delta^{18}O$ = 11.8 to 14.4 ‰ and $\delta^{13}C$ = -2.0 to 0.4 ‰ (Table 2; Fig. 7). Ankerite and ferroan dolomite from a dolostone layer in Quartet Group and from clasts of Quartet Group dolomitic siltstone and dolostone in Wernecke Breccia returned values similar to those of FLG with $\delta^{18}O$ and $\delta^{13}C$ values of 13.9 to 15.9 ‰and -1.9 to -0.3 ‰respectively. Dolomite from dolostone layers, stromatolitic dolostone and intraformational breccia within GLG returned $\delta^{13}C$ values similar to those of FLG and Quartet Group (-1.9 to 1.6 ‰) but significantly higher $\delta^{18}O$ values (16.4 to 24.6 ‰). Whole rock samples of Quartet Group carbonaceous shale returned $\delta^{13}C$ values of -26.7 to -20.8 ‰, consistent with an organic matter origin.

Slab: Samples of ankerite-magnetite alteration, veins and breccia that formed early in the brecciation process at Slab, i.e. Slab paragenetic stage 2 (Fig. 3a), returned $\delta^{13}C$ and $\delta^{18}O$ values of -3.7 to -1.2 ‰ and 10.9 to 14.8 ‰ respectively (Table 2; Fig. 7a). Samples from the main brecciation phase, i.e. Slab stage 3, returned $\delta^{18}O$ values between -2.1 and 15.3 ‰ and $\delta^{13}C$ values of -3.7 to 1.5 ‰ Results for samples from veins that cross-cut breccia, i.e. Slab stage 4, overlap those of stage 3 to some degree and range from $\delta^{18}O$ = 10.1 to 14.6 ‰and $\delta^{13}C$ = -2.7 to 1.24 ‰(Fig. 7 a).

One sample only (SB97-9-119.9 m, Appendix IV) contains coexisting calcite and dolomite. It returned $\delta^{18}O$ values of 13.0 and 14.1 ‰respectively. If isotopic equilibrium was attained then the difference in $\delta^{18}O$ values between the two types of carbonate indicates a fluid temperature of approximately 300°C (using the fractionation factors of Sheppard and Schwartz, (1970) or Golyshev *et al.* (1981).

Hoover: Syn-breccia calcite from the Hoover prospect, i.e. Hoover paragenetic stage 3 (Fig. 3b), returned $\delta^{18}O$ and $\delta^{13}C$ values of 9.4 to 13.5 ‰and -6.8 to -2.3 ‰ respectively (Table 2). The lowest $\delta^{13}C$ values were returned by samples from veins and breccia that cut Quartet Group carbonaceous slate/shale (Fig. 7b).

Slats-Frosty: Samples of syn- and syn to post-breccia carbonate from the Slats-Frosty area, i.e. paragenetic stages 2, 3 and 4 (Fig. 3c), returned $\delta^{18}O$ values between 13.7 and 20.1 ‰ with most samples falling between 13.7 and 15.6 ‰(Fig. 7 c; Table 2). $\delta^{13}C$ values range from -4.4 to -0.2 ‰ with the lowest values returned by veins that cross-cut carbonaceous shale (Fig. 7c).

Slats-Wallbanger: Syn- and syn to post-breccia carbonate from the Slats-Wallbanger area, i.e. paragenetic stages 5 and 6 (Fig. 3d), returned a narrow range of $\delta^{18}O$ values (14.1 to 16.8 ‰) and a wide range of $\delta^{13}C$ values (-10.6 to -2.2 ‰; Table 2). All but two $\delta^{13}C$ values are less than -4 ‰. The highest $\delta^{13}C$ values were returned by veins cutting interlayered metasiltstone and dolostone at the base of GLG (Fig. 7d). The lowest $\delta^{13}C$ values (-10.5, -10.6 ‰) were returned by stage 6 veins that cut a massive magnetite ± ankerite vein.

Igor: Syn- and syn to post-breccia siderite and ferroan dolomite from the Igor prospect, i.e. Igor paragenetic stages 3 and 4 (Fig. 3e) returned $\delta^{13}C$ values of -6.1 to -1.4 ‰ and $\delta^{18}O$ values of 14.6 to 20.0 ‰ (Table 2; Fig. 7e).

Olympic: Syn-breccia, syn to post-breccia and post-breccia carbonate from the Olympic area, i.e. paragenetic stages 1, 2, 3 and 5 (Fig. 3f), returned a fairly narrow range of oxygen and carbon isotope values with $\delta^{18}O$ between 14.8 to 18.7 ‰ and $\delta^{13}C$ from -5.1 to 0.4 ‰ (Table 2; Fig. 7f). One sample (OY94-4-38.90) contains coexisting dolomite and ankerite that returned $\delta^{18}O$ values of 14.8 and 15.6 ‰respectively.

Summary and discussion of carbon – oxygen isotope results

Mean carbon and oxygen isotope values for Paleoproterozoic carbonates, comparable in age to WSG, are $\delta^{18}O \approx 18$ to 22 ‰ and $\delta^{13}C \approx -2$ to 2 ‰ (*cf.* Shields and Veizer, 2002). Samples of WSG have $\delta^{13}C$ values similar to the mean values but variable $\delta^{18}O$ values (Fig. 8). The lower and middle parts of WSG, i.e. FLG and Quartet Group, returned $\delta^{18}O$ values lower than the mean values (~ 12-16 vs. 18-22 ‰; Table 2). GLG, which forms the upper part of WSG, returned $\delta^{18}O$ values similar to the mean values (~ 16-25 vs. 18-22 ‰; Table 2). Thus, although the number of samples collected from the WSG is not large, the results indicate that the lower and middle parts of the supergroup are significantly depleted in $\delta^{18}O$ compared to typical Proterozoic marine carbonate. Samples were collected from areas outside those with visible Wernecke Breccia-related alteration, hence this variation likely reflects either a meteoric water-dominated

diagenetic history of pre-GLG strata, or post-WSG carbonate alteration that preferentially affected the lower and middle WSG. Coincidentally, most mineralized Wernecke Breccia sites occur in the lower WSG, i.e. within the most $\delta^{18}O$ depleted stratigraphy.

In general $\delta^{18}O$ results for the prospects studied reflect those of the host strata. For example, the Hoover prospect which is located at the top of the FLG returned $\delta^{18}O$ values of 9.4 to 13.5 ‰ similar to those of the FLG (11.8-14.4 ‰). The Slats-Wallbanger prospect is hosted by strata at the top of the Quartet Group and $\delta^{18}O$ results (14.1 to 16.8 ‰) are comparable to those of the host rocks (13.9 to 15.9 ‰). Likewise, the Olympic prospect returned $\delta^{18}O$ results (14.8-18.7 ‰) similar to host GLG rocks (16.4-24.6 ‰). At Slab, most oxygen isotope results are similar to those of the host FLG, however some samples returned low $\delta^{18}O$ values. The three lowest $\delta^{18}O$ values (-2.1, 2.7, 3.0 ‰) are from breccia zones (Slab stage 3) that are made up of smaller and more rounded clasts than those in other breccia bodies, and appear to have been the focus of abundant fluid flow. Hence, the low $\delta^{18}O$ values are likely a reflection of interaction with large amounts of low $\delta^{18}O$ fluid such as meteoric and/or formation water.

Carbon isotope ratios also appear to be influenced by host rock type. For example, at Hoover, samples from breccia and veins hosted in carbonaceous shale returned values of $\delta^{13}C$ = -6.8 to -4.5 ‰while those h osted in calcareous metasiltstone returned higher values of $\delta^{13}C$ = -3.9 to -2.3 ‰(Fig. 7b). Similar results are seen at Slats-Frosty and Slats-Wallbanger where $\delta^{13}C$ results for samples from veins in carbonaceous shale or metasiltstone are lower than those from samples in calcareous metasiltstone or dolostone (Figs. 7c,d).

In general, carbon and oxygen isotope ratios for the prospects studied do not vary systematically with paragenetic stage. An exception to this is the Slab prospect where early ankerite-magnetite alteration (Slab stage 2) forms a distinct group with $\delta^{18}O$ = 10.9 to 14.8 ‰and $\delta^{13}C$ = -3.7 to -1.2 ‰ (Fig. 7a; Table 2). Some of the spread in $\delta^{18}O$ values seen at the prospects and in the WSG samples may be due to the expected fractionation of oxygen isotopes between different types of carbonate (*cf.* Rye and Ohmoto, 1974; Valley *et al.*, 1986; Zheng, 1999). For example, carbonate in a sample from the Olympic prospect (sample OY94-4-38.90 in Appendix IV) is composed of dolomite ($\delta^{18}O$ = 14.8 ‰) and ankerite ($\delta^{18}O$ = 15.6 ‰); The measured $\delta^{18}O$ difference, $\Delta_{dolomite\text{-}ankerite}$ = 0.8, is close to the expected value of 0.97 calculated for equilibrium

conditions using the fractionation factors of Zheng (1999), suggesting it may be due to oxygen isotope fractionation.

Measured oxygen isotope ratios of syn-breccia carbonates (stage 3 for Slab, Hoover, Slats-Frosty and Igor and stage 2 for Olympic) were used in conjunction with the fractionation factors of Zheng (1999) for calcite-H_2O, dolomite-H_2O, ankerite-H_2O and siderite-H_2O along with estimates of temperature for syn-breccia fluid: Slab = 300°C, Hoover = 285°C, Slats-Frosty = 235°C, Igor = 350°C and Olympic = 185°C (see section C.6.1 for temperature determination) to calculate $\delta^{18}O_{water}$ values for the prospects. Resulting (syn-breccia) $\delta^{18}O_{water}$ values range from: Slab = -7.9 to 9.5 ‰; Hoover = 3.0 to 7.2 ‰; Slats -Frosty = 5.4 to 11.6 ‰; Igor = 9.4 to 14. 7 ‰and Olympic = 5.7 to 7.8 ‰ (Table 3; shown for comparison on Fig. 11).

C.5.5 Results: sulphur isotopes

Slab: Pre to syn-breccia, syn-breccia and syn to post-breccia sulphide samples from the Slab area, i.e. Slab paragenetic stages 1 to 4 (Fig. 3a), returned overlapping $\delta^{34}S$ values between -11.5 and 7.1 ‰ (Table 4; Fig. 9a). Samples from the same paragenetic stage show a wide range of values. For example, two samples of chalcopyrite from a stage 3 vein returned $\delta^{34}S$ values of -11.5 and 2.4 ‰ (labelled 1 in Fig. 9a) and samples of pyrite from stage 4 veins returned values of $\delta^{34}S$ = -11.0 and 3.8 ‰ (labelled 2 in Fig. 9a).

Hoover: Syn-breccia and syn to post-breccia sulphide samples from the Hoover prospect, i.e. Hoover paragenetic stages 3 and 4 (Fig. 3b), returned a wide range of $\delta^{34}S$ values between -12.4 and 13.4 ‰ (Table 4; Fig. 9b) with no systematic variation with paragenetic stage. Though, based on the limited data, there is variation in $\delta^{34}S$ with host rock type. Samples from veins and breccia hosted in calcareous metasiltstone returned $\delta^{34}S$ = -12.4 to -1.6 ‰ and samples from those hosted in carbonaceous shale/slate returned $\delta^{34}S$ = 4.6 to 13.4 ‰ (Fig. 9b). However, unlike the C-O data, sulphur isotopic ratios in breccia-related samples cannot be compared to background diagenetic sulphide compositions as this aspect was not investigated during the study.

Slats: Syn-breccia and syn to post-breccia sulphides from the Slats-Wallbanger area, i.e. paragenetic stages 5 and 6 (Fig. 3d), returned $\delta^{34}S$ values between -6.8 and -1.7 ‰ (Table 4; Fig. 9c). The highest $\delta^{34}S$ value (-1.7 ‰) is from a stage 6 ankerite-chalcopyrite-quartz vein that cuts massive magnetite (labelled 1 in Fig. 9c). The

remaining values are from stage 5 veins that cut calcareous siltstone at the base of GLG. Pyrite from a hematite-pyrite-quartz vein (paragenetic stage unknown) cutting FLG phyllite at Slats-Frosty returned a $\delta^{34}S$ value of 4.2 ‰ (Fig. 9a).

Igor: Syn-breccia and syn to post-breccia sulphides from the Igor prospect, i.e. Igor paragenetic stages 3 and 4 (Fig. 3e), returned $\delta^{34}S$ values between -8.4 and 4.8 ‰ (Table 4; Fig. 9d). Igor is the only prospect in the study that contains significant amounts of sulphate, as stage 4 barite. Samples of the barite returned $\delta^{34}S$ values between 7.7 and 17.1 ‰. Three samples of co-existing sulphate and sulphide were analyzed and gave the following results: 1) pyrite from the selvage of a barite vein returned $\delta^{34}S$ = 3.3 ‰; $\delta^{34}S_{barite}$ = 7.7 ‰ (labelled 1 in Fig. 9d); 2) chalcopyrite and barite from a hematite-magnetite-chalcopyrite-barite vein/pod returned $\delta^{34}S$ values of -7.9 and 17.1 ‰ respectively (labelled 2 in Fig. 9d); and 3) chalcopyrite and barite from a siderite-chalcopyrite-pyrite-barite vein returned $\delta^{34}S$ values of -8.4 and 8.7 ‰ respectively (labelled 3 in Fig. 9d). Samples 2 and 3 give reasonable temperatures of 243 and 356°C based on the equations[2] of Ohmoto and Lasaga (1982). Sample 1 gives a temperature of 1026°C which is clearly unreasonable indicating this barite-pyrite pair are not in equilibrium (*cf.* Ohmoto and Goldhaber, 1997).

Olympic: Abundant sulphides were not observed in the Olympic area and only three samples were analysed. Syn-breccia (Olympic paragenetic stage 2, Fig 3f) and syn to post-breccia (stage 3) chalcopyrite returned $\delta^{34}S$ = -10.8 ‰ and 5.3 ‰ respectively (Table 4; Fig. 9e). Pyrite in Wernecke Breccia proximal to a diorite dyke, returned a $\delta^{34}S$ value of -0.5 ‰.

Summary and discussion of sulphur isotope results

Sulphur isotope results for sulphide samples from the Wernecke Mountains show a wide range in values from approximately $\delta^{34}S$ = -12 to 13 ‰ with a broad peak between -7 to 0 ‰ (Figs. 9 & 10). In general, the isotopic ratios do not vary systematically with paragenetic stage and can vary greatly even within a single stage. This is illustrated dramatically at Slab where chalcopyrite samples collected a few centimetres apart in a vein returned values of $\delta^{34}S$ = -11.5 and +2.4 ‰

Mechanisms to account for variations in the isotopic composition of sulphide and sulphate minerals include: 1) changes in the temperature of the fluid; 2) changes in

[2] $1000 \ln\alpha_{\text{sulphate-pyrite}} = 6.463 \times 10^6/T^2 + 0.56$; $1000 \ln\alpha_{\text{sulphate-chalcopyrite}} = 6.513 \times 10^6/T^2 + 0.56$

the redox state of the fluid; 3) changes in the environments where variations in the SO_4^{-2}/H_2S take place; and 4) multiple sources of sulphur (*cf.* Ohmoto and Rye, 1979; Ohmoto and Goldhaber, 1997). If the dominant species in a hydrothermal fluid is H_2S temperature variations cause little change in $\delta^{34}S$ (Ohmoto and Goldhaber, 1997). However, if the fluid contains significant amounts of SO_4^{-2} and H_2S (or other oxidised and reduced species) a change in temperature can cause large variations in the $\delta^{34}S$ values of minerals precipitating from the fluid (*ibid*).

In open systems, the ratio of oxidised to reduced sulphur species can be changed by reactions with wall rocks, for example by reaction with Fe^{+2}-or Fe^{+3}-bearing minerals such as magnetite and hematite, or by precipitation of sulphide or sulphate minerals (*ibid*). Oxidation of the fluid (i.e. an increase in the ratio of oxidised to reduced species) will cause a decrease in the $\delta^{34}S$ values of individual species in the fluid (if equilibrium between oxidised and reduced species is maintained) and reduction may cause an increase (*ibid*). Reduction of fluid can also occur by reaction with organic matter and causes increases in the $\delta^{34}S$ values of H_2S and SO_4^{-2} and subsequently in the $\delta^{34}S$ values of minerals precipitated from this fluid (*ibid*). Indications of this mechanism are seen at the Hoover prospect where veins and breccia hosted in carbonaceous shale returned higher $\delta^{34}S$ values than those hosted in calcareous metasiltstone (Fig. 9b).

The residence time of sulphur species in a particular environment (in addition to differences in pH, fO_2 and fS_2 conditions in the fluid) can affect the degree of isotopic equilibrium attained by sulphate and sulphide (Ohmoto and Rye, 1979). It takes a certain amount of time at given fluid conditions to attain equilibrium between SO_4^{-2} and H_2S (*ibid*). If a change occurs in the SO_4^{-2}/H_2O ratio of the fluid at the site of mineral deposition and minerals are precipitated before the SO_4^{-2} and H_2S have time to attain equilibrium the sulphide and sulphide minerals will reflect this isotopic disequilibrium (*ibid*). Limited isotopic data available for coexisting minerals at the IOCG prospects studied, e.g. pyrite-barite and chalcopyrite-barite at Igor (see above) indicates equilibrium and non-equilibrium conditions were present.

Hydrothermal fluids may acquire sulphur from more than one source by one or more mechanisms and the proportions of sulphur from different sources may vary during the history of ore formation as the plumbing system evolves (*ibid*). Possible sources of sulphur include: 1) seawater; 2) sulphur leached from host sedimentary rocks which may include biogenic and non-biogenic sulphur; 3) sulphur leached from igneous rocks; and 4) magmatic fluid. At Igor, one barite sample has a $\delta^{34}S$ value (17.1 ‰ – see

above) similar to that of Proterozoic seawater (18 ‰ – Strauss, 1993) suggesting possible derivation of sulphur from the seawater. At Hoover, some sulphur may have been leached from biogenic pyrite associated with organic matter because sulphide hosted in carbonaceous shale has different $\delta^{34}S$ values than sulphide hosted in metasiltstone (Fig. 9b). At Olympic, a sample of pyrite from Wernecke Breccia that is adjacent to a BPRI dyke has a $\delta^{34}S$ value of 0 ‰suggesting some sulphur may have been derived locally from igneous rocks.

Any, or a combination, of the above mechanisms can cause large differences in the observed sulphur isotopic ratios in an ore deposit. For example, if a fluid acquires aqueous SO_4^{-2} via dissolution of anhydrite that was precipitated from seawater (e.g. $\delta^{34}S$ = 20 ‰) sulphate minerals that precipitate from this fluid may have $\delta^{34}S$ values similar to that of the SO_4^{-2} (i.e. ~ 20 ‰). If the SO_4^{-2} is reduced to H_2S the value of $\delta^{34}S_{H_2S}$ will vary depending on the degree of sulphate reduction – for instance, reduction by interaction with Fe^{+2}-bearing minerals at 250°C would give $\delta^{34}S_{H_2S}$ values between -5 and +20 ‰(*ibid*).

The above explanations for heterogeneous sulphur isotope response will be revisited in the overall discussion of fluid properties (section C.6).

C.5.6 Results: hydrogen – oxygen isotopes

Samples of syn-breccia biotite, muscovite and actinolite were analysed for hydrogen and oxygen isotopes. Biotite from Wernecke Breccia matrix in the Slab area returned δD values of -115 and -84 ‰and $\delta^{18}O$ values of 8.3 and 9.5 ‰ (Table 5). Muscovite from breccia matrix returned δD = -45 ‰ and $\delta^{18}O$ = 10.6 ‰. Biotite from a vein in a breccia clast in the Slab area returned δD and $\delta^{18}O$ values of -141 and 6.7 ‰ respectively. Muscovite in veins cutting altered FLG proximal to Wernecke Breccia in the Slab area returned δD values of -54 and -21 ‰and $\delta^{18}O$ values of 11.1 and 11.6 ‰; actinolite from a vein returned δD = -22 and -18 ‰ and $\delta^{18}O$ = 11.0 ‰. Biotite from Wernecke Breccia matrix at the Hoover prospect returned δD and $\delta^{18}O$ values of -119 and 7.8 ‰ respectively (Table 5). Muscovite from Wernecke Breccia matrix in the Igor area returned δD and $\delta^{18}O$ values of -55 and 9.9 ‰ respectively (Table 5).

Hydrogen and oxygen isotope values for water co-existing with syn-breccia muscovite, biotite and actinolite were calculated using the measured hydrogen and oxygen isotopic ratios, fractionation factors for muscovite-H_2O, biotite-H_2O and

actinolite-H_2O (or tremolite-H_2O) and estimates of temperature (Slab = 300°C, Hoover = 285°C, Igor = 350°C – see section C.6.1 for temperature determination). Calculated $\delta^{18}O_{water}$ values for the three prospects fall within a fairly narrow range from 8 to 11 ‰; however, there is a wide spread in calculated δD_{water} values (Table 5, Fig. 11). δD_{water} values calculated from biotite and muscovite range from -73 to -16 ‰and -7 to +27 ‰ respectively; δD_{water} values calculated from actinolite are 0 and 4 ‰

Discussion of hydrogen – oxygen isotope results

Variations in δD are not well understood and may involve: 1) mixing of different waters; 2) evaporation; 3) magma degassing; 4) interaction with younger fluids; 5) exchange with hydrous minerals; and 6) exchange with H_2S of H_2 (Sheppard, 1986; Ohmoto, 1986; Hedenquist *et al.*, 1998). Low and/or variable δD values in the Wernecke samples could be due to any of these, however 1 and 2 seem to be most likely. Organic water derived from carbonaceous material in host WSG rocks would have low δD values (Fig. 11) and could be present in variable amounts in the fluid. Evaporation of meteoric water (or seawater) would cause a shift to higher δD values (*cf.* Sheppard, 1986). The presence of evaporites in the lower part of WSG (Hunt *et al.*, 2005) indicates arid conditions existed at least during the deposition of FLG, however it is not known how long these conditions persisted. Muscovite in Wernecke Breccia and associated veins demonstrates Ar-Ar re-equilibration (see Section B), most likely due to re-heating, and it is not clear what effect, if any, this would have had on the hydrogen isotopic ratios.

$\delta^{18}O$ values calculated for water co-existing with biotite, muscovite and actinolite in Wernecke samples are similar to those calculated for water co-existing with hydrothermal carbonate at the six prospects (Fig. 11). This could be due to their precipitation from fluid with the same oxygen isotope signature or may be an indication that the fluid(s) underwent isotopic exchange with host WSG sedimentary rocks (*cf.* Shepperd, 1986; Ohmoto, 1986). It is not possible to differentiate between the two scenarios, however, isotopic information from the Slab prospect suggests fluid-rock interaction may have been significant. At Slab, limestone layers in FLG have $\delta^{18}O$ values 6 to 10 ‰lower than expected for Proterozoic rocks of similar age (Fig. 8; Table 2), suggesting interaction with a fluid that had a low $\delta^{18}O$ value, such as meteoric, sea or formational water.

C.6 Discussion: fluid characteristics

C.6.1 Constraints on fluid P-T-X

Pressure and temperature

Isochores constructed from fluid inclusion microthermometry data (salinity, Tm_{ice}, Thv and Ths) were used in conjunction with **limited** independent estimates of temperature for Slab and Igor (Table 6) to determine fluid pressure using the methods of Shepherd and Rankin (1998). Independent temperature estimates for Slab and Igor are based on isotopic data, assuming isotopic equilibrium was attained. At Slab a co-existing dolomite-calcite pair indicates a temperature of approximately 300^{o}C (Section C.5.4). At Igor two barite-chalcopyrite pairs indicate temperatures of approximately 240 and 350^{o}C (Section C.5.5). The higher temperature was used to estimate pressure because fluid inclusion data indicate minimum temperatures at Igor were 250^{o}C (this study) to 300^{o}C (Hitzman, *et al.*, 1992). Results for the Slab area range from 2420 to 3000 bars which, assuming lithostatic confining pressure and a rock density of 2.7 g/cm^{3} (Shepherd *et al.*, 1985), correspond to depths of approximately 9.1 to 11.3 km (Fig. 12; Table 7). The results are similar to upper estimates for the combined thickness of Quartet Group and GLG (7.4 to 9 km) that overlie the Slab prospect (Fig. 2) based on stratigraphic sections measured by Delaney (1981) that take into account present day exposure and deformation. Results for Igor range from 1500 to 1900 bars (Fig. 12), corresponding to depths of approximately 5.7 to 7.2 km. This depth range is in agreement with the > 4 km estimated thickness for Quartet and GLG strata that overlie the Igor prospect.

The reasonable agreement between stratigraphic thickness obtained from estimates of pressure (this study) and from field mapping (Delaney, 1981; Thorkelson, 2000) allow approximate fluid inclusion trapping temperatures to be calculated for the Hoover, Slats-Frosty and Olympic areas. The Hoover and Slats-Frosty prospects are overlain by approximately 7 to 9 km of strata and the Olympic prospect by 0.4 to 1.5 km (based on stratigraphic sections of Delaney, 1981). Using the upper limit of these estimates on isochore diagrams gave average trapping temperatures of 285, 235 and 185 ^{o}C for syn-breccia fluids at Hoover, Slats-Frosty and Olympic respectively (Table 7). The upper estimates of measured thickness were used as these gave the best agreement with fluid inclusion data at Slab and Igor.

Composition

Fluid associated with the formation of Wernecke Breccia is a H_2O-NaCl-$CaCl_2$ plus iron system, based on: 1) the occurrence of halite and hematite daughter phases and 2) the presence of $CaCl_2$ in the fluid as indicated by the formation of brown ice during freezing and initial melting temperatures below -50 ^oC (*cf.* Potter *et al.*, 1978, Vanko *et al.*, 1988; Zwart and Touret, 1994*).*

The composition of syn-breccia fluid and the isotopic ratios of minerals precipitated from it appear to be controlled, to some degree, by the composition of the host rocks. Na-rich, high salinity fluids occur at the Slab prospect which is hosted in upper FLG rocks that contain metaevaporite (halite facies; Figs. 5, 6; Table 1; Hunt *et al.*, 2005). Ca-rich, lower salinity fluids occur at the Olympic prospect which occurs in GLG dolostone. Fluids of varied composition and salinity occur between these two end member types in prospects that are hosted by the Quartet Group. Lithological control on isotopic ratios is indicated by $\delta^{18}O$ values for the prospects, i.e. they are similar to those of the host WSG strata (Fig. 8). Carbon isotope results are also indicative of lithological control in that samples from veins hosted by carbonaceous shale have lower $\delta^{13}C$ values than those hosted by calcareous siltstone (Fig. 7b,c).

The composition of alteration that is associated with Wernecke breccia also suggests extensive fluid-rock interaction. Alteration extends for metres to hundreds of metres beyond the breccias and varies from sodic- to potassic- to calcic-dominant with changes in lithology from FLG to Quartet Group to GLG (Section A; Hunt *et al.,* 2005). However, at each prospect, syn to post-breccia alteration and veining are dominated by carbonate. The type of carbonate varies with host lithology. Calcite is the dominant phase at Slab and Hoover; dolomite and ankerite are dominant at Slats and Olympic (*ibid*). Igor is somewhat different in that the late carbonate phase includes siderite, as well as dolomite and ankerite, and is accompanied by abundant barite.

C.6.2 Constraints on fluid sources

Possible sources for fluids that formed Wernecke Breccia and associated IOCG mineralisation are: meteoric water, seawater, water derived from diagenesis and compaction of basinal sediments (including evaporites), water derived during

metamorphism of WSG, and magmatic water. Tracers for the origin of water are provided by its D/H and $^{18}O/^{16}O$ ratios (Sheppard, 1986). Calculated values for water co-existing with syn-breccia muscovite, biotite and actinolite in Wernecke Breccia show wide scatter, especially in δD (-73 to +27 ‰; Fig. 11) and thus do not uniquely constrain the fluid source. The fluid may have been a mixture of waters from a number of sources and several possibilities are outlined below, based on the limited data available.

Evolved seawater: The δD and $\delta^{18}O$ values of seawater are initially increased by evaporation as shown in Figure 11 (Knauth and Beeunas, 1986). Seawater evolved in this way could account for the high δD_{water} values calculated from muscovite in Wernecke Breccia samples and represents one of the few ways such values could be formed (assuming the δD values for muscovite have not been affected by younger events – see Section C.5.6). Some of the high $\delta^{18}O$ values could also be due to exchange between seawater and ^{18}O-rich minerals such as carbonates (Sheppard, 1986). Mixing of this evolved seawater with variable amounts of low δD water (e.g. organic water) could produce the remainder of the depleted δD_{water} values seen.

Evolved meteoric water: The evaporation of meteoric water can also lead to higher δD and $\delta^{18}O$ values and its interaction with ^{18}O-rich minerals in the host rocks can lead to marked enrichment in ^{18}O relative to local meteoric water (Sheppard, 1986; Fig. 11). It is typical for these meteoric-hydrothermal waters to acquire high $\delta^{18}O$ values as demonstrated by geothermal waters in the Salton Sea and Lanzarote areas (Fig. 11). Therefore, meteoric water that has undergone evaporation and/or water-rock isotope exchange is a possible source of Wernecke Breccia fluids; the range in δD values could be due to mixing with variable amounts of low δD water and/or evolved seawater.

Several syn-breccia calcite samples that returned highly depleted $\delta^{18}O$ values (Fig. 7a) may be giving a window into local meteoric waters at the time of breccia formation. Calculated $\delta^{18}O_{water}$ values for these samples range from approximately -8 to -3 ‰(Fig. 11). The $\delta^{18}O_{water}$ values correspond to calculated δD values of -54 to -14 ‰[3] assuming ancient and modern meteoric waters are comparable and that there were no local affects on isotopic compositions by geographic parameters (e.g. temperature, latitude, altitude; Sheppard, 1986). By analogy with present-day meteoric water patterns

[3] $\delta D = 8\delta^{18}O + 10$ (*cf.* Sheppard, 1986)

these values would require temperate (to arctic) latitudes (Sheppard, 1986). Paleogeographic reconstructions for the Proterozoic are ambiguous (*cf.* Moores, 1991; Karlstom *et al.*, 1999; Pisarevsky *et al.*, 2003) and it is not possible to determine if these values are reasonable for meteoric water of Proterozoic age. However, in general, the high salinity of Wernecke Breccia fluids is not consistent with a dominantly meteoric water source for the fluids.

Formation water/metamorphic water: Calculated δD_{water} and $\delta^{18}O_{water}$ values for Wernecke Breccia samples fall in the overlapping area between high temperature formation waters (these predominate at the heavy $\delta^{18}O$ end of this field) and metamorphic waters (Fig. 11). Thus, an origin as evolved formation water would be consistent with most of the calculated isotopic ratios.

Magmatic waters: Several of the samples have δD–$\delta^{18}O$ fluid values that fall within the magmatic fields on Figure 11. Magmatic waters are considered less likely as a fluid source than other sources because there are no magmatic rocks of appropriate age in the Wernecke area, but devolatilization of magmas beneath the WSG is geologically feasible. The breccias are spatially associated with BPRI however the *ca.* 1600 Ma age of Wernecke Breccia rules out a genetic link between BPRI magmatism (*ca.* 1710 Ma) and breccia/mineralizing fluids (Thorkelson *et al.*, 2001a,b). The age of the Slab volcanics is unknown however, they occur as clasts within Wernecke Breccia and so must also be older than the breccia (Thorkelson, 2000). High temperature volcanic vapour is also considered a less likely fluid source because no vapour-rich fluid inclusions were observed in the breccia samples; however, this could simply reflect trapping conditions.

Constraints from carbon and oxygen isotope data

Dissolution of limestone/dolostone and oxidation of organic matter are possible sources of carbon for hydrothermally precipitated carbonates (*cf.* Ohmoto and Rye, 1979; Giuliani *et al.*, 2000) associated with Wernecke Breccia. Magmatic waters as a source are considered less likely for reasons already discussed. Limestone/dolostone can provide CO_2 to hydrothermal fluids through dissolution and decarbonation reactions (Ohmoto and Rye, 1979). At high temperatures (> ~ 200°C) dissolution reactions should produce CO_2 that is isotopically similar to that of the original carbonate (*ibid*), i.e. $\delta^{13}C_{CO_2}$ produced by dissolution ≈ $\delta^{13}C$ of the limestone/dolostone (*ibid*). Decarbonation reactions may produce $\delta^{13}C$ enriched CO_2 (*ibid*). Organic components in sediments

typically have low $\delta^{13}C$ values (approx. -35 to -10 ‰) and oxidation of this material produces CO_2 with a similar isotopic composition (*cf.* Ohmoto and Rye, 1979; Ganor *et al.*, 1994). Thus, carbonates with $\delta^{13}C$ values approaching those of limestone/dolostone would precipitate from fluids containing carbon derived from limestone dissolution and carbonates with low $\delta^{13}C$ values would precipitate from fluids containing CO_2 derived from the oxidation of organic matter (*ibid*).

$\delta^{13}C$ values for carbonaceous shale in the Quartet Group range from -26.7 to -20.8 ‰. Calcite precipitated from the oxidation of this organic matter would have $\delta^{13}C$ values of -16.9 to -11.0 ‰ at Slab (300 ^{o}C), -16.5 to -10.6 ‰ at Hoover (285 ^{o}C), -14.9 to -9.0 ‰ at Slats-Frosty (235 ^{o}C), -18.1 to -12.2 ‰ at Igor (350 ^{o}C) and -12.9 to -7.0 ‰ at Olympic (185 ^{o}C) based on the fractionation factors of Chacko *et al.* (1991) for calcite-graphite; data are not available for other carbonate compositions at these temperatures. Measured $\delta^{13}C$ values for carbonates are higher than these values at all of the prospects (Table 2), thus organic matter is unlikely to have been the main source of carbon for the hydrothermal precipitates. However, low $\delta^{13}C$ values returned by veins that cut carbonaceous shale at the Hoover and Slats-Frosty prospects may have formed from fluid that contained minor amounts of carbon derived from organic matter in addition to carbon from limestone/dolostone sources (see below).

Carbon isotopic ratios for limestone/dolostone of the WSG range from -2.0 to 1.6 ‰(Table 2). Calculated $\delta^{13}C$ values for carbonate precipitated from a 200 to 300^{o}C fluid that contained carbon derived by dissolution of WSG limestone/dolostone range from -4.0 to 1.4 ‰for calcite and -3.3 to -1.2 ‰for dolomite – based on $\delta^{13}C_{\text{carbonate mineral}} = \delta^{13}C_{CO_2} + \Delta_{\text{carbonate mineral} - CO_2}$, which is valid for temperatures ≤ 300^{o}C, and fractionation factors for calcite-CO_2 and dolomite-CO_2 (Ohmoto and Rye, 1979). $\delta^{13}C$ values for hydrothermal carbonates from the prospects studied (Table 2) are similar to the calculated values suggesting dissolution of carbonates was the main source of carbon in the fluid. The influence of WSG strata on the isotopic composition of the fluid is also reflected in the $\delta^{18}O$ results for the hydrothermal carbonates, i.e. they are similar to those of the host rocks (Figs. 7 & 8).

Constraints from sulphur isotopes

Sulphur in hydrothermally precipitated sulphide and sulphate minerals associated with Wernecke Breccia could have been derived from several sources including: seawater, host sedimentary and igneous rocks and magmatic fluids. There is a wide spread in

sulphur isotopic ratios for the prospects studied and no sulphur reservoir is clearly defined (Fig. 10). Constraints on possible sulphur sources can be obtained from sulphur isotope contours on a log fO_2 versus pH diagram using the method of Ohmoto (1972). This approach was used at the Slab prospect as it had been examined in more detail than the other prospects in the study. Values of $\delta^{34}S$ were calculated for pyrite that would have precipitated from the fluid at Slab assuming: 1) a seawater/sedimentary source and 2) a magmatic source for sulphur. No published sulphur isotope contours were available for fluid conditions similar to those at Slab (i.e. highly saline, 300 ^oC fluids at 2.5 kb) and new diagrams were constructed as described below.

Oxygen and sulphur fugacity conditions were estimated by examining the mineral assemblages present. At Slab, magnetite (Slab stage 2) is replaced by hematite, but continues to occur in minor amounts in later paragenetic stages (Fig. 3a; Hunt *et al.*, 2005). The hematite occurs with pyrite and both are overprinted by chalcopyrite (Slab stages 3 & 4); pyrrhotite and bornite are not present. This assemblage indicates the oxygen and sulphur fugacity of the fluids changed through time but remained close to the magnetite-hematite-pyrite triple junction. Construction of an oxygen fugacity versus sulphur fugacity diagram at pressure (2.5 kb) and temperature (300 ^oC) appropriate for Slab fluids shows that in order for the above mineral assemblage to occur log fO_2 and log fS_2 values are limited to approximately -31 to -30 and -10 to -7 respectively (Fig. 13). The presence of calcite and/or ankerite, and the absence of graphite or anhydrite, with the above mineral assemblage puts constraints on possible CO_2 fugacity values and limits them to log $fCO_2 > -1$ and < 2 (Fig. 13).

pH versus log fO_2 diagrams (Fig. 14) were constructed for activities of H_2S determined from the range of sulphur fugacity values identified above. Sulphur isotope contours were constructed, as outlined in Ohmoto (1972), for the middle of this range and are shown on Fig. 14a. Expected pyrite $\delta^{34}S$ values were calculated for the contours assuming the initial source of sulphur was: 1) magmatic with $\delta^{34}S = 0$ ‰(*cf.* Ohmoto and Goldhaber, 1997) and 2) Paleoproterozoic seawater with $\delta^{34}S = 18$ ‰(Strauss, 1993). Calculated $\delta^{34}S_{pyrite}$ values that fall within fluid conditions at Slab (i.e. near the triple junction) range from about -22 to -15 ‰ for a magmatic source of sulphur and from -3.4 to +3.6 ‰ for a seawater source of sulphur (Fig. 14a). Measured sulphur isotope values for pyrite at Slab range from -5.8 to +7.1 ‰, similar to those calculated for a seawater source of sulphur. Thus, in the Slab area sulphur isotope results indicate that the source of sulphur was likely non-magmatic and may have been derived from

seawater or sediments/evaporite deposits precipitated from that seawater as these would have a similar isotopic composition to the seawater (*cf.* Strauss, 1997).

The wide range of $\delta^{34}S$ values at Slab may be due to small changes in fO_2 and/or pH because fluid conditions occur where the $\delta^{34}S$ contours are close together (Fig. 14a), hence sulphide minerals precipitated from the fluid may exhibit a large variation in $\delta^{34}S$ values that reflect only a slight variation in fO_2 or pH in the hydrothermal fluids (Ohmoto, 1972). Variability in $\delta^{34}S$ values from the Hoover, Slats, Igor and Olympic prospects may also be due to changes in fO_2 or pH in the hydrothermal fluids however, further data is required to determine this.

Constraints from composition

Fluid inclusion data indicate Wernecke Breccia fluids are high salinity (24-42 wt. % NaCl eq.) NaCl-$CaCl_2$-H_2O brines. This is consistent with their derivation from an evaporite-bearing sedimentary sequence deposited at a continental margin (*cf.* Yardley and Graham, 2002). Thus, derivation of the fluid from the shallow marine, halite-bearing WSG is plausible.

C.7 Conclusions

Fluid inclusion analyses of Wernecke Breccia samples allowed the estimation of PTX characteristics for the breccia forming-IOCG mineralizing fluids. Estimates of fluid pressure determined from fluid inclusion data are in reasonable agreement with those based on the thickness of overlying stratigraphy and vary from approximately 0.4 to 2.4 kb. Pressure adjusted fluid temperatures range from about 185 to 350 ^{o}C (Table 7). Mineral assemblages and cross-cutting relationships observed at all of the IOCG prospects indicate fluid conditions were close to the magnetite-hematite-pyrite triple junction during brecciation. The fluids are high salinity (24-42 wt. % NaCl equiv.) NaCl-$CaCl_2$-H_2O brines with compositions that appear to reflect those of the host strata. For example, at the Slab prospect which is hosted by upper FLG that contains metaevaporites (metahalite; Hunt *et al.*, 2005) the fluids are dominated by Na. Fluids at the Olympic prospect which is hosted by GLG dolostone are dominated by Ca.

Hydrogen isotope data indicate the source of fluids that formed Wernecke Breccia and associated IOCG mineralisation was most likely formational/metamorphic water mixed with variable amounts of low δD (e.g. organic) water ± evolved meteoric

water and/or evolved seawater (Fig. 11). The $\delta^{13}C$ values of hydrothermal carbonates indicate the carbon was derived in large part from the host WSG (Fig.7; Table 2). The $\delta^{34}S$ values of hydrothermal pyrite, chalcopyrite and barite point to seawater (or sediments/evaporites deposited from seawater) as a likely source for much of the sulphur (Fig. 14) with possible additional sources from the leaching of biogenic pyrite and/or sulphides in local igneous rocks (BPRI and/or Slab volcanics). The high salinity of the fluid is consistent with derivation from an evaporite-bearing sedimentary sequence deposited at a continental margin (Yardley and Graham, 2002).

Taken together these results suggest fluid that formed Wernecke Breccia and associated IOCG mineralisation was dominantly formation-metamorphic water. This is similar to the evaporitic-source model proposed by Barton and Johnson (1996, 2000). Wernecke Breccias have the features indicative of an "evaporitic component", i.e. direct association with an evaporite-bearing basin, voluminous sodic alteration and geochemical data that point to evaporitic rather than magmatic fluids. In Barton and Johnson's (1996, 2000) model evaporitic sources provide the chloride necessary for the transport of metals that are derived from igneous rocks. The source of metals in Wernecke Breccia fluids is unknown but it may have been derived from the host rocks. Mafic to intermediate BPRI and/or the Slab volcanics locally contain disseminated chalcopyrite and/or malachite and could have acted as a source of copper. Published geochemical analyses for BPRI and Slab volcanics indicate Cu contents of 2.7 to 2124 ppm (n = 20) and 10.2 to 11.6 ppm (n = 2) respectively (Thorkelson, 2000). However, the samples analysed were collected from locations proximal to Wernecke Breccia and the results may not represent background values. Geochemical analyses reported for unmineralized samples of WSG (Goodfellow, 1979; Lane, 1990; Thorkelson, 2000) indicate that, at least in part, the FLG and Quartet Group contain elevated levels of Cu, U and Co. Values range from - FLG: Cu = 3-890 ppm (n = 15, avg. = 75 ppm), U = 0.7-40 ppm (n = 10, avg. = 8 ppm) and Co = 1-24 ppm (n = 15, avg. = 12 ppm); and Quartet Group: Cu = 5-1230 ppm (n = 24, avg. = 72 ppm), U = 1.2-18.4 ppm (n = 19, avg. = 4) and Co = 3-27 ppm (n = 24, avg. = 11 ppm). Background values in the GLG are lower than those in the FLG and Quartet Group (*ibid*) and range from: Cu = 5-22 ppm (n = 14, avg. = 9 ppm), U = 0.6-5 ppm (n = 14, avg. = 2 ppm) and Co = 2-11 ppm (n = 14, avg. = 5 ppm). Thus, fluid could have leached metals from the FLG and Quartet Group rocks.

The Barton and Johnson (1996, 2000) model invokes magmatism as the source of heat to drive fluid circulation and generate the required high temperatures. This is problematic in the Wernecke Mountains where no intrusive rocks of appropriate age are known. Previous authors (*cf.* Thorkelson, 2000 for a review) have suggested buried intrusive as the source of heat. Another possible solution that would form fluids with the required high temperatures is to use a simple burial model. An average geothermal gradient of 25-30 ^{o}C/km (*cf.* Raymond, 1995, 2000) and a surface temperature of 25 ^{o}C would produce temperatures of 250 to 295 ^{o}C at depths of 7 to 9 km. The geothermal gradient may have been higher than average in the Wernecke Mountains area because it is postulated to have been a rifting/extensional environment during deposition of WSG and emplacement of BPRI (Thorkelson, 2000; Thorkelson *et al.*, 2001a). Wernecke Breccias were formed syn- to post-deformation (Thorkelson, 2000; Hunt *et al.*, 2005), thus fluid circulation could have been driven by tectonic processes.

Constrained by these new geochemical parameters, the genesis of Wernecke Breccia and associated IOCG mineralisation appears independent of a magmatic cycle and is likely related to temporal evolution of the basin. The circulation of high salinity brines, formed in part from dissolution of evaporites, being derived by deformation and mobilizing mineralizing components from the enclosing rocks. The emerging hypothesis is that periodic (tectonic-stratigraphic) over-pressuring of the fluids led to repeated brecciation and mineral precipitation within hydraulic breccias, vein networks and disseminations. Fluids that formed Wernecke Breccia are perhaps therefore similar to high temperature oil field brines, or to brines that formed emerald deposits in Columbia, the salinity of which is due to dissolution of evaporites (*cf.* Banks *et al.*, 1995; Cheilletz and Giuliani, 1996; Giuliani *et al.*, 2000). Wernecke Breccia-related fluids may also be similar to mineralizing brine described by Knutson *et al.* (1979) from the breccia-hosted Redbank copper deposits in the Northern Territory of Australia. The brine is interpreted to have been derived from sedimentary units and possibly seawater based on C and S isotopic data that indicate their source was the host sedimentary and igneous rocks (*ibid*). The circulation of this non-magmatic brine through fractured igneous and sedimentary rocks led to the precipitation of copper mineralisation within permeable breccia zones (*ibid*). However, the Redbank deposit differs from Wernecke Breccia in that the breccia pipes are interpreted to be the result of the explosive release of fluids from magma with mineralisation precipitated later from circulating non-magmatic fluids (*ibid*).

If, as is indicated by the new fluid data, Wernecke Breccia-related IOCG mineralisation is independent of magmatism this has implications in the search for IOCG deposits on a broader scale. Traditionally, exploration for IOCG deposits has focussed on areas where brecciation is temporally related to magmatism. However, the new information obtained from Wernecke Breccia suggests IOCG mineralisation may also be found in thick sedimentary sequences (thick enough to produce high temperature basinal fluids) that contain sources of metals (host sedimentary of igneous rocks), a source of chloride (evaporites) for metal transport and traps (e.g. breccia zones) for metal precipitation, plus a mechanism to drive fluid flow (e.g. tectonics, gravity).

C.8 References:

Archer A, Bell RT, Delaney GD and Godwin CI (1977).Mineralized breccias of Wernecke Mountains Yukon. Geological Association of Canada Program with Abstracts, 2:5.

Banks DA, Yardley BWD, Cheilletz A, Giuliani G and Rueda F (1995) Chemistry and source of high temperature brines in the Colombian emerald deposits. In: Pasava J, Kribek B and Karel Z (eds.) Mineral Deposits: from their origin to their environmental impacts. Proceedings of the third biennial SGA meeting, Prague. AA Balkema, Rotterdam, pp. 557-560.

Barton MD and Johnson DA (2000) Alternative brine sources for Fe-Oxide(-Cu-Au) systems: implications for hydrothermal alteration and metals. In: Porter TM (ed.) Hydrothermal Iron Oxide Copper-Gold & Related Deposits: A Global Perspective, Volume 1, PGC Publishing, Adelaide, pp. 43-60.

Barton MD and Johnson DA (1996) Evaporitic-source model for igneous-related Fe oxide-(REE-Cu-Au-U) mineralisation. Geology 24:3:259-262.

Bell RT (1986a) Megabreccias in northeastern Wernecke Mountains, Yukon Territory. Current Research, Part A, Geological Survey of Canada, Paper 86-1A, pp 375-384.

Bell RT (1986b) Geological map of north-eastern Wernecke Mountains, Yukon Territory. Geological Survey of Canada, Open File 1027.

Bell RT (1978) Breccias and uranium mineralisation in the Wernecke Mountains, Yukon Territory – a progress report. Current Research, Part A, Geological Survey of Canada, Paper 78-1A, pp317-322.

Bell RT and Delaney GD (1977) Geology of some uranium occurrences in Yukon Territory. Report of Activities, Part A, Geological Survey of Canada, Paper 77-1A, pp 33-37.

Bethke C (2000) The Geochemist's Workbench software package. University of Illinois, Urbana-Champaign.

Brown PE (1998) Fluid inclusion modeling for hydrothermal systems. In: Richards JP and Larson PB (eds.) Techniques in Hydrothermal Ore Deposits Geology, Reviews in Economic Geology 10, pp 151-171.

Chacko, T., Mayeda, T.K., Clayton, R.N. & Goldsmith, J.R. (1991). Oxygen and carbon isotope fractionations between CO2 and calcite, Geochimica et Cosmochimica Acta 55: 2867-2882.

Chambers LA (1982) Sulphur isotope study of a modern intertidal environment and the interpretation of ancient sulphides. Geochimica et Cosmochimica Acta 46: 721-728.

Chaussidon M, Albarede F and Sheppard SMF (1989) Sulphur isotope variations in the mantle from ion microprobe analysis of micro-sulphide inclusions. Earth and Planetary Science Letters 92: 144-156.

Cheilletz A and Giuliani G (1996) The genesis of Colombian emeralds: a restatement. Mineralium Deposita 31:359-364.

Delaney GD (1981) The Mid-Proterozoic Wernecke Supergroup, Wernecke Mountains, Yukon Territory; In: Proterozoic Basins of Canada, Geological Survey of Canada, Paper 81-10, pp 1-23.

Donnelly T, Waldron S, Tait A, Dougans J and Bearhop S (2001) Hydrogen isotope analysis of natural abundance and deuterium-enriched waters by reduction over chromium on-line to a dynamic dual inlet isotope-ratio mass spectrometer. Rapid Communications in Mass Spectrometry 15:1297-1303.

Epstein S (1970) Antarctic ice sheet: stable isotope analysis of Byrd Station coves and interhemispheric climactic implications. Science 168: 570-572.

Epstein S, Sharp RP and Gow AJ (1965) Six-year record of hydrogen and oxygen isotope variation in South Pole fur. Journal of Geophysical Research 70: 1809-1814.

Fallick AE, Macaulay CI and Haszeldine RS (1993) Implications of linearly correlated oxygen and hydrogen isotopic compositions for kaolinite and illite in the magnus sandstone, North Sea. Clays and Clay Minerals 41:2:184-190.

Gabrielse H (1967) Tectonic evolution of the northern Canadian Cordillera. Canadian Journal of Earth Sciences, 4:271-298.

Ganor J, Matthews A and Schliestedt M (1994) Post-metamorphic low $\delta^{13}C$ in the Cycladic complex (Greece) and their implications for modelling fluid infiltration processes using carbon isotope compositions. European Journal of Mineralogy 6:365-379.

Giggenbach WF (1992) Magma degassing and mineral deposition in hydrothermal systems along convergent plate boundaries. Economic Geology 87: 1927-1944.

Gillen D, Baker T and Hunt JA (2004) Fluid inclusion studies in Fe-oxide Cu-Au deposits, Wernecke Mountains. In: McPhie J and McGoldrick P (eds), 17th Australian Geological Convention, Hobart, Dynamic Earth: Past, Present and Future, Geological Society of Australia, Abstracts 73, pp 82.

Giuliani G, France-Lanford C, Cheilletz A, Coget P, Branquet Y and Laumomnier B (2000) Sulfate reduction by organic matter in Colombian Emerald deposits: chemical and stable isotope (C,O,H) evidence. Economic Geology 95: 1129-1153.

Graham CM and Harmon RS (1983) Stable isotope evidence on the nature of crust-mantle interactions. In: Hawkesworth CJ and Norry MJ (eds) Continental Basalts and Mantle Xenoliths. Shiva, Nantwich, pp. 20-45.

Graham CM, Harmon RS and Sheppard SMF (1984) Experimental hydrogen isotope exchange between amphibole and water. American Mineralogist 69:128-138.

Goodfellow WD (1979) Geochemistry of copper, lead and zinc mineralisation in Proterozoic rocks near Gillespie Lake, Yukon. Geological Survey of Canada Paper 79-1A: 333-348.

Golyshev SI, Padalko NL & Pechenkin SA (1981) Fractionation of stable oxygen and carbon isotopes in carbonate systems. Geochemistry International 18:85-99.

Hedenquist JW, Arribas A(Jr) and Reynolds TJ (1998) Evolution of an intrusion-centred hydrothermal system: far southwast Lepanto porphyry and epithermal Cu-Au deposits, Philippines. Economic Geology 93:4:373-404.

Hitzman MW, Oreskes N and Einaudi MT (1992) Geological characteristics and tectonic setting of Proterozoic iron oxide (Cu-U-Au-REE) deposits. Precambrian Research 58:241-287.

Hitzman MW (2000) Iron oxide-Cu-Au deposits: what, where, when, and why? In: Porter TM (ed) Hydrothermal iron oxide copper-gold & related deposits: a global perspective, volume 1, pp. 9-25.

Hoefs J (1987) Stable Isotope Geochemistry. 3rd edition, Spriner-Verlag, Berlin.

Hunt JA, Laughton JR, Brideau M-A, Thorkelson DJ, Brookes ML and Baker T (2002) New mapping around the Slab iron oxide-copper-gold occurrence, Wernecke Mountains. In: Emond DS, Weston LH and Lewis LL (eds) Yukon Exploration and Geology 2001, Exploration and Geological Services Division, Yukon Region, Indian and Northern Affairs Canada, pp 125-138.

Hunt, JA, Baker, T and Thorkelson, DJ (2005, in press). Regional-scale Proterozoic IOCG-mineralised breccia systems: examples from the Wernecke Mountains, Yukon, Canada. Mineralium Deposita, vol. X, no. x, p. x-x.

Johnson JW, Oelkers EH and Helgeson HC (1992) SUPCRT92: a software package for calculating the standard molal thermodynamic properties of minerals, gases, aqueous species, and reactions from 1 to 5000 bars and 0 to 1000 degrees C. Computers and Geosciences 18: 7: 899-947.

Karlstrom KE, Williams ML, McLelland J, Geissman JW and Ahall K-I (1999) Refining Rodinia: geologic evidence for the Australia-western U.S. connection in the Proterozoic. GSA Today 9:10:1-7.

Kerridge JF, Haymon RM and Kastner M (1983) Sulphur isotope systematics at the 21°N site, East Pacific Rise. Earth and Planetary Science Letters 66:91-100.

Knauth LP and Beeunas MA (1986) Isotope geochemistry of fluid inclusions in Permian halite with implications for the isotopic history of ocean water and the origin of saline formation waters. Geochimica et Cosmochimica Acta 50:419-433.

Knutson J, Fergurson J, Roberts WMB and Donnelly TH (1979) Petrogenesis of copper-bearing breccia pipes, Redbank, Northern Territory, Australia. Economic Geology 74:4:814-826.

Lane RA (1990) Geologic setting and petrology of the Proterozoic Ogilvie Mountains breccia of the Coal Creek Inlier, southern Ogilvie Mountains, Yukon Territory. MSc. Thesis, University of British Columbia, pp. 223.

McCrea T (1950) The isotopic chemistry of carbonates and a paleotemperature scale. Journal of Chemical Physics 18:849-857.

Moores EM (1991) Southwest U.S.-east Antarctic (SWEAT) connection: a hypothesis. Geology 19:425-428.

Norris DK (1997) Geology and mineral and hydrocarbon potential of northern Yukon Territory and northwestern district of Mackenzie. Geological Survey of Canada, Bulletin 422, 401pp.

Ohmoto H (1972) Systematics of sulfur and carbon isotopes in hydrothermal ore deposits. Economic Geology 67:5:551-578.

Ohmoto H (1986) Stable isotope geochemistry of ore deposits. In: Valley JW, Taylor HP Jr and O'Neil JR (eds.) Stable Isotopes in High Temperature Geological Processes, Reviews in Mineralogy, volume 16, Mineralogical Society of America, pp. 491-559.

Ohmoto H and Goldhaber MB (1997) Sulphur and carbon isotopes. In: Barnes HL (ed.) Geochemistry of hydrothermal ore deposits. John Wiley and Sons, New York, USA, pp. 517-612.

Ohmoto H and Lasaga AC (1982) Kinetics of reactions between aqueous sulfates and sulfides in hydrothermal systems. Geochimica et Cosmochimica Acta 46:1727-1745.

Ohmoto H and Rye RO (1979) Isotopes of sulfur and carbon. In: Barnes HL (ed) Geochemistry of hydrothermal ore deposits. John Wiley & Sons, pp. 509-567.

Pisarevsky SA, Wingate MTD and Harris LB (2003) Late Mesoproterozoic (*ca*. 1.2 Ga) palaeomagnetism of the Albany-Fraser orogen: no pre-Rodinia Australia-Laurentia connection. Geophysics Journal International, 155:F6-F11.

Pitzer KS (1991) Activity coefficients in electrolyte solutions. Chapter 3, CRC Press, Boca Raton, Florida.

Potter RW, Clynne MA and Brown DL (1978) Freezing point depression of aqueous NaCl solutions. Economic Geology 73:284-285.

Raymond, J. (2000) Mantle of the earth. In: Sigurdsson H (ed) Encyclopedia of Volcanoes, Academic Press, San Diego, USA, pp 41-54.

Raymond, J. (1995) Petrology: The study of igneous, metamorphic and sedimentary rocks. McGraw-Hill Higher Education, New York, 742p.

Reynolds LJ (2000) Geology of the Olympic Dam Cu-U-Au-Ag-REE deposit. In: Porter TM (ed) Hydrothermal Iron Oxide-Copper-Gold & Related Deposits: A Global Perspective, volume 1, PGC Publishing, Adelaide, pp. 93-104.

Robinson BW and Kusabe M (1975) Quantitative preparation of SO_2 for $^{34}S/^{32}S$ analyses, from sulphides by combustion with cuprous oxide. Analytical Chemistry 47:1179-1181.

Roedder E (1984) Fluid inclusions. Rev Mineral 12:1-644.

Rollinson H (1993) Using geochemical data: evaluation, presentation, interpretation. Longman Group, UK, 352p.

Ryan (1998) Ernest Henry copper-gold deposit. In: Australasian Institute of Mining and Metallurgy Monograph 22, pp. 759-768.

Rye RO and Ohmoto H (1974) Sulfur and carbon isotopes and ore genesis: a review. Economic Geology 69:826-842.

Sharp ZD (1990) A laser-based microanalytical method for the in situ determination of oxygen isotope ratios in silicates and oxides. Geochimica et Cosmochimica Acta 54:1353-1357.

Shepherd TJ and Rankin AH (1998) Fluid inclusion techniques of analysis. In: Richards JP and Larsen PB (eds.) Techniques in Hydrothermal Ore Deposits Geology, Reviews in Economic Geology Volume 10, Society of Economic Geologists, pp. 125-150.

Shepherd TJ, Rankin AH and Alderton DHM (1985) A practical guide to fluid inclusion studies. Blackie & Son Limited, Glasgow, 200pp.

Sheppard SMF (1977) The Cornubian batholith, SW England: D/H and $^{18}O/^{16}O$ studies of kaolinite and other alteration minerals. Journal of the Geological Society 133: 573-591.

Sheppard SMF (1981) Stable isotope geochemistry of fluids. In: Rickard DT and Wickman FE (eds) Chemistry and Geochemistry of Solutions at High Temperatures and Pressures. Physical Chemistry of the Earth 13/14: 419-445.

Sheppard SMF (1986) Characterization and isotopic variations in natural waters. In: Valley JW, Taylor HP Jr and O'Neil JR (eds.) Stable Isotopes in High Temperature Geological Processes, Reviews in Mineralogy, volume 16, Mineralogical Society of America, pp. 165-183.

Sheppard SMF and Schwarcz HP (1970) Fractionation of carbon and oxygen isotopes and magnesium between coexisting metamorphic calcite and dolomite. Contributions to Mineralogy and Petrology 26:161-198.

Shields G and Veizer J (2002) Precambrian marine carbonate isotope database: version 1.1. Geochemistry, Geophysics Geosystems, 3:6, 12pp. An electronic journal of the earth sciences published by AGU and the Geochemical Society

Sillitoe RH (2003) Iron oxide copper-gold deposits: an Andean view. Mineralium Deposita 38:787-812.

Strauss H (1997) The isotopic composition of sedimentary sulphur through time. Palaeogeography, Palaeoclimatology, Palaeoecology 132: 97-118.

Strauss H (1993) The sulphur isotope record of Precambrian sulfates: new data and a critical evaluation of the existing record. Precambrian Research 63:225-246.

Suzuoki T and Epstein S (1976) Hydrogen isotope fractionation between OH-bearing minerals and water. Geochimica et Cosmochimica Acta 40:1229-1240.

Taylor BE (1992) Degassing of H_2O from rhyolite magma during eruption and shallow intrusion, and the isotopic composition of magmatic water in hydrothermal systems. Japan Geological Survey Report 279: 190-194.

Taylor HP (1974) The application of oxygen and hydrogen isotope studies to problems of hydrothermal alteration and ore deposition. Economic Geology 69:843-883.

Thorkelson DJ (2000) Geology and mineral occurrences of the Slats Creek, Fairchild Lake and "Dolores Creek" areas, Wernecke Mountains, Yukon Territory. Exploration and Geological Services Division, Yukon Region, Indian and Northern Affairs Canada, Bulletin 10, 73pp.

Thorkelson DJ, Laughton JR and Hunt JA (2002) Geological map of Quartet Lakes area (106E/1), Wernecke Mountains, Yukon (1:50,000 scale). Exploration and Geological Services Division, Yukon Region, Indian and Northern Affairs Canada, Geoscience map 2002-2.

Thorkelson DJ, Mortensen JK, Creaser RA, Davidson GJ and Abbott JG (2001a) Early Proterozoic magmatism in Yukon, Canada: constraints on the evolution of northwestern Laurentia. Canadian Journal of Earth Science 38:1479-1494.

Thorkelson DJ, Mortensen JK, Davidson GJ, Creaser RA, Perez WA and Abbott JG (2001b) Early Mesoproterozoic intrusive breccias in Yukon, Canada: The role of hydrothermal systems in reconstructions of North America and Australia. Precambrian Research 111:31-55.

Valley JW, Taylor HP Jr. and O'Neil JR (1986) Stable isotopes in high temperature geological processes. Reviews in Mineralogy Volume 16, Mineralogical Society of America, 570p.

Vanko DA, Bodnar RJ and Sterner SM (1988) Synthetic fluid inclusions: VIII. Vapour-saturated haltite solubility in part of the system NaCl-$CaCl_2$-H_2O, with application to fluid inclusions from oceanic hydrothermal systems. Geochimica et Cosmochimica Acta 52:2451-2456.

Yardley BWD and Graham JT (2002) The origins of salinity in metamorphic fluids. Geofluids 2:249-256.

Yukon MINFILE, 2003. Database of Yukon mineral occurrences. Exploration and Geological Services Division, Yukon Region, Indian and Northern Affairs Canada, CD-ROM (2).

Zhang Y-G and Fratz JD (1987) Determination of the compositional limits of immiscibility in H (sub 2) O-CO (sub 2) -CaCl (sub 2) fluids to 600 degrees C and 2.0 kbar using synthetic fluid inclusions. AGU 1987 fall meeting, EOS Transactions, American Geophysical Union 68, 44:1539.

Zheng YF (1993) Calculation of oxygen isotope fractionation in hydroxyl-bearing silicates. Earth and Planetary Science Letters 120:247-263.

Zheng YF (1999) Oxygen isotope fractionation in carbonate and sulfate minerals. Geochemical Journal 33:109-126.

Zwart EW and Touret JLR (1994) Melting behaviour and composition of aqueous fluid inclusions in fluorite and calcite: applications within the system H_2O-$CaCl_2$-NaCl. European Journal of Mineralogy 6:773-786.

SECTION D

Wernecke Breccias, Yukon, Canada: an example of a non-magmatic end-member IOCG system and implications for IOCG genesis and classification

D.1 Abstract

Genetic models for iron oxide-copper-gold (IOCG) systems typically invoke formation from magmatic or hybrid magmatic – non-magmatic fluids. New data from Wernecke Breccia indicates IOCG systems can also form in non-magmatic environments. Bodies of Wernecke Breccia are hosted by Early Proterozoic sedimentary rocks of the Wernecke Supergroup (WSG). The location of the breccias is structurally controlled on a regional and local scale. They occur in weak zones and likely formed during the expansion of over-pressured fluids. IOCG mineralisation occurs as veins and disseminations within the breccia bodies and surrounding WSG and is largely made up of early magnetite and/or hematite and later chalcopyrite and pyrite. The breccia bodies are associated with extensive sodic or potassic metasomatic alteration and they are cut by late-stage carbonate, or rarely, barite veins. Cross-cutting relationships indicate multiple phases of brecciation, alteration and mineralisation have occurred. The breccias were formed by low to moderate temperature (185-350 ^{o}C), moderate to high salinity (24-42 wt % NaCl eq.) brines that were likely derived from basinal/metamorphic fluids. Magmatic waters are considered less likely as a fluid source because isotopic data for the breccias do not have a magmatic signature and spatially associated mafic to igneous rocks are significantly older (i.e. *ca*. 1710 vs. 1600 Ma) thus ruling out a genetic connection. Metals and sulphur were probably derived from host strata and fluids circulated via tectonic (and/or gravity) processes.

Modifications to the definition of IOCG systems are proposed that reflect the degree of involvement of magmatic and/or non-magmatic fluids. A division into magmatic, non-magmatic and hybrid types is suggested. Typical magmatic end-member IOCG deposits include Lightning Creek, Osborne and Eloise. Hybrid examples include Ernest Henry, Olympic Dam and Aitik. Wernecke Breccia and Redbank are representative of non-magmatic end members. End-member magmatic deposits such as Lightning Creek have similarities to some porphyry deposits and non-magmatic end-members share characteristic with some sediment hosted Cu deposits (e.g. Tsumeb, Mount Isa) suggesting the range of IOCG deposits may form a link between intrusive- and sedimentary-related deposits.

D.2 Introduction

The discovery of the giant Olympic Dam deposit (Fig. 1, Table 1) in the 1970's and the ensuing increase in exploration and research aimed at the discovery of similar deposits led to proposals for a new deposit class: iron oxide (Cu-U-Au-REE) deposits (*cf.* Meyer, 1988; Einaudi and Oreskes, 1990; Gandhi and Bell, 1990). A description of general characteristics, was first published in Hitzman *et al.* (1992), based largely on studies of Olympic Dam and prospects in the Stuart Shelf (Australia), the Kiruna district (Sweden), the southeast Missouri iron district (USA) and the Wernecke Breccias (Canada). The definition was refined in Hitzman (2000) and "Kiruna-type" deposits were no longer included, instead magnetite-apatite deposits and iron oxide-Cu-Au (IOCG) deposits were considered to form end members of a continuum.

The IOCG end of the spectrum is loosely defined and incorporates deposits worldwide of Archean to Tertiary age that are linked primarily by the presence of abundant Ti-poor (< 2% TiO_2) magnetite and/or hematite and extensive alteration, particularly Fe-, Na- and K-metasomatism (Hitzman *et al.*, 1992; Hitzman, 2000; Sillitoe, 2003). However, there are also noteworthy differences both between deposits within a district and between districts and this has led to a number of genetic models. Some authors propose formation from dominantly magmatic fluids (*cf.* Hitzman *et al.*, 1992; Pollard *et al.*, 1998; Wyborn, 1998; Skirrow, 1999; Perring *et al.*, 2000; Pollard, 2000, 2001). Others propose magmatic fluid as the main source of metals (and sulphur) but invoke mixing with other fluids, usually cooler, less saline and more oxidising, as the mechanism responsible for metal precipitation (*cf.* Mark *et al.*, 2000; Baker, 1998; Reeve *et al.*, 1990; Marschik and Fontboté, 2001); the contribution made to the metal budget by these additional fluids is not clear. Several authors suggest non-magmatic fluids are *necessary* for the formation of IOCG mineralisation (*cf.* Haynes *et al.*, 1995, Haynes, 2000; Barton and Johnson, 1996, 2000; Barton *et al.*, 2000; Hitzman, 2000) and that magmatism is important primarily as a source of heat to drive hydrothermal convection (Barton and Johnson, 1996; 2000).

New information from Wernecke Breccia-associated IOCG prospects suggests the above spectrum of magmatic and hybrid magmatic–non-magmatic models for IOCG deposits should be expanded to accommodate systems formed in an environment unrelated to magmatism, i.e. IOCG mineralisation formed from non-magmatic fluid circulated by non-magmatic processes. This paper presents a summary of new

information for Wernecke Breccia and explores variations in IOCG systems. To reflect this variability modifications to the definition of IOCG systems are proposed that accommodate the degree of involvement of magmatic and/or non-magmatic fluids and it is suggested that IOCG systems be divided into non-magmatic and magmatic end-members with hybrid IOCG types in between. Brief descriptions are given of the characteristics of typical end-member IOCG deposits and of those that best fit a hybrid IOCG magmatic – non-magmatic model. Such changes will enable the characteristics of individual types to be better delineated, thus providing more narrowly defined attributes to be used in mineral exploration models.

The range of IOCG systems may form a link between intrusive- and sedimentary-related deposits. Those systems dominated by magmatic and magmatic – non-magmatic fluids have been compared to porphyry deposits (*cf.* Pollard, 2000; Barton and Johnson, 2000; Sillitoe, 2003) and the two deposit types considered to form a continuum of intrusive-related deposits (*cf.* Pollard, 2000; Sillitoe, 2003). IOCG systems dominated by highly saline non-magmatic fluids have similarities with some sediment-hosted Cu deposits, e.g. Mount Isa, Zambian Copper Belt. Thus, IOCG systems may provide valuable information that can be used in the study of, and in exploration for, other types of mineral deposits.

D.3 Wernecke Breccia – Canada

Proterozoic Wernecke Breccia is found in areas of the north-central Yukon Territory that are underlain by the Early Proterozoic Wernecke Supergroup (WSG; Fig. 2). The WSG is an approximately 13 km-thick package of marine fine-grained sandstone, siltstone, dolostone and minor limestone (*cf.* Gabrielse, 1967; Delaney, 1981; Bell, 1986b; Thorkelson, 2000) that was metamorphosed to greenschist facies and multiply deformed during the Proterozoic Racklan Orogeny (*cf.* Thorkelson, 2000; Brideau *et al.*, 2002). Bodies of Wernecke Breccia cross-cut the WSG and are made up largely of clasts of the supergroup in a matrix of rock flour and hydrothermal precipitates (Fig. 3; Table 2). At least 65 bodies of Wernecke Breccia are known and all are associated with iron oxide-Cu(±U±Au±Co) mineralisation, including the Slab (Table 1), Hoover, Slats, Igor and Olympic prospects that were examined in this study (Fig. 2). Mineralisation occurs as disseminations and veins within Wernecke Breccia and surrounding WSG rocks and is largely made up of early magnetite and/or hematite and later chalcopyrite

and pyrite (Fig. 3; *cf.* Brookes *et al.*, 2002; Hunt *et al.*, 2002, 2005; Thorkelson *et al.*, 2003; Yukon MINFILE, 2003). Gold-bearing phases were not observed but gold reports with copper in assay results (*cf.* Yukon MINFILE, 2003). Minor uranium (pitchblende, brannerite) and cobalt (cobaltian pyrite, erythrite) mineralisation occurs locally. Gangue is dominantly composed of carbonate (calcite, dolomite, siderite), quartz, albite and K-feldspar with lesser biotite, muscovite, chlorite and fluorite and locally includes minor rutile, epidote (some is allanite), apatite, tourmaline and monazite (*cf.* Brookes *et al.*, 2002; Hunt *et al.*, 2002, 2005). Extensive sodic or potassic metasomatic alteration is spatially associated with the breccia bodies and they are cut by late-stage carbonate veins dominantly composed of calcite and/or dolomite/ankerite that contain minor pyrite and chalcopyrite and trace molybdenite (Fig. 3; Table 3; Hunt *et al.*, 2002, 2005). At the Igor prospect late stage veins are composed dominantly of barite ± siderite.

The breccia bodies are associated with faults on a regional (Richardson Fault array) and local scale (Fig. 2; *cf.* Bell, 1978, 1986a,b; Bell and Delaney, 1977; Thorkelson, 2000) and were emplaced into weak zones such as fault and shear zones, fold axes and lithological contacts during the expansion of over-pressured fluids (Hunt *et al.*, 2005; Section A). Wernecke Breccia occurs throughout the WSG but is most abundant in the lower part of the stratigraphy (Delaney, 1981; Lane, 1990) where there is a transition from calcareous sedimentary strata that contain halite facies meta-evaporites to overlying carbonaceous shale (Hunt *et al.*, 2005; Section A). Fluid pressure calculated from fluid inclusion data for breccias at this stratigraphic level ranges from approximately 2.5 to 3 kbars indicting depth of emplacement of about 7.5 to 9.0 km, roughly equivalent to the thickness of overlying WSG strata (see section C for details).

Cross-cutting relationships indicate multiple phases of brecciation and mineralisation occurred after peak metamorphism and syn- to post-deformation (*cf.* Thorkelson, 2000; Brideau *et al.*, 2002; Hunt *et al.*, 2005). The best estimate for the age of Wernecke Breccia comes from a U-Pb (titanite) date of *ca.* 1595 Ma from the matrix of breccia (Slab prospect) emplaced into the FLG, the lowermost unit of the WSG (Thorkelson, 2000; Thorkelson *et al.*, 2001a). This date is supported by *ca.* 1600 Ma Re-Os dates (R. Creaser and D. Selby pers. comm, 2003, 2004) obtained during this study from molybdenite in late-stage carbonate veins at the Slab prospect (see Section B for details).

All Wernecke Breccia prospects examined in this study are spatially associated with Bonnet Plume River intrusions (BPRI). The BPRI are mafic to intermediate in composition and generally form narrow (< 1 to 5 m) dykes and sills and small stocks throughout the study area (Thorkelson, 2000; Thorkelson *et al.*, 2001b). Clasts of the intrusive rocks are locally abundant in Wernecke Breccia and they are thus, clearly older than the breccia bodies (*ibid*). U-Pb (zircon) dating of four BPRI bodies shows they are *ca*. 1710 Ma (Thorkelson *et al.*, 2001b) and thus rules out a genetic link between BPRI magmatism and breccia/mineralising fluids. Clasts of Slab volcanics are also locally abundant in Wernecke Breccia. Attempts at dating the Slab volcanics have been unsuccessful and their age remains poorly constrained. Cross-cutting relationships show they are older than Wernecke Breccia (Thorkelson, 2000; Thorkelson *et al.*, 2001a; Laughton, 2004; Laughton *et al.*, in review) but the difference in age between the timing of breccia emplacement and volcanism is unknown. However, Slab volcanics have been observed only locally (*ibid.*) and thus are unlikely to have been responsible for brecciation that is observed over hundreds of kilometres (Fig. 2).

The coincidence of Wernecke Breccia and BPRI (and Slab volcanics) appears to be a consequence of the use of the same fluid pathways. The coincident location of some *ca*. 1270 Ma dykes of the Bear River suite indicates these fluid pathways were important for hundreds of millions of years. In addition, ductility contrasts between BPRI and host WSG sedimentary rocks may have produced dilational zones during folding that focussed hydrothermal fluids leading to the preferential development of breccia in these sites, similar to the mechanism proposed by Bell *et al.* (1988) for the Mount Isa deposit.

Fluids that formed Wernecke Breccia and the associated mineralisation were low to moderate temperature (185-350 ^{o}C), moderate to high salinity (24-42 wt. % NaCl eq.) NaCl-$CaCl_2$ brines (Fig. 4; Table 4; Hunt *et al.*, 2004; see Section C for details). Carbon isotopic compositions for hydrothermal carbonates at the prospects studied range from: $\delta^{13}C_{carbonate} \approx$ -7 to +1 ‰ (V-PDB) and $\delta^{18}O_{carbonate}$ values are between -2 and 20 ‰ (V-SMOW). Calculated $\delta^{18}O_{fluid}$ values derived from carbonate range from approximately -8 to +14 ‰ (Fig. 5). Sulphur isotope values for hydrothermal pyrite, chalcopyrite and barite range from: $\delta^{34}S_{pyrite/chalcopyrite} \approx$ -13 to +14 ‰ (CDT) and $\delta^{34}S_{barite} \approx$ 7 to 18 ‰ (CDT; Fig. 5). The $\delta^{18}O$ values for hydrothermal carbonates generally reflect those of the host WSG strata and $\delta^{13}C$ values indicate that carbon was derived in large part from the WSG. The $\delta^{34}S$ values of pyrite, chalcopyrite and barite point to a seawater (or

sediments/evaporites deposited from seawater) as a likely source for much of the sulphur with possible additional sulphur from the leaching of biogenic pyrite and/or sulphides in local igneous rocks (Section C). The carbon, oxygen and sulphur isotopic compositions combined with limited hydrogen isotope data indicate fluids were likely derived from formation/metamorphic water mixed with variable amounts of low δD (e.g. organic) water ± evolved meteoric and/or evolved seawater (Section C). The high salinity of the fluid is consistent with derivation from an evaporite-bearing sedimentary sequence (*cf.* Yardley and Graham, 2002). Magmatic waters are considered less likely as a fluid source because the isotopic data do not have a magmatic signature and there are no igneous rocks of appropriate age.

The isotopic signature of Wernecke Breccia fluids and the lack of an obvious intrusive heat source suggest fluid circulation and the high temperatures reached by the fluid(s) occurred via mechanisms other than those related to magmatic heat flow. Temperatures would have increased within the basin during intrusion of the BPRI and throughout prograde metamorphism. The presence of marialitic scapolite in metahalite layers in the lower part of the WSG indicates temperatures reached at least 400 ^{o}C (*cf.* Kwak, 1977) in the deep part of the basin during metamorphism. However, metamorphism occurred prior to brecciation and metamorphic/basinal fluids may have cooled considerably before breccia emplacement and mineralisation occurred. Nevertheless, fluid temperatures in at least the deeper part of the WSG would have been elevated due to the thickness of overlying sediments. A simple burial model would produce fluids with the required high temperatures. An average geothermal gradient of 25-30 ^{o}C (*cf.* Raymond, 1995, 2000) and a surface temperature of 25^{o}C would produce temperatures of 250-295 ^{o}C at depths of 7 to 9 km. The geothermal gradient may have been higher than average in the Wernecke Mountains area because it is postulated to have been a rifting/extensional environment during deposition of the WSG and emplacement of the BPRI (Thorkelson, 2000; Thorkelson *et al.*, 2001b). Cross-cutting relationships indicate Wernecke Breccias were formed syn- to post-deformation (Thorkelson, 2000; Hunt *et al.*, 2005), thus fluid circulation could have been driven by tectonic (and/or gravity) processes (*cf.* Torgerson, 1990; Garven *et al.*, 2001). Another possible mechanism to provide high temperature fluids and drive circulation is the method proposed by Deming (1992) whereby heat is released periodically from continental crust by the onset of free convection in orogenic zones. In this mechanism orogeny increases the permeability of the crust and causes the deep, transitory

circulation of fluids through the upper crust setting up free convection cells. The free convection cells supply a tectonically/gravity-driven flow system periodically with heat (and possibly metals) as they form, release heat from the crust and then die out. Thus the influx of heat is transitory but may be large.

The source of metals that formed IOCG mineralisation associated with Wernecke Breccia is unknown but may have been the host strata. BPRI and Slab volcanics locally contain disseminated chalcopyrite and/or malachite and could have acted as sources of copper. Published geochemical analyses indicate Cu contents of 2.7-2124 ppm and 10.2-11.6 ppm respectively for the BPRI and Slab volcanics (Thorkelson, 2000), however, the samples were collected proximal to Wernecke Breccia and the results may not represent background values. Analyses of reportedly unmineralised samples of WSG (Goodfellow, 1979; Lane, 1990; Thorkelson, 2000) indicate the FLG and Quartet Group contain elevated levels of Cu (up to 1230 ppm), U (up to 40 ppm) and Co (up to 27 ppm; see Section C for details) and thus could have acted as a source of metals.

D.4. IOCG systems

IOCG deposits are highly variable and at present the classification scheme is very broad (*cf.* Hitzman *et al.*, 1992; Hitzman, 2000). A single genetic model is not able to explain all the variations seen within this broad class of deposits and the genesis of IOCG mineralisation is variably interpreted to be related to magmatic (*cf.* Hitzman *et al.*, 1992; Baker, 1998; Rotherham *et al.*, 1998; Pollard, 2000; Sillitoe, 2003), non-magmatic (Section C) or hybrid mixtures (*cf.* Barton and Johnson, 1996, 2000; Haynes, 2000; Hitzman, 2000) of fluids. Narrower definitions of IOCG systems would be useful for mineral exploration and research purposes and could be facilitated by dividing up the broad spectrum of deposits. A division into magmatic and non-magmatic end-member IOCG systems with hybrid IOCG systems in between is suggested to reflect the various genetic models (Fig. 6). The proposed division is based on new data for Wernecke Breccia and on existing studies in other areas that include temperature, salinity, fluid composition and stable isotope data. It is intended to reflect the degree of involvement of magmatic fluids and of non-magmatic fluids such as formation and metamorphic waters, (evolved) seawater and/or meteoric waters. The environment of formation, i.e.

magmatic or non-magmatic, is also taken into account in this classification scheme as shown in the lower part of figure 6.

D.4.1 End-member non-magmatic IOCG systems

New geological, fluid inclusion and stable isotope data indicate IOCG mineralisation associated with Wernecke Breccia formed from highly saline non-magmatic fluid (Section C). Ore fluids were low to moderate temperature brines derived from basinal or metamorphic fluids, (evolved) seawater and/or meteoric water that were circulated by tectonic, gravity and/or density related processes. Sulphur isotope values are more consistent with an evaporitic rather than a magmatic source for sulphur. Metals may have been leached from host strata, transported as chloride complexes and precipitated due to changes in temperature, pressure and fluid-rock interaction when fluid expanded forming breccia and possibly subsequently as fluid flowed through the high permeability breccia zones and mixed with meteoric and/or seawater.

Other possible non-magmatic end-member systems include deposits in the Tennant Creek Inlier and Redbank areas of the Northern Territory of Australia (Fig. 1). Tennant Creek mineralisation is interpreted by some authors to have formed from metamorphic/ formation water (*cf.* Large, 1975; Skirrow and Walshe, 2002) and at Redbank isotopic data indicate carbonate and sulphide minerals related to copper mineralisation were deposited from non-magmatic fluids (Knutson *et al.*, 1979). Although there is a spatial relationship with igneous rocks in both areas no genetic connection has been demonstrated.

The Salton Sea geothermal system, where iron oxide-Cu-REE-Co-Au mineralisation is precipitated from evaporite-derived brines may be a modern analogue of a non-magmatic system (*cf.* McKibben and Hardie, 1997; Barton and Johnson, 2000). However, it occurs in a magmatic environment and fluid is interpreted to be circulated by igneous-driven convection (*ibid*). Thus, it cannot be considered an end-member non-magmatic IOCG system, but would lie between hybrid IOCG systems and end-member non-magmatic IOCG systems.

Tennant Creek - Iron oxide-associated Au(-Cu-Bi) mineralisation in the Tennant Creek area, e.g. the West Peko and Eldorado deposits (Table 1), occurs within *ca.* 1860 Ma (*cf.* Compston, 1995) weakly metamorphosed greywacke, siltstone and shale of the

Warramunga Formation (Table 2; *cf.* Large, 1975; Skirrow and Walshe, 2002). Magnetite (and/or hematite)-chlorite-quartz ± talc ± carbonate ironstone bodies occur within the sedimentary rocks in dilatent zones that were generated by shearing and folding during the *ca.* 1860-1840 Ma Barramundi orogeny (*cf.* Skirrow and Walshe, 2002). Au(-Cu-Bi) mineralisation overprinted selected ironstones during later deformation (at or before *ca.* 1830-1825 Ma) and appears to be structurally controlled (*cf.* Wedekind and Love, 1990; Huston *et al.*, 1993; Skirrow and Walshe, 2002). For example, the West Peko deposit is proximal to the axis of a regional-scale syncline and the Eldorado deposit is located within parasitic folds on the limb of a regional-scale anticline (Skirrow and Walshe, 2002).

Mineralisation ranges from reduced to oxidised and occurs as: 1) magnetite-pyrrhotite-pyrite Cu-rich deposits; 2) magnetite-dominant Au-Bi deposits and 3) hematite-dominant Au deposits (*ibid*). At West Peko the central parts of two magnetite-hematite-quartz-chlorite ironstone bodies were overprinted by sulphides (pyrrhotite, chalcopyrite ± pyrite), gold, chlorite ± stilpnomelane ± minnesotaite ± talc ± siderite and ± calcite resulting in lenses and zones of (reduced) chalcopyrite-gold-bismuthinite mineralisation (Table 3; *ibid*). At the Eldorado deposit hematite-magnetite-quartz ironstone occurs as discontinuous, discordant bodies proximal to hematitic shale and siltstone units of the Warramunga Formation (*ibid*). Au-Bi (oxidised) mineralisation occurs near a change in the trend of the ironstones and occurs mainly in stringer and breccia zones that broadly correlate with areas of pervasive silicification and zones of higher magnetite/(hematite + martite; *ibid*).

The ironstone bodies formed from hot (350-400 ^{o}C) NaCl + $CaCl_2$ brines (probably formation waters) at pressures of approximately 2.5 to 5 kbars (Fig. 4; Wedekind and Love, 1990; Skirrow and Walshe, 2002). Au-Cu-Bi mineralisation at the West Peko deposit is interpreted to have formed from pyrrhotite ± magnetite-stable, 300-340 ^{o}C, weakly acidic, sulphur- and N_2±CH_4-rich, low salinity (3-10 wt% NaCl eq.) hybrid metamorphic–formation water(s) as it reacted with pre-existing magnetite ± hematite-rich ironstone (Fig. 4; Table 4; Skirrow and Walshe, 2002). Fluid flowed along shear and fault zones that tapped reduced rock packages (that may have included mafic and felsic rocks) beneath the oxidised Warramunga Formation (Skirrow, 1999; Skirrow and Walshe, 2002). The deposition of gold and native bismuth likely occurred due to desulphidation ± oxidation of the reduced fluid as it reacted with ironstone. Desulphidation of the fluid was likely driven by precipitation of chalcopyrite, pyrite,

pyrrhotite, and Bi sulphides or sulphosalts in response to increased pH of the fluids (*ibid*). Eldorado mineralisation is interpreted to have formed from intermediate fO_2, low to moderate salinity ore fluid (a variant of the reducing fluid that formed West Peko mineralisation) that mixed with hematite-stable Ca-Na-Cl brine in the presence of pre-existing magnetite-rich ironstone (Skirrow and Walshe, 2002). Fluid mixing likely caused an increase in copper solubility leading to undersaturation of copper minerals and the deposition of gold-bismuth mineralisation without copper phases (*ibid*).

The mechanism of fluid circulation and the source of heat and metals for the Tennant Creek deposits are not clear (*cf.* Large, 1975; Wedekind and Love, 1990; Skirrow and Walshe, 2002). The West Peko deposit occurs several hundred metres above a 300-500 m-thick stratiform quartz-potassium feldspar-plagioclase porphyry and geophysical data for the Eldorado area indicate granite occurs nearby (Skirrow and Walshe, 2002), however the age of the intrusive rocks is not well constrained, hence their role as a potential heat or metal source is not known. The deposits are associated with regional-scale structures and Au(-Cu-Bi) mineralisation occurred during deformation (*cf.* Wedekind and Love, 1990; Skirrow and Walshe, 2002) suggesting fluid flow may have been driven by tectonic and/or gravity processes. Metals may have been derived from the host sedimentary strata and/or igneous rocks as fluid flowed along shear and fault zones.

Redbank – IOCG prospects in the Redbank area (Fig. 1) are hosted by sedimentary and volcanic rocks of the Paleoproterozoic Tawallah Group (< 1780 to 1720 Ma) in the McArthur Basin (Knutson *et al.*, 1979; Jackson and Southgate, 2000; Betts *et al.*, 2003). Mineralisation occurs within breccia pipes located along a series of basement faults (Orridge and Mason, 1975). Approximately 50 pipes have been recognised and significant copper mineralisation occurs in several, e.g. Bluff and Sandy Flat (Table 1; Knutson *et al.*, 1979). Chalcopyrite and minor covellite and chalcocite occur as breccia infill and as veins and disseminations in breccia clasts and host rocks; sulphur isotope values for chalcopyrite range from $\delta^{34}S \approx 4$ to 16 ‰ (*ibid*). Brecciation was accompanied by pervasive potassium and iron metasomatism and abundant K-feldspar, hematite and chlorite occurs in breccia and host strata (*ibid*). Mineralisation is associated with carbonate alteration and isotopic values for hydrothermal dolomite range from $\delta^{13}C$ = -4.6 to +3.2 ‰and $\delta^{18}O$ = 13.1 to 22.6 ‰, indicating a fluid temperature of 150-300°C (*ibid*). The carbon and oxygen isotopic compositions reflect

those of the host strata and fluid related to the copper mineralisation was probably derived from the sedimentary units (*ibid*). Sulphur was likely derived from marine sulphate and dissolved sedimentary and magmatic sulphides; copper may have been leached from host sedimentary and igneous strata (*ibid*).

D.4.2 End-member magmatic IOCG systems

IOCG deposits at the magmatic end of the spectrum formed from ore fluids with a dominantly magmatic origin and are typified by deposits such as Lightning Creek, Osborne and Eloise (Tables 1 to 4; Fig. 1). The deposits are generally temporally associated with igneous rocks, e.g. Lightning Creek (*cf.* Perring *et al.*, 2000). However, exposed, coeval igneous rocks are not always present and the presence of buried intrusions may be inferred from geophysical data, for example at Eloise (Baker, 1998). Fluid was moderate to high temperature, saline (Fig. 4; Table 4), probably a source of metals, and circulated by heat from magmatism (*cf.* Adshead *et al.*, 1998; Pollard, 2000, 2001). Isotopic values indicate sulphur and fluids were derived from a magmatic source (Fig 5).

Lightning Creek, Osborne and Eloise: regional setting – The Lightning Creek, Osborne and Eloise deposits are located in the Cloncurry district of Australia in the eastern part of the Mount Isa inlier (Fig. 1; *cf.* Adshead *et al.*, 1998; Williams and Skirrow, 2000). They occur within an intracratonic basin (Table 2) that consists of metamorphosed pelitic, psammitic, calcareous and evaporitic sedimentary rocks and felsic and basic volcanic rocks (*cf.* Beardsmore *et al.*, 1988; Blake and Stewart, 1992) that have been divided into three superbasin sequences: Leichhardt (*ca.* 1800-1750 Ma), Calvert (*ca.* 1730-1690 Ma) and Isa (*ca.* 1670-1575 Ma; *cf.* Southgate *et al.*, 2000; Scott *et al.*, 2000). Deformation and metamorphism of the host rocks occurred during the Diamantina (*ca.* 1600 Ma) and Isan orogenies (*ca.* 1550-1500 Ma; *cf.* O'Dea *et al.*, 1997; Betts *et al.*, 1998; Laing, 1998; MacCready *et al.*, 1998) and significant granitoid igneous activity occurred *ca.* 1550 Ma and *ca.* 1540-1500 Ma (Page and Sun, 1998; Pollard *et al.*, 1998; Wyborn, 1998). Intense, widespread sodic-calcic alteration is temporally and spatially associated with emplacement of the intrusions and is concentrated along regional-scale, deep-seated structures such as the Cloncurry fault (*cf.* De Jong and Williams, 1995; Mark and De Jong, 1996).

Lightning Creek – The Lightning Creek prospect is hosted by a suite of *ca.*1540-1500 Ma (Page and Sun, 1998) intrusive rocks (Table 2; Perring *et al.*, 2000). The suite is largely made up of porphyritic quartz monzodiorite (that contains enclaves of quartz diorite) intruded by porphyritic monzogranite and fine-grained alkali feldspar granite (*ibid*). High temperature (> 500 ^{o}C) waters with a composition similar to primary magmatic fluid caused widespread sodic-calcic alteration of the host rocks and removed K, Fe, Cl and Cu (Fig. 4; Tables 3, 4; *ibid*).

Quartzofeldspathic and aplitic sills that are interpreted to be late-stage differentiates cut the altered intrusive rocks (Perring *et al.*, 2000). The sills crystallised at temperatures > 500^{o}C and pressures > 1.5 kbars under hydrous conditions and episodically released a fluid phase (*ibid*). The released fluid underwent phase separation that resulted in CO_2-rich vapour and a hypersaline (33-55 wt. % NaCl eq.) aqueous phase (Williams *et al.*, 1999; *ibid*). The hypersaline fluid contained significant amounts of Fe (~ 10 wt %) and Cu (~1wt %) plus Na, Ca, K, Cl and Ba and led to the formation of Ca-Fe ± Na alteration (pyroxene-albite ± magnetite) within the sills and quartz-magnetite ± clinopyroxene ± albite ± pyrite veins outside the sills (Williams *et al.*, 1999; Perring *et al.*, 2000). Calculated $\delta^{18}O_{water}$ values for quartz in the quartz-magnetite veins range from +7.8 to +9.9 ‰ and sulphur isotope values for pyrite range from -4.9 to -3.3 ‰, compatible with a magmatic fluid source (Fig. 5; *ibid*).

Narrow, steeply-dipping calcite ± chlorite ± pyrite veins cut the quartz-magnetite veins and contain minor Cu(-Au) mineralisation. The carbonate veins likely formed from cooler (< 200 ^{o}C), lower salinity (15-28 wt % NaCl eq.) fluid that may have been produced by mixing meteoric water with magmatic hydrothermal fluid (Fig. 4; Table 4). Sulphur isotope values for pyrite and chalcopyrite in the carbonate veins are -3.2 and -9.7 ‰respectively (Fig. 5; *ibid*).

Osborne – The Osborne deposit occurs within the Isa Superbasin in the Soldiers Cap Group of Cover Sequence 3 (*ca*. 1670-1600 Ma; Table 2; *cf.* Beardsmore *et al.*, 1988). Host rocks include feldspathic psammite (± pelite) and banded ironstone (magnetite-quartz-apatite) cut by tholeiitic amphibolite dykes and a body of ultra mafic rock (*cf.* Adshead *et al.*, 1998). Host rocks were metamorphosed and deformed *ca*. 1595 Ma (Perkins and Wyborn, 1998; Gauthier *et al.*, 2001; Rubenach *et al.*, 2001). Na-Ca-Fe metasomatism accompanied this deformation and produced albitites and metasomatic

ironstones (Rubenach *et al.*, 2001). Pegmatite dykes were emplaced late syn- to immediately post-deformation (*ibid*) and pre-date and cross-cut the mineralisation (Adshead *et al.*, 1998). A second generation of albitisation and calc-silicate alteration (also dated at *ca.* 1595 Ma) replaced country rocks adjacent to the pegmatite dykes and the Osborne orebodies (Table 3; *cf.* Rubenach *et al.*, 2001).

Magnetite-pyrite-chalcopyrite mineralisation occurs in zones of silicification mainly along contacts between ironstone and psammite (*cf.* Adshead *et al.*, 1998). The mineralisation has high copper and gold grades and contains anomalous concentrations of cobalt, molybdenum, silver, selenium, bismuth, mercury, tellurium, tin, fluorine and chlorine (Table 1; Adshead, 1995). Disseminated mineralisation occurs within the banded ironstone units and is associated with secondary hematite-pyrite-magnetite. One ore body (3E) is not associated with ironstone and is hosted by pegmatite, psammite, metatholeiite and schist (Adshead *et al.*, 1998). This ore body contains abundant pyrrhotite and pyrite-magnetite (Adshead, 1995). Cu:Au ratios vary across the deposit and pyrrhotite-bearing associations have higher ratios than hematite-stable alteration. Gangue minerals include quartz, calcite, chlorite, muscovite, magnetite, pyrite and/or pyrrhotite, iron-cobalt sulphides, apatite, molybdenite and tourmaline plus bismuth sulphides and sulphosalts (Adshead, 1995).

Primary fluid inclusions in pre-mineralisation silica flooding contain high temperature (>450 ^{o}C), chemically complex (Na, Fe, Ca, K, Mn, Ba, CO_2, CH_4) hypersaline (60-70 wt % salts) brines or $CO_2 \pm CH_4$ vapours (Fig. 4; Table 4; Adshead, 1995; Adshead *et al.*, 1998). Fluid inclusions related to mineralisation contain lower temperature (~300 ^{o}C), aqueous, less saline (20-37 wt % salts) fluids (*ibid*). Fluids are interpreted to have a magmatic and/or retrograde metamorphic origin (*ibid*). Sulphur isotope values for chalcopyrite range from -3 to +2.5 ‰consistent with a magmatic source for sulphur (Fig. 5; *cf.* Rotherham *et al.*, 1998). Calculated oxygen isotope values for water in equilibrium with magnetite range from +5 to +12 ‰, overlapping the magmatic and metamorphic fluids fields (Fig. 5; *cf.* Rotherham *et al.*, 1998). Gold and copper were likely carried as chlorocomplexes and precipitated due to decreases in temperature and salinity and an increase in pH of the fluid (Adshead, 1995; Adshead *et al.*, 1998).

Eloise – The Eloise deposit is hosted within altered and deformed meta-arkose, quartz-biotite schist and amphibolite of the Soldiers Cap Group (Table 2; Cover Sequence 3;

Baker, 1996, 1998). No granitic rocks have been found in the Eloise area however, a large gravity low 10 km east of the deposit may be a pluton related to the Williams batholith (Baker, 1998). The deposit occurs proximal to a bend in a regional shear zone (Baker, 1996) and metasomatism and mineralisation are interpreted to have occurred synchronous with ductile-brittle deformation during the waning stages of the Isan Orogeny and emplacement of the Williams and Naraku batholiths (*ca.* 1540-1490 Ma; Baker and Laing, 1998).

Pyrrhotite-chalcopyrite mineralisation (Table 1; *ca*. 1530 Ma; Baker *et al.*, 2001) occurs in veins, silicified zones and massive sulphide bodies, within highly strained, hornblende-biotite-altered, metasedimentary rocks proximal to and within the Eloise shear zone (*cf.* Baker, 1998). Gold is associated with chalcopyrite. The mineralised system is zoned, i.e. minor magnetite-pyrite occurs south of the pyrrhotite-chalcopyrite mineralisation and pyrrhotite occurs to the northwest (*ibid*). Gangue minerals include quartz, calcite, actinolite/hornblende, chlorite, biotite, muscovite and potassium feldspar. Host rocks were affected by pervasive albitisation and ± hornblende ± biotite ± quartz veins and alteration prior to mineralisation (Table 3). Post mineralisation veins are dominantly composed of potassium feldspar, siderite-hematite or chlorite and are overprinted by silicification and chlorite-calcite veins and late pyrite-quartz ± adularia veins (*ibid*).

Fluid that formed the pervasive pre-mineralisation albite alteration was high temperature (400-500 ^{o}C) ultrasaline brine (Fig. 4; Table 4; Baker, 1996; 1998). Pre-mineralisation hornblende-biotite assemblages that cross-cut the albite alteration also formed from high temperature (450-600 ^{o}C), ultrasaline (32-68 wt% total salts) brines. Fluid that formed mineralisation was lower temperature (200-450 ^{o}C) and lower salinity (30-47 wt% total salts). Calculated oxygen isotope values for water in equilibrium with pre-mineralisation assemblages and with mineralisation overlap those of typical magmatic and metamorphic fluids (Fig. 5; Baker *et al.*, 2001). Sulphur isotope values for pyrite, chalcopyrite and pyrrhotite range from 0.0 to 2.3 ‰, consistent wi th a magmatic source for sulphur (Fig. 5; *ibid*). The source of fluid is interpreted to be magmatic based on the high salinity of fluid inclusions and on sulphur isotope data (and to a lesser degree oxygen and hydrogen isotope data) that have a magmatic signature (*ibid*). Metals were likely carried as chlorocomplexes with H_2S as the dominant sulphur species. Ore deposition is interpreted to have been predominantly controlled by decreasing fluid temperature and the sulphidation of early Fe-rich alteration (*ibid*).

D.4.3 Hybrid magmatic – non-magmatic IOCG systems

Hybrid magmatic – non-magmatic IOCG systems formed from fluids with a significant non-magmatic component (*cf.* Barton and Johnson, 1996, 2000). They include the large deposits at Olympic Dam (*cf.* Haynes *et al.*, 1995), Aitik (*cf.* Wanhainen *et al.*, 2003), Candelaria (*cf.* Ullrich and Clark, 1999), Salobo (*cf.* Souza and Vieira, 2000) and Ernest Henry (*cf.* Mark *et al.*, 2000; Fig. 1; Table 1). Hybrid IOCG systems are generally spatially and/or temporally associated with igneous rocks (Table 2) and fluid circulation is inferred to have been driven by heat from magmatism; the magmatic fluid may be a source of metals and/or sulphur (*cf.* Barton and Johnson, 1996; 2000). Isotopic and geochemical data indicate input from non-magmatic fluids such as basinal brines or meteoric water (*cf. ibid*). Non-magmatic fluids are commonly highly saline and may be evaporite-derived (*cf. ibid*, Yardley and Graham, 2002). For example, highly saline surficial water is interpreted to have mixed with magmatic water during the formation of the Olympic Dam deposit (*cf.* Reeve *et al.*, 1990; Haynes *et al.*, 1995) and mixing with evaporite-derived brines is invoked at Aitik (Wanhainen *et al.*, 2003).

Olympic Dam – The Olympic Dam deposit (Table 1) occurs in the eastern part of the Gawler Craton (Fig.1), a region largely underlain by *ca.* 1845 Ma deformed granite (Donington Suite) unconformably overlain by metasedimentary and metaigneous units of the Wallaroo Group (*cf.* Creaser, 1995; Ferris *et al.*, 2002). Dominantly felsic lavas and ignimbrites, and minor mafic lavas, of the Gawler Range Volcanics overlie the Wallaroo Group and are intruded by/coeval with (*ca.* 1595-1575 Ma) Hiltaba Suite K-feldspar dominant granite (to granodiorite; *cf.* Ferris *et al.*, 2002). The deposit formed at shallow depth during the late stages of intrusion of voluminous, felsic melts *ca.* 1590 Ma (Table 2; *cf.* Roberts and Hudson, 1983; Reeve *et al.*, 1990; Oreskes and Einaudi, 1990; Cross *et al.*, 1993; Oreskes and Hitzman, 1993; Johnson and Cross, 1995; Haynes *et al.*, 1995; Reynolds, 2000; Skirrow *et al.*, 2002).

Olympic Dam is hosted by fractured, hematite-sericite-altered granite over an ~ 7 x 3 km area and is associated with a zone of dilation related to a regional-scale fault zone (*ibid*). The deposit consists of multi-stage hematitic breccias around a core of barren hematite-quartz breccias (*ibid*). Mineralisation was broadly contemporaneous with brecciation (Oreskes and Einaudi, 1990; Reeve *et al.*, 1990) and occurs dominantly within breccia matrix as disseminated Cu-Fe sulphides and uraninite (*cf.* Roberts and

Hudson, 1983; Oreskes and Hitzman, 1993; Reynolds, 2000). Multiple mineralising episodes have occurred and each has the following general paragenetic assemblages (*cf.* Oreskes and Einaudi, 1990; Haynes *et al.*, 1995): a) magnetite (± hematite), chlorite, sericite, siderite and minor pyrite, chalcopyrite and uraninite, b) hematite, sericite, chalcocite, bornite, pitchblende, barite, fluorite and chlorite, and c) hematite, or hematite + quartz ± barite (Table 3). Assemblages a to c overlap in time and space and there is a transition from chalcopyrite-bearing assemblages to bornite (± chalcocite)-bearing assemblages about 100-300 m below the top of the deposit that locally follows upflow zones (*ibid*).

The repeated brecciation and alteration events that occurred during the formation of the Olympic Dam deposit created complex zoning and structural patterns that make it difficult for any one study area to be representative of the whole deposit. This has led to significant differences in detailed published accounts of the geology and to a number of proposed models for ore formation. Most models indicate formation from a combination of magmatic and non-magmatic fluids (*cf.* Roberts and Hudson, 1983; Oreskes and Einaudi, 1990, 1992; Reeve *et al.*, 1990; Haynes *et al.*, 1995), but at least one model (Johnson and Cross, 1991) suggests fluids were dominantly magmatic. Interaction between hot, saline, relatively reduced metal-bearing brine and cooler, oxidised saline meteoric waters was proposed by Reeve *et al.*, (1990). Haynes *et al.*, (1995) proposed a model involving the repeated mixing of hot, relatively oxidized, iron-rich, F, Ba and CO_2-bearing hydrothermal fluid (magmatic or deeply circulated meteoric water derived from a felsic volcanic or granitic source) with cooler, highly oxidized meteoric or connate fluid that contained Cu, U, Au, Ag and sulphate derived from the interaction of saline lacustrine (or ground) water with mafic volcanic rocks. Oreskes and Einaudi (1990, 1992) suggested fluids that deposited early magnetite were hot (~400 ^{o}C), had oxygen isotope characteristics ($\delta^{18}O_{water}$ = 8-10 ‰) similar to those of primary magmatic fluid or deeply circulating fluid that equilibrated with metamorphic basement, were possibly highly saline (31-42 wt % NaCl eq.) and carried Fe, Cu and other metals (Figs. 4, 5; Table 4). They suggest the hot fluids were followed by cooler (200-?360 ^{o}C), lower salinity fluids with low $\delta^{18}O_{water}$ values (-2.5 to +4.5 ‰) that may have been derived from surficial fluids (evolved meteoric, closed-basin, ground and/or seawater). Johnson and Cross (1991) presented a model that involves two fluids based on Sm-Nd isotopic evidence: 1) fluid in isotopic equilibrium with Hiltaba Suite granites led to the precipitation of early magnetite and 2) fluid derived from an ascending volatile phase

exsolved from mafic/ultramafic magma and enriched in Cu and REE led to the precipitation of copper mineralisation. Reynolds (2000) suggests ore fluids and metals have magmatic sources and Knutson *et al.* (1992) report that Mesoproterozoic basalts are a possible source of copper.

Sulphur isotope data indicate mean $\delta^{34}S$ values of: pyrite = -6 ‰, chalcopyrite = -7 ‰, bornite = -7 ‰, chalcocite = -10 ‰ and barite = 11 ‰ (Fig. 5; Eldridge and Danti, 1994). Differences between sulphur isotope values for different minerals are broadly compatible with a temperature of formation of approximately 300 °C (*ibid*). Bimodal results for sulphur isotope data in an area with elevated gold values suggest boiling may have been important in gold deposition (*ibid*).

Aitik - The Aitik deposit (Table 1) is located in northern Fennoscandia (Fig. 1) in a 40 x 5 km NNW-trending belt of Cu(-Au) mineralisation (*cf.* Frietsch *et al.*, 1997, Carlon, 2000). The belt is spatially associated with a regional-scale fault/shear zone and is underlain by terrestrial and marine intermediate to felsic metavolcanic rocks of the *ca.* 1910-1880 Ma Porphyry Group (Table 2; *cf.* Skiöld and Cliff, 1984; Skiöld, 1987; *ibid*). Cu(-Au) mineralising events occurred within the belt *ca.* 1870 and 1770 Ma and the genesis of the mineralisation is interpreted to be related to large-scale Na-Cl-rich fluid fluxes synchronous with granitic igneous activity *ca.* 1890-1860 Ma and *ca.* 1830-1770 Ma (*cf.* Skiöld, 1987; Frietsch *et al.*, 1997, Carlon, 2000).

Aitik is hosted by intermediate composition volcanic and clastic sedimentary rocks that have been metamorphosed to amphibolite facies; *ca.* 1870 Ma porphyritic quartz monzodiorite occurs in the footwall (*cf.* Frietsch *et al.*, 1997; Wanhainen *et al.*, 2003). Mineralisation is controlled by a NNW-trending fault zone and exhibits multiple phases of brittle-ductile deformation (*ibid*; Carlon, 2000). Chalcopyrite and pyrite and minor magnetite, pyrrhotite, bornite, chalcocite and molybdenite occur as disseminations and stringers in garnet-bearing biotite schist and gneiss and muscovite schist (*cf.* Frietsch *et al.*, 1997; Wanhainen and Martinsson, 1999; Carlon, 2000; Wanhainen *et al.*, 2003). Stockwork quartz-chalcopyrite-pyrite veins extend into the underlying quartz monzodiorite (Wanhainen *et al.*, 2003). Barite-magnetite-actinolite-chalcopyrite-pyrite veins occur locally. Native gold and gold alloys occur with chalcopyrite and pyrite and are intergrown with non-sulphide minerals (*ibid*). Gangue minerals include quartz, barite, fluorite, calcite, tourmaline, scapolite and apatite. Pervasive sericitisation, scapolitization and tourmalinization have affected host rocks

(Table 3; *cf.* Frietsch *et al.*, 1997). Mineralisation is associated with extensive biotite and sericite alteration (Wanhainen *et al.*, 2003). K-feldspar and epidote alteration occurs along fault zones that bound the ore zone (*ibid*).

Chalcopyrite mineralisation was deposited prior to bornite from moderate temperature (140-373 ^{o}C), highly saline (31-37 eq. wt% NaCl) fluids (Fig. 4; Table 4; Wanhainen *et al.*, 2003). Bornite mineralisation was deposited from moderate temperature (100-222 ^{o}C), less saline (18-27 eq. wt% NaCl + $CaCl_2$) fluids (*ibid*). Sulphur isotope values for pyrite and chalcopyrite range from -3.4 to +3.3 ‰and from +6.7 to +13.8 ‰for barite (Fig. 5; Frietsch *et al.*, 1995).

The Aitik deposit has been interpreted to be genetically related to hydrothermal fluids exsolved from the underlying syntectonic quartz monzodiorite (Monro, 1988) with a contribution to the fluid from evaporitic sources (Wanhainen *et al.*, 2003). Based on isotopic data (Fig. 5) sulphur is interpreted to have been derived from a magmatic source, either from magmatic fluid or by dissolution of igneous sulphides (Frietsch *et al.*, 1995). The high calcium content (in addition to Na) of fluid inclusions related to the main chalcopyrite mineralisation is interpreted to indicate at least some fluid was derived from evaporitic sources (Wanhainen *et al.,* 2003). Highly saline hydrothermal fluids derived from an evaporitic source have also been invoked to explain pervasive scapolite and albite alteration that is widespread in the region (Frietsch *et al.,* 1997).

Candelaria (Punta del Cobre Belt) – An approximately 5 x 20 km belt of IOCG and iron deposits, that includes Candelaria (Table 1) and deposits within the Punta del Cobre district, occurs along the eastern margin of the coastal batholith, near Copiapó, Chile (Fig. 1; *cf.* Marschik and Fontboté, 2001). The deposits are located east of, but proximal to, the Atacama fault zone a >1000 km-long, arc-parallel, strike-slip fault system (*cf.* Scheuber and Andriessen, 1990). The area is underlain by an Early Cretaceous continental arc and marine back-arc basin terrane made up of andesitic volcanic flows and volcaniclastic rocks overlain by limestones and minor evaporites (Table 2; *cf.* Ullrich and Clark, 1999; Marschik *et al.*, 2000; Marschik and Fontboté, 2001). Significant iron oxide-Cu-Au(-Zn-Ag) mineralisation, including the large Candelaria deposit, occurs at the intersection of northwest-trending brittle faults with the contact between massive relatively impermeable volcanic rocks and overlying porous and permeable volcaniclastic rocks (*cf.* Marschik *et al.*, 2000; Marschik and Fontboté, 1996, 2001). Marschik *et al.* (2000) and Marschik and Fontboté (2001)

suggest ore-forming fluids were focussed along faults and formed sub-vertical orebodies in low permeability strata and lens-shaped concordant bodies in permeable horizons.

Copper mineralisation occurs as veins and hydrothermal breccia infill, or overprints massive magnetite replacement bodies (*cf.* Marschik *et al.*, 2000; Marschik and Fontboté, 1996, 2001). Ore consists mainly of magnetite and/or hematite, chalcopyrite and pyrite, locally abundant pyrrhotite and sphalerite and trace amounts of molybdenite and arsenopyrite. Gold occurs as inclusion in chalcopyrite, in fractures within pyrite and as Hg-Au-Ag alloy. Malachite, chrysocolla, chalcocite and covellite occur in poorly developed supergene oxidation and enrichment zones (Sillitoe and Clark, 1969). Gangue consists mainly of quartz and anhydrite at Candelaria and calcite and/or quartz in the Punta del Cobre district (*cf.* Marschik *et al.*, 2000; Marschik and Fontboté, 1996, 2001).

Alteration and mineralisation in the Punta del Cobre belt is multiphase with numerous cross-cutting relationships that can be divided into six general stages (*cf.* Ullrich and Clark, 1999; Marschik and Fontboté, 1996, 2001). Stage 1: large-scale pervasive albitization. Stage 2: intense biotite-quartz-magnetite ± K-feldspar alteration associated with emplacement of large magnetite-quartz bodies; coeval specular hematite formed in dilational zones but is replaced by later magnetite. Stage 3: Ca-Na metasomatism (calcic amphibole, albite) ± K-feldspar associated with the main ore stage (Cu-Au); sodic scapolite occurs in sedimentary strata (limestones and metaevaporites of the Abundancia Formation) that overlie the volcanic rocks which host mineralisation. Stage 4: epidote-chlorite alteration. Stage 5: hematite-calcite-chalcopyrite. Stage 6: anhydrite and calcite-chlorite alteration (Table 3).

Mineralisation was broadly contemporaneous with regional uplift and emplacement of calc-alkaline diorite to quartz monzonite of the *ca.* 119-97 Ma Copiapó Batholith (Ullrich and Clark, 1999; Marschik and Fontboté, 2001) and likely occurred at 2 to 3 km depth (Marschik and Fontboté, 2001). Intrusion of the batholith created an extensive contact metamorphic aureole and peak contact metamorphism occurred between stages 2 and 3 (Marschik and Fontboté, 2001). The temperature of oxide mineralisation (stage 2) is interpreted to be 500-600 ^{o}C (*cf.* Marschik *et al.*, 2000). Fluid inclusions in quartz associated with main stage Cu-Au mineralisation are hypersaline and CO_2-rich with homogenisation temperatures from ~ 330 to 440 ^{o}C (Fig. 4; Table 4; Ullrich and Clark, 1999; Marschik *et al.*, 2000). Fluid inclusions in late stage

calcite have homogenisation temperatures of ≤ 236 °C. Sulphur isotopes values for main ore stage (stage 3) sulphides at Candelaria range from -1.3 to + 5.7 ‰and from 14.5 to 17.5 ‰for anhydrite associated with the chalcopyrite (Fig. 5; Ullrich and Clark, 1999; Marschik and Fontboté, 2001). $\delta^{34}S$ values for late stage chalcopyrite at Candelaria range from +0.8 to +7.2 ‰(*ibid*). Oxygen isotope values for fluid in equilibrium with ore stage quartz at Candelaria range from approximately 6 to 9 ‰(Fi g. 5; *cf.* Marschik and Fontboté, 2001). $\delta^{18}O_{fluid}$ values in equilibrium with late stage calcite range from -5.4 to +1.3, +4.6 to +7.7 and -2.8 to + 4.7 respectively for the Candelaria, Carola and Santos/Socavón Rampa IOCG deposits in the Punta del Cobre district (*ibid*).

Magmatic and non-magmatic fluids are interpreted to have been involved in ore formation at Candelaria and deposits in the Punta del Cobre district (*cf.* Ullrich and Clark, 1999; Marschik *et al.*, 2000; Marschik and Fontboté, 2001). A magmatic fluid contribution to the hydrothermal system is based on calculated fluid oxygen isotope values, the presence of hypersaline, CO_2-rich and saline fluid inclusions, the oxidised nature of the ore fluid as indicated by early formed hematite, coeval ages for mineralisation and intrusive activity, similar Pb isotope values for sulphides, volcanic and intrusive rocks, and similar initial $^{187}Os/^{188}Os$ ratios for magnetite, sulphides and magmatic magnetite (*cf.* Marschik *et al.*, 2000; Marschik and Fontboté, 2001). The presence of non-magmatic fluid (basinal brines, formation or meteoric waters) is inferred from the low calculated $\delta^{18}O$ values for fluid in equilibrium with calcite (*ibid*) and from sulphur isotopic data that indicate early, reduced, Cu-depositing fluids with near magmatic S compositions ($\delta^{34}S_{fluid}$ = -1.3 to +5.7 ‰in early stage 3) w ere replaced by more oxidised and probably evaporite-sourced brines ($\delta^{34}S_{fluid}$ = 11.7 to 16.8 ‰in late stage 3; $\delta^{34}S_{fluid}$ = 13 to 20.2 ‰in stage 5 ; Ullrich and Clark (1999). Thus, suggesting the main ore forming event may have been dominated by the mixing of sulphur-bearing fluids from magmatic and evaporitic sources (*ibid*).

Salobo – The Carajás metallogenic province in Brazil (Fig. 1) is host to Salobo (Table 1) and a number of other Fe oxide-Cu-Au (± Mo,Ag,U,REE) deposits including Igarapé Bahia, Alemão, Cristalino, Sossego and Águas Claras (*cf.* Tazava and Olivera, 2000). The deposits occur within the Carajás Basin which is underlain by Late Archaean (*ca.* 2750 Ma) volcano-sedimentary rocks of the Itacaiúnas Supergroup unconformably overlain by Archaean (*ca.* 2680 Ma) marine siliciclastic rocks of the Águas Claras Formation or Rio Fresco Group, all of which were likely deposited in an extensional

continental environment (*cf.* DOCEGO, 1988; Lindenmayer, 1990; Machado *et al.*, 1991; Pinheiro, 1997). Rocks within the basin were intruded by *ca.* 2750 Ma mafic-ultramafic rocks (Luanga complex), *ca.* 2740 Ma granitoids and diorites (Plaquê Suite), *ca.* 2570 Ma granite (Old Salobo granite/Estrela granitoid complex) and *ca.* 1880 Ma granitoids (Carajás Suite; (*cf.* Machado *et al.*, 1991; Barros *et al.*, 1997). The IOCG deposits are enriched in LREE, Co, Ni, Pb, Zn, As, Bi, W and U, are associated with abundant magnetite and/or hematite and are structurally controlled (*cf.* Requia and Fontboté, 2000; Souza and Vieira, 2000; Tazava and de Olivera, 2000, Ronzê *et al.*, 2000).

The Salobo deposit is situated at the western termination of the Cinzento Transcurrent System and is located within a lens of Itacaiúnas Supergroup bounded by basement gneiss (Table 2; *cf.* Pinheiro, 1997; Souza and Vieira, 2000). The deposit is hosted by metagreywackes that contains lenses or layers of amphibolite (*cf.* Requia and Fontboté, 2000) and are cut by *ca.* 2573 (Old Salobo Granite) and *ca.* 1880 Ma (Young Salobo Granite) granitoids and *ca.* 550-560 Ma diabase dykes (*cf.* Machado *et al.*, 1991; Souza and Vieira, 2000). Cross-cutting relationships demonstrate mineralisation at Salobo is post metamorphic and isotopic dating, based on Re-Os and Pb-Pb analyses of sulphides and magnetite, indicates an age of *ca.* 2500 Ma (*cf.* Machado *et al.*, 1991; Souza and Vieira, 2000), roughly coeval with emplacement of Old Salobo Granite.

Mineralisation occurs along a NNW-trending shear zone (*ibid*) and consists dominantly of steeply-dipping lenses of: 1) abundant early magnetite with minor hematite and local graphite and 2) less abundant, later, chalcopyrite, bornite and chalcocite (Requia and Fontboté, 2000). Copper sulphides also occur in veins cutting iron-rich rocks. Accessory minerals include hematite, molybdenite, ilmenite, uraninite, digenite and covellite; native gold occurs as inclusions in cobaltite, safflorite and copper sulphides, or interstitial to magnetite and chalcopyrite grains (*cf.* Machado *et al.*, 1991; Souza and Vieira, 2000).

Alteration around the deposit includes early Na-metasomatism (Na-plagioclase) overprinted by extensive K-metasomatism (K-feldspar, biotite; Requia and Fontboté, 2000). Intense K-metasomatism is spatially associated with the main ore zone (Table 3; Requia and Fontboté, 2000). Propylitic alteration overprints earlier phases and is characterized by the infiltration of Ca-bearing fluids. Veinlets with quartz, stilpnomelane, fluorite, allanite, chalcopyrite, molybdenite, cobaltite and gold formed during propylitic alteration (Lindenmayer, 1990; Souza and Vieira, 2000).

Chloritization associated with brittle shearing accompanied the propylitic alteration (Lindenmayer, 1990; Souza and Vieira, 2000).

The interaction of a mixture of magmatic and connate brines with a more oxidized fluid is suggested as an ore forming mechanism (*cf.* Requia and Fontboté, 2000). Sulphur isotope values of 0.2 to 1.6 ‰suggest a dominantly magmatic source for sulphur (Fig. 5 ; *ibid*).

Ernest Henry – The Ernest Henry deposit (Table 1), like the magmatic end-member Lightning Creek, Osborne and Eloise deposits, occurs in the Cloncurry district of Australia (Fig. 1). The deposit is hosted by strata of Cover Sequence 2 that include *ca.* 1740 Ma plagioclase-phyric volcanic rocks intercalated with siliciclastic, calc-silicate-rich (scapolite-bearing) and graphitic metasedimentary rocks; *ca.* 1660 Ma metadiorite also occurs in this area (Table 2; *cf.* Mark *et al.*, 2000). Host rocks have been affected by: 1) Na-Ca alteration characterised by hematite-bearing albite and 2) disseminated biotite-magnetite alteration and garnet-K feldspar-biotite alteration (Ryan, 1998; Mark *et al.*, 2000). Mineralisation (*ca.* 1510-1500 Ma) was roughly coeval with emplacement of the Williams and Naraku batholiths *ca.* 1540-1500 Ma (Blake *et al.*, 1990; Ryan, 1998; Mark *et al.*, 2000) and is associated with extensive K-feldspar-hematite alteration (Table 3; Ryan, 1998; Mark *et al.*, 2000). Post ore alteration is dominated by carbonate (Mark *et al.*, 2000).

The location of the orebody is structurally controlled and occurs within volcanic rocks that were brecciated during reverse fault movement along bounding shear zones (Mark *et al.*, 2000). Breccia infill is made up dominantly of a magnetite-carbonate-sulphide assemblage but also contains biotite, K-feldspar, hematite, garnet, barite, fluorite and quartz (Ryan, 1998; Mark *et al.*, 2000). Primary and supergene mineralisation occur. Chalcopyrite and pyrite are the dominant sulphide minerals in the primary zone and there is a strong correlation between copper and gold (*ibid*). The supergene zone extends to 150 m depth and contains chalcocite, bornite, secondary chalcopyrite and native copper (*ibid*). In this zone gold is largely decoupled from copper, magnetite has been oxidised to hematite and secondary calcite and siderite are ubiquitous. Anomalous amounts of cobalt, molybdenum, uranium, REE, arsenic, fluorite and barium are associated with the copper mineralisation in both zones (*ibid*).

Ore fluids were high temperature (~ 400-450 ^{o}C) and high salinity (>26 wt % NaCl eq; Fig. 4; Table 4; Mark *et al.*, 2000). Stable isotope data are compatible with a

significant magmatic contribution to ore-forming fluid(s) and/or sulphur ($\delta^{34}S_{chalcopyrite}$ = -1 to 4 ‰; $\delta^{18}O_{fluid}$ = 8-11 ‰; Fig. 5; *ibid*). However, the wide range of elements enriched in Ernest Henry ore (Table 1) suggest involvement of more than one fluid (*ibid*). Cu and Au (+ Fe, Ba) were probably carried as chloride complexes and pyrite and chalcopyrite (plus magnetite and barite) were likely deposited via a mechanism(s) that involved fluid mixing and/or cooling during brecciation (*ibid*).

D.5 Discussion

IOCG deposits do not appear to form in any one specific geological setting (Tables 1 to 4 and references therein). They are found in a variety of environments that are able to provide basic ingredients for formation, i.e. hot, saline (oxidized) fluid(s), permeable flow paths (e.g. faults, shear zones), source(s) of metals and sulphur (either in original fluid or leached from rocks en route), mechanism(s) to drive fluid flow (e.g. heat, tectonics, gravity, density gradients), and means to precipitate ore minerals (e.g. fluid mixing, cooling, changes in pH and/or fO_2). Thus, unlike other types of mineral deposits which form in a restricted range of geological environments (e.g. volcanic-associated massive sulphide, porphyry copper, skarn, Mississippi Valley-type) IOCG deposits can form in a variety of environments ranging from those containing abundant igneous rocks (e.g. Lightning Creek, Olympic Dam) to those with large volumes of igneous and sedimentary rocks (e.g. Cloncurry district) to those dominated by sedimentary rocks (e.g. Wernecke Breccia). The type of alteration and mineralisation in any IOCG district or at any one deposit will be affected by, for instance, the abundance of fluid of various types (e.g. magmatic, metamorphic, basinal, meteoric), the composition of host strata (e.g. igneous rocks, evaporites), the degree of interaction between fluid and rocks along the fluid pathway (e.g. function of fluid temperature, pH, fO_2) and the degree of permeability of the host rocks (e.g. presence of major structures to act as fluid paths, permeable lithologies; *cf.* Williams and Blake, 1993; Barton and Johnson, 1996, 2000). Thus, IOCG systems can be viewed as forming a spectrum of deposits ranging from those dominated by magmatic environments and fluids to those where non-magmatic fluids dominate.

D.5.1 Comparison of IOCG systems

Tectonic setting – The tectonic and structural settings at the time of mineralisation are poorly understood for most IOCG districts, however, in general this deposit type commonly occurs in extensional settings (*cf.* Hitzman *et al.*, 1992). For example, Candelaria, Aitik and possibly Olympic Dam were emplaced within arc-back arc systems above subducting slabs (*cf.* Ullrich and Clark, 1999; Marschik *et al.*, 2000; Marschik and Fontboté, 2001; Gorbatschev and Bogdanova, 1993; Ferris *et al.*, 2002) and deposits within the Carajás region likely formed in a continental rift environment (*cf.* DOCEGO, 1988; Lindenmayer, 1990; Machado *et al.*, 1991; Pinheiro, 1997). Wernecke Breccia-related IOCG mineralisation may also have formed in an extensional environment. WSG sediments that host Wernecke Breccia were likely deposited in a rift-related basin (Thorkelson, 2000). Mafic to intermediate sills and dykes of the BPRI that cut the WSG have major and trace element chemistry compatible with a rift setting (Thorkelson, 2000; Thorkelson *et al.*, 2001) as do the Slab volcanics (Laughton, 2004). However, further work is required to determine if an extensional setting still existed at the time of emplacement of Wernecke Breccia.

The deposits are largely coeval with tectonic activity, are spatially related to regional-scale fault and/or shear zones and also exhibit structural control on a smaller scale (Table 2 and references therein). For example, the Ernest Henry and Olympic Dam deposits occur in dilational zones (*cf.* Ryan, 1998; Mark *et al.*, 2000; Roberts and Hudson, 1983; Reeve *et al.*, 1990; Oreskes and Einaudi, 1990; Cross *et al.*, 1993; Oreskes and Hitzman, 1993; Johnson and Cross, 1995; Haynes *et al.*, 1995; Reynolds, 2000; Skirrow *et al.*, 2002), the ore zone at Candelaria is located at the intersection of shear/fault zones with a lithological contact between relatively impermeable rocks and overlying permeable strata (*cf.* Marschik *et al.*, 2000; Marschik and Fontboté, 1996, 2001) and Wernecke Breccia mineralisation occurs in structurally weak, permeable zones such as fractured fold hinges (Section A).

Host rocks – IOCG systems are not restricted to particular types of host rocks and can occur in intrusive, volcanic, sedimentary and ironstone hosts (Table 2 and references therein). Magmatic and hybrid IOCG systems are temporally and, generally, spatially related to intrusive rocks (*ibid*). Non-magmatic IOCG systems are not temporally related to igneous rocks but may be spatially related, e.g. Wernecke Breccia. A single area may host various types of IOCG systems. For example the Cloncurry district is

host to magmatic (Lightning Creek, Eloise, Osborne) and hybrid (Ernest Henry) IOCG systems (Tables 1 to 4 and references therein), reflecting different fluid pathways and sources present in the area. The Tennant Creek Inlier hosts non-magmatic IOCG systems (*cf.* Skirrow and Walshe, 2002). The presence of evaporites in the host rock package appears to be important (*cf.* Haynes *et al.*, 1995; Barton and Johnson, 1996, 2000; Hitzman, 2000). For example, Wernecke Breccia is most abundant proximal to a metahalite horizon (Section A). New Br/Cl data for the Cloncurry area suggests a variable but significant contribution of evaporitic halite to the fluid locally (Williams *et al.*, in progress).

Alteration – Most IOCG systems are associated with regional, pervasive alteration (Table 3 and references therein). For example, extensive sodic-calcic alteration occurs in the Cloncurry district, widespread sodic alteration occurs in the Aitik and Candelaria regions, and Salobo, Wernecke Breccia and Redbank are associated with abundant sodic and or potassic alteration (*ibid*). Extensive hematite-sericite-chlorite alteration occurs in the Olympic Dam area (*cf.* Reynolds, 2000). In general, late alteration in IOCG systems is dominated by carbonate (Table 3 and references therein).

Fluid composition, temperature and salinity – IOCG deposits were formed by moderate to high temperature, complex brines largely made up of H_2O-NaCl-$CaCl_2$ with variable amounts of K, Mn, Fe, Sr, Ba, Si, Zn, CH_4, CO_2 and/or Cu (*cf.* Table 4 and references therein; Barton and Johnson, 1996, 2000; Williams *et al.*, in progress). The fluids were varied and different brine compositions occur within a deposit, between deposits in a given district, and between districts (*ibid*). The sulphur content of the brines was typically low and oxygen fugacity was variable (*ibid*).

In general, early-stage alteration in magmatic IOCG systems formed from high temperature, high salinity fluids (Fig. 4). For example, pre-mineralisation quartz-magnetite veins at Lightning Creek formed from fluids with a temperature > 500 ^{o}C and a salinity of 33 to 55 weight % (NaCl eq.) and early silica flooding at Osborne was produced by > 450 ^{o}C , highly saline (60-70 wt % NaCl eq) fluid (Tables 1 to 4, Figs. 4 & 5 and references therein). Early phases in some hybrid IOCG systems also formed from fluids with high temperatures and salinities, e.g. pre-mineralisation biotite-quartz-magnetite alteration at Candelaria and early magnetite at Olympic Dam (*ibid*). Fluid temperature and salinity generally decrease towards later stages and differences between IOCG types are less apparent. For example, mineralisation stage fluid temperature varies from < 200 to 450, 100 to 450 and 150 to 350 ^{o}C and salinity ranges from 15 to

47, 18 to 37 and 3 to 42 weight % (NaCl eq.) respectively for the magmatic, hybrid and non-magmatic IOCG systems listed in Table 1(*ibid*).

Oxygen isotopic composition of fluid – Calculated $\delta^{18}O_{fluid}$ values for magmatic IOCG systems generally overlap values for magmatic fluid (5-10 ‰; Fig. 5 and references therein). For example, $\delta^{18}O_{fluid}$ = 7 to 10, 5 to 12 and 5 to 10 ‰ respectively for Lightning Creek, Osborne and Eloise (*ibid*). Fluids related to hybrid IOCG systems show a wider range of isotopic compositions and commonly vary temporally from early magmatic values to those reflecting the later input of other fluids (Fig. 5). For example, $\delta^{18}O_{fluid}$ = 8 to 10 ‰ and -2 to +5 ‰ for fluid in equi librium with early magnetite and later hematite, respectively, at Olympic Dam (Oreskes and Hitzman, 1993). At Candelaria $\delta^{18}O_{fluid}$ = 6 to 9 ‰ for ore stage mineralisation and $\delta^{18}O_{fluid}$ = -5 to +2 ‰ for later mineralisation (Marschik and Fontboté, 2001). Non-magmatic IOCG systems have a wide range of fluid oxygen isotopic compositions, for example $\delta^{18}O_{fluid}$ = 0 to +16 and -7 to +14 respectively for Redbank and Wernecke Breccia (Knutson *et al.*, 1979; Section C).

Sulphur isotopes – Sulphur isotope values for magmatic IOCG systems are generally close to those of mantle-derived sulphur (Fig. 5), e.g. $\delta^{34}S$ = 0 to 2.3 ‰ at the Eloise deposit (*cf.* Baker, 1998). Some hybrid IOCG systems also have sulphur isotopic compositions close to those of mantle-derived sulphur but others show a wider range. Non-magmatic IOCG systems have a wide range of sulphur isotope values, for example $\delta^{34}S$ values for chalcopyrite and pyrite from Wernecke Breccia range from -12 to +14 ‰ (Section C) and $\delta^{34}S$ values for Redbank vary from -1 to +16 ‰ In general, the large hybrid IOCG systems in Figure 5 do not show as large a variation in sulphur isotopic compositions as the non-magmatic IOCG systems, although Eldridge and Danti (1994) report one value of -47 ‰ from Olympic Dam. However, at least one small hybrid IOCG system has a wide range of sulphur isotope compositions, i.e. pyrite and chalcopyrite from Monakoff, which is interpreted to have formed from the mixing of granite-derived and metaevaporite-derived fluids returned $\delta^{34}S$ values of -10 to +12 ‰ (*cf.* Davidson *et al.*, 2002).

Deposit size and grade – Mineralisation occurs dominantly as disseminations, veins and breccia infill in all IOCG types, however, the size of deposits varies widely (Table 1 and references therein). In general, based on those listed in Table 1, magmatic IOCG deposits tend to be small and higher grade. For example, Eloise has a resource of 3.2 million tonnes of 5.8 % Cu, 1.5 g/t Au and 19 g/t Ag (*cf.* Baker and Laing, 1998).

Hybrid IOCG deposits are generally low grade but have the potential to be very large, for example Olympic Dam is reported to have had a pre-mining resource of 2320 million tonnes of 1.3 % Cu, 0.5 g/t Au, 2.9 g/t Ag and 0.4 kg/t U_3O_8 (*cf.* Reeve *et al.*, 1990). Non-magmatic IOCG deposits can be small to medium in size and high or low grade (Table 1). Most IOCG systems contain a variety of associated elements including cobalt, molybdenum, REE and bismuth (Table 1 and references therein). Eloise and Olympic Dam are reported to contain elevated levels of Ni which may be the reflection of primitive magmatic contribution (*cf.* Baker *et al.*, 2001; Reynolds, 2000).

Mechanisms that would cause the precipitation of mineralisation include: fluid mixing, possibly with less saline, oxidised, and/or sulphur-bearing fluid (*cf.* Table 4 and references therein; Barton and Johnson, 1996, 2000; Williams *et al.*, in progress); CO_2 unmixing (e.g. Osborne; *cf.* Adshead, 1995; Mustard *et al.*, 2003); and the sulphidation of pre-existing iron silicates (e.g. Eloise; Baker, 1998). The presence of abundant fluid (i.e. magmatic + other sources) and a magmatic source of heat ± metals ± sulphur (*cf.* Barton and Johnson, 2000) may account for the large tonnage potential of hybrid systems (Fig. 7). During fluid circulation Fe and base metals could be leached from host rocks along the fluid pathway. For example, in the Cloncurry district K, Fe and Cu were leached from host rocks during widespread sodic-calcic alteration creating a fluid with the potential to contribute to the overall metal budget of the district (*cf.* Williams and Blake, 1993; De Jong and Williams, 1995; Adshead *et al.*, 1998; Baker, 1998; Rotherham *et al.*, 1998; Mark *et al.*, 1999; Perring *et al.*, 2000). Metals and/or sulphur could also be supplied by magmatic fluid, for example PIXE analyses of fluid inclusions from the Lightning Creek deposit indicates a copper content of up to 1 weight % (Perring *et al.* 2000; Williams *et al.* in progress). In magmatic environments fluid flow tends to be focussed into permeable zones and fluid generally cools rapidly as it migrates away from the heat source (*cf.* Barton and Johnson, 2000). The rapid cooling causes precipitation of sulphides and the focussed flow concentrates precipitation in a relatively limited area. The amount of sulphides precipitated would be limited largely by the sulphur content of the fluid (*ibid*). In end member magmatic IOCG systems fluid is derived only from plutons and may be less abundant leading to smaller more focussed deposits. In non-magmatic environments fluid flow may not be focussed and widely disseminated sulphides may result, rather than concentrated sulphide deposits (*ibid*). Metal concentrations may also be lower because there is no contribution from magmatic

fluid. In all cases metals present in the fluid will be lost if the sulphur content is low and/or if there is no favourable trap (*ibid*).

D.5.2 Relationship to other deposit types

Non-magmatic end-member IOCG systems have potential links to other sediment-hosted copper systems, e.g. Tsumeb and Mount Isa. Wernecke Breccia, Tsumeb and Mount Isa all occur in rift-related settings (*cf.* Thorkelson, 2000; Frimmel *et al.*, 1996; O'Dea *et al.*, 1997; Betts *et al.*, 1998). All are hosted by thick sedimentary packages that contain(ed) evaporite horizons and they are not temporally associated with igneous intrusions (*cf.* Thorkelson *et al.*, 2001b; Frimmel *et al.*, 1996; Heinrich *et al.*, 1995). Mineralisation is structurally controlled and at least partly synchronous with tectonic activity (*cf.* Section A; Frimmel *et al.*, 1996; Perkins, 1984; Swager, 1985). In each region the onset of deformation may have been a driving force for the movement of hydrothermal fluid. All were formed from hot, high salinity brines that indicate the involvement of evaporites and are likely evolved basinal/metamorphic waters (*cf.* Section C; Hughes, 1987; Chetty and Frimmel, 2000; Heinrich *et al.*, 1993). Sulphur isotopic compositions for sulphides have a wide range of values in each area: -12 to +14; -8 to +26 and +8 to +21 ‰respectively for Wernecke Breccia, Tsumeb and Mount Isa, indicating a dominantly non-magmatic source for sulphur (Section C; Hughes, 1987; Andrew *et al.*, 1989). Host-strata and mafic rocks are likely sources of copper in each area (*cf.* Section C; Chetty and Frimmel, 2000; Heinrich *et al.*, 1995).

End-member magmatic IOCG deposits are similar to some porphyry Cu(-Au) deposits (*cf.* Pollard, 2000; Sillitoe, 2003). For example Lightning Creek is associated with K-rich, magnetite-series metaluminous intrusive rocks that are similar to intrusive rocks associated with Cu-Au porphyry systems (Pollard *et al.*, 1998; Perring *et al.*, 2000). Pollard (2000) suggests the development of the two styles of mineralisation is related to the composition of the granitoids and the evolution of the hydrothermal fluids, i.e. boiling of magmatic-derived H_2O-salt fluids can lead to porphyry deposits and unmixing of magmatic-derived H_2O-CO_2-salts fluids can lead to IOCG deposits. The variable CO_2 content of the magmas is suggested as a key factor in the evolution of the mineralising system.

D.6 Conclusions

Wernecke Breccia-associated IOCG mineralisation was formed by low to moderate temperature (185-350 ^{o}C), moderate to high salinity (24-42 wt % NaCl eq.) brines that were likely derived from basinal/metamorphic fluids. Magmatic waters are considered less likely as a fluid source because isotopic data for the breccias do not have a magmatic signature and spatially associated mafic to igneous rocks are significantly older (i.e. *ca*. 1710 vs. 1600 Ma) thus ruling out a genetic connection. Metals and sulphur were probably derived from host strata and fluids circulated via tectonic (and/or gravity) processes. This suggests that IOCG systems can form in non-magmatic environments that are able to provide basic ingredients for formation, i.e. hot, saline (oxidized) fluid(s), permeable flow paths (e.g. faults, shear zones), source(s) of metals and sulphur (either in original fluid or leached from rocks en route), mechanism(s) to drive fluid flow (e.g. heat, tectonics, gravity, density gradients), and means to precipitate ore minerals (e.g. fluid mixing, cooling, changes in pH and/or fO_2).

A division of the broad class of IOCG deposits in to end-member magmatic and non-magmatic IOCG systems with hybrid IOCG systems in between would allow their attributes to be more narrowly defined and these could be used in exploration models. For example, large low grade deposits, e.g. Olympic Dam, Aitik, Ernest Henry, are hybrid IOCG systems. Magmatic end-member IOCG deposits are generally smaller but can be higher grade e.g. Osborne, Eloise. Non-magmatic end-member IOCG deposits are small to medium in size and low to high grade (Table 1).

End-member magmatic IOCG deposits such as Lightning Creek have similarities to some porphyry deposits (*cf.* Pollard, 2000). Non-magmatic end-member IOCG deposits share characteristic with some sediment hosted Cu deposits, e.g. Tsumeb, Mount Isa (& Zambian Copper Belt?). This suggests that the range of IOCG deposits may form a link between intrusive- and sedimentary-related deposits, thus, information obtained through the study of IOCG deposits may also be useful in the search for other types of deposits.

D.7 References:

Adshead ND (1995) Geology, alteration and geochemistry of the Osborne Cu-Au deposit, Cloncurry district, NW Queensland, Australia. PhD Thesis, James Cook University, Australia.

Adshead ND, Voulgaris P and Muscio VN (1998) In: Berkman DA and Mackenzie DH (eds.) Geology of Australian and Papua New Guinean Mineral Deposits, The Australasian Institute of Mining and Metallurgy, Melbourne, pp. 793-799.

Ahmad M, Wygralak AS and Ferenczi PA (1999) Gold deposits of the Northern Territory: Northern Territory Geological Survey Report 11, 95p.

Andrew AS, Heinrich CA, Wilkins RWT and Patterson DJ (1989) Sulphur isotope systematics of copper ore formation at Mount Isa, Queensland. Economic Geology 84:1614-1626.

Baker T (1996) The geology and genesis of the Eloise Cu-Au deposit, Cloncurry district, NW Queensland, Australia. PhD Thesis, James Cook University, Australia.

Baker T (1998) Alteration, mineralization, and fluid evolution at the Eloise Cu-Au deposit, Cloncurry district, northwest Queensland, Australia. Economic Geology 93:1213-1236.

Baker T and Laing WP (1998) Eloise Cu-Au deposit, East Mount Isa block: structural environment and structural controls on ore. Australian Journal of Earth Sciences 45:429-444.

Baker T, Perkins C, Blake KL and Williams PJ (2001) Radiogenic and stable isotope constraints on the genesis of the Eloise Cu-Au deposit, Cloncurry district, northwest Queensland. Economic Geology 96:4:723-742.

Barros CE de M, Dall'Agnoll R, Barbey P and Boullier, AM (1997) Geochemistry of the Estrela Granite complex, Carajás region, Brazil: and example of an Archaean A-type granitoid. Journal of South American Earth Sciences 10:321-330.

Barton MD and Johnson DA (2000) Alternative brine sources for Fe-Oxide(-Cu-Au) systems: implications for hydrothermal alteration and metals. In: Porter TM (ed.) Hydrothermal Iron Oxide Copper-Gold & Related Deposits: A Global Perspective, volume 1, PGC Publishing, Adelaide, pp. 43-60.

Barton MD and Johnson DA (1996) Evaporitic-source model for igneous-related Fe oxide-(REE-Cu-Au-U) mineralisation. Geology 24, 3:259-262.

Barton MD, Johnson DA and Zurcher L (2000) Phanerozoic iron oxide (-REE-Cu-Au-U) systems in southwestern North America and their origins. In: Roberts MD and Fairclough MUSCOVITE (eds), Fe-oxide-Cu-Au Deposits: A Discussion of Critical Issues and Current Developments. EGRU contribution 58, James Cook University, pp 5-11.

Beardsmore TJ, Newbery SP and Laing WP (1988) The Maronan Supergroup: an inferred early volcanosedimentary rift sequence in the Mount Isa Inlier, and its implications for ensialic rifting in the Middle Proterozoic of northwest Queensland. Precambrian Research 40/41:487-507.

Bell RT (1978) Breccias and uranium mineralisation in the Wernecke Mountains, Yukon Territory – a progress report. Current Research, Part A, Geological Survey of Canada, Paper 78-1A, pp317-322.

Bell RT (1986a) Megabreccias in northeastern Wernecke Mountains, Yukon Territory. Current Research, Part A, Geological Survey of Canada, Paper 86-1A, pp 375-384.

Bell RT (1986b) Geological map of north-eastern Wernecke Mountains, Yukon Territory. Geological Survey of Canada, Open File 1027.

Bell TH, Perkins WG and Swager CP (1988) Structural controls on development and localization of syntectonic copper mineralisation at Mount Isa, Queensland. Economic Geology: 83:1:69-85.

Bell RT and Delaney GD (1977) Geology of some uranium occurrences in Yukon Territory. Report of Activities, Part A, Geological Survey of Canada, Paper 77-1A, pp 33-37.

Betts PG, Lister GS and O'Dea MG (1998) Asymmetric extension of the Middle Proterozoic lithosphere, Mount Isa Inlier, Queensland, Australia. Tectonophysics 296:293-316.

Betts PG, Giles D and Lister GS (2003) Tectonic environment of shale-hosted massive sulphide Pb-Zn-Ag deposits of Proterozoic northeastern Australia. Economic Geology 98: 3: 557-576.

Blake DH and Stewart AJ (1992) Stratigraphic and tectonic framework, Mount Isa Inlier. In: Stewart AJ and Blake DH (eds.) Detailed studies of the Mount Isa Inlier, Bureau of Mineral Resources Bulletin 243, pp 1-11.

Blake DH, Etheridge MA, Page RW, Stewart AJ, Williams PR and Wyborn LAI (1990) Mount Isa Inlier – regional geology and mineralisation. In: Hughes FE (ed.) Geology of the mineral deposits of Australia and Papua New Guinea, Australasian Institute of Mining and Metallurgy: Melbourne, pp 915-925.

Brideau M-A, Thorkelson DJ, Godin, L and Laughton JR (2002) Paleoproterozoic deformation of the Racklan Orogeny, Slats Creek (106D/16) and Fairchild Lake (106C/13) map areas, Wernecke Mountains, Yukon. In: Emond DS, Weston LH and Lewis LL (eds.) Yukon Exploration and Geology 2001, Exploration and Geological Services Division, Yukon Region, Indian and Northern Affairs Canada, pp 65-72.

Brooks M, Baker T and Hunt J (2002) Alteration zonation, veining and mineralisation associated with the Wernecke Breccias at Slab creek, Yukon Territory, Canada. In: Emond DS, Weston LH and Lewis LL (eds.) Yukon Exploration and Geology 2001, Exploration and Geological Services Division, Yukon Region, Indian and Northern Affairs Canada, pp 249-258.

Carlon, CJ (2000) Iron oxide systems and base metal mineralisation in northern Sweden. . In: Porter TM (ed.) Hydrothermal Iron Oxide Copper-Gold & Related Deposits: A Global Perspective, volume 1, PGC Publishing Adelaide, pp 283-296.

Chetty D and Frimmel HE (2000) The role of evaporites in the genesis of base metal sulphide mineralisation in the Northern Platform of the Pan-African Damara Belt, Namibia: geochemical and fluid inclusion evidence from carbonate wall rock alteration. Mineralium Deposita 35:364-376.

Compston DM (1995) Time constraints on the evolution of the Tennant Creek block, northern Australia. Precambrian Research 71:107-129.

Creaser RA (1995) Neodymium isotopic constraints for the origin of Mesoproterozoic felsic magmatism, Gawler Craton, South Australia. Canadian Journal of Earth Science 32:460-471.

Cross KC, Daly SJ and Flint RB (1993) Olympic Dam deposit. In: Drexel JF, Preiss WV and Parker AJ (eds.) The geology of South Australia. Geological Survey of South Australia, Bulletin 54, volume 1, pp 132-138.

Davidson GJ, Davis BK and Garner A (2002) Structural and geochemical constraints on the emplacement of the Monakoff oxide Cu-Au (-Co-U-REE-Ag-Zn-Pb) deposit, Mt Isa Inlier, Australia. In: Porter TM (ed.) Hydrothermal Iron Oxide Copper-Gold & Related Deposits: A Global Perspective, volume 2, PGC Publishing Adelaide, pp 49-75.

De Jong G and Williams PJ (1995) Evolution of metasomatic features during exhumation of mid crustal Proterozoic rocks in the vicinity of the Cloncurry fault, NW Queensland. Australian Journal of Earth Sciences 42: 281-290.

Delaney GD (1981) The Mid-Proterozoic Wernecke Supergroup, Wernecke Mountains, Yukon Territory; In: Proterozoic Basins of Canada, Geological Survey of Canada, Paper 81-10, pp. 1-23.

Deming D (1992) Catastrophic release of heat and fluid flow in the continental crust. Geology 20:83-86.

DOCEGEO, (1988) Revisão litoestratigráfica da Província Mineral de Carajás. In: SBG, Congresso Brasileiro de Geologia, 35, Belém, Anexo aos Anais, pp. 11-56.

Einaudi MT and Oreskes N (1990) Progress towards an occurrence model for Proterozoic iron oxide (Cu, U, REE, Au) deposits – a comparison between the ore provinces of South Australia and SE Missouri. In: Pratt WP and Sims P (eds.) The midcontinent: Permissive terrane for an Olympic Dam deposit? US Geological Survey Bulletin, 1392: 58-69.

Eldridge CS and Danti K (1994) Low sulphur isotope ratios; high gold values – a closer look at the Olympic Dam deposit via SHRIMP. Geological Society of America Abstracts with Programs, 1994 Annual Meeting, pp. A-498 – A-499.

Ferris GM, Schwarz MP and Heithersay P (2002) The geological framework, distribution and controls of Fe oxide Cu-Au mineralisation in the Gawler Craton, South Australia – Part 1 – Geological and tectonic framework. In: Porter TM (ed.), Hydrothermal Iron Oxide Copper-Gold & Related Deposits: A Global Perspective, volume 2, PGC Publishing, Adelaide, pp. 9-31.

Frietsch R, Billström K and Perdahl JA (1995) Sulphur isotopes in Lower Proterozoic iron and sulphide ores in northern Sweden. Mineralium Deposita 30: 275-284.

Frietsch R, Tuisku P, Martinsson O and Perdahl, J (1997) Early Proterozoic Cu(-Au) and Fe ore deposits associated with regional Na-Cl metasomatism in northern Fennoscandia. Ore Geology Reviews 12: 1-34.

Frimmel HE, Deane JG and Chadwick PJ (1996) Pan-African tectonism and the genesis of base metal sulphide deposits in the northern foreland of the Damara orogen, Namibia. Society of Economic Geologists, Special Publication 4:204-217.

Gabrielse H (1967) Tectonic evolution of the northern Canadian Cordillera. Canadian Journal of Earth Sciences, 4:271-298.

Gandhi SS and Bell RT (1990) Metallogenic concepts to aid exploration for the giant Olympic Dam-type deposits and their derivatives. 8th IAGOD Symposium, Program with Abstracts, Ottawa, August 1990, Canada, pp. A7.

Garven G, Bull SW and Large RR (2001) Hydrothermal fluid flow models of stratiform ore genesis in the McArthur Basin, Northern Territory, Australia. Geofluids 1:4:289-311.

Gauthier L, Hall G, Stein H and Schaltegger U (2001) The Osborne deposit, Cloncurry district: a 1595 Ma Cu-Au skarn deposit. In: Williams PJ (ed.) 2001: A hydrothermal odyssey. Extended Conference Abstracts, Economic Geology Research Unit, James Cook University, Contribution 59, pp. 58 -59.

Goodfellow WD (1979) Geochemistry of copper, lead and zinc mineralization in Proterozoic rocks near Gillespie Lake, Yukon. Geological Survey of Canada Paper 79-1A: 333-348.

Gorbatshev R and Bogdanova S (1993) Frontiers in the Baltic Shield. Precambrian Research 64:3-21.

Haynes DW (2000) Iron oxide copper (-gold) deposits: their position in the ore deposit spectrum and modes of origin. In: Porter TM (ed.) Hydrothermal iron oxide copper-gold & related deposits: a global perspective, volume 1, pp. 71-90.

Haynes DW, Cross KC, Bills RT and Reed MH (1995) Olympic Dam ore genesis: a fluid-mixing model. Economic Geology 90:281-307.

Heinrich CA, Bain JHC, Fardy JJ and Waring C (1993) Bromine/chlorine geochemistry of hydrothermal brines associated with Proterozoic metasediment-hosted copper mineralisation at Mount Isa, northern Australia. Geochimica Cosmochimica Acta 57:2991-3000.

Heinrich CA, Bain JHC, Mernagh TP, Wyborn LAI, Andrew AS and Waring C (1995) Fluid and mass transfer during metabasalt alteration and copper mineralisation at Mount Isa, Australia. Economic Geology 90:705-730.

Hitzman MW (2000) Iron oxide-Cu-Au deposits: what, where, when, and why? In: Porter TM (ed.) Hydrothermal iron oxide copper-gold & related deposits: a global perspective, volume 1, pp. 9-25.

Hitzman MW, Oreskes N and Einaudi MT (1992) Geological characteristics and tectonic setting of Proterozoic iron oxide (Cu-U-Au-REE) deposits. Precambrian Research 58:241-287.

Hughes MJ (1987) The Tsumeb ore body, Namibia, and related dolostone-hosted base metal ore deposits of Central Africa. PhD Thesis, University of Witwatersrand, Johannesburg, 448pp. University Microfilms International, Ann Arbor, Michigan, USA.

Hunt JA, Laughton JR, Brideau M-A, Thorkelson DJ, Brookes ML and Baker T (2002) New mapping around the Slab iron oxide-copper-gold occurrence, Wernecke Mountains. In: Emond DS, Weston LH and Lewis LL (eds.) Yukon Exploration and Geology 2001, Exploration and Geological Services Division, Yukon Region, Indian and Northern Affairs Canada, pp 125-138.

Hunt JA, Baker T, Davidson G, Fallick AE, and Thorkelson DJ (2004) Origin of Wernecke Breccia: results of fluid inclusion and stable isotope analyses. Abstract, GSA Convention, Hobart, Tasmania, February 2004.

Hunt JA, Baker, T and Thorkelson, DJ (2005, in review). Regional-scale Proterozoic IOCG-mineralised breccia systems: examples from the Wernecke Mountains, Yukon, Canada. Mineralium Deposita, X:x:x-x.

Huston DL, Bolger C and Cozens G (1993) A comparison of mineral deposits at the Gecko and White Devil deposits: implications for ore genesis in the Tennant Creek district, Northern Territory, Australia. Economic Geology 88: 5: 1198-1225.

Jackson MJ and Southgate PN (2000) Evolution of three unconformity-bounded sand-carbonate successions in the McArthur River region of Northern Australia: the Lawn, Wide and Doom Supersequences in a proximal part of the Isa Superbasin. Australian Journal of Earth Sciences 47: 3: 625-636.

Johnson JP and Cross KC (1991) Geochronological and Sm-Nd constraints on the genesis of the Olympic Dam Cu-U-Au-Ag deposit, South Australia. In: Pagel M and Leroy JL (eds.) Source, Transport and Deposition of Metals: Proceedings, 25 Years' SGA Anniversary Meeting, Nancy, Aug. 30 – Sept. 3, 1991, AA Balkema, Rotterdam, The Netherlands, pp 395-400.

Johnson JP and Cross KC (1995) U-Pb geochronological constraints on the genesis of the Olympic Dam Cu-U-Au-Ag deposit, South Australia. Economic Geology 90:1046-1063.

Knutson J, Ferguson J, Roberts WMB, Donnelly TH and Lambert, IB (1979). Petrogenesis of the copper-bearing breccia pipes, Redbank, Northern Territory, Australia. Economic Geology 74:4:814-826.

Knutson J, Donnely TH, Eadington PJ and Tonkin DG (1992) Hydrothermal alteration of Middle Proterozoic basalts, Stuart shelf, South Australia – a possible source for copper mineralization. Economic Geology 87:1054-1077.

Kwak TAP (1977) Scapolite compositional change in metamorphic gradient and its bearing on the identification of metaevaporite sequences. Geological Magazine, 114:343-354.

Laing WP (1998) Structural-metasomatic environment of the East Mt Isa Block base metal-gold province. Australian Journal of Earth Sciences 45:413-428.

Large RR (1975) Zonation of hydrothermal minerals at the Juno mine, Tennant Creek goldfield, central Australia. Economic Geology 70: 1387-1413.

Lane RA (1990) Geologic setting and petrology of the Proterozoic Ogilvie Mountains breccia of the Coal Creek Inlier, southern Ogilvie Mountains, Yukon Territory. MSc. Thesis, University of British Columbia, pp. 223.

Laughton JR (2004) The Proterozoic Slab volcanics of northern Yukon, Canada: megaclasts of a volcanic succession in Proterozoic Wernecke Breccia, and implications for the evolution of northwestern Laurentia. PhD Thesis, Simon Fraser University, Burnaby, British Columbia, Canada.

Laughton JR, Thorkelson DJ, Brideau M-A, Hunt JA and Marshall DD (in review) Early Proterozoic orogeny and exhumation of Wernecke Supergroup revealed by vent facies of Wernecke Breccia, Yukon, Canada. Canadian Journal of Earth Sciences, xx: x-x.

Lindenmayer ZG (1990) Salobo sequence, Carajás, Brazil. PhD Thesis, University of Western Ontario, Canada, 406p.

MacCready T, Goleby BR, Goncharov A, Drummond BJ and Lister GS (1998) A framework of overprinting orogens based on the interpretation of the Mount Isa deep seismic transect. Economic Geology 93:1422-1434.

Machado N, Lindenmayer ZG, Krogh TE and Lindenmayer D (1991) U-Pb geochronology of Archean magmatism and basement reactivation in the Carajás area, Amazon Shield, Brazil. Precambrian Research 49:329-354.

Mark G and De Jong G (1996) Synchronous granitoid emplacement and episodic sodic-calcic alteration in the Cloncurry district: styles, timing and metallogenic significance. Economic Geology Research Unit, James Cook University, Townsville, Queensland, Australia, Contribution 55, pp 77-80.

Mark G and Crookes RA (1999) A hydrothermal origin for the Ernest Henry Fe oxide-(Cu-Au) deposit, Cloncurry district, Australia. In: Stanley CJ *et al.* (eds.) Mineral Deposits: Processes to Processing. Balkema, Rotterdam pp. 235-238.

Mark G, Oliver NHS, Williams PJ, Valenta RK and Crookes RA (2000) The evolution of the Ernest Henry Fe-oxide-(Cu-Au) hydrothermal system. In: Porter TM (ed.) Hydrothermal Iron Oxide Copper-Gold & Related Deposits: A Global Perspective, volume 1, PGC Publishing, Adelaide, pp 123-136.

Marschik R and Fontboté L (1996) Copper(-iron) mineralisation and superposition of alteration events in the Punta del Cobre belt, northern Chile. In: Camus F, Sillitoe RH, Peterson R (eds.) Andean Copper Deposits: New Discoveries, Mineralisation, Styles and Metallogeny. Society of Economic Geologists Special Publication #5, pp. 171-190.

Marschik R and Fontboté L (2001) The Candelaria – Punta del Cobre iron oxide Cu-Au (-Zn-Ag) deposits, Chile. Economic Geology 96:1799-1826.

Marschik R, Leveille RA and Martin W (2000) La Candelaria and the Punta del Cobre district, Chile: Early Cretaceous iron oxide Cu-Au(-Zn-Ag) mineralisation. In: Porter TM (ed.) Hydrothermal Iron Oxide Copper-Gold & Related Deposits: A Global Perspective, volume 1, PGC Publishing, Adelaide, pp 163-175.

McKibben MA and Hardie LA (1997) Ore-forming brines in active continental rifts. In: Barnes HL (ed.) Geochemistry of Hydrothermal Ore Deposits. John Wiley and Sons, pp. 877-936.

Meyer C (1988) Proterozoic ore-forming habitats – tectonic and chemical transitions. In: Kisvarsanyi G and Grant SK (eds.) Tectonic controls of ore deposits and vertical and horizontal extent of ore systems. Conference Proceedings, University of Missouri, Rolla, October 6-8, 1987, pp. 217-235.

Monro D (1988) The geology and genesis of the Aitik copper-gold deposit, Arctic Sweden. PhD Thesis, Cardiff College, University of Wales, U.K.

Mustard R, Baker T, Williams P, Ulrich T, Mernagh T, Ryan CG, VanAchterbergh E and Adshead N (2003) Cu-rich brines at the Osborn and Starra deposits: implications for immiscibility in Fe-oxide Cu-Au systems. Applied Earth Science Transactions of the Institute of Mining and Metallurgy: Section B: 112: B189-B191.

O'Dea MG, Lister GS and MacCready T (1997) Geodynamic evolution of the Proterozoic Mt Isa Terrain. In: Burg J-P and Ford M (eds.) Orogeny Through Time. Geological Society of London Special Publication 121 pp 99-122.

Ohmoto H and Goldhaber MB (1997) Sulphur and carbon isotopes. In: Barnes HL (ed.) Geochemistry of hydrothermal ore deposits. John Wiley and Sons, New York, USA, pp. 517-612.

Oreskes N and Einaudi MT (1990) Origin of REE-enriched hematite breccias at the Olympic Dam Cu-U-Au-Ag deposit, Roxby Downs, South Australia. Economic Geology 85:1-28.

Oreskes N and Einaudi MT (1992) Origin of hydrothermal fluids at Olympic Dam: preliminary evidence from fluid inclusions and stable isotopes. Economic Geology 87:1:64-88.

Oreskes N and Hitzman MW (1993) A model for the origin of Olympic Dam-type deposits. In: Kirkham RV, Sinclair WD, Thorpe RI and Duke JM (eds.) Mineral Deposit Modeling. Geological Association of Canada, Special Paper 40, pp 615-633.

Orridge GR and Mason AAC (1975) Redbank copper deposits. In: Knight CL (ed.) Economic Geology of Australia and Papua New Guinea, 1, Metals. Australian Institute of Mining and Metallurgy Monograph 5 pp. 339-343.

Page RW and Sun S-S (1998) Aspects of geochronology and crustal evolution in the Eastern fold belt, Mount Isa inlier. Australian Journal of Earth Sciences 45:343-361.

Perkins WG (1984) Mount Isa silica dolomite and copper orebodies: the result of a syntectonic hydrothermal system. Economic Geology 79:601-637.

Perkins C and Wyborn L (1996) The age of Cu-Au mineralisation, Cloncurry district, Mount Isa Inlier, as determined by $^{40}Ar/^{39}Ar$ dating. Australian Geological survey Organisation Research Newsletter, 25:8-9.

Perkins C and Wyborn L (1998) Age of Cu-Au mineralisation, Cloncurry district, Mount Isa Inlier, as determined by $^{40}Ar/^{39}Ar$ dating. Australian Journal of Earth Sciences 45:233-246.

Perring CS, Pollard PJ, Dong G, Nunn AJ and Blake KL (2000) The Lightening Creek sill complex, Cloncurry district, northwest Queensland: a source of fluids for Fe oxide Cu-Au mineralisation and sodic-calcic alteration. Economic Geology 95: 1067-1090.

Pinheiro RVL (1997) Reactivation history of the Carajás and Cinzento strike-slip systems, Amazon, Brazil. PhD Thesis, University of Durham, England, 408p.

Pollard PJ (2001) Sodic(-calcic) alteration in Fe oxide-Cu-Au districts: an origin via unmixing of magmatic-derived H_2O-CO_2-NaCl±$CaCl_2$-KCl fluids. Mineralium Deposita 36:93-100.

Pollard PJ (2000) Evidence of a magmatic fluid and metal source for Fe oxide Cu-Au mineralisation. In: Porter TM (ed.) Hydrothermal Iron Oxide-Copper-Gold & Related Deposits: A Global Perspective, volume 1, PGC Publishing, Adelaide, pp. 27-41.

Pollard PJ, Mark G and Mitchell L (1998) Geochemistry of post-1540 Ma granites in the Cloncurry district. Economic Geology 93:1330-1344.

Raymond, J. (2000) Mantle of the earth. In: Sigurdsson H (ed.) Encyclopaedia of Volcanoes, Academic Press, San Diego, USA, pp 41-54.

Raymond, J. (1995) Petrology: The study of igneous, metamorphic and sedimentary rocks. McGraw-Hill Higher Education, New York, 742p.

Reeve JS, Cross KC, Smith RN and Oreskes N (1990) Olympic Dam copper-uranium-gold-silver deposit. In: Hughes FE (ed.) Geology of the Mineral Deposits of Australian and Papua New Guinea, Australasian Institute of Mining and Metallurgy, Monograph 14, pp. 1009-1035.

Requia K and Fontboté L (2000) The Salobo iron oxide-copper-gold deposit, Carajás, northern Brazil. In: Porter TM (ed.) Hydrothermal iron oxide copper-gold & related deposits: a global perspective, volume 1, pp. 225-236.

Reynolds LJ (2000) Geology of the Olympic Dam Cu-U-Au-Ag-REE deposit. In: Porter TM (ed.) Hydrothermal Iron Oxide-Copper-Gold & Related Deposits: A Global Perspective, volume 1, PGC Publishing, Adelaide, pp. 93-104.

Roberts DE and Hudson GRT (1983) The Olympic Dam copper-uranium-gold deposit, Roxby Downs, South Australia. Economic Geology 78:5:799-822.

Roberts DE and Hudson GRT (1984) The Olympic Dam copper-uranium-gold deposit, Roxby Downs, South Australia – A reply. Economic Geology 79:1944-1945.

Rollinson H (1993) Using geochemical data: evaluation, presentation, interpretation. Longman Group, UK, 352p.

Ronzê PC, Soares ADV, Giovanni S and Berreira CF (2000) Alemão copper-gold (U-REE) deposit, Carajás, Brazil. In: Porter TM (ed.) Hydrothermal Iron Oxide-Copper-Gold & Related Deposits: A Global Perspective, volume 1, PGC Publishing, Adelaide, pp. 191-202.

Rotherham JF, Blake KL, Cartwright I and Williams PJ (1998) Stable isotope evidence for the origin of the Mesoproterozoic Starra Cu-Au deposit, Cloncurry district, northwest Queensland. Economic Geology, 93:1435-1449.

Rubenach M, Adshead N, Oliver N, Tullemans F, Esser D and Stein H (2001) The Osborne Cu-Au deposit: geochronology and genesis of mineralisation in relation to host albitites and ironstones. In: Williams PJ (ed.) 2001: A hydrothermal odyssey. Extended Conference Abstracts, Economic Geology Research Unit, James Cook University, Contribution 59, pp. 172-173.

Ryan (1998) Ernest Henry copper-gold deposit. In: Berkman DA and Mackenzie DH (eds.) Geology of Australian and Papua New Guinean Mineral Deposits, Australasian Institute of Mining and Metallurgy: Melbourne, Monograph 22, pp. 759-768.

Scheuber E and Andriessen PAM (1990) The kinematic and geodynamic significance of the Atacama Fault Zone, northern Chile. Journal of Structural Geology 12:243-257.

Scott DL, Rawlings DJ, Page RW, Tarlowski CZ, Idnurm M, Jackson MJ and Southgate PN (2000) Basement framework and geodynamic evolution of the Paleoproterozoic superbasins of north-central Australia: an integrated review of geochemical, geochronological and geophysical data. Australian Journal of Earth Sciences 47:341-380.

Sheppard SMF (1986) Characterization and isotopic variations in natural waters. In: Valley JW, Taylor HP Jr and O'Neil JR (eds.) Stable Isotopes in High Temperature Geological Processes, Reviews in Mineralogy, volume 16, Mineralogical Society of America, pp. 165-183.

Sillitoe RH (2003) Iron oxide copper-gold deposits: an Andean view. Mineralium Deposita, 38:787-812.

Sillitoe RH and Clark AH (1969) Copper and copper iron sulphides as the initial products of supergene oxidation, Copiapó mining district, northern Chile. American Mineralogist 54:1684-1710.

Skiöld, T (1987) Aspects of Proterozoic geochronology on northern Sweden. Precambrian Research, 35: 161-167.

Skiöld, T and Cliff RA (1984) Sm-Nd and U-Pb dating of Early Proterozoic mafic-felsic volcanism in northernmost Sweden. Precambrian Research, 26: 1-13.

Skirrow RG (1999) Proterozoic Cu-Au-Fe mineral systems in Australia: filtering key components in exploration models. In: Stanley CJ *et al.* (eds.) Mineral Deposits: Processes to Processing. Balkema, Rotterdam pp. 1361-1364.

Skirrow RG and Walshe JL (2002) Reduced and oxidized Au-Cu-Bi iron oxide deposits of the Tennant Creek Inlier, Australia: an integrated geologic and chemical model. Economic Geology 97:1167-1202.

Southgate PN, Bradshaw BE, Domagala J, Jackson MJ, Idurnam M, Krassay AA, Page RW, Sami TT, Scott DL, Lindsay JF, McConachie BA and Tarlowski C (2000) Chronostratigraphic basin framework for Paleoproterozoic rocks (1730-1575 Ma) in northern Australia and implications for base-metal mineralisation. Australian Journal of Earth Sciences 47:3:461-483.

Souza, LH and Vieira EA (2000) Salobo 3 Alpha Deposit: geology and mineralisation. In: Porter TM (ed.) Hydrothermal iron oxide copper-gold & related deposits: a global perspective, volume 1, pp. 213-224.

Swager CP (1985) Syndeformational carbonate-replacement model for the copper mineralisation at Mount Isa, Queensland: a microstructural study. Economic Geology 80:107-125.

Tazava E and de Olivera CG (2000) The Igarape Bahia Au-Cu(-REE-U) deposit, Carajás mineral province, northern Brazil. In: Porter TM (ed.) Hydrothermal iron oxide copper-gold & related deposits: a global perspective, volume 1, pp. 203-212.

Thorkelson DJ (2000) Geology and mineral occurrences of the Slats Creek, Fairchild Lake and "Dolores Creek" areas, Wernecke Mountains, Yukon Territory. Exploration and Geological Services Division, Yukon Region, Indian and Northern Affairs Canada, Bulletin 10, 73pp.

Thorkelson DJ, Mortensen JK, Davidson GJ, Creaser RA, Perez WA and Abbott JG (2001a) Early Mesoproterozoic intrusive breccias in Yukon, Canada: The role of hydrothermal systems in reconstructions of North America and Australia. Precambrian Research 111:31-55.

Thorkelson DJ, Mortensen JK, Creaser RA, Davidson GJ and Abbott JG (2001b) Early Proterozoic magmatism in Yukon, Canada: constraints on the evolution of northwestern Laurentia. Canadian Journal of Earth Science 38:1479-1494.

Thorkelson DJ, Laughton JR and Hunt JA (2002) Geological map of Quartet Lakes area (106E/1), Wernecke Mountains, Yukon (1:50,000 scale). Exploration and Geological Services Division, Yukon Region, Indian and Northern Affairs Canada, Geoscience map 2002-2.

Thorkelson DJ, Laughton JR, Hunt JA and Baker T (2003) Geology and mineral occurrences of the Quartet Lakes map area (NTS 106E/1), Wernecke and Mackenzie mountains, Yukon. In: Emond DS and Lewis LL (eds.) Yukon Exploration and Geology 2002, Exploration and Geological Services Division, Yukon Region, Indian and Northern Affairs Canada, pp 223-239.

Torgersen T (1990) Crustal-scale fluid transport, magnitude and mechanisms. EOS (Transactions, American Geophysical Union) 71:1,4,13.

Twyerould SC (1997) The geology and genesis of the Ernest Henry Fe-Cu-Au deposit, northwest Queensland, Australia. University of Oregon, PhD Thesis, 494 p.

Ullrich TD and Clark AH (1999) The Candelaria copper-gold deposit, Region III, Chile: paragenesis, geochronology and fluid composition. In: Stanley CJ *et al.* (eds.) Mineral deposits: Processes to Processing, volume 1. Proceedings of the 5th Biennial SGA Meeting and 10th Quadrennial IAGOD Symposium, London, UK, AA Balkema, Rotterdam, pp 201-204.

Wanhainen C and Martinsson O (1999) Geochemical characteristics of host rocks to the Aitik Cu-Au-Ag deposit, Gellivare area, northern Sweden. Proceedings of the fifth biennial SGA meeting and the tenth quadrennial IAGOD meeting, London, 22-25 August 1999, Extended Abstracts, pp. 1443-1446.

Wanhainen C, Broman C and Martinsson O (2003) The Aitik Cu-Au-Ag deposit in northern Sweden: a product of high salinity fluids. Mineralium Deposita 38: 715-726.

Wedekind MR and Love RJ (1990) Warrego gold-copper-bismuth deposit. In: Hughes FE (ed) Geology of the Mineral Deposits of Australia and Papua New Guinea, The Australian Institute of Mining and Metallurgy, Melbourne, pp 839-843.

Williams PJ and Blake KL (1993) Alteration in the Cloncurry district: Roles of recognition and interpretation on exploration for Cu-Au and Pb-Zn-Ag deposits. Economic Geology Research Unit Contribution 49, James Cook University, Australia, 75pp.

Williams PJ and Skirrow RG (2000) Overview of iron oxide-copper-gold deposits in the Curnamona Province and Cloncurry District (eastern Mount Isa block), Australia. In: Porter TM (ed.) Hydrothermal Iron Oxide Copper-Gold & Related Deposits: A Global Perspective, volume. 1, PGC Publishing, Adelaide, pp 105-122.

Williams PJ, Dong G, Pollard PJ and Perring CS (1999) Fluid inclusion geochemistry of Cloncurry (Fe)-Cu-Au deposits. In: Stanley CJ *et al.* (eds.) Mineral deposits: processes to processing. Rotterdam, Balkema, pp 111-114.

Williams PJ, Broman C, Guoyi D, Mark G, Martinsson O, Mernagh TP, Pollard PJ, Ryan CG and Win TT (in progress) PIXIE characterization of fluid inclusion brines from Proterozoic Fe oxide-bearing Cu-Au deposits, Norbotten (Sweden) and the Cloncurry district (NW Queensland), 50 pp.

Wyborn LA (1998) Younger *ca.* 1500 Ma granites of the Williams and Naraku batholiths, Cloncurry district, eastern Mt Isa inlier: geochemistry, origin, metallogenic significance and exploration indicators. Australian Journal of Earth Sciences 45:397-411.

Yardley BWD and Graham JT (2002) The origins of salinity in metamorphic fluids. Geofluids, 2:249-256.

Yukon MINFILE, 2003. Database of Yukon mineral occurrences. Exploration and Geological Services Division, Yukon Region, Indian and Northern Affairs Canada, CD-ROM (2).

THE GEOLOGY AND GENESIS OF IRON OXIDE-COPPER-GOLD MINERALISATION ASSOCIATED WITH WERNECKE BRECCIA, YUKON, CANADA

VOLUME II

Thesis submitted by
Julie Hunt B.Sc., M.Sc., PGeo.

in April 2005
for the degree of Doctor of Philosophy
in the School of Earth Sciences,
James Cook University, Queensland, Australia

SECTION A - FIGURES

Regional-scale Proterozoic iron oxide-copper-gold-mineralised breccia systems: examples from the Wernecke Mountains, Yukon, Canada

Figure 1:

Location of study area, distribution of WSG and Wernecke Breccia plus location of breccia-associated IOCG prospects included in this study (modified from Thorkelson, 2000).

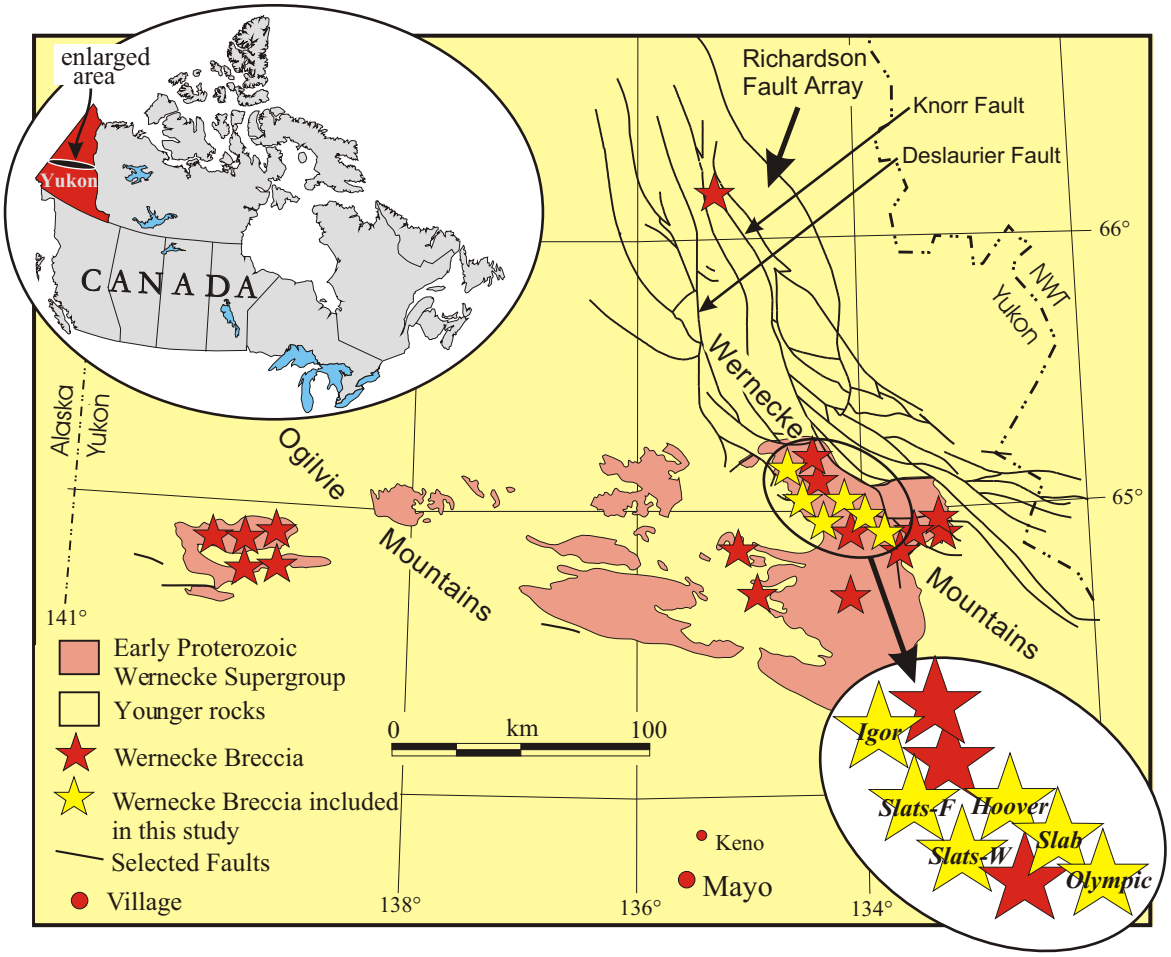

Section A: Figure 1

Figure 2:

Simplified geology map of the study area (for details see Thorkelson, 2000 and Thorkelson *et al.*, 2002). Legend shows approximate stratigraphic position of IOCG prospects included in this study.

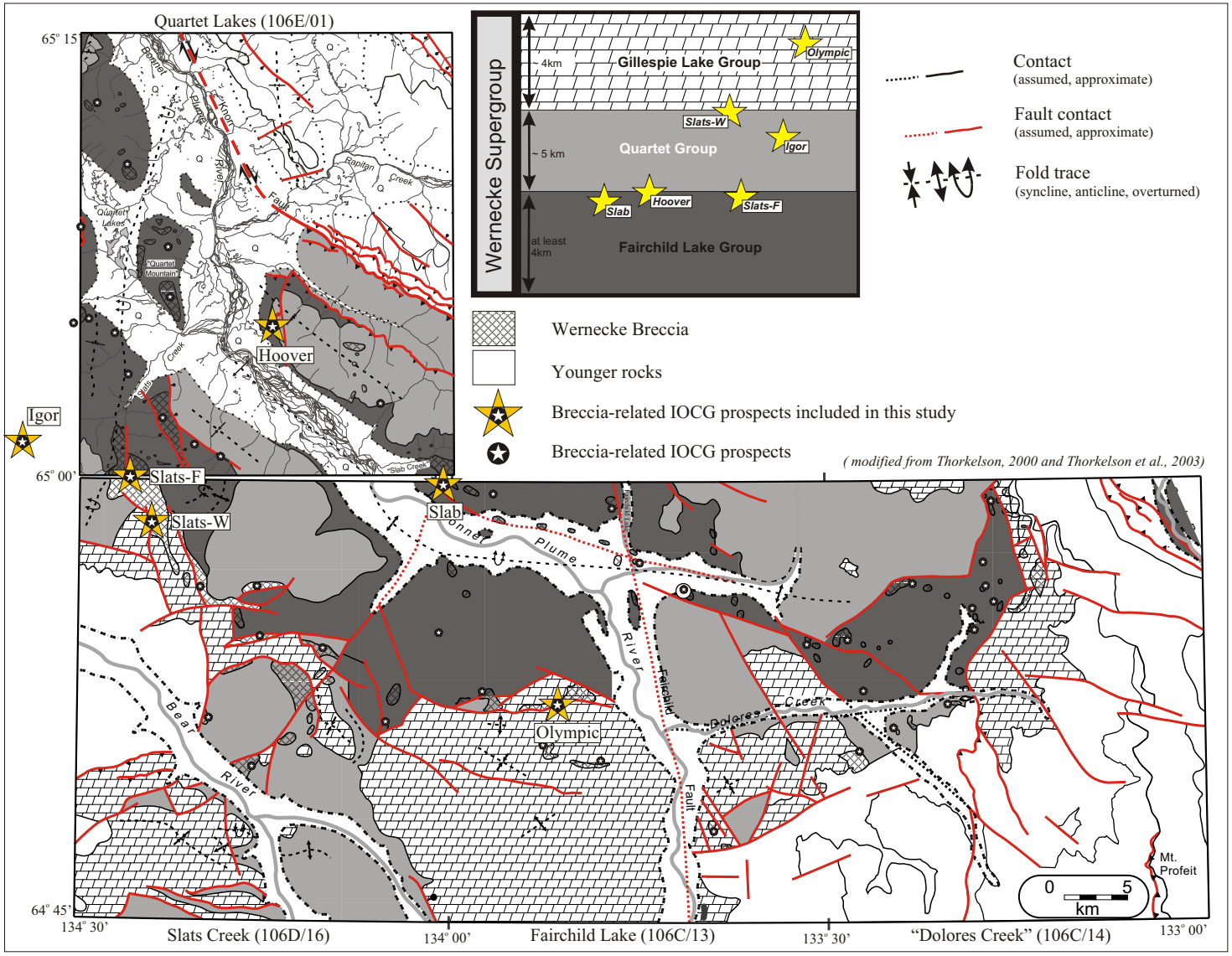

Section A: Figure 2

Figure 3:

Time stratigraphic column of the study area showing major depositional, intrusive and deformational events (modified from Thorkelson, 2000).

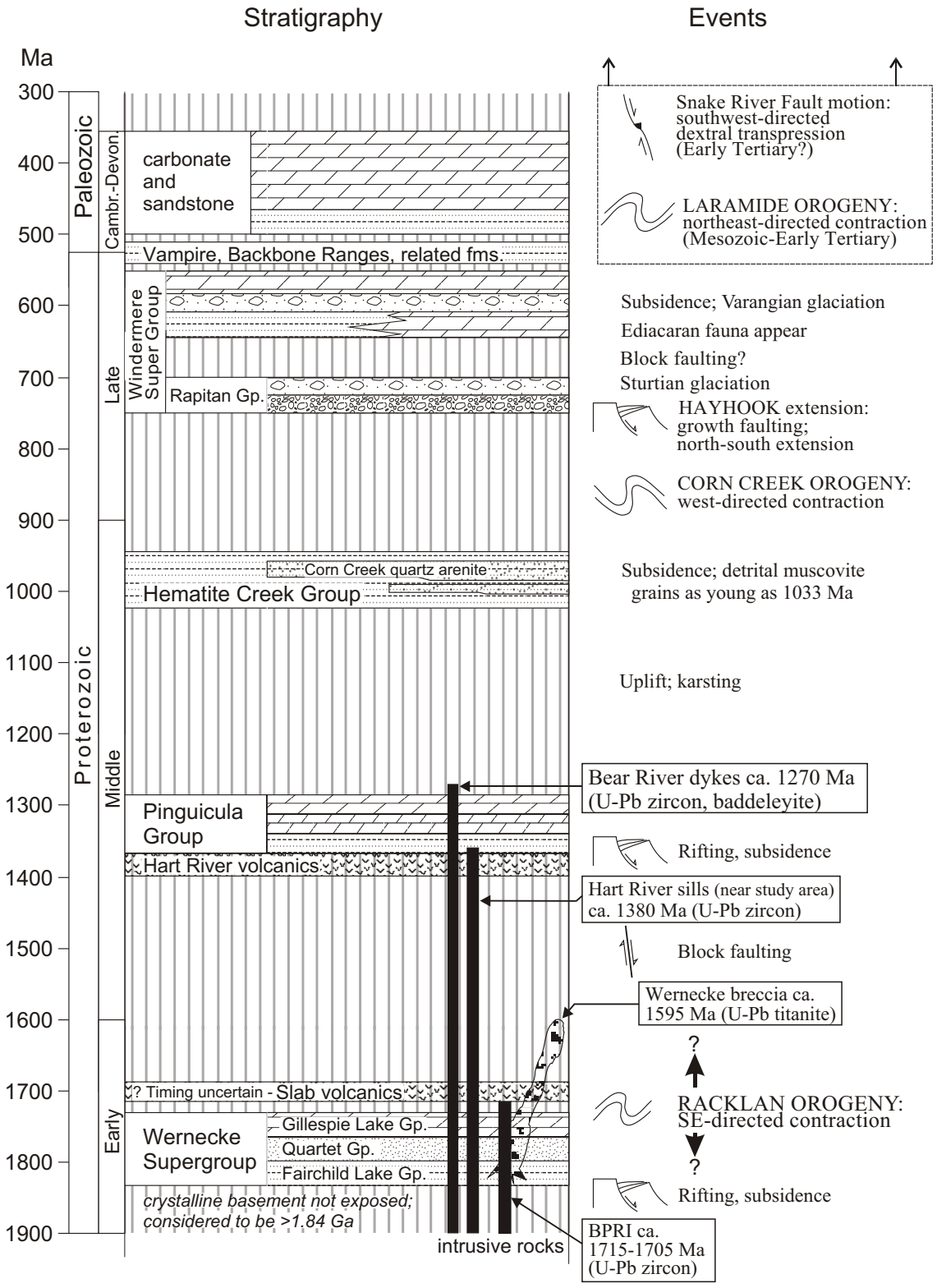

Section A: Figure 3

Figure 4:

WSG a) stratigraphic column, see text and Table 1 for unit descriptions (information from Delaney, 1981), b) typical FLG, c) probable meta-evaporite in F-Tr, d) typical Quartet Group and e) GLG stromatolitic dolostone.

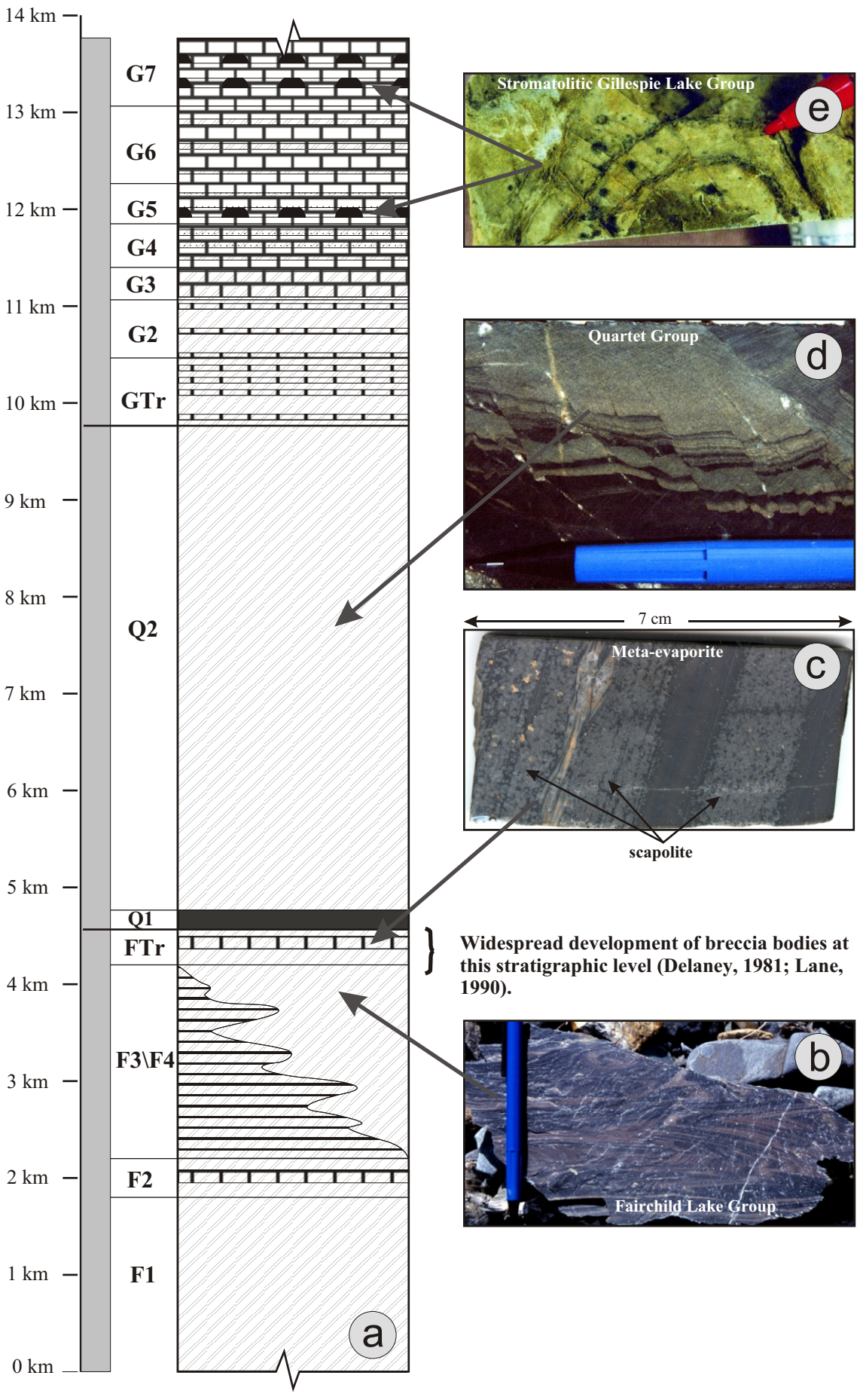

Section A: Figure 4

Figure 5:

View of Slab mountain and Slab ridge (looking south) showing location of metaevaporites. Insets: detail of metaevaporites in outcrop showing one thick (labelled) and several narrow (light coloured) scapolite-rich layers and detail of solution breccia that overlies metaevaporites.

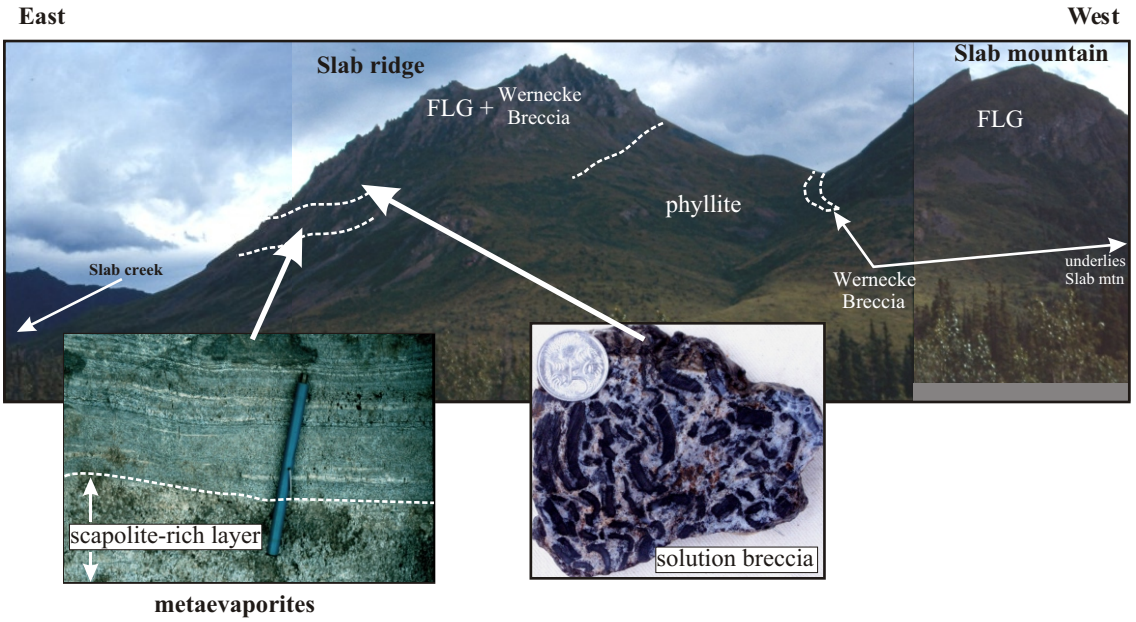

Section A: Figure 5

Figure 6:

Examples of Wernecke Breccia: a) clast supported breccia, Slab area, b) matrix supported breccia, Olympic area, c) breccia with abundant clasts of earlier breccia, Slab area, d) photomicrograph of Wernecke Breccia matrix (crossed polars) made up dominantly of sedimentary rock fragments, carbonate, feldspar, lesser quartz and minor hematite and magnetite, e) sharp contact between breccia and phyllitic metasiltstone, Hoover area, f) crackle brecciated metasiltstone from a gradational breccia contact, Hoover area.

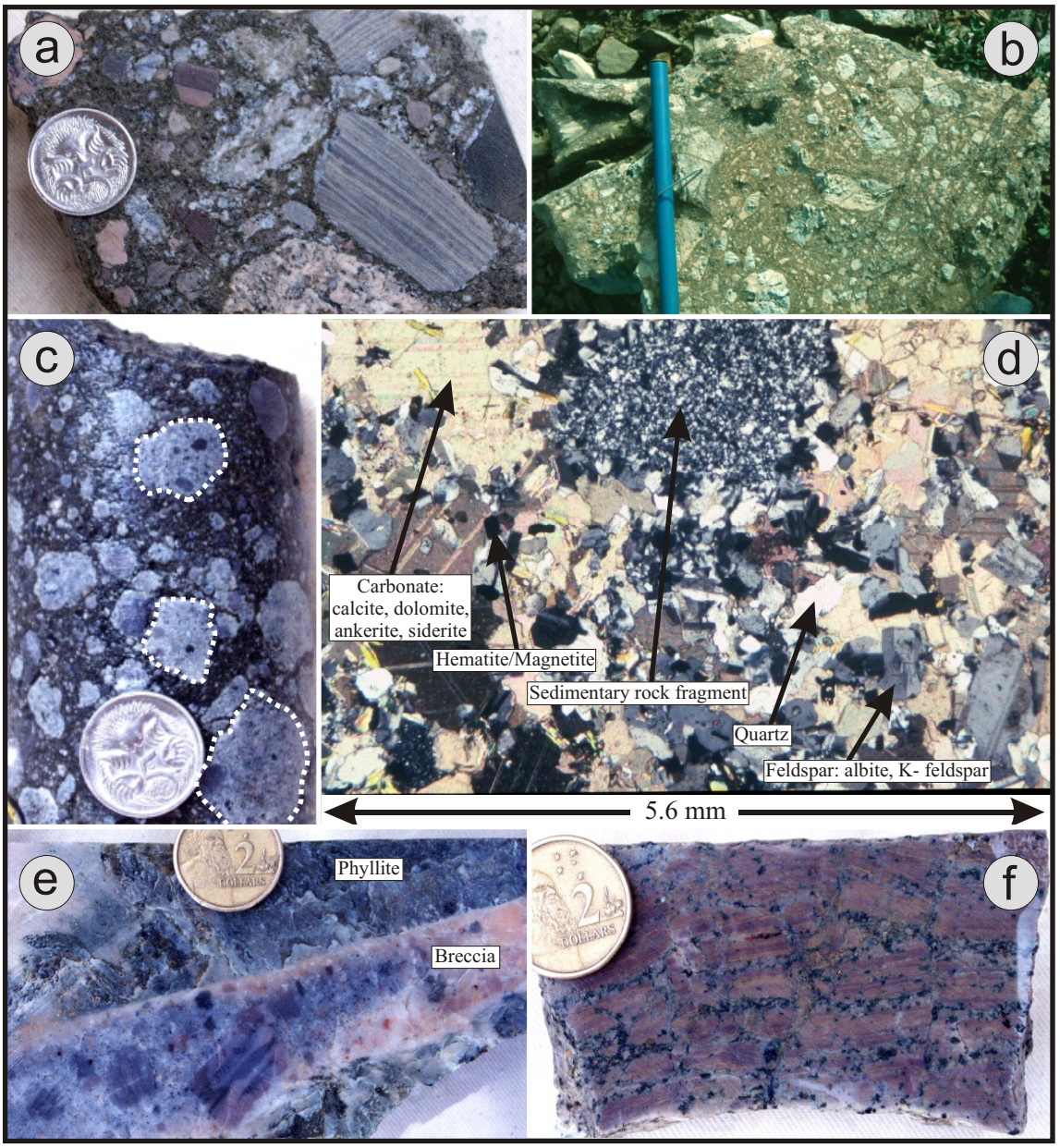

Section A: Figure 6

Figure 7:

Slab mountain area showing location of 'Slab mountain', 'Slab ridge', 'Slab creek', Bonnet Plume River, fold axial trace in the river valley, Wernecke Breccia, high strain zone, breccia that contains deformed clasts of phyllite and large clast of Slab volcanics with some of the flows outlined.

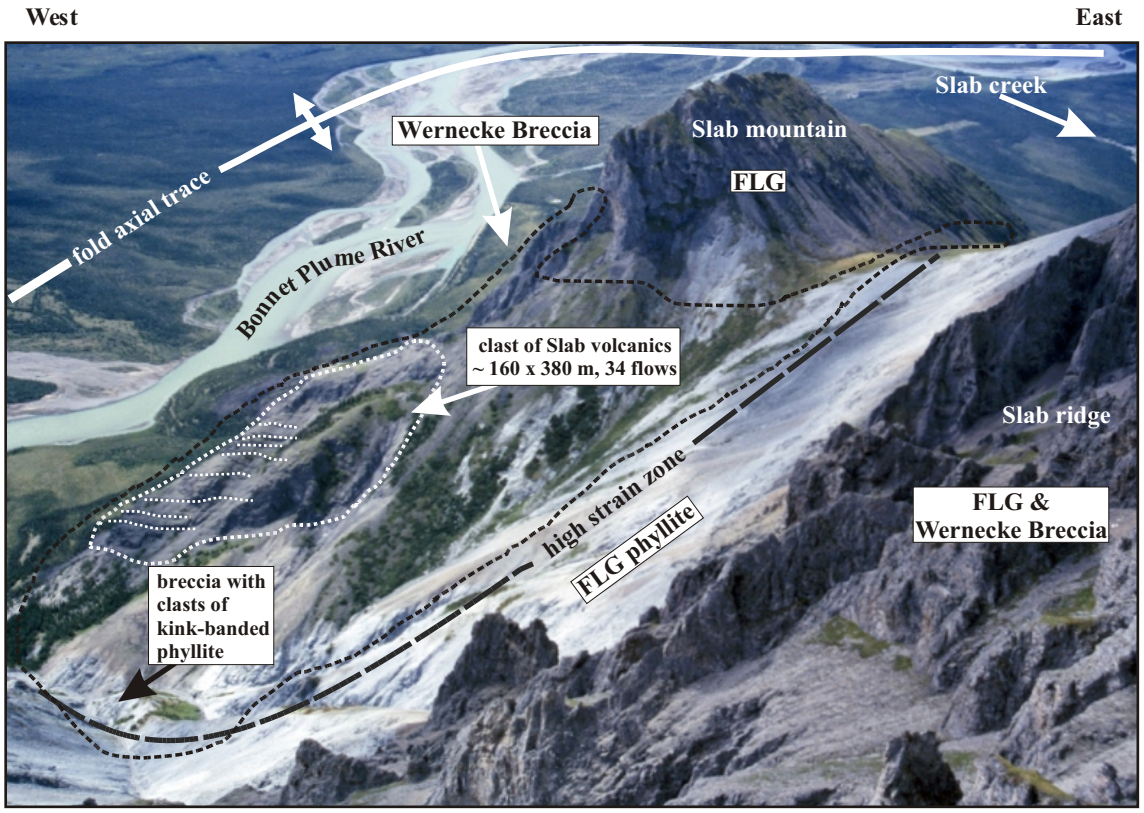
West
East
Slab creek
Wernecke Breccia
Slab mountain
FLG
fold axial trace
Bonnet Plume River
clast of Slab volcanics
~ 160 x 380 m, 34 flows
Slab ridge
high strain zone
FLG &
Wernecke Breccia
FLG phyllite
breccia with
clasts of
kink-banded
phyllite

Figure 8:

Hoover area showing location of FLG, Quartet Group, marker carbonate horizon and upper and lower breccias. (Photo taken by DJ Thorkelson).

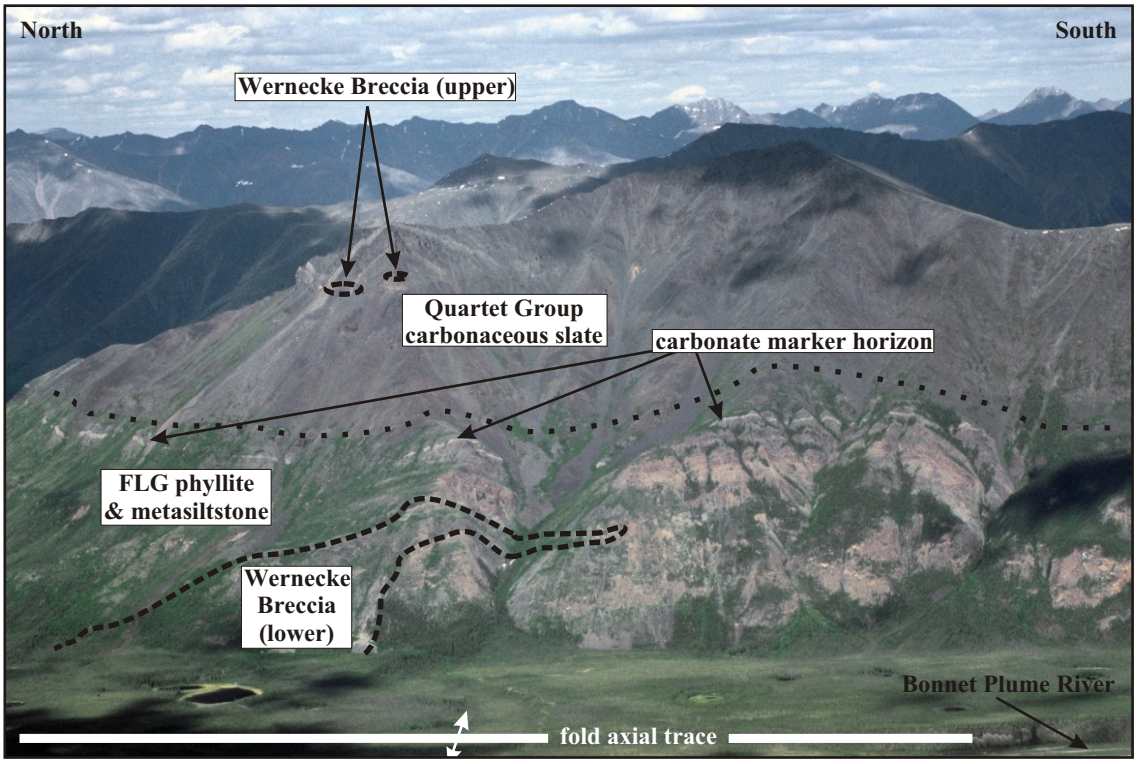
North
South
Wernecke Breccia (upper)
Quartet Group
carbonaceous slate
carbonate marker horizon
FLG phyllite
& metasiltstone
Wernecke
Breccia
(lower)
Bonnet Plume River
fold axial trace

Figure 9:

Igor area showing location of 'Igor ridge', fold axial trace in 'Igor creek', Wer necke Breccia, Quartet Group and Cambrian strata.

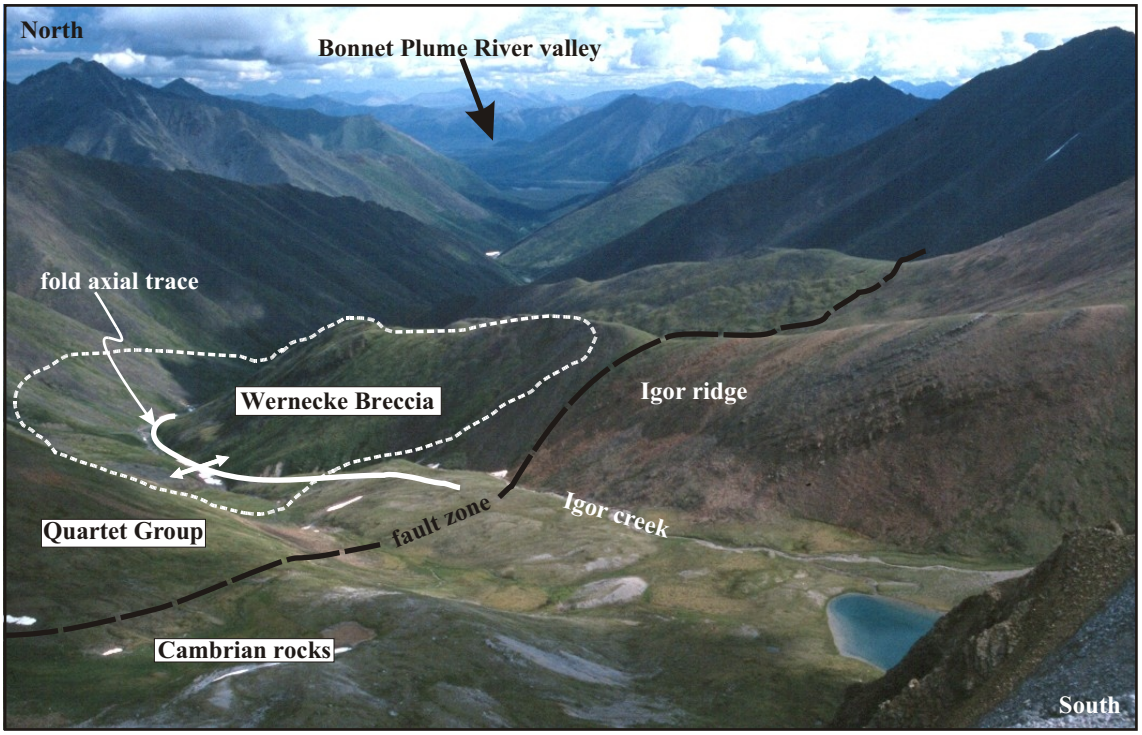

Section A: Figure 9

Figure 10:

Examples of alteration and mineralization: a) grey sodic-altered breccia, b) red potassic-altered breccia, c) biotite-scapolite alteration in FLG metasiltstone cut by albite veins, cross-cut by calcite vein, d) potassic-altered Quartet Group metasiltstone cut by dolomite-chalcopyrite vein, e) ankerite-magnetite vein cutting FLG, Slab prospect, f) massive chalcopyrite-pyrite vein cutting FLG, Slab prospect, g) clast of massive sulphide in breccia, Slab prospect, h) calcite-chalcopyrite vein cutting FLG, Slab prospect and i) chalcopyrite forming matrix to breccia, Hoover prospect.

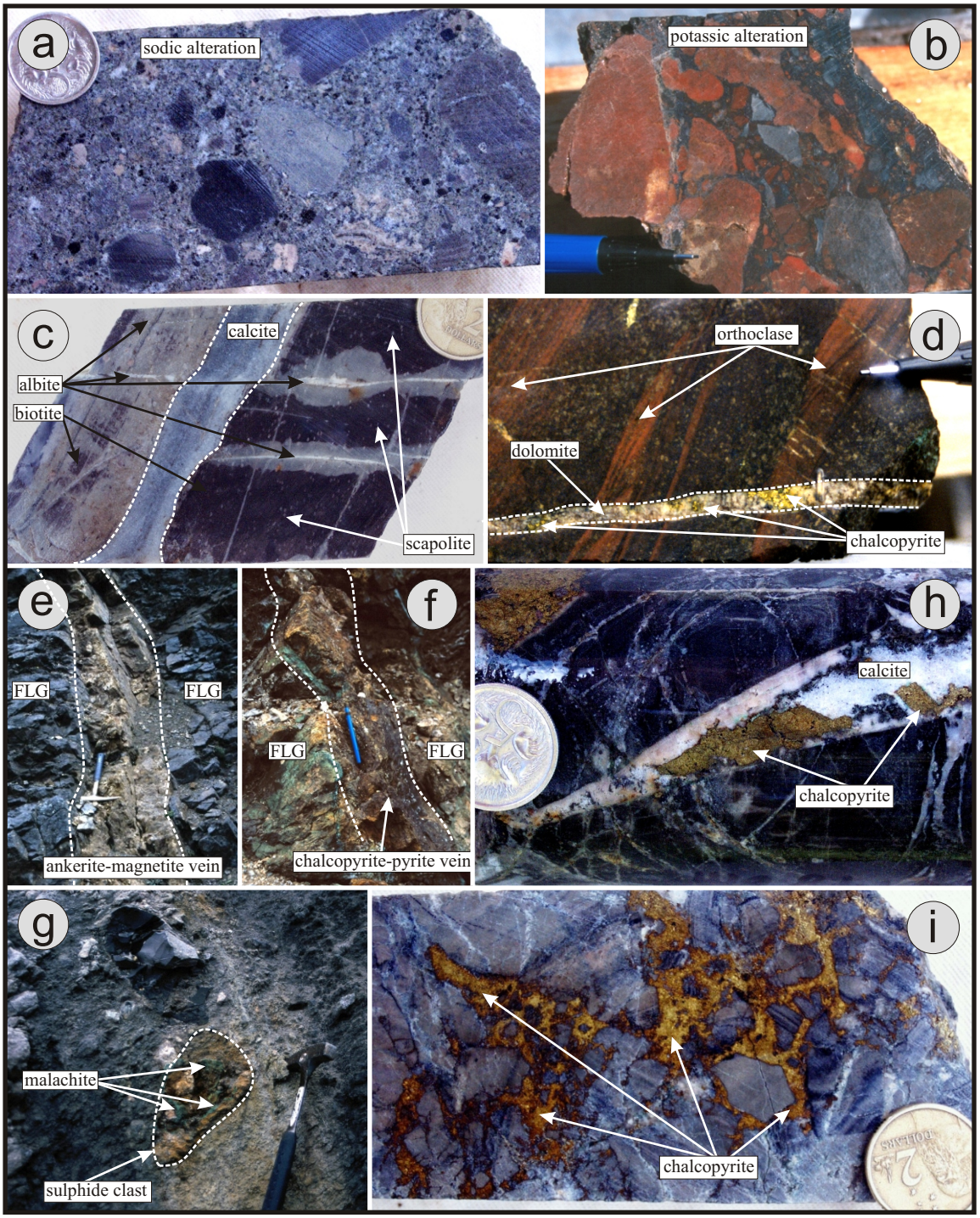

Section A: Figure 10

Figure 11:

Composition of a) feldspar and b) carbonate in Wernecke samples, based on microprobe data. Analyses were obtained with the James Cook University electron microprobe in wavelength dispersive mode, at an accelerating voltage of 15 kV and a current of 20 nA.

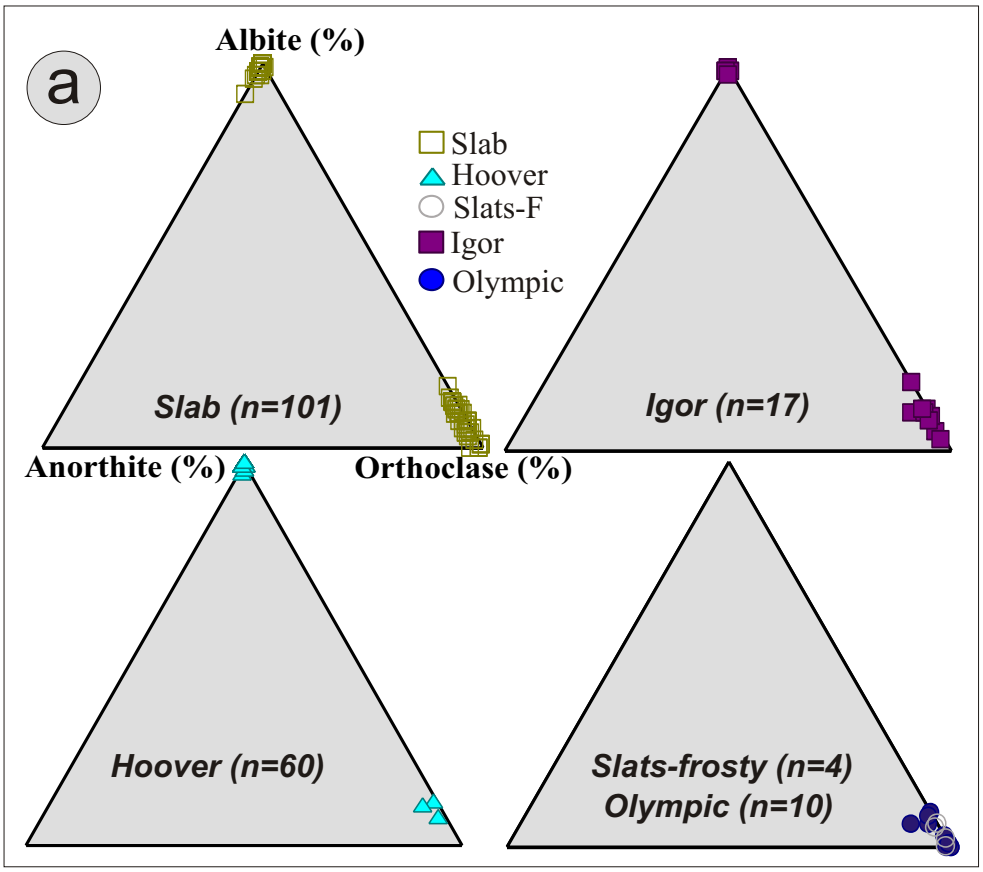
a
Albite (%)
Slab
Hoover
Slats-F
Igor
Olympic
Slab (n=101)
Igor (n=17)
Anorthite (%)
Orthoclase (%)
Hoover (n=60)
Slats-frosty (n=4)
Olympic (n=10)

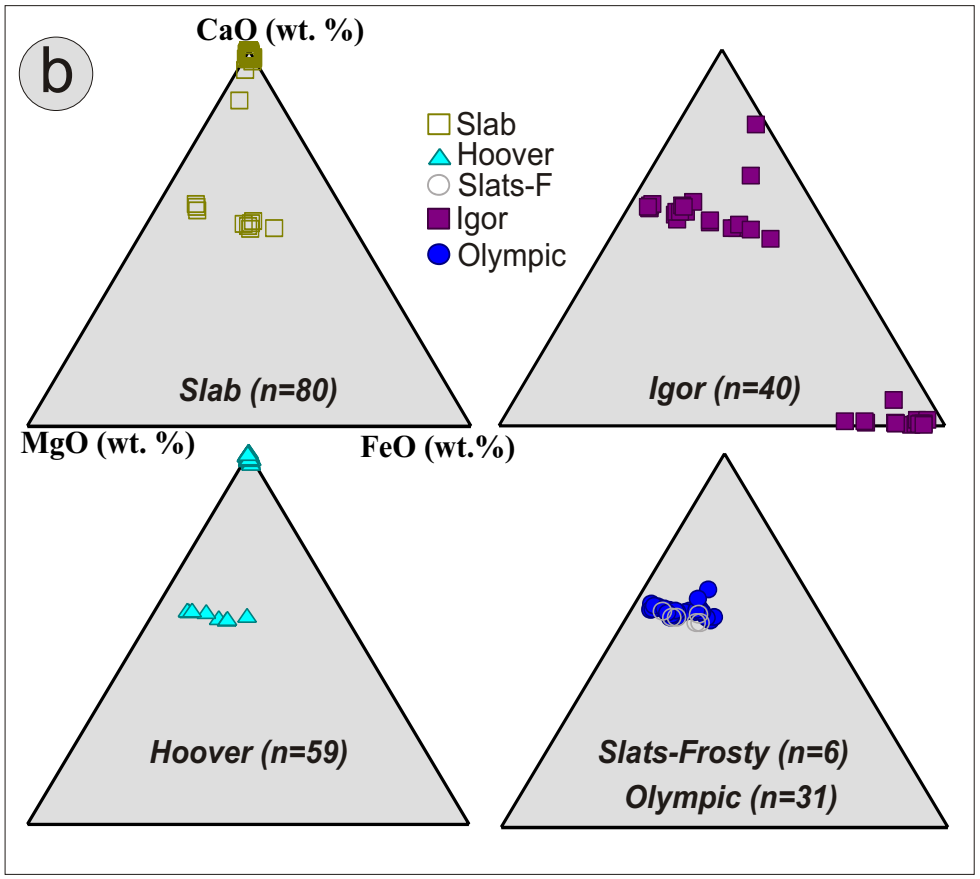
b
CaO (wt. %)
Slab
Hoover
Slats-F
Igor
Olympic
Slab (n=80)
Igor (n=40)
MgO (wt. %)
FeO (wt.%)
Hoover (n=59)
Slats-Frosty (n=6)
Olympic (n=31)

Figure 12:

Examples of mineralization and deformation: a) massive magnetite-coarsely crystalline hematite-ankerite-quartz vein, Slats-Frosty area, b) euhedral magnetite replaced by hematite (rl), Igor prospect, c) euhedral magnetite overgrown by pyrite (rl), Igor prospect, d) hematite overgrown by pyrite with chalcopyrite filling fractures (rl), Olympic prospect, e) clasts of foliated metasiltstone in Wernecke Breccia, f) foliated FLG cut by ankerite vein, both have been kinked during Racklan deformation and g) flattened clasts in foliated breccia. rl = reflected light.

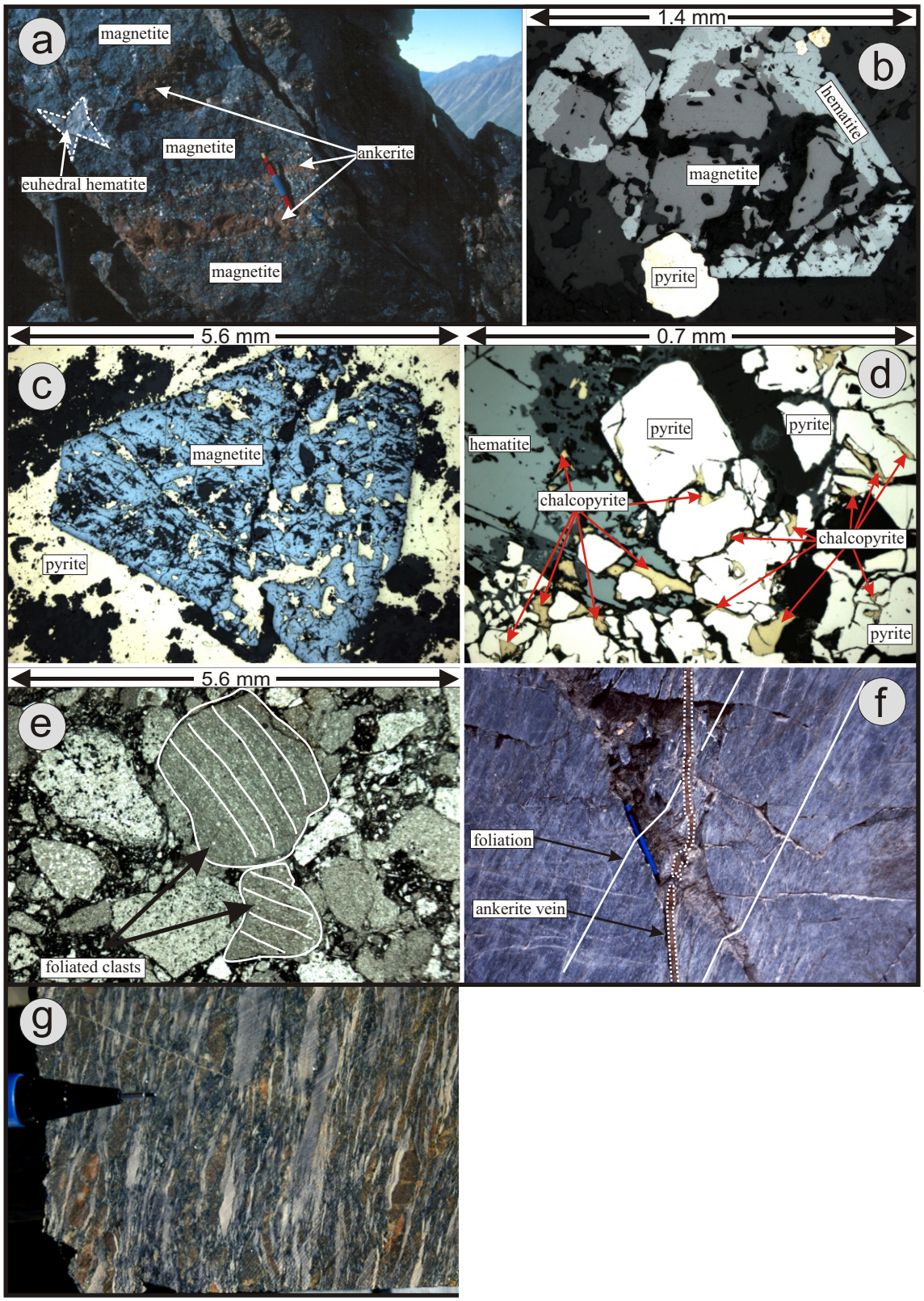

Section A: Figure 12

Figure 13:

Simplified paragenesis for prospects in the Wernecke Mountains : a) Slab, b) Hoover, c) Slats-Frosty, d) Slats-Wallbanger, e) Igor and f) Olympic prospects. NB: paragenetic stages apply only to a specific area, e.g. Slab stage 3 ≠ Hoover stage 3 ≠ Igor stage 3.

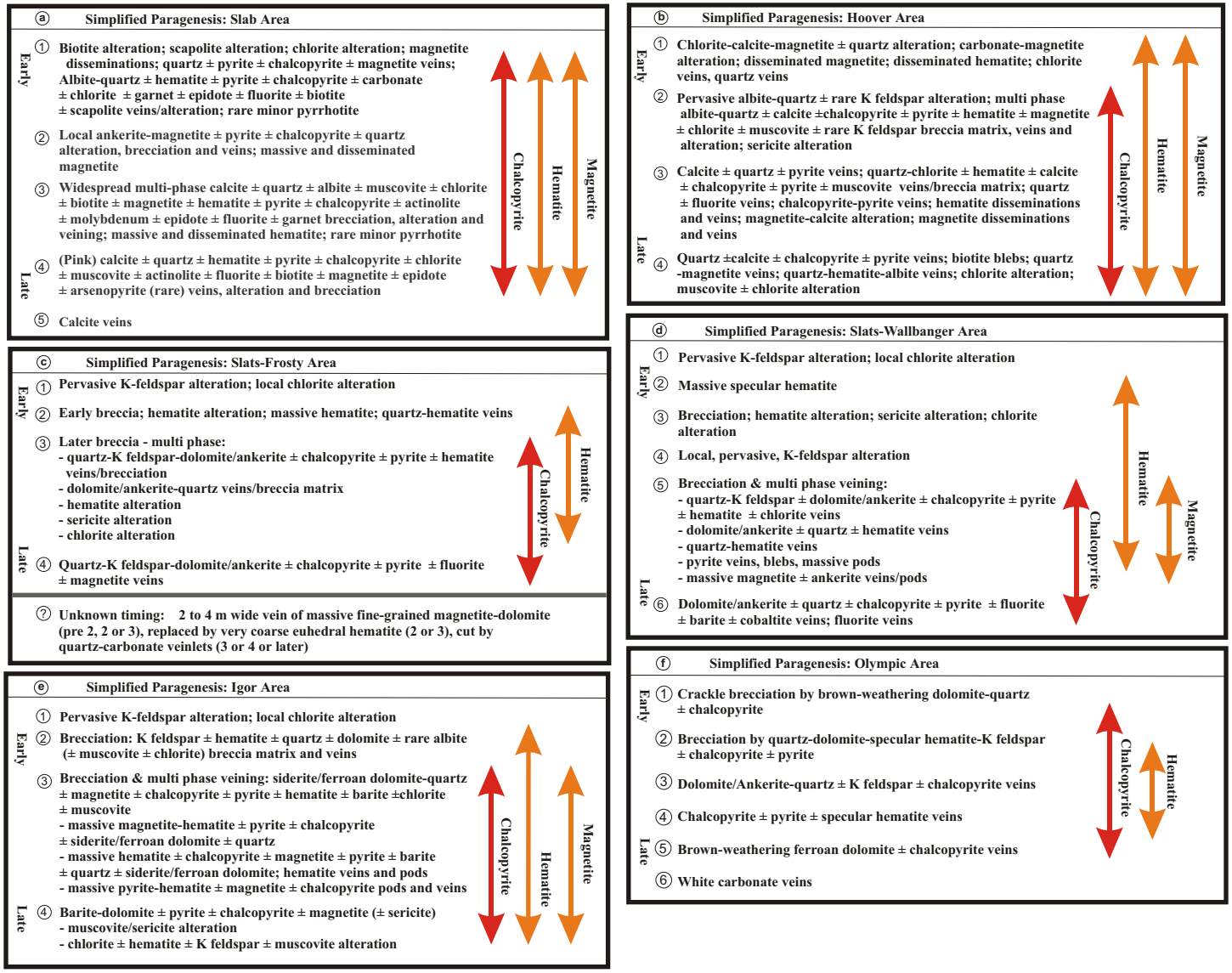
ⓐ Simplified Paragenesis: Slab Area
Early
① Biotite alteration; scapolite alteration; chlorite alteration; magnetite disseminations; quartz ± pyrite ± chalcopyrite ± magnetite veins; Albite-quartz ± hematite ± pyrite ± chalcopyrite ± carbonate ± chlorite ± garnet ± epidote ± fluorite ± biotite ± scapolite veins/alteration; rare minor pyrrhotite
② Local ankerite-magnetite ± pyrite ± chalcopyrite ± quartz alteration, brecciation and veins; massive and disseminated magnetite
③ Widespread multi-phase calcite ± quartz ± albite ± muscovite ± chlorite ± biotite ± magnetite ± hematite ± pyrite ± chalcopyrite ± actinolite ± molybdenum ± epidote ± fluorite ± garnet brecciation, alteration and veining; massive and disseminated hematite; rare minor pyrrhotite
Late
④ (Pink) calcite ± quartz ± hematite ± pyrite ± chalcopyrite ± chlorite ± muscovite ± actinolite ± fluorite ± biotite ± magnetite ± epidote ± arsenopyrite (rare) veins, alteration and brecciation
⑤ Calcite veins
Chalcopyrite
Hematite
Magnetite
ⓑ Simplified Paragenesis: Hoover Area
Early
① Chlorite-calcite-magnetite ± quartz alteration; carbonate-magnetite alteration; disseminated magnetite; disseminated hematite; chlorite veins, quartz veins
② Pervasive albite-quartz ± rare K feldspar alteration; multi phase albite-quartz ± calcite ±chalcopyrite ± pyrite ± hematite ± magnetite ± chlorite ± muscovite ± rare K feldspar breccia matrix, veins and alteration; sericite alteration
③ Calcite ± quartz ± pyrite veins; quartz-chlorite ± hematite ± calcite ± chalcopyrite ± pyrite ± muscovite veins/breccia matrix; quartz ± fluorite veins; chalcopyrite-pyrite veins; hematite disseminations and veins; magnetite-calcite alteration; magnetite disseminations and veins
Late
④ Quartz ±calcite ± chalcopyrite ± pyrite veins; biotite blebs; quartz -magnetite veins; quartz-hematite-albite veins; chlorite alteration; muscovite ± chlorite alteration
Chalcopyrite
Hematite
Magnetite
ⓒ Simplified Paragenesis: Slats-Frosty Area
Early
① Pervasive K-feldspar alteration; local chlorite alteration
② Early breccia; hematite alteration; massive hematite; quartz-hematite veins
③ Later breccia - multi phase:
- quartz-K feldspar-dolomite/ankerite ± chalcopyrite ± pyrite ± hematite veins/brecciation
- dolomite/ankerite-quartz veins/breccia matrix
- hematite alteration
- sericite alteration
- chlorite alteration
Late
④ Quartz-K feldspar-dolomite/ankerite ± chalcopyrite ± pyrite ± fluorite ± magnetite veins
Chalcopyrite
Hematite
? Unknown timing: 2 to 4 m wide vein of massive fine-grained magnetite-dolomite (pre 2, 2 or 3), replaced by very coarse euhedral hematite (2 or 3), cut by quartz-carbonate veinlets (3 or 4 or later)
ⓓ Simplified Paragenesis: Slats-Wallbanger Area
Early
① Pervasive K-feldspar alteration; local chlorite alteration
② Massive specular hematite
③ Brecciation; hematite alteration; sericite alteration; chlorite alteration
④ Local, pervasive, K-feldspar alteration
⑤ Brecciation & multi phase veining:
- quartz-K feldspar ± dolomite/ankerite ± chalcopyrite ± pyrite ± hematite ± chlorite veins
- dolomite/ankerite ± quartz ± hematite veins
- quartz-hematite veins
- pyrite veins, blebs, massive pods
- massive magnetite ± ankerite veins/pods
Late
⑥ Dolomite/ankerite ± quartz ± chalcopyrite ± pyrite ± fluorite ± barite ± cobaltite veins; fluorite veins
Chalcopyrite
Hematite
Magnetite
ⓔ Simplified Paragenesis: Igor Area
① Pervasive K-feldspar alteration; local chlorite alteration
Early
② Brecciation: K feldspar ± hematite ± quartz ± dolomite ± rare albite (± muscovite ± chlorite) breccia matrix and veins
③ Brecciation & multi phase veining: siderite/ferroan dolomite-quartz ± magnetite ± chalcopyrite ± pyrite ± hematite ± barite ±chlorite ± muscovite
- massive magnetite-hematite ± pyrite ± chalcopyrite ± siderite/ferroan dolomite ± quartz
- massive hematite ± chalcopyrite ± magnetite ± pyrite ± barite ± quartz ± siderite/ferroan dolomite; hematite veins and pods
- massive pyrite-hematite ± magnetite ± chalcopyrite pods and veins
Late
④ Barite-dolomite ± pyrite ± chalcopyrite ± magnetite (± sericite)
- muscovite/sericite alteration
- chlorite ± hematite ± K feldspar ± muscovite alteration
Chalcopyrite
Hematite
Magnetite
ⓕ Simplified Paragenesis: Olympic Area
Early
① Crackle brecciation by brown-weathering dolomite-quartz ± chalcopyrite
② Brecciation by quartz-dolomite-specular hematite-K feldspar ± chalcopyrite ± pyrite
③ Dolomite/Ankerite-quartz ± K feldspar ± chalcopyrite veins
④ Chalcopyrite ± pyrite ± specular hematite veins
Late
⑤ Brown-weathering ferroan dolomite ± chalcopyrite veins
⑥ White carbonate veins
Chalcopyrite
Hematite

Figure 14:

Cartoon depicting evolution of Wernecke Basin and structural controls on location of Wernecke Breccia. Stage I: deposition of FLG. Stage II: deposition of Quartet Group and GLG. Stage III: emplacement of Wernecke Breccia into pre-existing weak zones in deformed and metamorphosed WSG. Breccia bodies are widespread at the top of FLG in metaevaporite-bearing stratigraphy. See text for detailed description of stages.

I: deposition of FLG

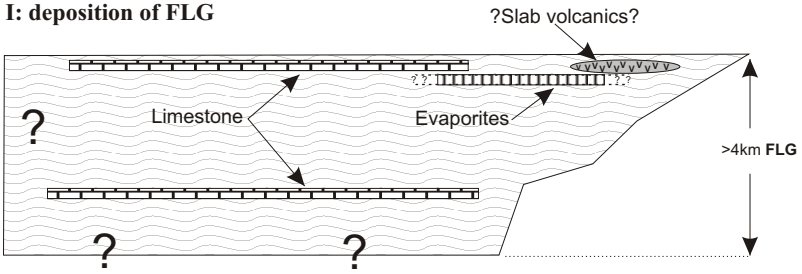

II: subsidence and thermal deepening of the basin; deposition of QG and GLG, followed by intrusion (pre- or syn-Racklan Orogenesis) of BPRI

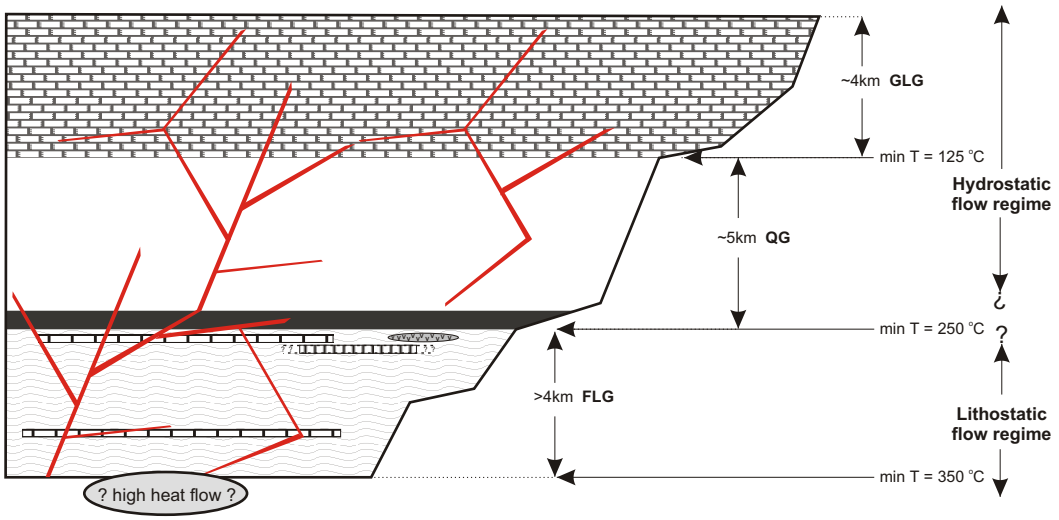

III: Racklan orogenesis - greenschist facies metamorphism (~ 450 °C, 3-6 kbars), deformation and syn- to post-deformation breccia emplacement

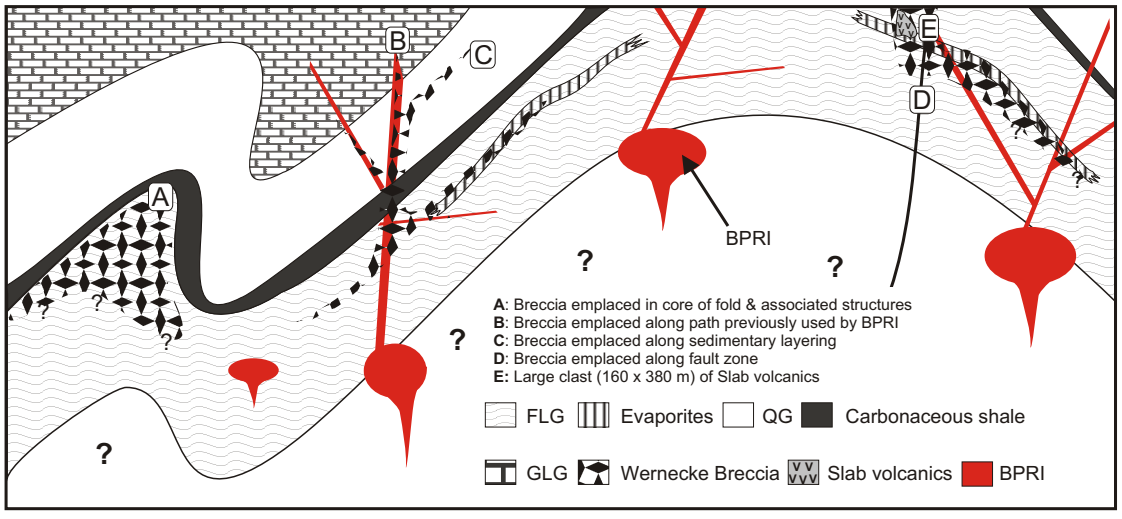

SECTION A - TABLES

Regional-scale Proterozoic iron oxide-copper-gold-mineralised breccia systems: examples from the Wernecke Mountains, Yukon, Canada

Table 1: Description of formations within WSG. Information from Delaney (1981).

Formation	Thickness (m)	Description	Sedimentary Structures
G-7	400 to 700	Thin to thick beds of orange-, buff-, and grey-weathering dolostone (patches of limestone); locally stromatolitic, locally carbonaceous. Lenses and nodules of grey chert.	Wavy and lenticular beds, parallel to crinkly laminations, oolites, pisolites, stromatolites, molar-tooth structure
G-6	500 to 800	Thin to thick beds of buff-, grey-, and maroon-weathering dolostone (locally carbonaceous), limestone, mudstone and siltstone.	Lenticular and wavy beds, parallel and cross laminations, load structures, microstylolites
G-5	~ 500	Thin to medium beds of buff-, grey, to locally maroon- or orange-weathering dolostone (locally carbonaceous) and claystone, minor siltstone and mudstone. Local thin to thick interbeds of stromatolitic dolostone conglomerate (granule- to pebble-sized clasts) and mounds, up to 3m high, of brecciated stromatolitic dolostone (pebble- to cobble-sized clasts). Pods and lenses of dark grey chert.	Wavy and flaser beds, parallel and cross laminations, ripple marks, slump structures, stromatolites
G-4	~ 450	Thin beds of brown-, buff-, grey-, locally orange- or maroon-, recessive-weathering dolostone, mudstone and siltstone interlayered with up to 20% thin beds and lenses of grey chert.	Parallel to wavy laminations
G-3	At least 50	Medium to thick beds of buff-weathering silty dolostone.	Parallel laminations, tent structures
G-2	400 to 600	Brown-, grey- and orange-weathering mudstone and lesser siltstone and silty dolostone. Minor lenses of black chert.	Laminations, lenticular beds, load structures
G-Tr	25 to 700	Grey-weathering siltstone, fine-grained sandstone and mudstone interlayered with thin beds of orange- to brown-weathering silty dolostone and dolomitic siltstone.	Parallel- and cross-laminations, wavy, lenticular and flaser-bedding, graded bedding, ripple marks, load structures, flame structures, shrinkage cracks, slump folds
Q-2	≤ 5000	Thin-, medium- to thick-bedded grey-weathering siltstone, mudstone, fine-grained sandstone and claystone.	Parallel- and cross-laminations, wavy, lenticular and flaser-bedding, graded bedding, ripple marks, load structures, flame structures, shrinkage cracks, slump folds
Q-1	~ 200	Dark grey-weathering, thin-bedded, locally pyritic, carbonaceous claystone, clayey siltstone and carbonaceous mudstone.	None – sediments have generally been metamorphosed to slate
F-Tr	≤ 365	Grey-, brown- to white-weathering slate, mudstone, siltstone, dolomitic mudstone, silty dolostone and limestone. 7-14 m-thick limestone marker.	Cross-beds, molar tooth structures
F-4	> 500	Thin to thick beds of grey-weathering siltstone, fine-grained sandstone and mudstone.	Parallel- to cross-laminations to wavy beds, ripple marks, cross-beds
F-3	~ 2000	Thin to medium beds of grey-weathering siltstone, mudstone and fine-grained sandstone, minor intercalated thin beds of silty limestone.	Parallel laminations to lenticular beds, ripple marks, load structures, flutes
F-2	~ 400	Thin-bedded grey to buff-weathering siltstone, mudstone, fine-grained sandstone and silty to sandy limestone.	Wavy to planar to lenticular beds/laminations, cross-beds, load structures
F-1	> 1800	Thin to medium beds of grey-weathering siltstone, mudstone and fine-grained sandstone, minor limestone.	Laminated to lenticular beds, asymmetrical cross-beds, ripple marks, load structures

Table 2: Representative results of scapolite and biotite microprobe analyses. % meionite = 100 (Ca+Mg+Fe+Mn+Ti) / (Na+K+Ca+Mg+Fe+Mn+Ti); marialite = 100 - meionite (after Deer *et al*., 1992). Analyses were obtained with the James Cook University JEOL electron microprobe in wavelength dispersive mode, at an accelerating voltage of 15 kV and a current of 20 nA, ZAF corrections were used. [1] average of 70 analyses, [2] average of 10 analyses.

Oxide (weight %)	Scapolite Min - Max	Scapolite [1] Average	Biotite Min - Max	Biotite[2] Average
SiO_2	54.61-57.73	56.08	37.27-40.64	38.92
TiO_2	0.00-0.04	0.01	1.33-2.57	2.00
Al_2O_3	21.12-22.54	21.78	14.79-13.23	14.00
FeO	0.00-0.09	0.04	12.97-15.53	14.28
MnO	0.00-0.04	0.01	0.04-0.43	0.19
MgO	0.00-0.01	0.00	12.76-14.59	13.75
CaO	5.34-7.13	6.34	0.00-0.37	0.17
Na_2O	7.94-10.24	9.68	0.00-0.61	0.08
K_2O	0.44-1.21	0.55	9.96-10.63	10.27
Cl	2.90-3.55	3.29	0.46-0.72	0.59
Total	96.09-98.97	97.77	91.21-97.49	94.25
% meionite $Ca_4[Al_6Si_6O_{24}]CO_3$	22.12-30.44	25.98		
% marialite $Na_4[Al_3Si_9O_{24}]Cl$	69.56-77.88	74.02		

Table 3 (next page): Main characteristics of IOCG prospects included in this study, see text for details. In mineralization column: V = vein, D = disseminated, B = forms breccia matrix. [1]Yukon MINFILE (2003) database number. Information from: [2](Thorkelson *et al.*, 2003), [3](Yukon MINFILE, 2003), [4](Stammers, 1995), [5](Eaton & Archer, 1981) and [6](Caulfield, 1994).

Prospect	Resource/best intersection	Metals	Mineralization (dominant)	Alteration (dominant)	Stratigraphic setting	Structural setting
Slab (106D 070)[1]	20 million tons of 0.35% Cu & 0.17 gpt Au[2]	Fe, Cu, Au ± Mo, Co, U	Magnetite^{VD}, hematite^{VDB} chalcopyrite^{VDB}, pyrite^{VDB} ± brannerite^{VD}, molybdenite^{D}, cobaltite^{D}	Pervasive albite-scapolite ± orthoclase; calcite veins	Upper FLG interlayered fine-grained calcareous metasedimentary rocks & minor carbonate; halite-facies metaevaporites	Folds, high strain zone(s), permeable strata
Hoover (106E 002)[1]	0.32 gpt Au & 0.42% Cu over 73m[2]; 3.6% Cu over 3.1m[2,3]	Fe, Cu, Au ± U, Co	Magnetite^{VD}, hematite^{VDB}, pyrite^{VDB}, chalcopyrite^{VDB} ± brannerite^{VD}	Pervasive albite ± scapolite; calcite ± dolomite veins	Transition from FLG fine-grained calcareous metasedimentary rocks to Quartet Group carbonaceous shale/slate	Folds, high strain zone
Slats-F (106D 075)[1]	1380 ppb Au & 9650 ppm Cu from a grab sample[2]	Fe, Cu, Au ± Co	Magnetite^{VD}, hematite^{VDB}, minor chalcopyrite^{VD}, pyrite^{VD}	Pervasive orthoclase; dolomite-ankerite veins	?FLG fine-grained calcareous metasedimentary rocks	Fold, high strain zone, fractures, pathways previously used by BPRI, permeable strata
Slats-W (106D 075)[1]	450 ppb Au, 1115 ppm Cu & 5800 ppm Co over 1m[4]	Fe, Cu ± Co, U, Au	Magnetite^{VD}, pyrite^{VDB}, hematite^{VDB}, chalcopyrite^{VD} ± cobaltite^{D}, brannerite^{VD}	Pervasive orthoclase; dolomite-ankerite veins	Interlayered shale and fine-grained calcareous metasedimentary rocks at the transition from Quartet Group to GLG	pathways previously used by BPRI, permeable strata
Igor (106E 009)[1]	4.74% Cu, 0.088% U_3O_8 & 325 ppm Co over 19.7m[5]; 6.14% Cu, 0.89% U_3O_8 & 358 ppm Co over 10.6m[5]	Fe, Cu, U ± Co, Au	Magnetite^{VDB}, hematite^{VDB}, pyrite (some is cobaltian)^{VDB}, chalcopyrite^{VDB}, barite^{VD} ± pitchblende^{VD}	Pervasive orthoclase-sericite ± albite; dolomite-ankerite-siderite veins; disseminated siderite; disseminated and vein barite	Quartet Group fine-grained calcareous metasedimentary rocks with well preserved sedimentary structures, e.g. ripple marks	Fold, high strain zone
Olympic (106C 095)[1]	1593 ppm Cu, 40 ppm Co & 23 ppb Au over 11m[6]; 0.8% Cu & 14 ppm Co over 1.7m[6]	Fe, Cu ± Co, Au	Hematite^{VDB}, pyrite^{VD}, chalcopyrite^{VD} ± cobaltite^{D}	Pervasive and vein dolomite-ankerite; locally pervasive orthoclase;	GLG dolostone (locally stromatolitic)	Folds, faults, pathways previously used by BPRI

SECTION B - FIGURES

Constraints on the age of Wernecke Breccia and associated iron oxide-copper-gold mineralisation: new Ar-Ar, U-Pb, Pb-Pb and Re-Os dates

Figure 1:

Location of study area, distribution of WSG and Wernecke Breccia (modified from Thorkelson, 2000) plus simplified geology map of the study area (for details see Thorkelson, 2000 and Thorkelson *et al.*, 2002). Legend shows approximate stratigraphic position of IOCG prospects included in this study.

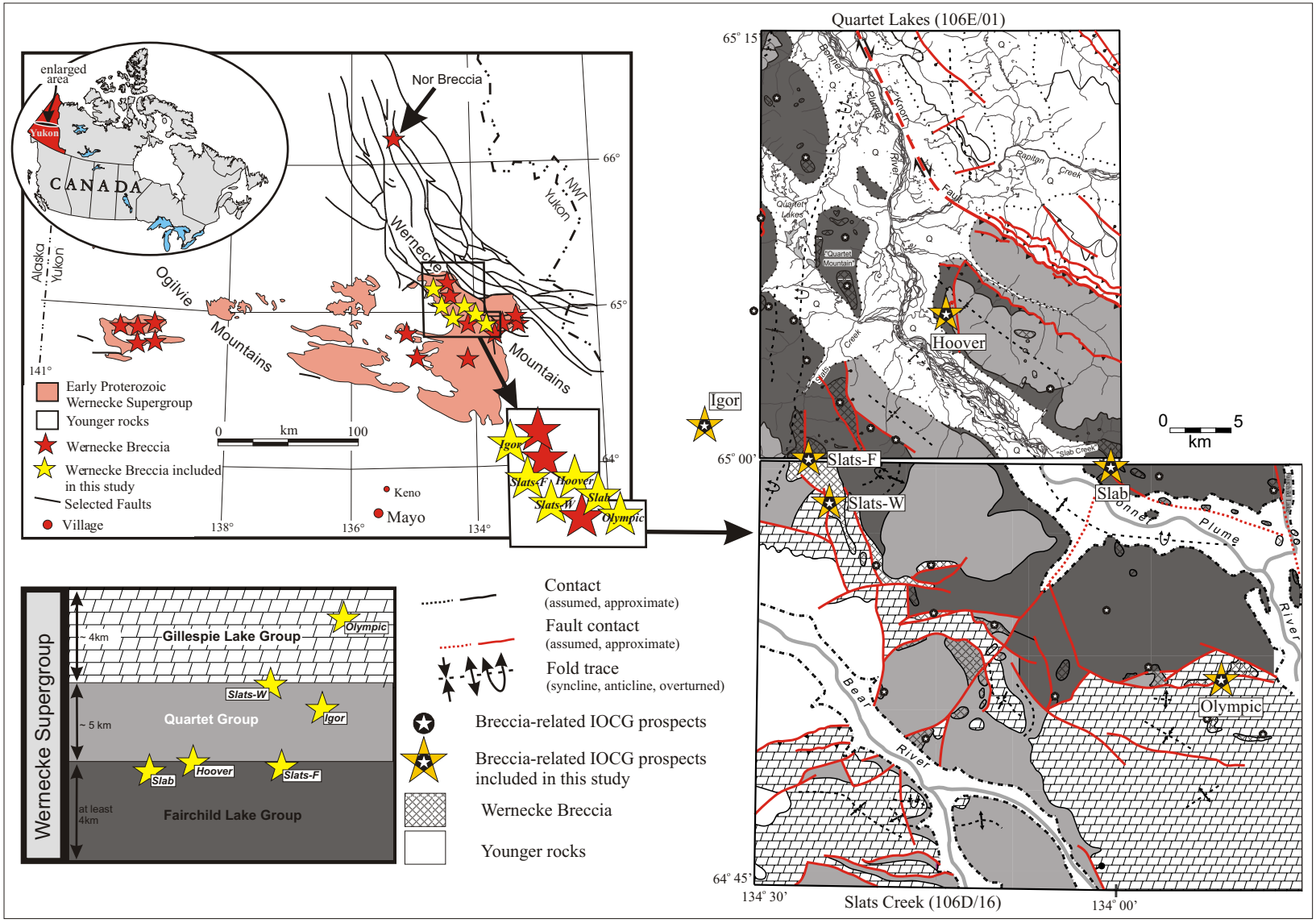

Section B: Figure 1

Figure 2:

Time stratigraphic column of the Wernecke area showing major depositional, intrusive and deformational events (modified from Thorkelson, 2000). Ar-Ar dates in bold are from this study.

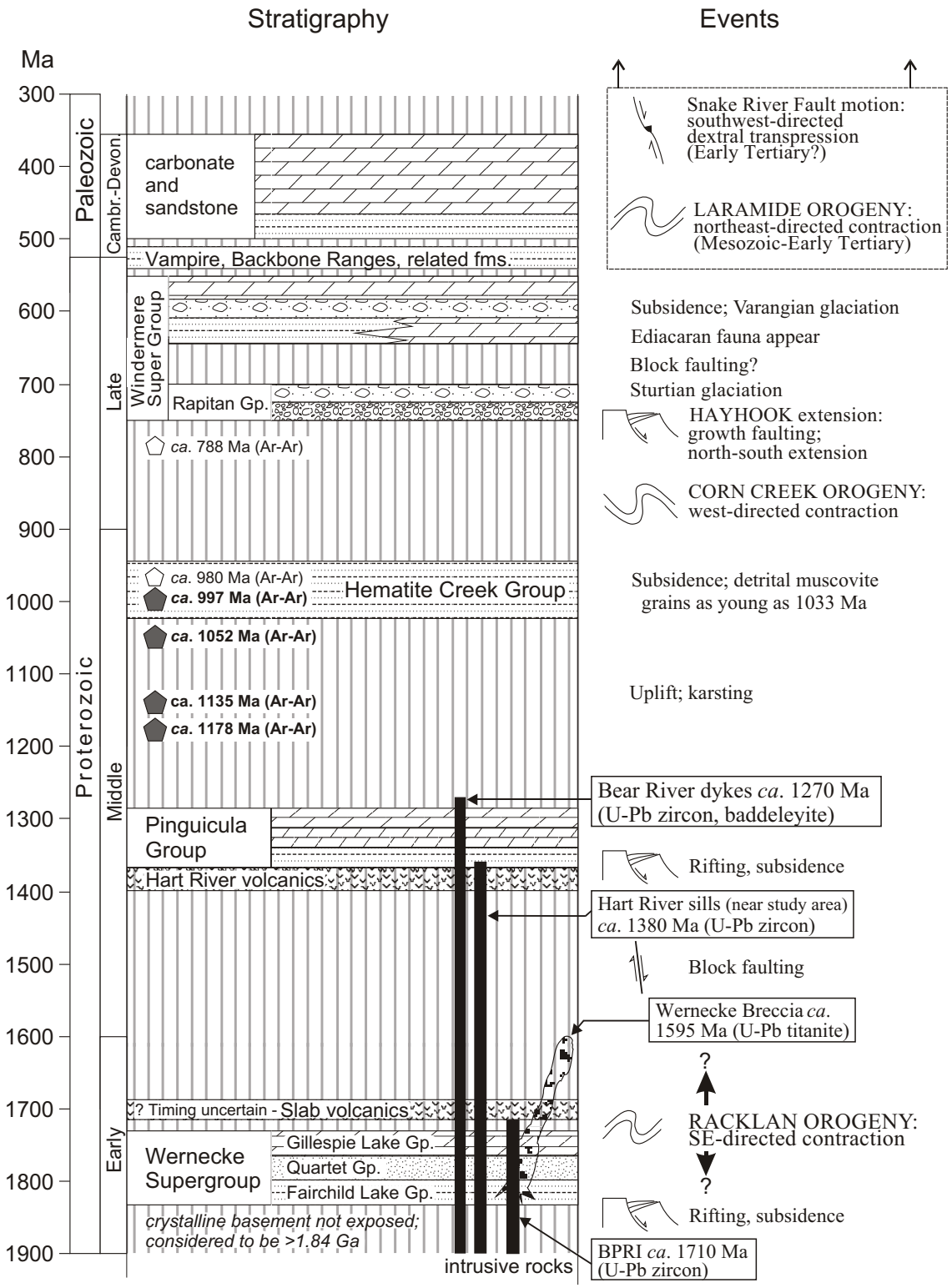

Section B: Figure 2

Figure 3:

Release spectra for ^{40}Ar-^{39}Ar ages for muscovite from four Wernecke Breccia-related samples.

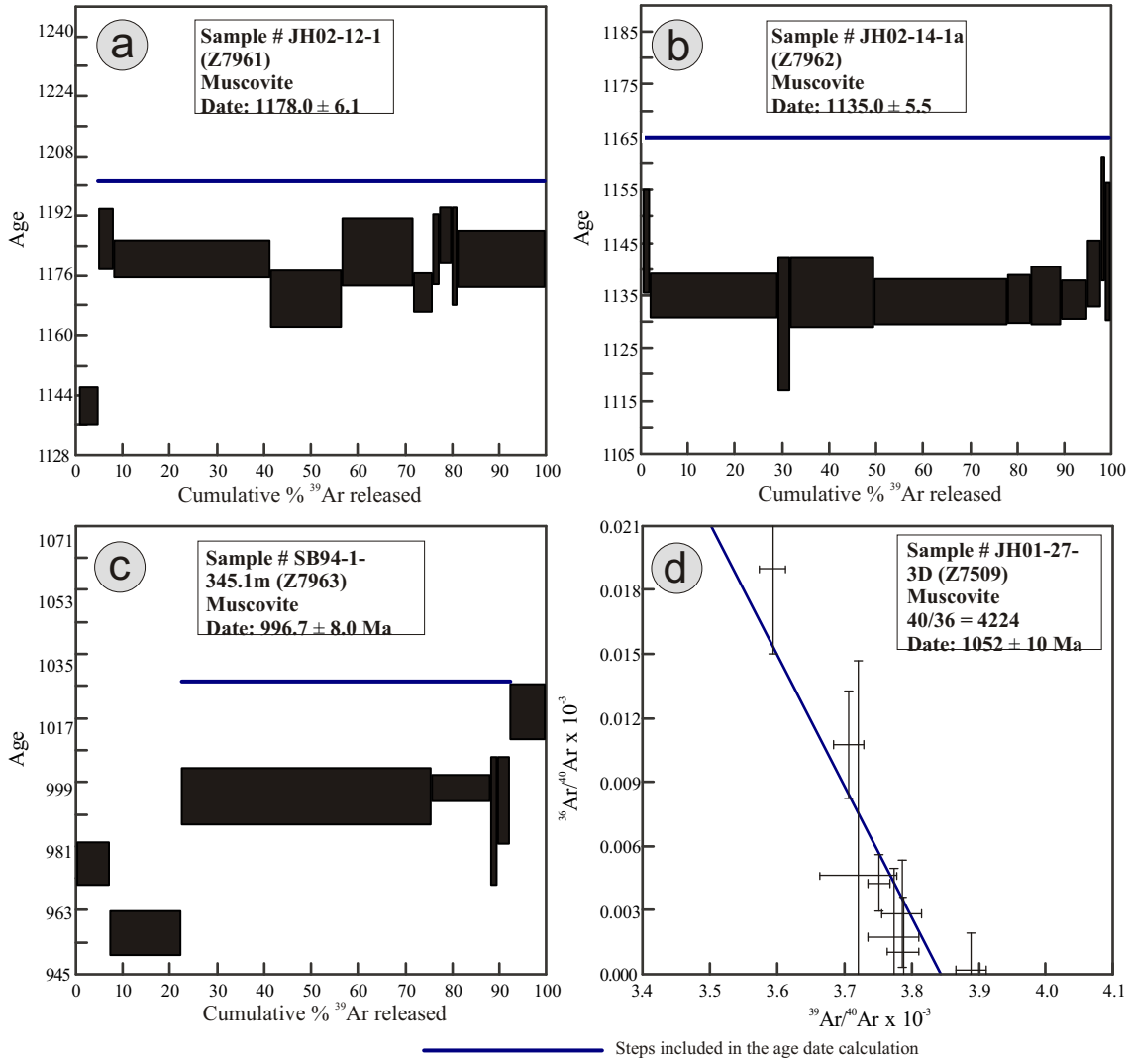

Section B: Figure 3

Figure 4:

$^{207}Pb/^{235}U$ versus $^{206}Pb/^{238}U$ plot for three fractions of titanite from a Wernecke Breccia-related vein. Error for Pb/Pb age is quoted at the 2σ level.

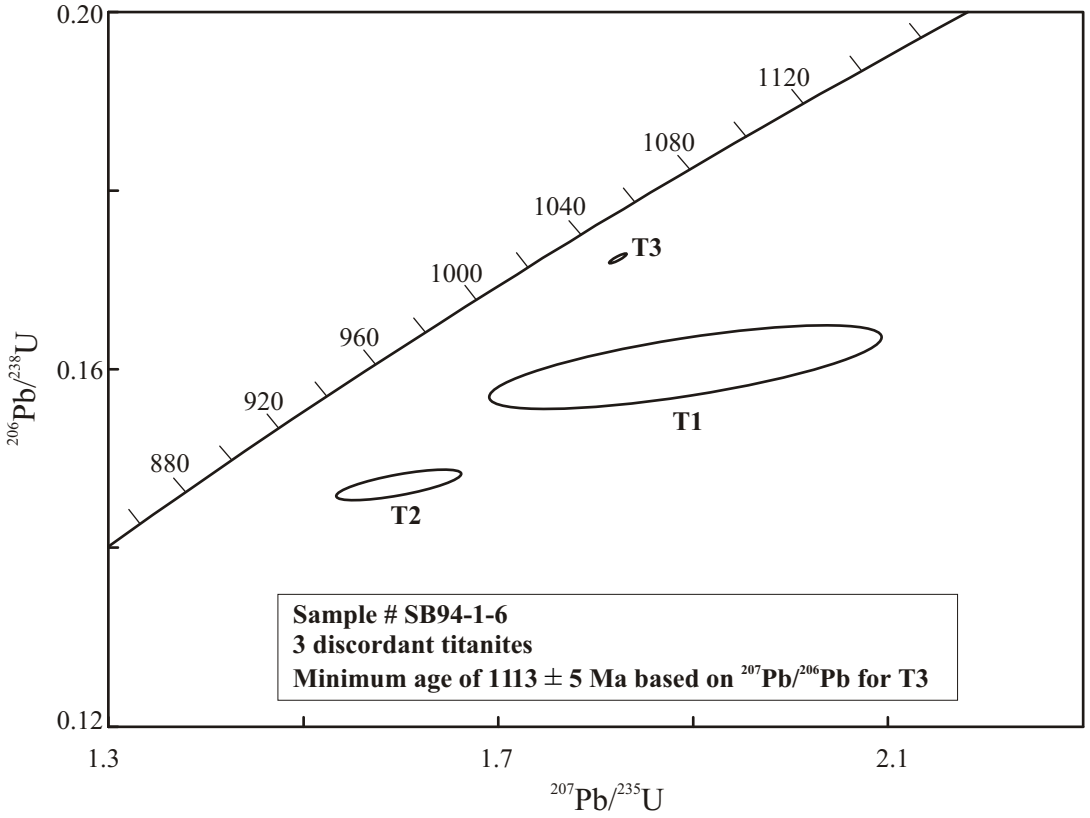
0.20
0.16
0.12
1.3
1.7
2.1
$^{206}Pb/^{238}U$
$^{207}Pb/^{235}U$
1120
1080
1040
1000
960
920
880
T3
T1
T2
Sample # SB94-1-6
3 discordant titanites
Minimum age of 1113 ± 5 Ma based on $^{207}Pb/^{206}Pb$ for T3

Figure 5:

$^{206}Pb/^{204}Pb$ versus $^{207}Pb/^{204}Pb$ plot for 5 analyses of a sample of GLG dolostone.

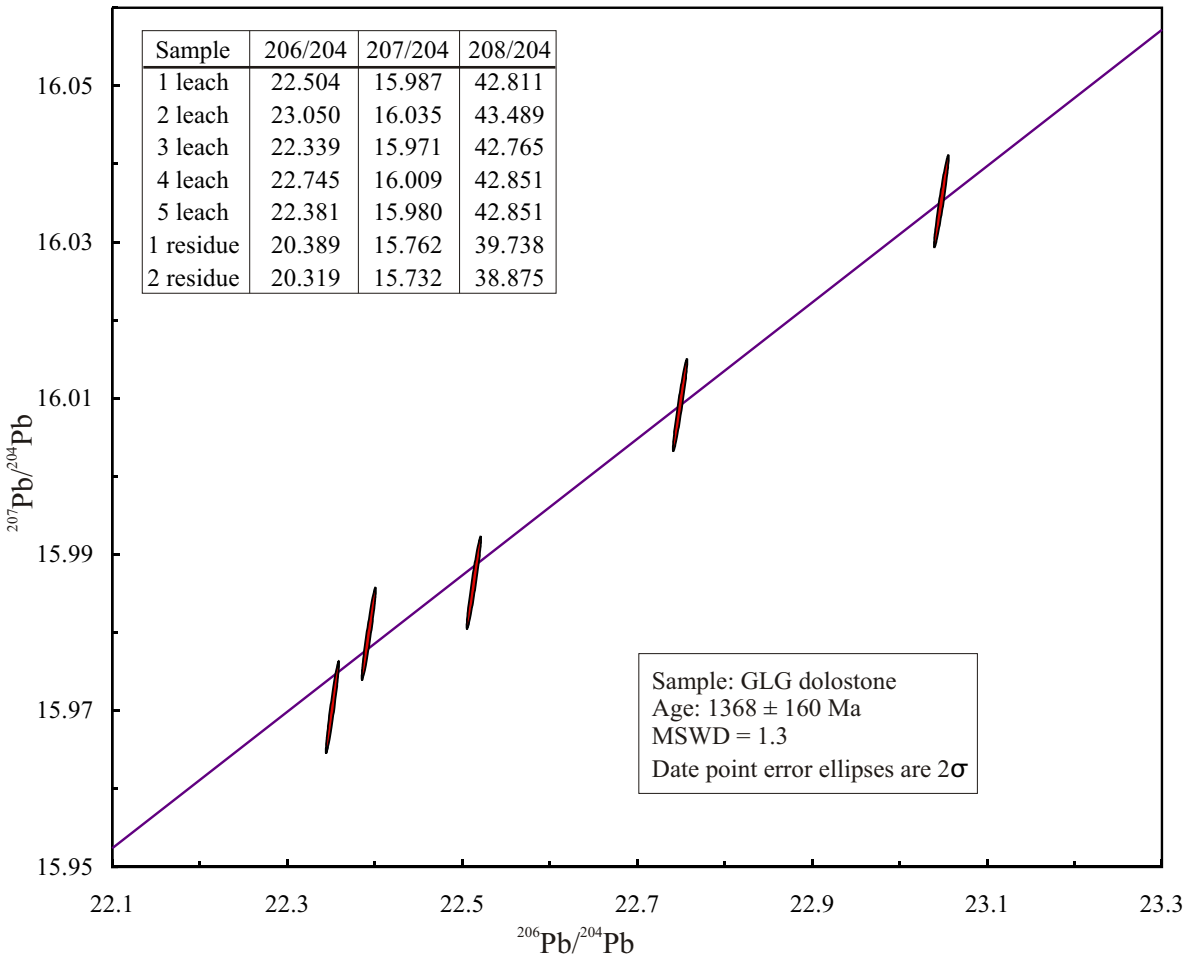
Sample | 206/204 | 207/204 | 208/204
1 leach | 22.504 | 15.987 | 42.811
2 leach | 23.050 | 16.035 | 43.489
3 leach | 22.339 | 15.971 | 42.765
4 leach | 22.745 | 16.009 | 42.851
5 leach | 22.381 | 15.980 | 42.851
1 residue | 20.389 | 15.762 | 39.738
2 residue | 20.319 | 15.732 | 38.875
16.05
16.03
16.01
15.99
15.97
15.95
207Pb/204Pb
22.1
22.3
22.5
22.7
22.9
23.1
23.3
206Pb/204Pb
Sample: GLG dolostone
Age: 1368 ± 160 Ma
MSWD = 1.3
Date point error ellipses are 2σ

SECTION B - TABLES

Constraints on the age of Wernecke Breccia and associated iron oxide-copper-gold mineralisation: new Ar-Ar, U-Pb, Pb-Pb and Re-Os dates

Table 1: Summary of published age dates for Wernecke Breccia-related samples, WSG and Slab volcanics.

Date (Ma)	Analysis	Description	Reference
Wernecke Breccia			
1500	K-Ar - biotite	Breccia complex cutting upper FLG on Quartet Mountain	Archer *et al.* (1977)
1153	U-Pb - pitchblende	Fractures associated with breccia in lower Quartet Group west of Quartet Lakes	Archer & Schmidt (1978)
1249	U-Pb - pitchblende	Fractures associated with breccia in lower Quartet Group west of Quartet Lakes	Archer & Schmidt (1978)
ca. 1200 to 400	U-Pb - pitchblende, brannerite	17 analyses of U minerals from breccia, veins & whole rock samples	Archer et al. (1986)
1270 ± 40	U-Pb - monazite	Nor breccia	Parrish & Bell (1987)
1594.8 ± 4.6	U-Pb - titanite	Matrix of breccia zone on east side of Slab mountain	Thorkelson (2000); Thorkelson et al. (2001a)
Wernecke Supergroup			
980 +/- 4	white mica	FLG schist	Thorkelson et al. (in review)
788 ± 8	white mica	FLG schist	Thorkelson et al. (in review)
Slab volcanics			
1382.8 ± 7.4	Rutile	Intermediate composition lava in a large clast of Slab volcanics within Wernecke Breccia	Thorkelson (2000)

Table 2: Summary of sample characteristics and new age dates obtained during this study.

Sample #	JH02-12-1 (Z7961)	JH02-14-1a (Z7962)	SB94-1-345.1m (Z7963)	JH01-27-3D (Z7509)	SB94-1-6.9 m	JH02-21-1
Location	Igor NAD 83, Zone 8 E0517196, N7213545	Slab NAD 83, Zone 8 E0545492, N7209860	Slab NAD 27, Zone 8 E0545727, N7208459	Slab NAD 27, Zone 9 E0545639, N7208014	Slab NAD 27, Zone 8 E0545727, N7208459	Olympic NAD 83, Zone 8 E0555311, N7195674
Sample description	Breccia with abundant hydrothermal musc. in the matrix	Abundant muscovite in the selvage of a massive pyrite-chalcopyrite vein that cross-cuts FLG adjacent to breccia	Quartz-calcite-muscovite-albite-molybdenum-chlorite vein that cross-cuts FLG meta-siltstone	Quartz-calcite-muscovite-albite-molybdenite-chalcopyrite vein that cross-cuts Wernecke Breccia	Calcite-biotite-titanite vein that cuts FLG metasiltstone proximal to breccia	GLG stromatolitic dolostone
Reason for dating	To date breccia emplacement into middle WSG strata	To date breccia-associated mineralising event	To date late-stage carbonate alteration and constrain age of brecciation	To date late-stage carbonate alteration and constrain age of brecciation	To date late-stage carbonate alteration and constrain age of brecciation	To constrain age of WSG
Paragenetic stage	Breccia matrix	Main breccia-associated mineralization	Late stage vein	Late stage vein	Late stage vein	upper WSG
Phase	Muscovite	Muscovite	Muscovite, Molybdenite	Muscovite, Molybdenite	Titanite	Dolostone
Analysis	^{40}Ar-^{39}Ar	^{40}Ar-^{39}Ar	^{40}Ar-^{39}Ar, Re-Os	^{40}Ar-^{39}Ar, Re-Os	U-Pb	Pb-Pb
Age (Ma)	1178.0 ± 6.1	1135.0 ± 5.5	Ar-Ar: 996.7 ± 8.0 Re-Os: 1601 ± 6 Re-Os: 1609 ± 6	Ar-Ar: 1052 ± 10 Re-Os: 1648.1 ± 5.97	minimum of 1113 ± 5	1368 ± 160
Age spectra	Fig. 3b	Fig. 3c	Fig. 3d	Fig. 3a	Fig. 4	Fig. 5

SECTION C - FIGURES

Stable isotope (C,O,S,H) and fluid inclusion constraints on the origin of Wernecke Breccia and associated iron oxide-copper-gold mineralisation

Figure 1:

Location of study area, distribution of WSG and Wernecke Breccia plus location of breccia-associated IOCG prospects included in this study (modified from Thorkelson, 2000).

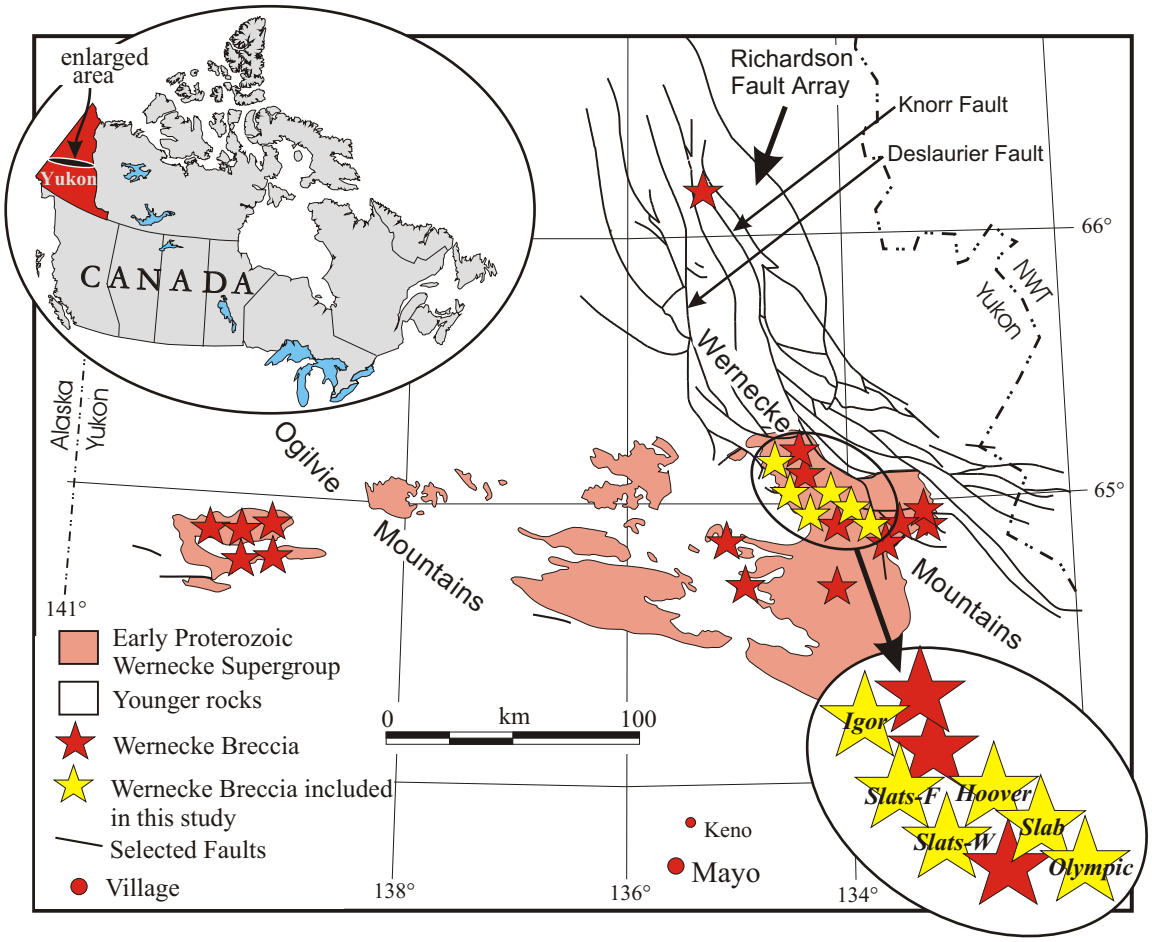

Section C: Figure 1

Figure 2:

Simplified geology map of the study area (for details see Thorkelson, 2000 and Thorkelson *et al.*, 2002). Legend shows approximate stratigraphic position of IOCG prospects included in this study. Slats-F = Slats-Frosty, Slats-W = Slats Wallbanger.

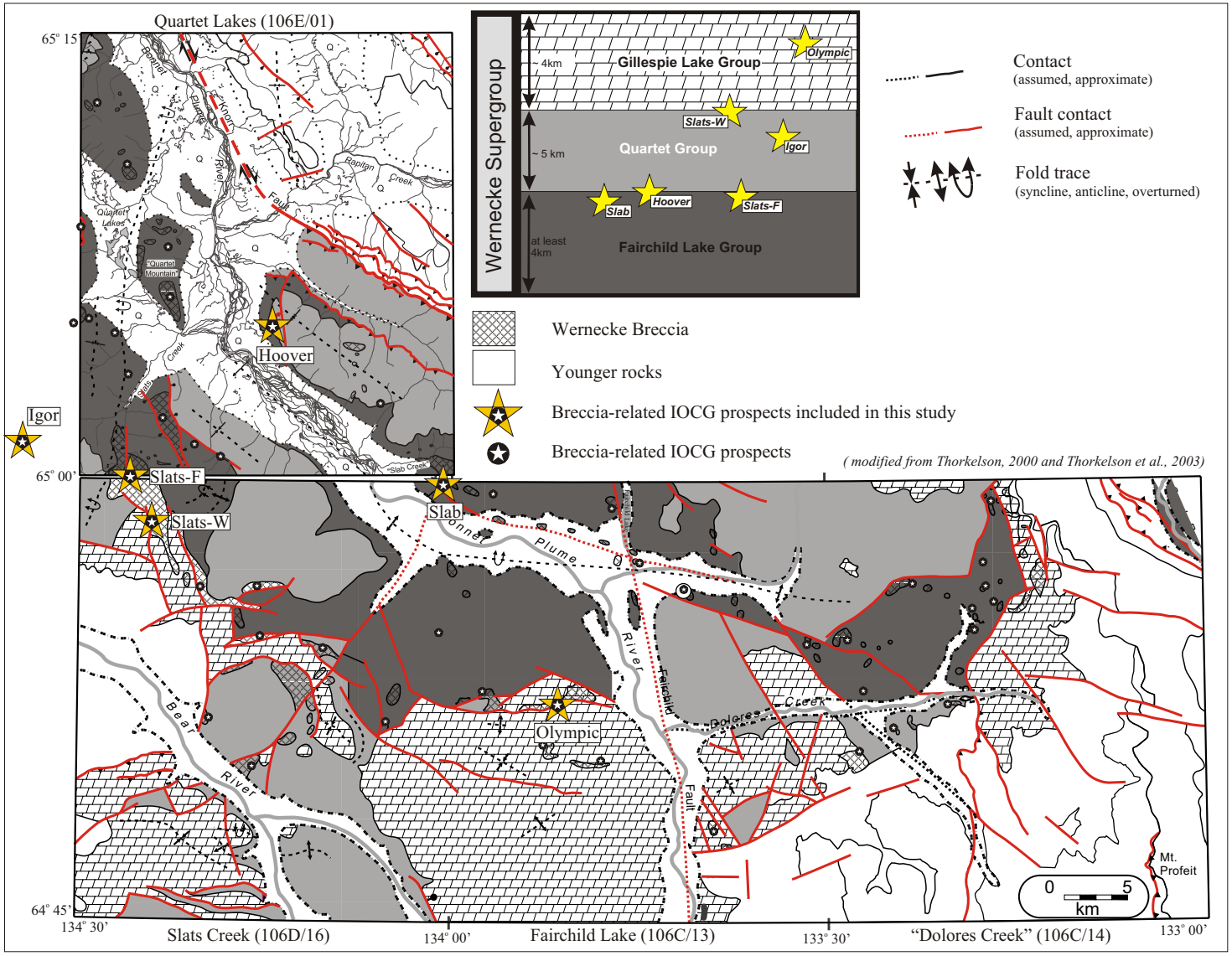

Section C: Figure 2

Figure 3:

Simplified paragenesis for prospects in the Wernecke Mountains: a) Slab, b) Hoover, c) Slats-Frosty, d) Slats-Wallbanger, e) Igor and f) Olympic prospects. NB: paragenetic stages apply only to a specific area, e.g. Slab stage 3 ≠ Hoover stage 3 ≠ Igor stage 3.

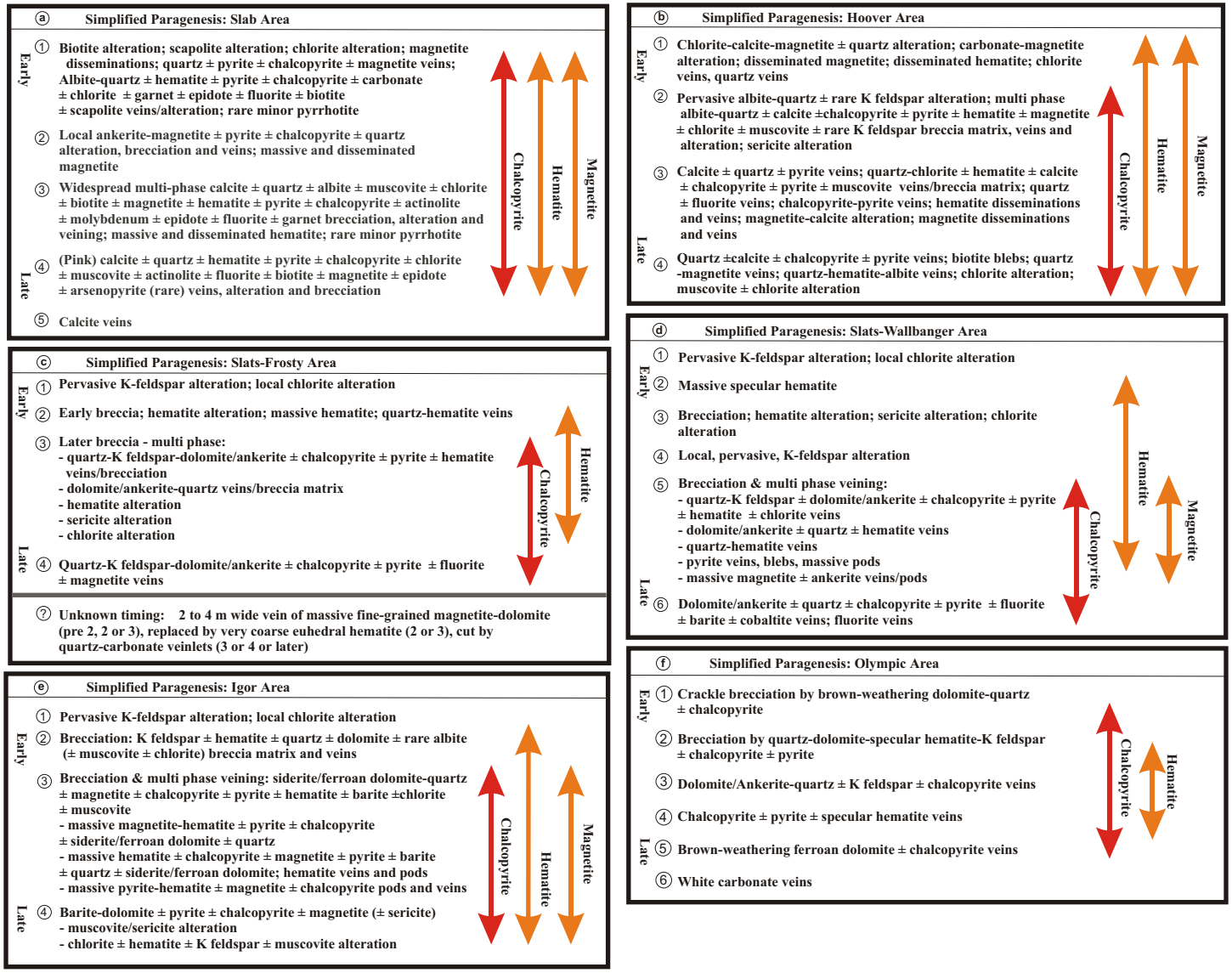

Section C: Figure 3

Figure 4:

Photographs of fluid inclusion samples: Slab area - **a)** large crystals of quartz, calcite and fluorite locally make up the matrix of Wernecke Breccia, **b)** fluid inclusions in quartz crystal, **c)** fluid inclusions containing L + V + H and **d)** fluid inclusion containing L + V + H + h. L=liquid, V=vapour, H=halite, h=hematite; Hoover area – **e)** metasedimentary clast in Wernecke Breccia, **f)** trails of secondary fluid inclusions parallel to fractures within quartz in the clast; **g)** closer view of inclusions in f; Slats-Frosty area - **h)** ferroan dolomite-pyrite-fluorite vein cutting hematite-altered metasiltstone; the fluorite contains pseudosecondary fluid inclusions, **i)** fluorite in h), note fluid inclusion trails parallel to fractures that do not extend beyond the fluorite crystal, **j)** and **k)** liquid + vapour fluid inclusions in fluorite; Igor area – **l)** Wernecke Breccia sample with large barite and magnetite crystals, **m)** barite crystal in area shown in l); and Olympic area – **n**) Wernecke Breccia sample used for fluid inclusion analysis, **o**) quartz grain from breccia matrix with fluid inclusions in the outer rim, **p**) ferroan dolomite-quartz-chalcopyrite±pyrite vein and **q**) dolomite with primary fluid inclusions.

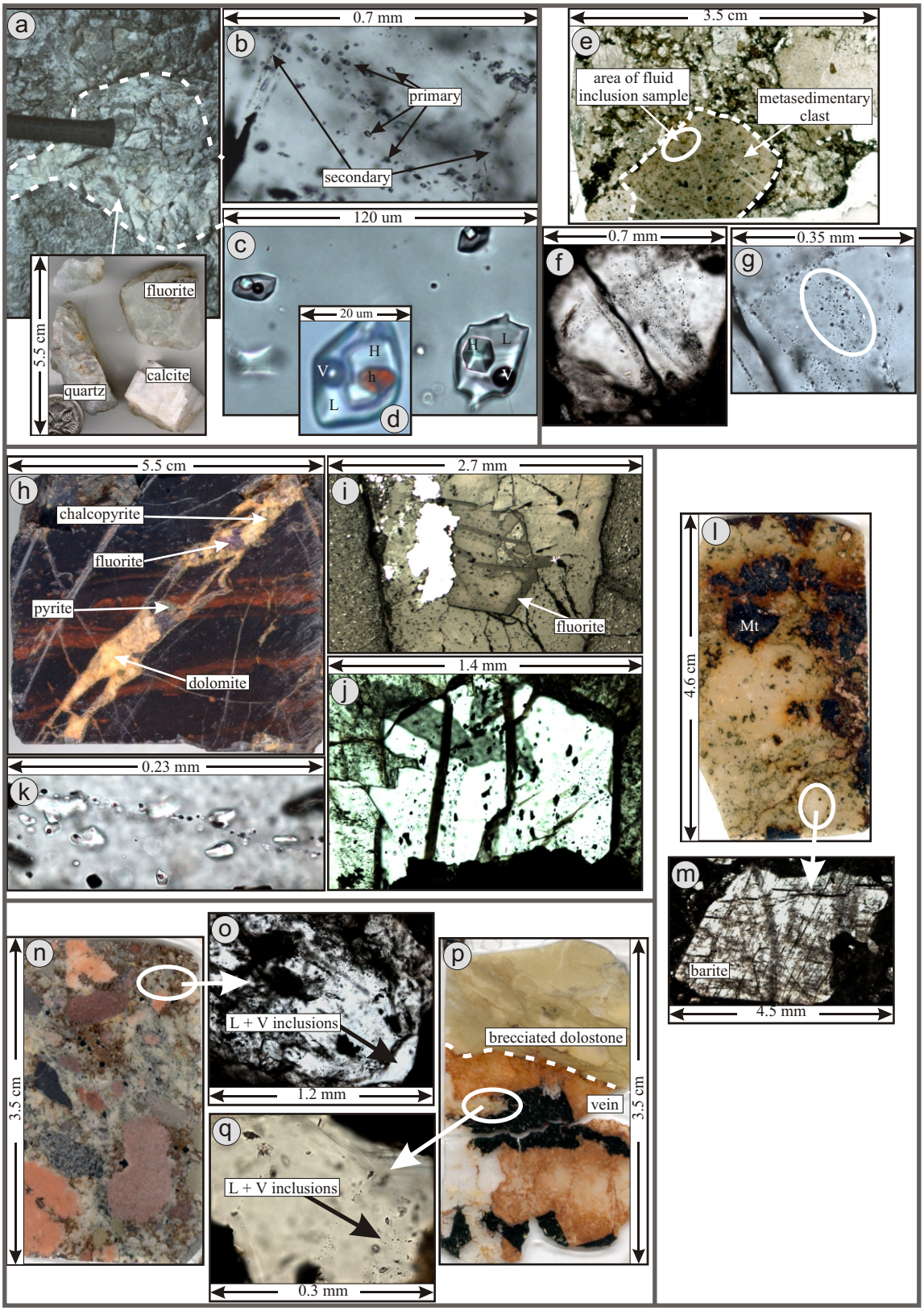

Section C: Figure 4

Figure 5:

Summary of fluid inclusion data for samples from the Wernecke Mountains area. Th = final homogenization temperature; NaCl eq. wt. % = equivalent weight % NaCl. See Table 1 caption for details of salinity calculations.

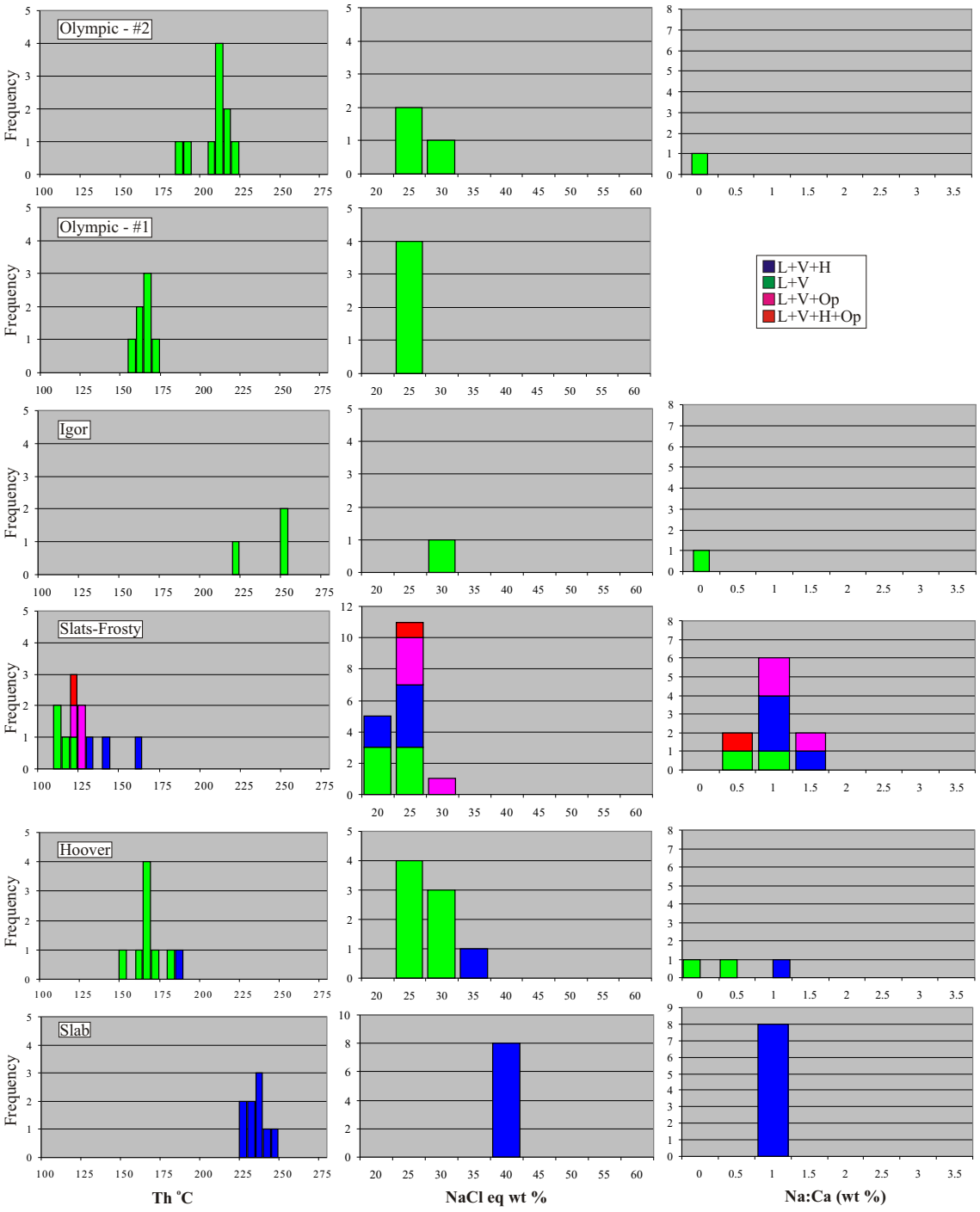
Olympic - #2
Olympic - #1
Igor
Slats-Frosty
Hoover
Slab
Frequency
L+V+H
L+V
L+V+Op
L+V+H+Op
Th °C
NaCl eq wt %
Na:Ca (wt %)

Figure 6:

Comparison of fluid composition for inclusions from the Slab, Hoover, Slats-Frosty, Igor and Olympic areas using the NaCl-$CaCl_2$-H_2O system.

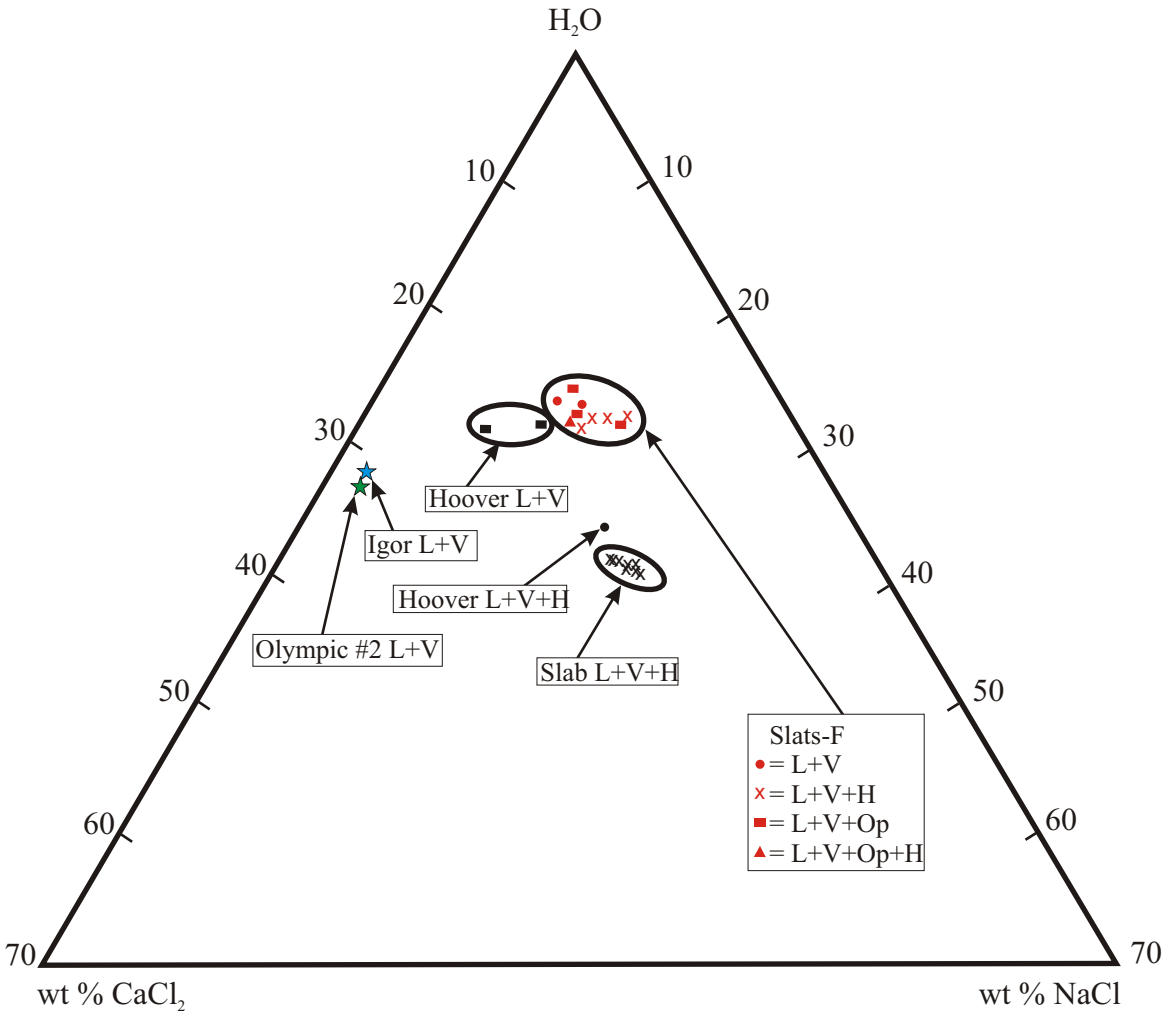
H2O
10
20
30
40
50
60
70
10
20
30
40
50
60
70
wt % CaCl2
wt % NaCl
Hoover L+V
Igor L+V
Hoover L+V+H
Olympic #2 L+V
Slab L+V+H
Slats-F
= L+V
= L+V+H
= L+V+Op
= L+V+Op+H

Figure 7:

$\delta^{18}O$ versus $\delta^{13}C$ results for samples of hydrothermal carbonate from the Slab, Hoover, Slats-Frosty, Slats-Wallbanger, Igor and Olympic areas. Also shown are results for samples of host WSG limestone/dolostone from FLG, Quartet Group and GLG.

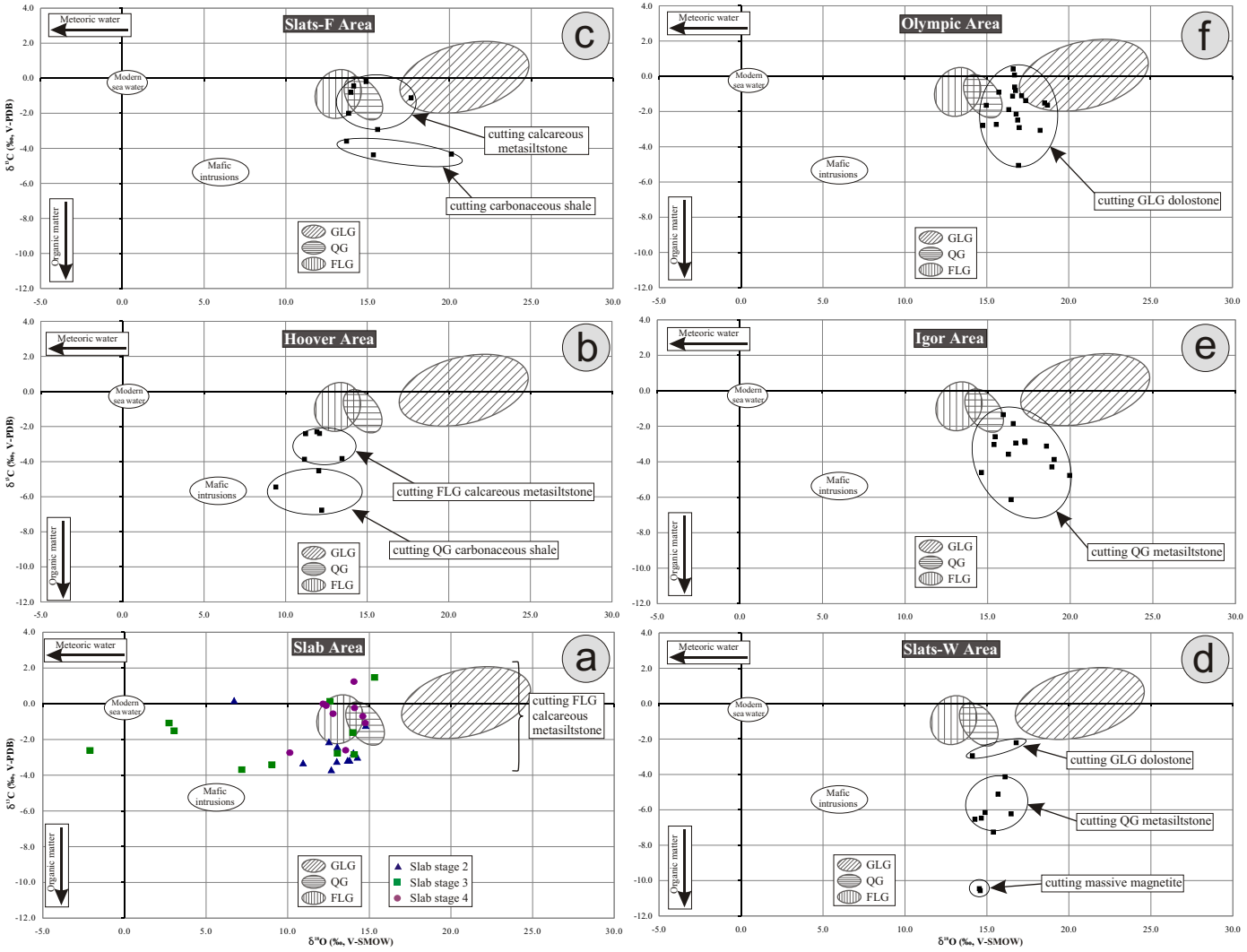

Section C: Figure 7

Figure 8:

Overall $\delta^{18}O$ versus $\delta^{13}C$ results for carbonate samples from the Wernecke Mountains. Also shown are fields for common large earth reservoirs that are important in hydrothermal systems. Fields are from Taylor (1974), Sheppard (1977), Graham and Harman (1983), and Hoefs (1987) as compiled in Rollinson (1993). Mean values for Paleoproterozoic carbonates are from Shields and Veizer (2002). FLG = Fairchild Lake Group, Quartet Group = Quartet Group, GLG = Gillespie Lake Group.

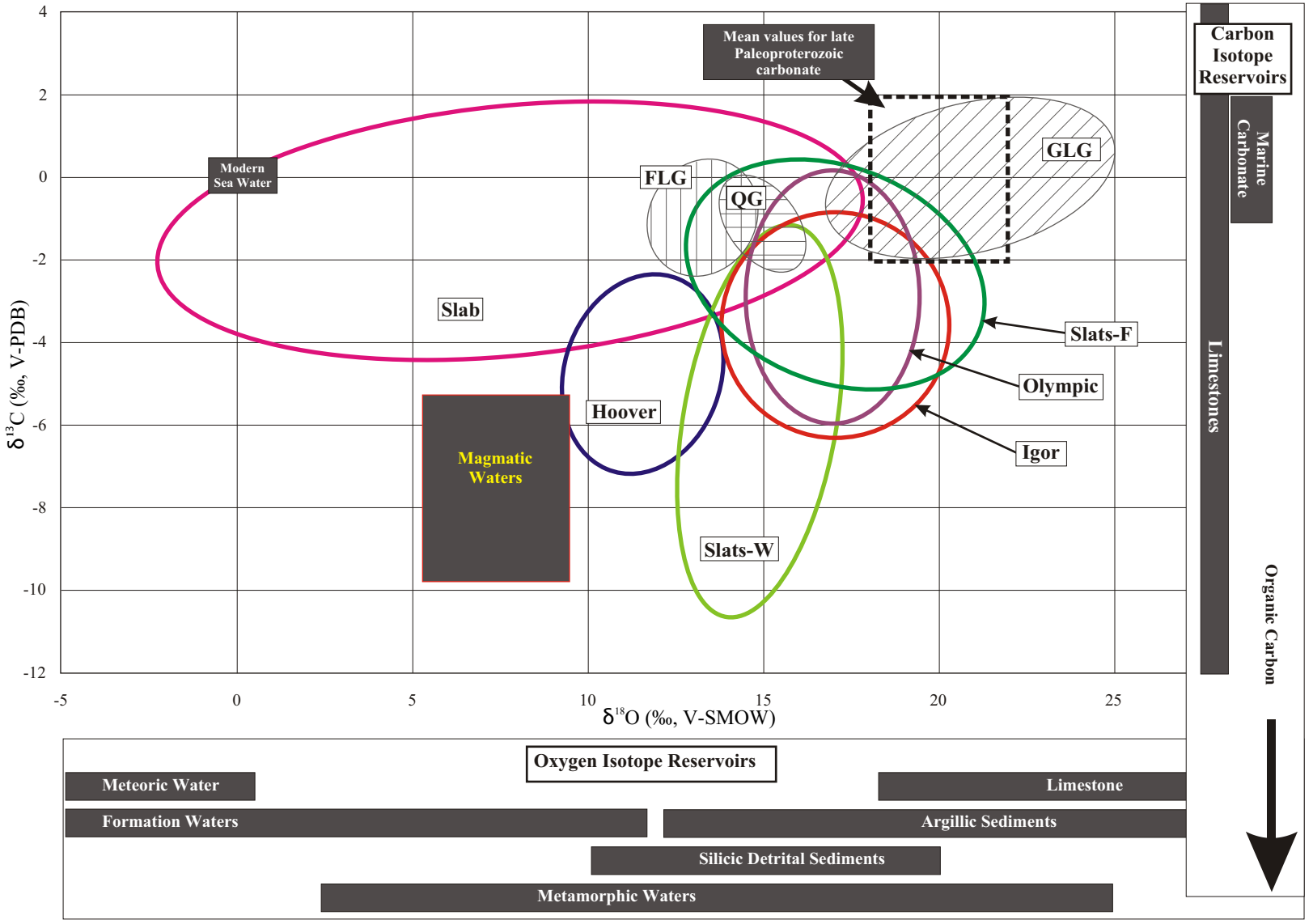
Mean values for late Paleoproterozoic carbonate
Modern Sea Water
FLG
QG
GLG
Slab
Slats-F
Olympic
Igor
Hoover
Magmatic Waters
Slats-W
Carbon Isotope Reservoirs
Marine Carbonate
Limestones
Organic Carbon
δ13C (‰, V-PDB)
δ18O (‰, V-SMOW)
4
2
0
-2
-4
-6
-8
-10
-12
-5
0
5
10
15
20
25
Oxygen Isotope Reservoirs
Meteoric Water
Formation Waters
Limestone
Argillic Sediments
Silicic Detrital Sediments
Metamorphic Waters

Figure 9:

$\delta^{34}S$ results for samples from the Slab, Hoover, Slats-Frosty, Slats-Wallbanger, Igor and Olympic areas. See text for discussion.

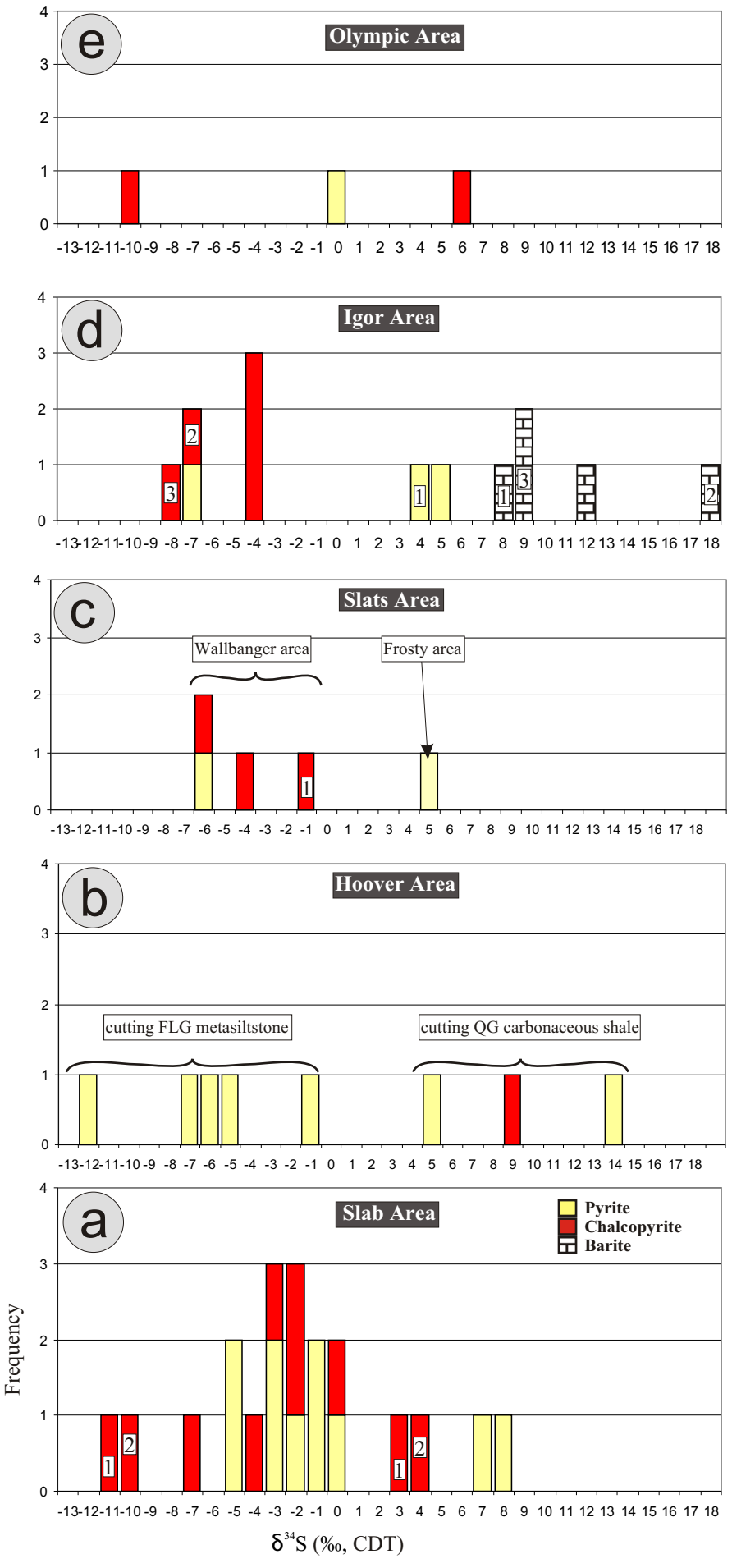

Section C: Figure 9

Figure 10:

Overall $\delta^{34}S$ results for samples from the Wernecke Mountains. Also shown are fields for common large earth reservoirs that are important in hydrothermal systems. Fields are from Chambers (1982), Kerridge *et al.* (1983) and Chaussidon *et al.* (1989) as compiled in Rollinson (1993).

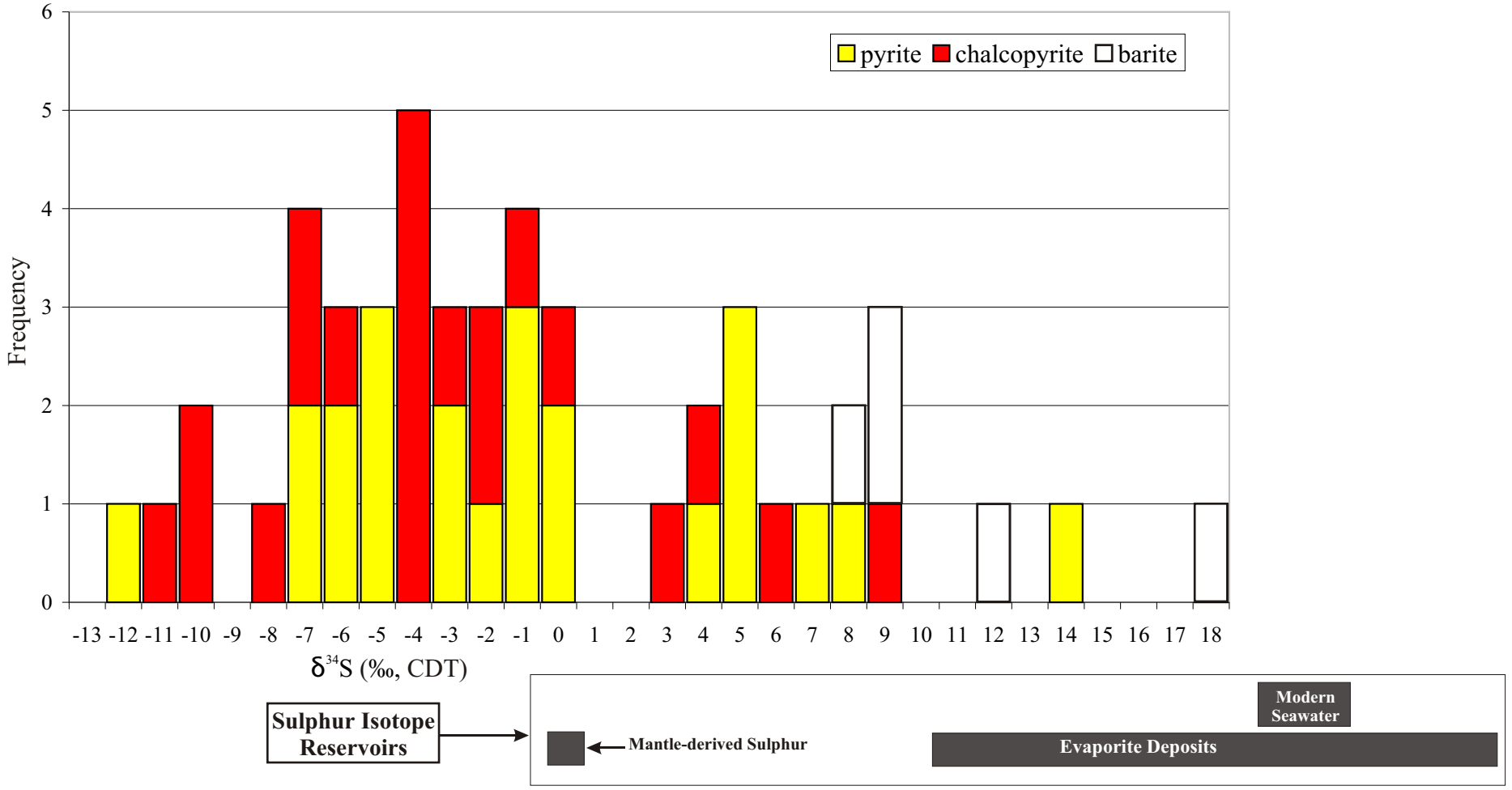
pyrite
chalcopyrite
barite
Frequency
0
1
2
3
4
5
6
-13 -12 -11 -10 -9 -8 -7 -6 -5 -4 -3 -2 -1 0 1 2 3 4 5 6 7 8 9 10 11 12 13 14 15 16 17 18
δ34S (‰, CDT)
Sulphur Isotope Reservoirs
Mantle-derived Sulphur
Modern Seawater
Evaporite Deposits

Figure 11:

Plot of calculated $\delta^{18}O_{water}$ versus δD_{water} values for mineral separates of biotite, muscovite and actinolite from Wernecke samples. See Appendix VII for sample descriptions. $\delta^{18}O_{water}$ values for biotite and muscovite were calculated using the fractionation equations of Zheng (1993). δD_{water} values for biotite and muscovite were calculated using the fractionation equations of Suzuoki and Epstein (1976). $\delta^{18}O_{water}$ and δD_{water} values for actinolite were calculated using the fractionation equations of Zheng (1993) and Graham *et al.* (1984) respectively for tremolite. Magmatic water and formation waters fields are from Taylor (1974). Meteoric water line is from Epstein *et al.* (1965) and Epstein (1970). The metamorphic waters field is from values in Taylor (1974) and Sheppard (1981) as compiled by Rollinson (1993). The fields for felsic magma and high temperature volcanic vapour are from Taylor (1992) and Giggenbach (1992) as shown in Hedenquist *et al.* (1998). Composition of ancient seawater from Sheppard (1986). Isotopic trends are given for: 1) seawater undergoing evaporation (Knauth and Beeunas, 1986), 2) meteoric waters undergoing exchange with ^{18}O in minerals, 3) evaporation of meteoric water and 4) isotopic compositions of Salton Sea and Lanzarote geothermal waters compared to their local meteoric waters (Sheppard, 1986).

Black bars beneath the main figure are calculated $\delta^{18}O_{water}$ values for calcite, dolomite and siderite from the Slab, Hoover and Igor areas using the fractionation factors of Zheng (1999).

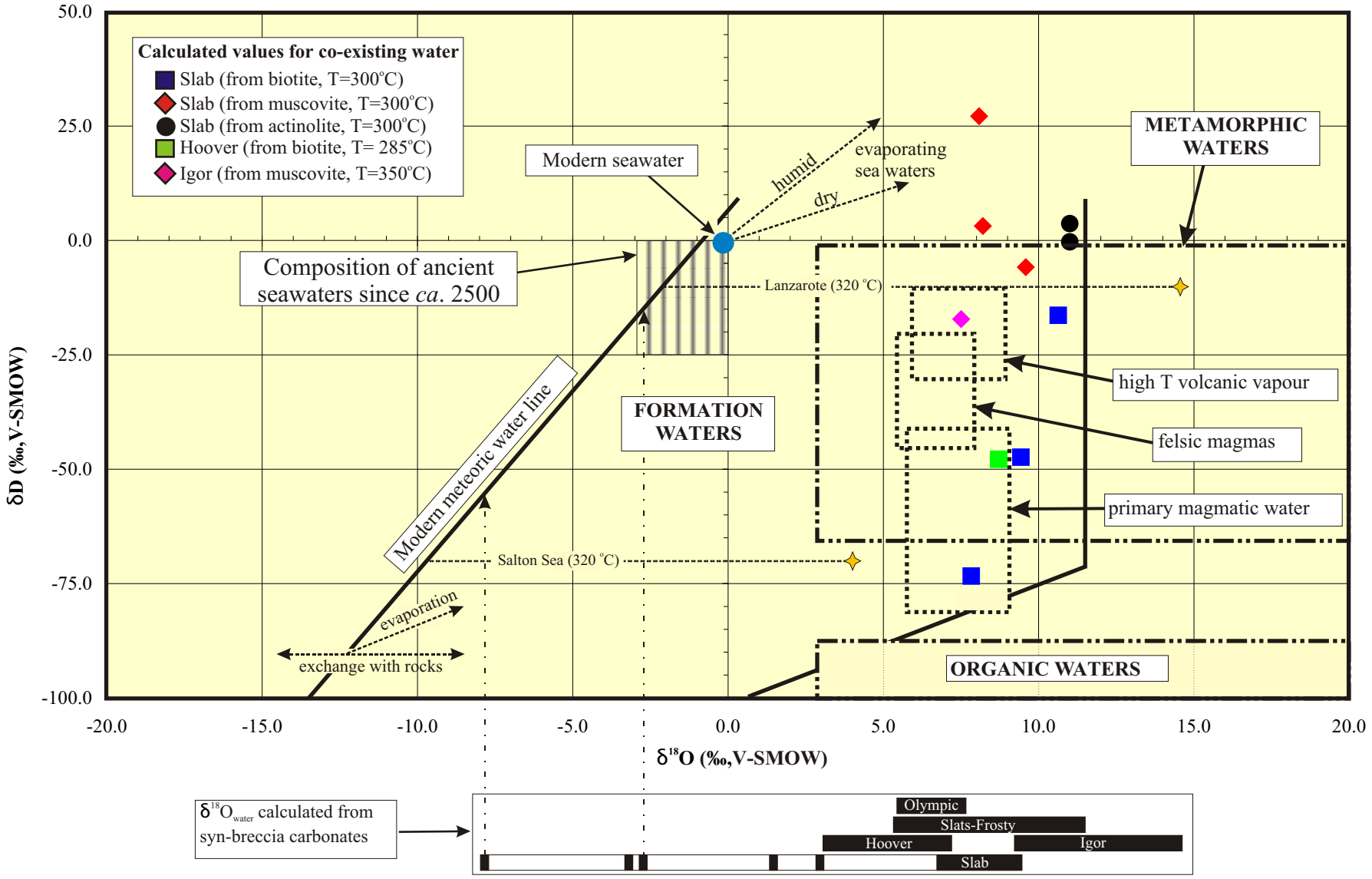

Section C: Figure 11

Figure 12:

Examples of isochores from the Slab and Igor prospects. Diagrams were constructed using the programme Flinc-Calc that is based on the equations of Zhang and Fratz (1987) and Brown (1998).

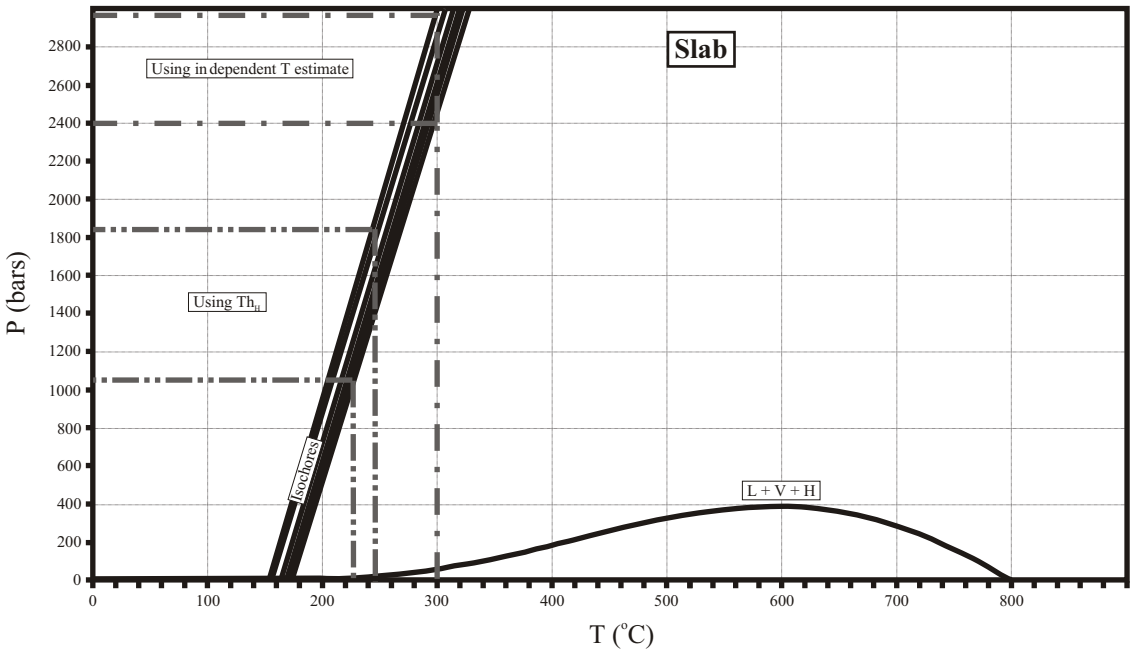
Slab
Using in dependent T estimate
Using Th_{H}
Isochores
L + V + H
P (bars)
T (°C)
0
200
400
600
800
1000
1200
1400
1600
1800
2000
2200
2400
2600
2800
0
100
200
300
400
500
600
700
800

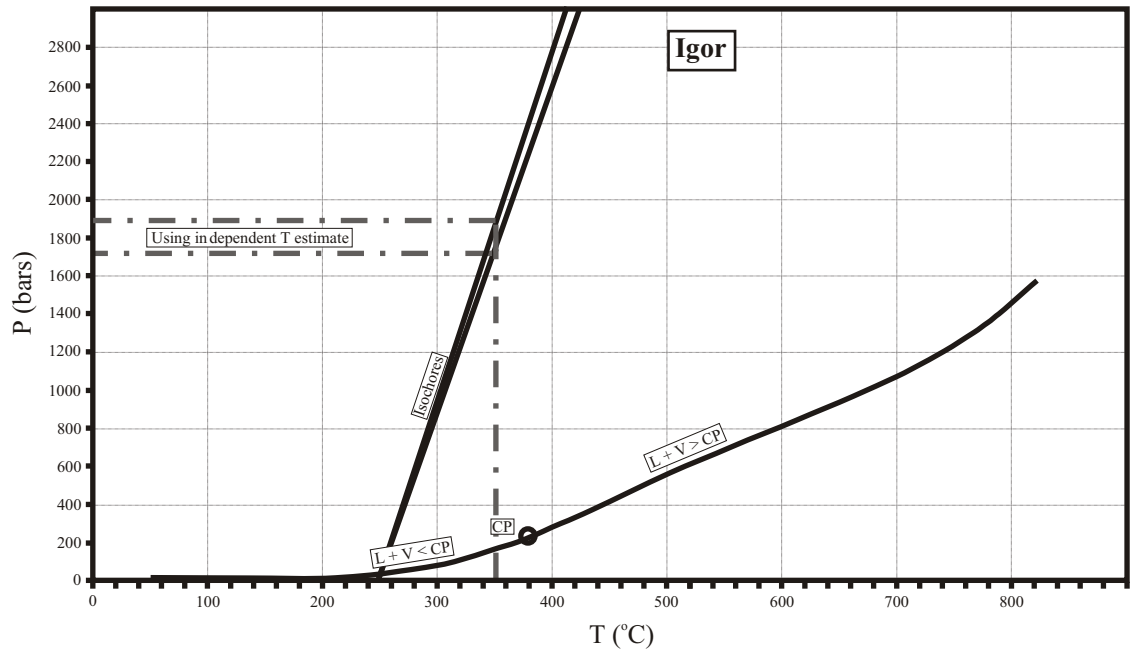
Igor
Using in dependent T estimate
Isochores
L + V > CP
CP
L + V < CP
P (bars)
T (°C)
0
200
400
600
800
1000
1200
1400
1600
1800
2000
2200
2400
2600
2800
0
100
200
300
400
500
600
700
800

Figure 13:

Log fO_2 – log fS_2 plot for Slab area fluids. The following equations were used to define the mineral stability fields; Log K values were calculated for temperature = 300 ^{o}C and pressure = 2500 bars.

Reaction used	**Equation**	**Log K**
Pyrite-Magnetite:	$3\ FeS_2 + 2\ O_{2(g)} = Fe_3O_4 + 3\ S_{2(g)}$	-4.6
Pyrite-Hematite:	$4\ FeS_2 + 3\ O_{2(g)} = 2\ Fe_2O_3 + 4\ S_{2\ (g)}$	33.88
Pyrrhotite-Magnetite:	$6\ FeS + 4\ O_{2(g)} = 2\ Fe_3O_4 + 3\ S_2$	55.34
Bornite-Chalcopyrite:	$Cu_5FeS_4 + 4\ FeS_2 = 5\ CuFeS_2 + S_2$	83.64
Graphite-CO2(g):	$C + O_{2(g)} = CO_{2(g)}$	-6.93
Calcite-gypsum:	$2\ CaCO_3 + S_{2(g)} + 3\ O_{2(g)} + 4\ H_2O = 2\ CaSO_4 + 2\ CO_{2(g)}$	36.13

Calculations were carried out using the programme “The Geochemists Workbench”® release 4.0.2. (Bethke, 2000). GWB uses information developed by numerous researchers, as compiled for example by Pitzer, 1991 and Johnson *et al.*, 1992.

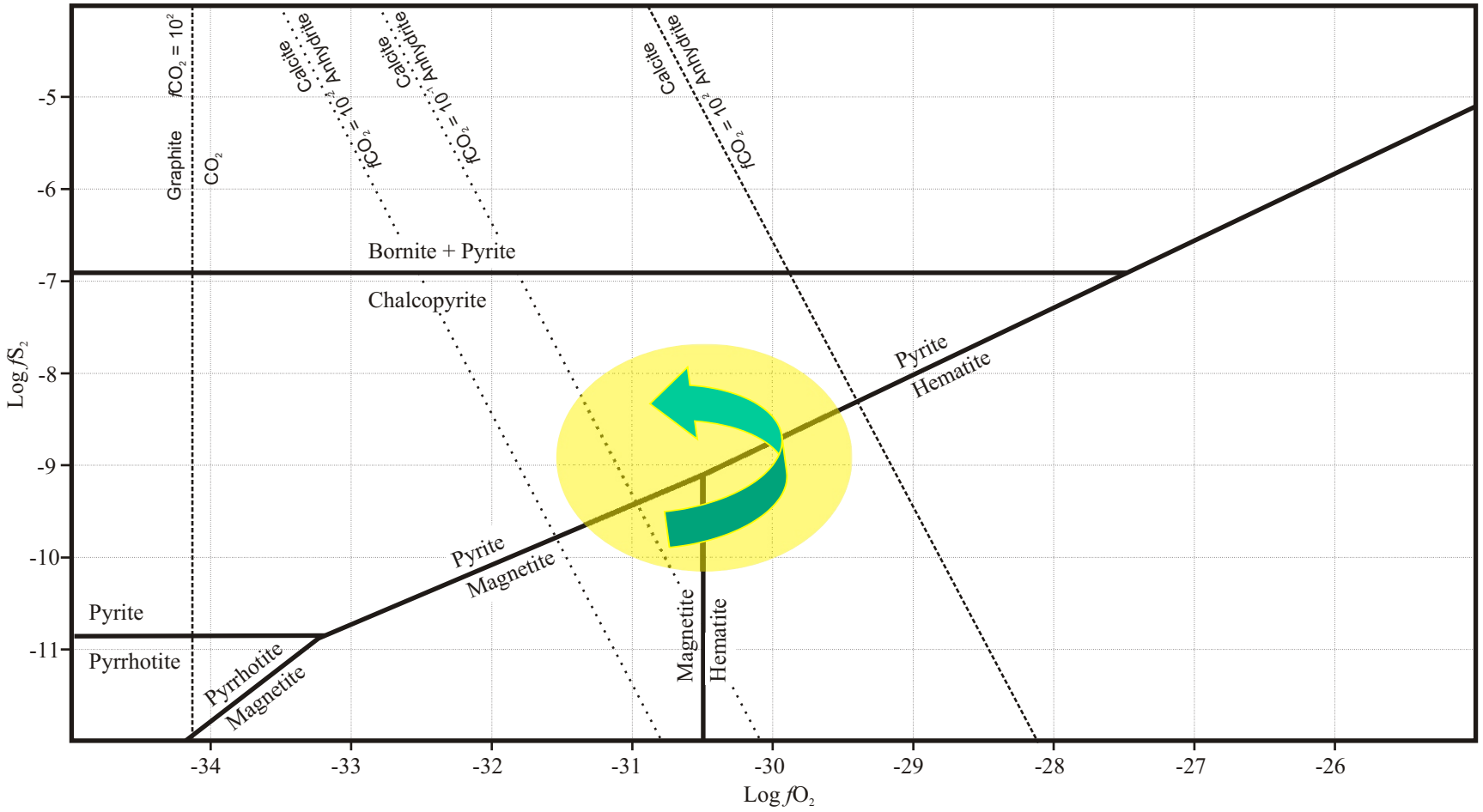

fS_2 - fO_2 mineral stability relationships at 300°C and 2.5 kb.

Figure 14:

Plots of pH versus log fO_2 for the Slab area. a) using a medium value for log aH_2S of -2.6, b) using a low value for log aH_2S of -3.23 and c) using a high value for log aH_2S of -1.97. The positions of δS^{34}_{i} contours are also shown in a); Numbers in boxes on contours are δS^{34}_{pyrite} values calculated using $\delta S^{34}_{\Sigma S} = 0$ ‰ (right side) and $\delta S^{34}_{\Sigma S} = 18$ ‰ (left side). The shaded oval shows approximate fluid conditions at Slab.

The position of sulphur isotope contours were calculated using the method of Ohmoto (1972) and the following conditions: temperature = 300 °C, pressure = 2.5 kb, ionic strength = 3.2 (based on fluid inclusion data). Molality of species was calculated using the programme "The Geochemists Workbench"® release 4.0.2; the following species were most abundant.

Species	Molality	Mole Fraction
$NaSO_4^-$	0.6985	0.497
$CaSO_4(aq)$	0.3741	0.266
KSO_4^-	0.165	0.117
SO_4^{--}	0.1623	0.115
$H_2S(aq)$	2.51E-03	0.002
HSO_4^-	1.54E-03	0.001
HS^-	1.30E-03	0.001

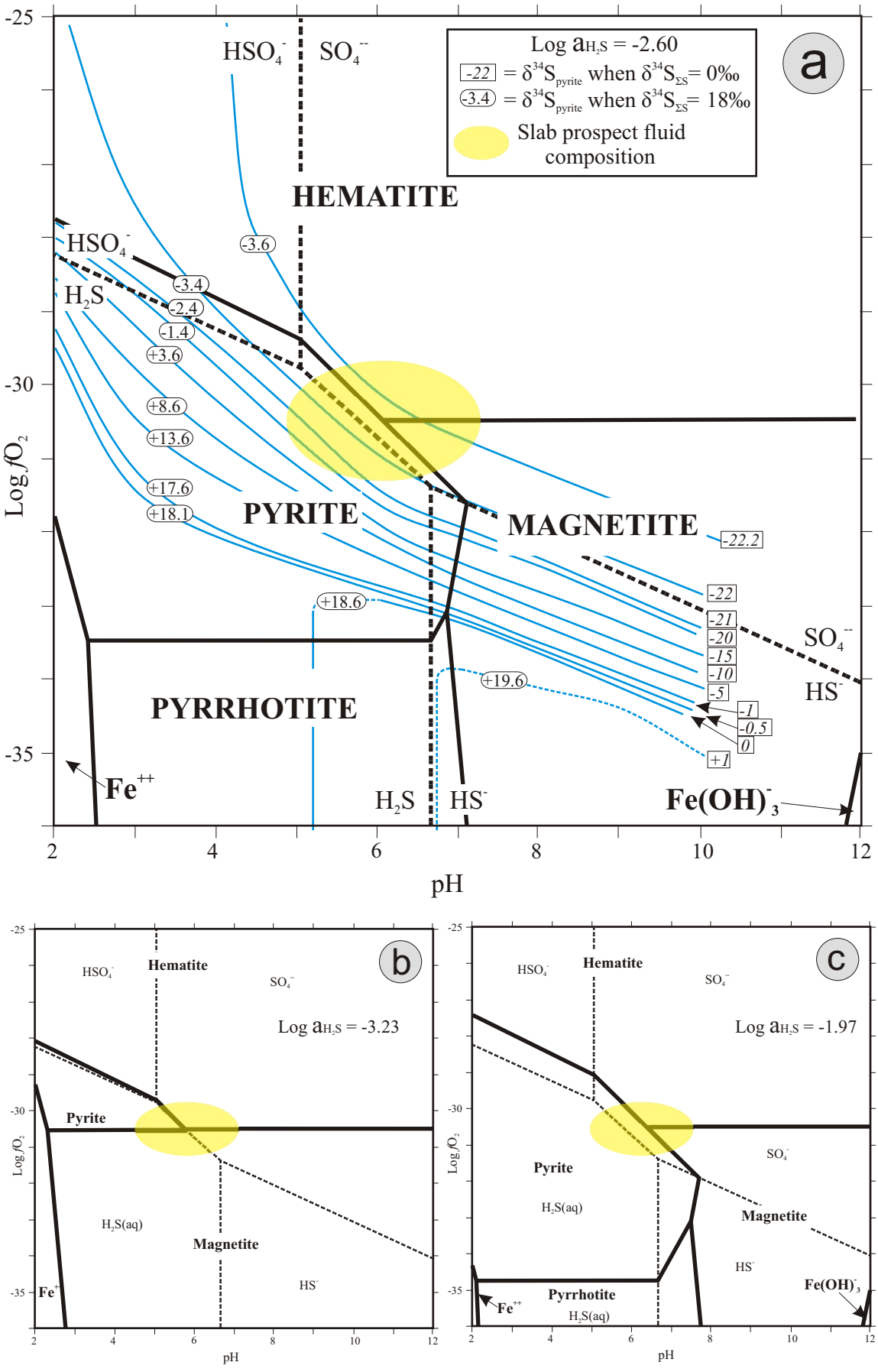
a
Log a_{H_2S} = -2.60
-22 = $\delta^{34}S_{pyrite}$ when $\delta^{34}S_{\Sigma S}$= 0‰
-3.4 = $\delta^{34}S_{pyrite}$ when $\delta^{34}S_{\Sigma S}$= 18‰
Slab prospect fluid composition
HEMATITE
PYRITE
MAGNETITE
PYRRHOTITE
HSO_4^-
SO_4^{--}
H_2S
HS^-
Fe^{++}
$Fe(OH)_3^-$
Log fO_2
pH
b
Log a_{H_2S} = -3.23
Hematite
Pyrite
H_2S(aq)
Magnetite
c
Log a_{H_2S} = -1.97
Pyrrhotite

SECTION C - TABLES

Stable isotope (C,O,S,H) and fluid inclusion constraints on the origin of Wernecke Breccia and associated iron oxide-copper-gold mineralisation

Table 1: Summary of fluid inclusion data for samples from the Wernecke Mountains area. Tfm = temperature of first melting, Tm_{ice} = ice melting temperature, Tm_{hh} = hydrohalite melting temperature, Thv = vapour homogenization temperature, Ths = halite dissolution temperature, Th = final homogenization temperature. Temperatures in ^{o}C. NaCl eq. wt. % = equivalent weight % NaCl. NaCl eq. wt. % values for Slab were approximated using the graphical methods of Vanko *et al.* (1988) and Zwart & Touret (1994). Values for other areas were calculated from Tm_{ice}, $Tm_{hydrohalite}$, Th_{halite} using the programme FlinCalc (J. Cleverly, written communication) which uses information from Zhang and Frantz (1987) and Brown (1998). In the paragenesis column P = primary, S = secondary and PS = pseudo secondary. In the FI (fluid inclusion) Type column L = liquid, V = vapour, H = halite and Op = opaque.

Location (sample #)	**Paragenesis**	**n**	**FI Type**	**Tfm**	**Tm_{ice}**	**Tm_{hh}**	**Thv**	**Ths**	**Th**	**NaCl eq wt %**	**Na:Ca (wt %)**
Slab (Slab SW)	P, Stage 3	10	L+V+H	-92 to -83	-50 to -36	na	154 - 175	226 - 245	226 - 245	41 - 42	1.3 - 1.4
Hoover (JH01-5-7A)	S, Stage 3	7	L+V	-78 to -67	-34 to -25	na	153 - 172	na	153 - 172	26 - 32	0.4, 0.7
Hoover (JH01-5-7A)	S, Stage 3	1	L+V+H	-64	-30	na	165	188	188	38	1.20
Slats-F (STF95-1-20.30 m)	PS, Stage 3	6	L+V	-91 to -72	-28 to -23	-12, -8	112 - 160	na	112 - 160	24 - 28	0.8 - 1.1
Slats-F (STF95-1-20.30 m)	PS, Stage 3	6	L+V+H	-89 to -75	-28 to -23	-4 to 3	89 - 160	> 160	> 160	24 - 29	1.0 - 1.6
Slats-F (STF95-1-20.30 m)	PS, Stage 3	4	L+V+Op	-103 to -77	-35 to -26	-22 to 0	68 - 130	> 130	> 130	27 - 32	1.0 - 1.6
Slats-F (STF95-1-20.30 m)	PS, Stage 3	1	L+V+H+Op	-77	-28	-7	124	> 124	> 124	29	0.9
Igor (JH02-10-17B)	P, Stage 3	3	L+V	-77	-54 to -50	-26	220 - 250	na	220 - 250	~ 34	~ 0.1
Olympic 1 (JH02-21-5A)	P, Stage 2	7	L+V	-67 to -60	-29 to -26	na	158 - 170	na	158 - 170	26 - 28	na
Olympic 2 (OY94-3-24.70 m)	P, Post stage 2	11	L+V	-64	-30 to -25	na	188 - 223	na	188 - 223	26 - 35	~ 0.1

Table 2: Summary of carbon and oxygen isotope results. * mean value for *ca*. 1.8 to 1.7 Ba carbonates is from Shields and Veizer (2002).

Sample	**n**	**$\delta^{13}C$ ‰ V-PDB**	**$\delta^{18}O$ ‰ V-SMOW**
All WSG Limestone & dolostone	23	-2.0 to 1.6	11.8 to 24.6
Fairchild Lake Group	6	-2.0 to 0.5	11.8 to 14.4
Quartet Group carbonate	3	-1.9 to -0.3	13.9 to 15.9
Quartet Group carbonaceous shale	4	-26.7 to -20.8	N/A
Gillespie Lake Group	14	-1.9 to 1.6	16.4 to 24. 6
*Mean value for *ca*. 1.8-1.7 Ba carbonates		-2 to 2	18 to 22
All breccia-related carbonates	94	-10.6 to 1.5	-2.1 to 20.0
Slab (stage 2)	11	-3.7 to -1.2	10.9 to 14.8
Slab (stage 3)	13	-3.7 to 1.5	-2.1 to 15.3
Slab (stage 4)	6	-2.7 to 1.2	10.1 to 14.6
Hoover (stage 3)	8	-6.8 to -2.3	9.4 to 13.5
Slats F (stages 2, 3 & 4)	9	-4.4 to -0.2	13.7 to 20.1
Slats W (stages 5 & 6)	11	-10.6 to -2.2	14.1 to 16.8
Igor (stage 3 & 4)	14	-6.1 to -1.4	14.6 to 20.0
Olympic (stages 1,2, 3 & 5)	19	-5.1 to 0.4	14.8 to 18.7

Table 3: $\delta^{18}O_{water}$ values calculated from measured $\delta^{18}O$ values of syn-breccia carbonate samples. (See text for discussion)

Prospect name	**Measured $\delta^{18}O_{carbonate}$ ‰ V-SMOW**	**Calculated $\delta^{18}O_{water}$ ‰ V-SMOW**
Slab (Stage 3: 300 ^{o}C)	-2.1 to 15.3	-7.9 to 9.5
Hoover (Stage 3: 285 ^{o}C)	9.4 to 13.5	3.0 to 7.2
Slats-Frosty (Stage 3: 235 ^{o}C)	13.7 to 20.1	5.4 to 11.6
Igor (Stage 3: 355 ^{o}C)	14.6 to 20.0	9.4 to 14.7
Olympic (Stage 2: 185 ^{o}C)	16.6 to 18.7	5.7 to 7.8

Table 4: Summary of sulphur isotope results

Sample	**n**	**$\delta^{34}S$ ‰ CDT**
All breccia-related samples	49	-12.4 to 17.1
Slab	20	-11.5 to 7.1
Hoover	8	-12.4 to 13.4
Slats W	4	-6.8 to -1.7
Slats F	1	4.2
Igor (sulphides)	8	-8.4 to 4.8
Igor (barite)	5	7.7 to 17.1
Olympic	3	-10.8 to 5.3

Table 5: Summary of hydrogen and oxygen isotope results. Also shown are calculated δD and $\delta^{18}O$ values for co-existing water. #duplicate analysis. See figure 11 caption for calculation details.

Area	**Sample**	**Mineral**	**δD ‰ V-SMOW**	**$\delta^{18}O$ ‰ V-SMOW**	**δD_{water} ‰ V-SMOW**	**$\delta^{18}O_{water}$ ‰ V-SMOW**
Slab	SB94-1-33.7m	Muscovite	-21	11.6	27.2	10.2
Slab	01JH-20-3	Muscovite	-45	10.6	3.2	9.2
Slab	02JH-14-IA2	Muscovite	-54	11.1	-5.8	9.7
Igor	02JH-12-1	Muscovite	-55	9.9	-6.8	8.5
Slab	01JH-19-1	Biotite	-141	6.7	-73.4	7.8
Slab	01JH-20-6A	Biotite	-115	8.3	-47.4	9.4
Slab	02JH-20-2	Biotite	-84	9.5	-16.4	10.6
Hoover	HV94-1-695'	Biotite	-119	7.8	-38.4	8.1
Slab	JH01-20-10C	Actinolite	-22	10.96	-0.3	11.0
Slab	JH01-20-10C	Actinolite	-18	10.96	3.7	11.0
Not used in figure						
Hoover	JH01-8-2	Muscovite	no data	11.1		
Slab	SB94-1-345.1m	Muscovite	no data	11.5		
Slab	SB97-19-70.1m	Muscovite	no data	10.1		
Slab	JH01-20-10C**	Biotite	-23	8.1		
Slab	JH01-35-2**	Biotite	-34	8.7		
	** possible chloritization of biotite					

Table 6: Estimates of fluid temperature from fluid inclusion and stable isotope data. * All direct fluid inclusion analyses are minimum temperatures, i.e. not trapped during phase separation. ** Using fractionation factors of Sheppard and Schwarcz (1970) and Golyshev *et al.* (1981). *** Using fractionation factors of Ohmoto and Lasaga (1982).

Location	Analysis	T ^{o}C
Slab	Fluid inclusion analyses	226 – 245*
Slab	δ^{18}O: dolomite-calcite mineral pair	~300**
Hoover	Fluid inclusion analyses	153 - 188
Slats-F	Fluid inclusion analyses	> 160
Igor	Fluid inclusion analyses	220 - 250
Igor	δ^{34}S: barite-chalcopyrite mineral pair	~350***
Olympic	Fluid inclusion analyses	158 - 170

Table 7: Estimates of: 1) thickness of strata overlying the IOCG prospects based on stratigraphic measurements (Delaney, 1981); 2) depth of the prospects based on pressure estimates; 3) pressure from fluid inclusion data + stable isotope geothermometry; and 4) trapping temperature of fluid (see text for discussion).

Location	Thickness km	Depth km	Estimated P kb	Estimated T ^{o}C
Slab	7.4 – 9.0	9.1 – 11.3	2.4 – 3.0	300
Hoover	7.0 – 9.0			285
Slats-F	7.0 – 9.0			235
Igor	> 4	5.7 – 7.2	1.5 – 1.9	350
Slats-W	2.1 – 4.0			N/A
Olympic	0.4 – 1.5			185

SECTION D - FIGURES

Wernecke Breccias, Yukon, Canada: an example of a non-magmatic end-member IOCG system and implications for IOCG genesis and classification

Figure 1:

Location of selected IOCG districts. Modified from Hitzman (2000).

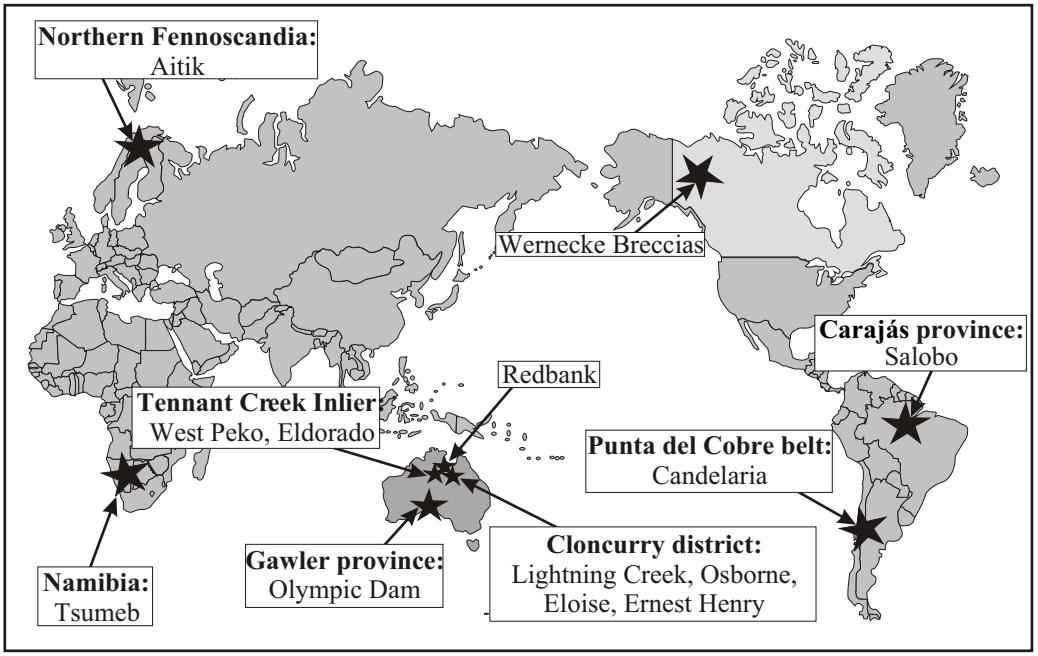

Section D: Figure 1

Figure 2:

Location of Wernecke belt, distribution of Wernecke Breccia and location of breccia-associated IOCG prospects included in this study (modified from Thorkelson, 2000) plus simplified bedrock geology map of the study area (for details see Thorkelson, 2000 and Thorkelson *et al.*, 2002, 2003). Legend shows approximate stratigraphic position of IOCG prospects studied.

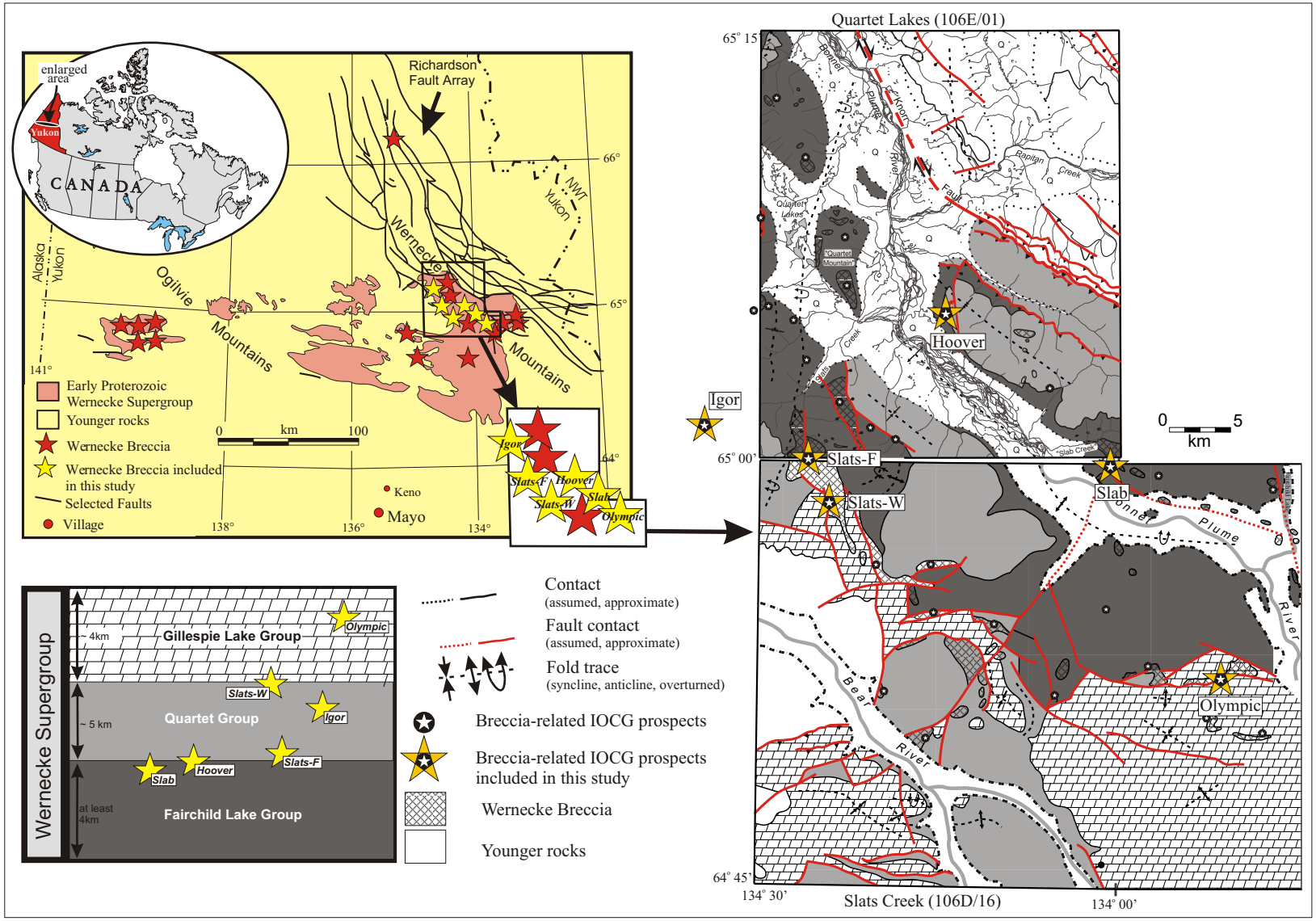

Section D: Figure 2

Figure 3:

Typical examples of Wernecke Breccia and associated IOCG mineralisation and alteration: a) grey sodic-altered breccia, b) red potassic-altered breccia, c) breccia with abundant clasts of earlier breccia, Slab area, d) photomicrograph of Wernecke Breccia matrix (crossed polars) made up dominantly of sedimentary rock fragments, carbonate, feldspar, lesser quartz and minor hematite and magnetite, e) calcite-chalcopyrite vein cutting FLG, Slab prospect, f) massive chalcopyrite-pyrite vein cutting FLG, Slab prospect, g) chalcopyrite forming matrix to breccia, Hoover prospect, h) massive magnetite-coarsely crystalline hematite-ankerite-quartz vein, Slats-Frosty area and i) photomicrograph of hematite overgrown by pyrite with chalcopyrite filling fractures (reflected light), Olympic prospect.

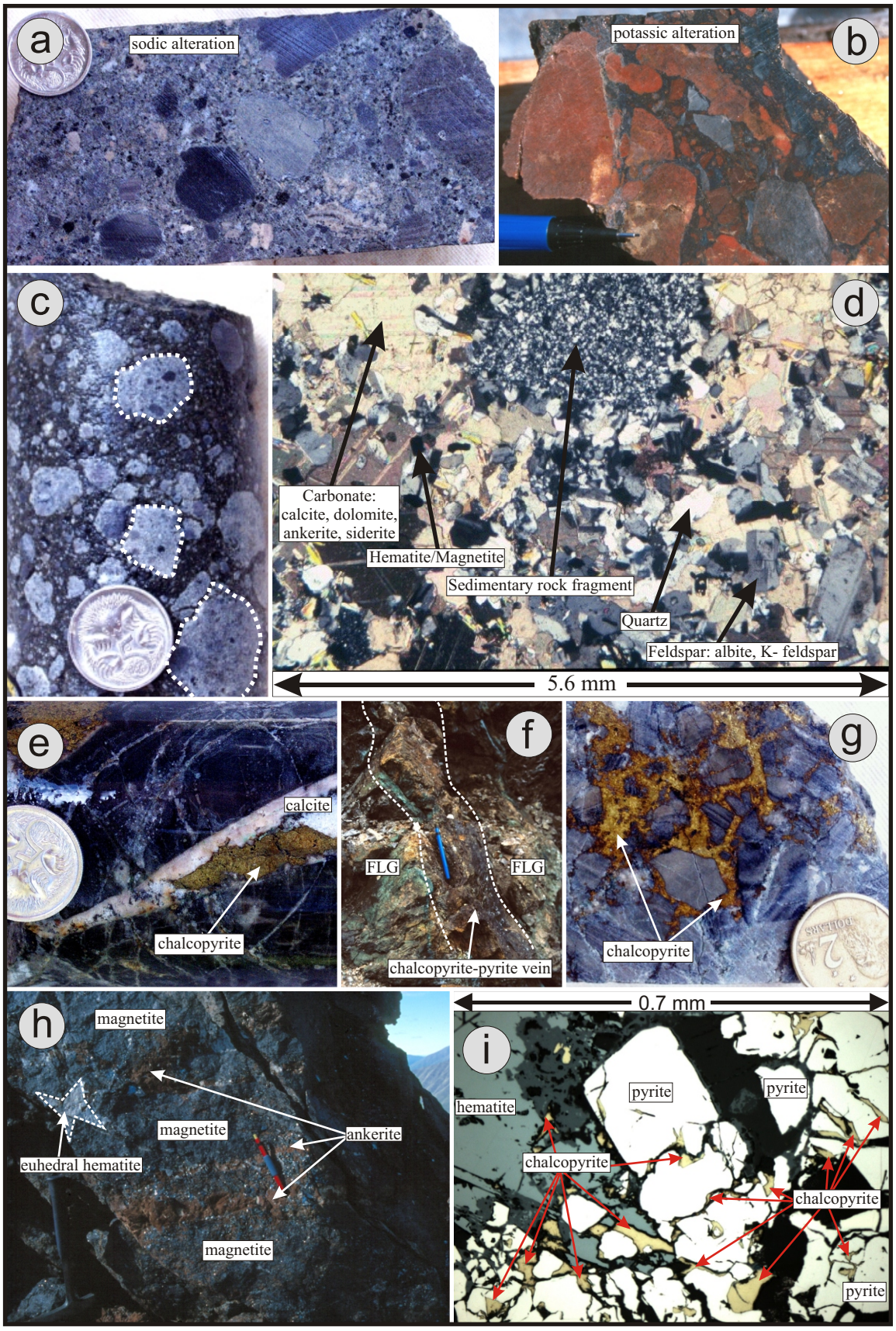
a
sodic alteration
b
potassic alteration
c
d
Carbonate:
calcite, dolomite,
ankerite, siderite
Hematite/Magnetite
Sedimentary rock fragment
Quartz
Feldspar: albite, K- feldspar
5.6 mm
e
calcite
chalcopyrite
f
FLG
FLG
chalcopyrite-pyrite vein
g
chalcopyrite
h
magnetite
magnetite
ankerite
euhedral hematite
magnetite
0.7 mm
i
pyrite
pyrite
hematite
chalcopyrite
chalcopyrite
pyrite

Figure 4:

Fluid temperature and salinity for selected IOCG deposits and prospects. References and abbreviations as in Table 1.

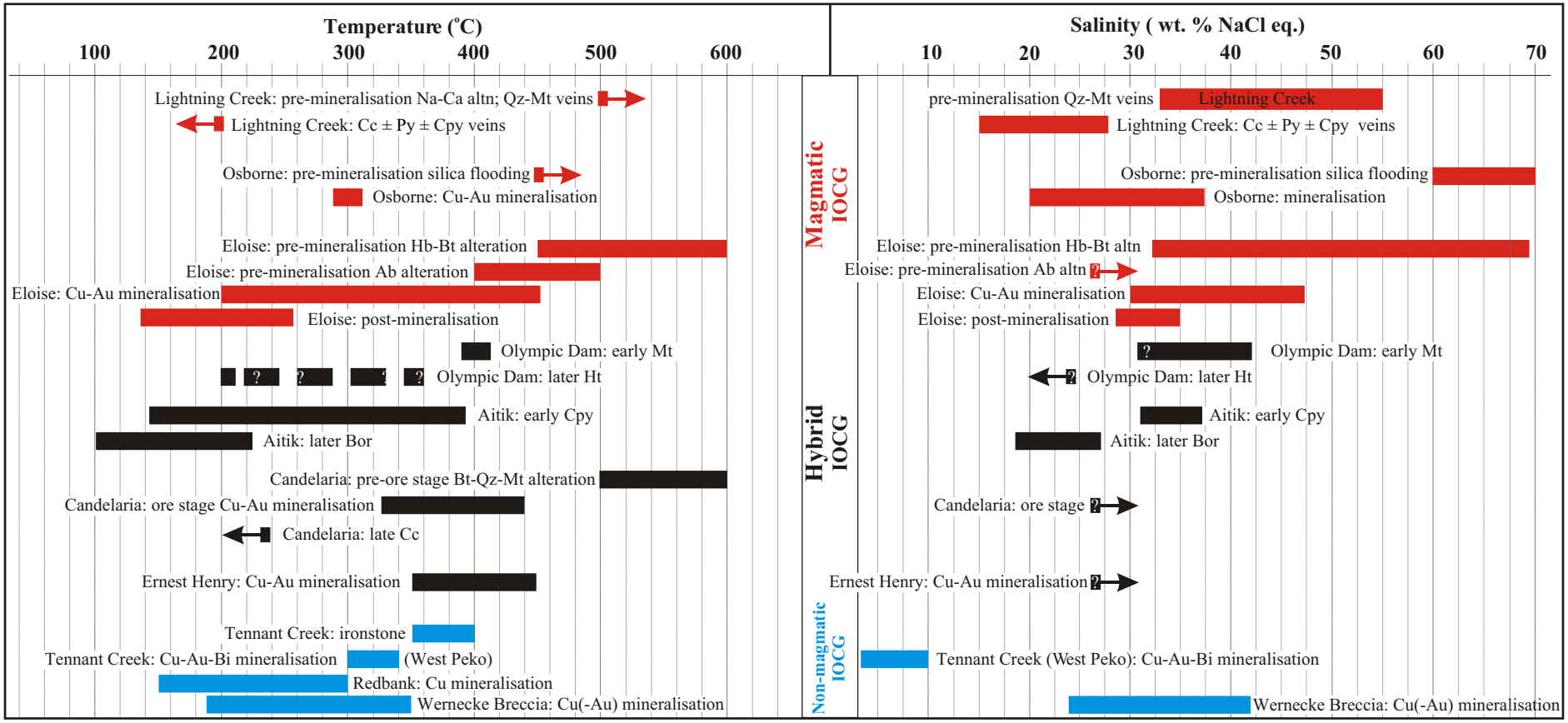

Section D: Figure 4

Figure 5:

Measured sulphur isotope compositions for mineralisation and calculated oxygen isotope compositions for mineralising fluid from various IOCG deposits. Legend shows mineral(s) used for sulphur isotope analysis and mineral used to calculated oxygen isotopic composition of fluid. References and abbreviations as in Table 1. * Values calculated from actinolite are 5.4 if temperature of 200 ^{o}C is used or 9.5 if temperature of 450 ^{o}C is used (see text for details). For $\delta^{18}O$ values for magmatic, metamorphic, formation and meteoric waters and modern seawater – *cf.* Sheppard, 1986; Rollinson, 1993. For $\delta^{34}S$ values for mantle and evaporite sources –*cf.* Ohmoto and Goldhaber, 1997.

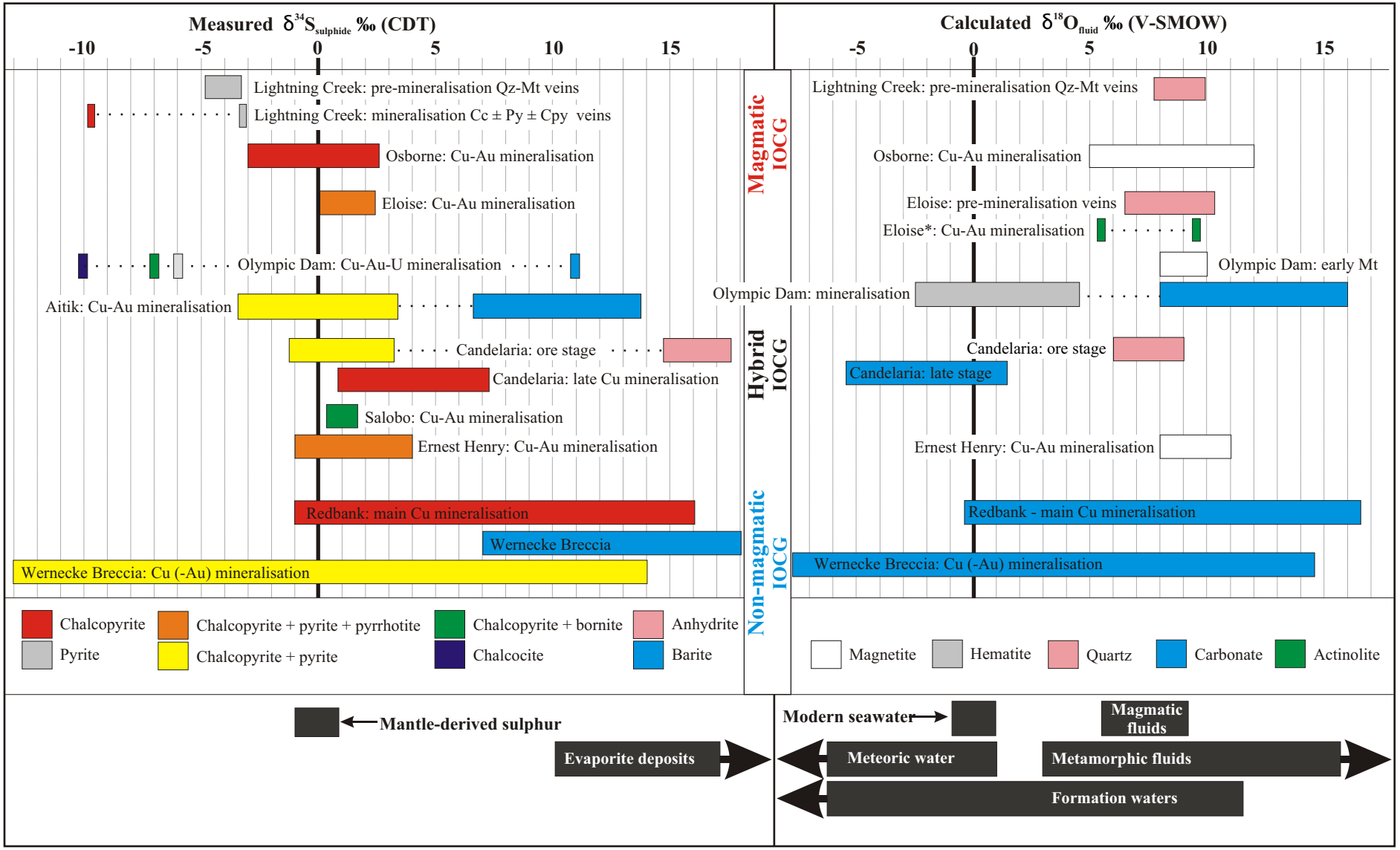

Section D: Figure 5

Figure 6:

Suggested classification of IOCG systems into magmatic and non-magmatic end-members with hybrid IOCG systems in between. Placement in the classification indicates the degree of involvement of magmatic and/or non-magmatic fluids in the formation of the IOCG system. Placement is also affected by the environment of formation of the IOCG system, i.e., magmatic or non-magmatic, which is determined by whether or not there is a **temporal** association with igneous rocks. At the non-magmatic end of the IOCG spectrum it is possible for an IOCG system to have formed from non-magmatic fluids but to have a temporal relationship with a magmatic system, e.g. Salton Sea. See text for discussion and references.

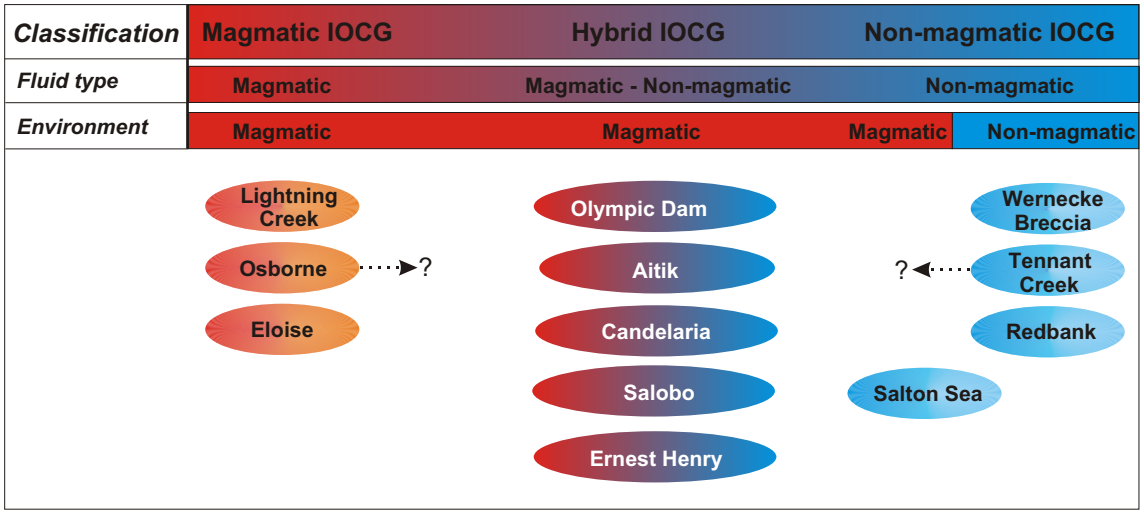
Classification
Magmatic IOCG
Hybrid IOCG
Non-magmatic IOCG
Fluid type
Magmatic
Magmatic - Non-magmatic
Non-magmatic
Environment
Magmatic
Magmatic
Magmatic
Non-magmatic
Lightning Creek
Osborne
?
Eloise
Olympic Dam
Aitik
Candelaria
Salobo
Ernest Henry
Wernecke Breccia
?
Tennant Creek
Redbank
Salton Sea

Figure 7:

Schematic model showing examples of hydrothermal alteration and mineralisation produced by the circulation of non-magmatic fluids (adapted from Barton and Johnson, 2000). Voluminous metal-depleted, sodic(-calcic) ± shallow K feldspar-hematite alteration forms in inflow zones and along the fluid pathway(s) (*cf.* Barton and Johnson, 1996, 2000). Fluids are heated and as they rise and cool they produce intense sodic and/or potassic alteration (depends on host rock composition) plus overprinting and shallow hydrolytic alteration. Metals are leached along the flow path and precipitate due to cooling and/or fluid mixing.

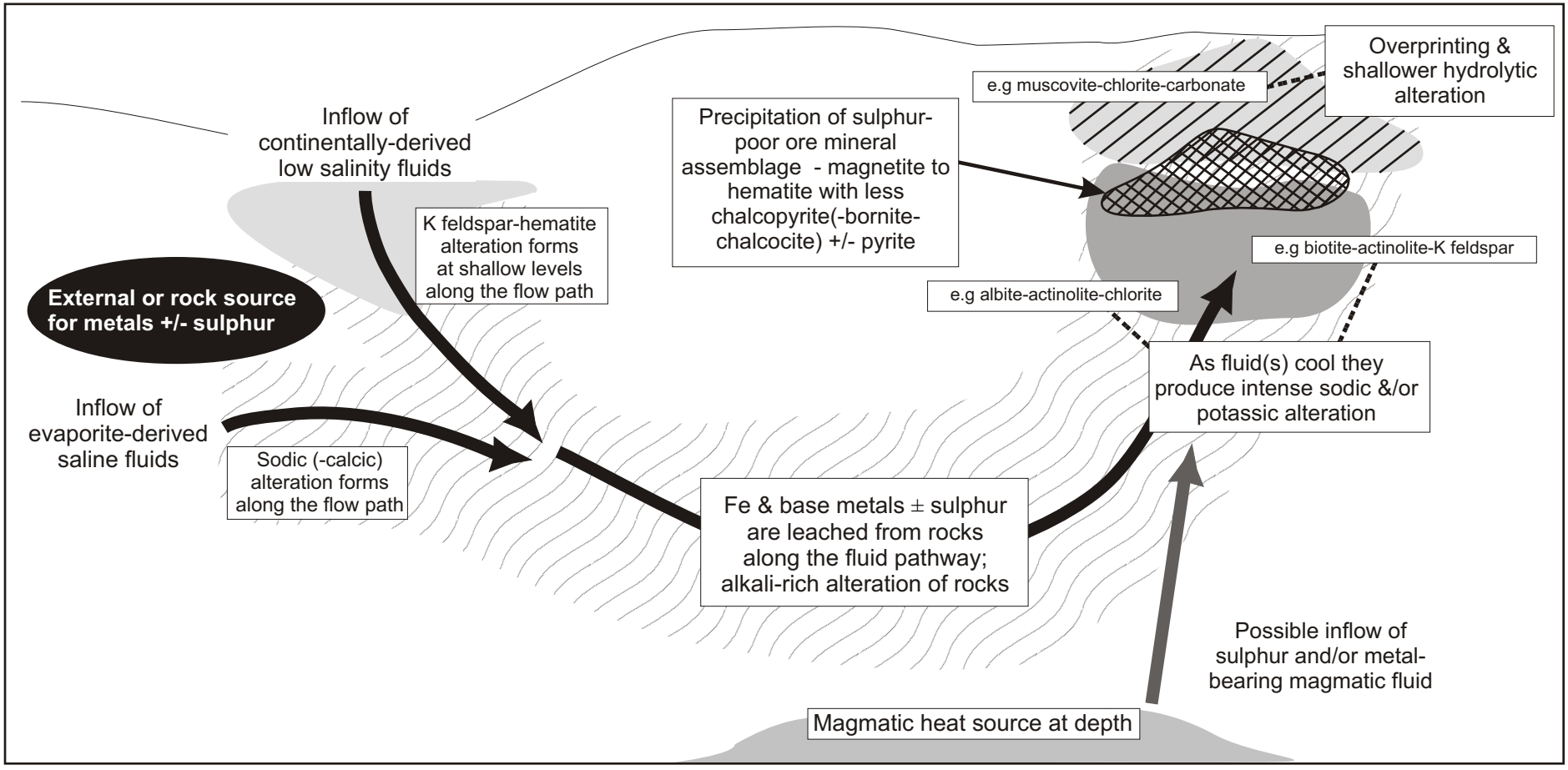

Section D: Figure 7

SECTION D - TABLES

Wernecke Breccias, Yukon, Canada: an example of a non-magmatic end-member IOCG system and implications for IOCG genesis and classification

Table 1: Size and grade of selected IOCG deposits. References: **Lightning Creek** – Perring *et al.*, 2000; Williams *et al.*, 1999; **Osborne** – Adshead, 1995; Perkins and Wyborn, 1996, 1998; Adshead *et al.*, 1998; Gauthier *et al.*, 2001; Rubenach *et al.*, 2001; **Eloise** – Baker, 1998; Baker and Laing, 1998; Baker *et al.*, 2001; **Olympic Dam** – Roberts and Hudson, 1983, 1984; Creaser, 1989; Reeve *et al.*, 1990; Johnson and Cross, 1991; Oreskes and Einaudi, 1992; Oreskes and Hitzman, 1993; Eldridge and Danti, 1994; Haynes *et al.*, 1995; Reynolds, 2000; **Aitik** – Frietsch *et al.*, 1995, 1997; Carlon, 2000; Wanhainen *et al.*, 2003; **Candelaria** – Ullrich and Clark, 1999; Marschik and Fontboté, 1996, 2001; Marschik *et al.*, 2000; **Salobo** – Requia and Fontboté, 2000; Souza and Vieira, 2000; **Ernest Henry** – Twyerould, 1997; Ryan, 1998; Mark and Crookes, 1999; Mark *et al.*, 2000; Williams *et al.*, in progress; **Wernecke Breccia (Slab)** – Hunt *et al.*, 2004, 2005; **Tennant Creek (West Peko, Eldorado)** – Ahmad *et al.*, 1999; Skirrow and Walshe, 2002; **Redbank** – Orridge and Mason (1975); Knutson *et al.* (1979).

Abbreviations used in tables and figures:

Ab = albite
Act = actinolite
Altn = alteration
Anhy = anhydrite
Ank = ankerite
Assoc = associated
Avg = average
Bar = barite
Bor = bornite
Bt = biotite
Bx = breccia
Cc = calcite
Cct = chalcocite
Cl = chlorite
Cov = covellite
Cpy = chalcopyrite
CS = cover sequence
Dec = decrease
Diss = disseminated
Dt = dolomite
dst = dolostone
Ep = epidote
eq = equivalent
Ft = fluorite
Gt = garnet
Hb = hornblende
Ht = hematite
Inc = increase
Ksp = potassium feldspar
lst = limestone
Mal = malachite
minz = mineralisation
mm = metamorphism
mtm = metasomatism
Musc = muscovite
Mt = magnetite
Pitch = pitchblende
Py = pyrite
Qz = quartz
Sd = siderite
Ser = sericite
SG = Supergroup
Spg = supergene
ss = sandstone
sst = siltstone
St = salinity
T = temperature
Th = homogenisation temperature
Tour = tourmaline
Urt = uraninite
wt = weight

Deposit	Tonnes (x 10^6)	Commodity	Grade	Associated metals	Mineralisation styles
MAGMATIC END MEMBER					
Lightning Ck	-	Cu (%) Au (g/t)	minor minor	-	Narrow Cc ± Cl ± Py ± Cpy veins x-cut Qz-Mt veins
Osborne	11.2	Cu (%) Au (g/t)	3.51 1.49	Co, Ag, Mo, Bi, Te, Se, Hg, Sn, W	Mineralisation occurs mainly in silicified zones at the contact between psammite & iron stone
Eloise	3.2	Cu (%) Au (g/t) Ag (g/t)	5.8 1.5 19	Co, Ni, Zn, As, Bi	Veins, stockwork veins, massive sulphide
HYBRID MAGMATIC - NON-MAGMATIC					
Olympic Dam	2320	Cu (%) Au (g/t) Ag (g/t) U_3O_8 (kg/t)	1.3 0.5 2.9 0.4	Co, REE (dominantly La & Ce), Ni, As	Disseminations, veinlets & fragments within bx zones, primarily within bx matrix
Aitik	800	Cu (%) Au (g/t) Ag (g/t)	0.3 0.2 2	Mo	Disseminations & veins
Candelaria	470	Cu (%) Au (g/t) Ag (g/t)	0.95 0.22 3.1	Zn, Mo, As, LREE	Vein, bx hosted, mantos, overprints Mt replacement bodies
Salobo	450	Cu (%) Au (g/t)	1.15 0.5	Ag, U, Co, Mo, F, LREE	Lenses, veins
Ernest Henry	166	Cu (%) Au (g/t)	1.1 0.54	Co, Mo, U, REE, F, Mn, As, Ba	In bx
NON-MAGMATIC END MEMBER					
Wernecke Bx	Slab: 20	Cu (%)	0.35	U, Co, Mo	Disseminations, veins, bx infill
Tennant Creek	West Peko: 3.2 Eldorado: 0.0292	Cu (%) Au (g/t) Ag (g/t) Bi (%) Au (g/t)	4 3.5 14 0.2 20.8	Bi	Massive & vein mineralisation overprinting ironstone
Redbank	Bluff: 2 Sandy Flat: 1.5	Cu (%) Cu (%)	1.66 2	Pb, Zn, REE	Breccia infill, veins, disseminations

Table 2 Tectonic setting, main host rocks, confining structure(s) and age of mineralisation for selected IOCG deposits. References and abbreviations as in Table 1. ** *The tectonic settings for most IOCG districts are poorly understood, even in areas that host well studied deposits such as Olympic Dam.*

Deposit	Tectonic setting**	Main host rocks	Confining structure(s)	Age of mineralization (Ma)	Coeval intrusions
MAGMATIC END MEMBER					
Lightning Ck	Intracratonic basin associated with high heat flow & plutonism	*ca* . 1540-1500 intrusive rocks	-	Coeval with late stage sills	Yes
Osborne		Feldspathic psammite & Mt-Qz iron stone of the Soldiers Cap Group of CS 3 (*ca* . 1670-1600 Ma)	Fault bends	*ca* . 1595 (Ar-Ar, Hb,Bt; U-Pb, titanite; Re-Os, Moly)	?
Eloise		Meta-arkose, schist, amphibolite of the Soldiers Cap Group of CS 3 (*ca* . 1670-1600 Ma)	Shear zones	*ca* . 1536-1512 (Ar-Ar, Bt, Hb)	Inferred
HYBRID MAGMATIC - NON-MAGMATIC					
Olympic Dam	Anorogenic intracontinental environment above a mantle plume; or arc - back-arc	Granite & felsic, mafic & ultramafic volcanic rocks of the *ca* . 1590 Ma Hiltaba Suite/Gawler Range volcanics	Dilational zone in regional-scale fault	*ca.* 1590	Yes
Aitik	Volcanic arcs-back arc basins above a subduction zone	*ca* . 1910-1880 Ma intermediate to felsic metavolcanic rocks	Fault/shear zones	*ca* . 1870	Yes
Candelaria	Arc - back-arc	Early Cretaceous intrusive, volcanic, volcaniclastic & sedimentary rocks	Intersection of shear zone & faults with lithologic contact	Oxide: *ca* . 116-114; copper sulphide: *ca* . 112-110	Yes
Salobo	Continental rift	Metagreywacke & amphibolite of the *ca* . 2750 Ma Itacaiúnas Super Group	Shear zone	*ca* . 2500 (Re-Os, Pb-Pb)	Yes
Ernest Henry	Intracratonic basin associated with high heat flow & plutonism	Brecciated, altered, intermediate to felsic *ca* . 1740 Ma volcanic rocks of CS 2 (*ca* . 1780-?1720 Ma)	Shear zones	*ca* . 1510-1500 (Ar-Ar, Bt)	Yes
NON-MAGMATIC END MEMBER					
Wernecke Breccia	Rifted continent	> *ca* . 1710 Ma meta-ss, siltstone, dlst, lst & evaporites of the WSG	Shear zones, faults, fold axes	> *ca.* 1860 & ≤ *ca* . 1830	No
Tennant Creek	Pull apart sedimentary basin	*ca* . 1860 Ma Warramunga Formation	Iron stone in shear zones & Fold axes	-	?
Redbank	Rifted continent	Middle Proterozoic Tawallah Group, in part ca. 1575 ± 120 Ma	Faults	-	?

Table 3: Regional and ore-related alteration types for selected IOCG deposits. References and abbreviations as in Table 1. Main copper minerals in the ore stage are shown in brackets.

Deposit	Regional alteration	Dominant IOCG-related mineralisation		
		Early	Main	Late
MAGMATIC END MEMBER				
Lightning Ck	Sodic-calcic	Ca-Fe ± Na	Ca ± Cl	-
Osborne	Na, Ca, Fe, Si	Na, Ca, Fe, Si	Na, Ca, Fe, Si	-
Eloise	Pervasive albitisation	Hb, Bt, Qz veins & alteration	Qz, Cc, Act/Hb, Cl, Bt, Musc, Ksp	Cl, Ksp, Sd-Ht, Cc veins; silicification & Cl-Cc veins; Py-Qz-adularia veins
HYBRID MAGMATIC - NON-MAGMATIC				
Olympic Dam	Weak pervasive Ht, Ser, & Cl.	Mt ± Ht, Cl, Ser, Sd	Intense Ht & Cl is assoc. with minz. in the lower part of the deposit; Ser & silica predominates in the upper part	Ht ± Qz ± Bar
Aitik	Scapolite, Ab ± Tour	-	Bt and Ser in the ore zone; Ksp and Ep in fault zones	Ser/musc
Candelaria	Pervasive albitization	Bt-Qz-Mt ± Ksp	Calcic amphibole-Ab ± Ksp	Ep-Cl; Ht-Cc-Cpy; Anhy & Cc-Cl
Salobo	Na, K	Mt, Ht	Ksp, Bt	Calcic; Cl
Ernest Henry	Na-Ca	Diss Bt-Mt; Gt-Ksp-Bt.	Ksp-Ht	Dominantly Cc-Dt; minor Qz-Bt-Act-Py-Mt-± Gt ± Cpy veins and bx
NON-MAGMATIC END MEMBER				
Wernecke Breccia	Greenschist facies mm	Sodic ± potassic; potassic ± sodic; local pervasive Bt; local Mt-Ank	Sodic ± potassic; potassic ± sodic; Ca; local Ser	Cc or Dt-Ank or Bar ± Sd ± Ank-Dt; local overprinting Cl-Mt
Tennant Ck	Weakly mm	Mt-Ht-Qz ± Cl ironstone	Cl ± stilpnomelane ± talc ± Sd ± Cc (reduced end member); Cl-Ser-Ht (oxidised end member)	-
Redbank	Pervasive K	Cl-Ht-Ksp	Dt	-

Table 4: Fluid temperature, salinity, composition and source plus precipitation mechanisms for selected IOCG deposits. References and abbreviations as in Table 1.

Deposit	Phase	Temperature (°C)	Salinity (wt. % NaCl eq)	Fluid source(s)	Precipitation mechanism(s)
MAGMATIC END MEMBER					
Lightning Creek	Na-Ca alteration	> 500	-	Magmatic	Dec. in T & St; fluid mixing
	Quartz-Mt veins	> 500	33 - 55	Magmatic	
	Cc±Cl±Py±Cpy	< 200	15 - 28	Magmatic + meteoric	
Osborne	Pre-minz silica flooding	> 450	60 - 70	-	Dec. in T & St & inc. in pH
	Mineralisation	~ 300	20 - 37	Magmatic &/or retrograde mm	
Eloise	Pre-minz Hb-Bt altn	450 - 600	32 - 68	? Magmatic	Dec. in T & St, inc. in pH & dilution due to fluid mixing; sulphidation of Fe-silicates
	Pre-minz Ab altn	400 - 500	> 26	? Magmatic	
	Mineralisation	200 - 450	30 - 47	Magmatic	
	Post-mineralisation	137 - 258	29 - 35	?Magmatic mixed with meteoric	
HYBRID MAGMATIC - NON-MAGMATIC					
Olympic Dam	Early Mt & Sd	~ 400	?31 - 42	Magmatic or deeply circulating water	Fluid mixing; superimposed hot & cooler fluids; cooling
	Ore formation (Ht)	200-300	< 24	Surficial/connate	
	Ft & Qz with Bor & Cct	Th = avg 240	-	-	
	Ft & Qz with Cpy	Th = avg 160	-	-	
Aitik	Cpy	140 - 373	31 - 37	Magmatic ± evaporitic	?Fluid mixing
	Bor	100 - 222	18 - 27		
Candelaria	Bt-Qz-Mt altn	500 - 600	-		Cooling ± fluid mixing
	Cu-Au	330 - 440	> 26	Magmatic ± non Magmatic	
	Late Cc	≤ 236	-		
Salobo	-	-	-	Magmatic + connate + more oxidized fluid	Fluid mixing
Ernest Henry	Ore fluid	350-450	> 26	Magmatic + ?	Fluid mixing &/or cooling
NON-MAGMATIC END MEMBER					
Wernecke Bx	Ore fluid	185 - 350	24 - 42	Formation/mm water	? Cooling, ? fluid mixing
Tennant Creek	West Peko: ore fluid	300 - 340	3 to 10 (low)	Mm/formation water	Reaction of reducing fluid with ironstone
	Eldorado: ore fluid	~ 300	low to moderate	Mm/formation water + ?	Fluid mixing in presence of iron stone
Redbank	Carbonate	150 - 300	-	Formation water ± sea water	Cooling, ? fluid mixing

APPENDIX I

Results of microprobe analyses

JCU #	Sample #	SiO_2	TiO_2	Al_2O_3	FeO	MnO	MgO	CaO	Na_2O	K_2O	Cl	TOTAL	Meionite	Marialite
Slab - metaevaporite-related scapolite													(Atomic %)	
70569	band 1 outer edge	55.70	0.00	22.41	0.03	0.03	0.00	6.86	1.60	0.65	3.26	97.15	30.44	69.56
70569	band 1 middle	55.90	0.00	22.22	0.03	0.02	0.00	6.85	1.61	0.68	3.21	98.41	27.47	72.53
70569	band 1 middle	55.74	0.00	22.13	0.06	0.01	0.00	6.59	9.41	0.45	3.19	97.59	27.43	72.57
70569	band 1 middle	55.39	0.03	22.39	0.00	0.00	0.00	7.00	9.15	0.48	3.12	97.55	29.08	70.92
70569	band 1 middle	55.73	0.00	22.03	0.02	0.03	0.00	7.13	9.36	0.44	2.90	97.63	29.05	70.95
70569	band 1 middle	56.37	0.02	21.52	0.09	0.00	0.00	6.12	9.84	0.56	3.26	97.78	25.14	74.86
70569	band 1 middle	55.84	0.02	22.20	0.02	0.04	0.00	6.67	9.67	0.50	3.17	98.13	27.01	72.99
70569	band 1 middle	56.15	0.00	21.79	0.05	0.04	0.00	6.31	9.60	0.51	3.28	97.73	26.09	73.91
70569	band 1 middle	55.92	0.00	22.18	0.05	0.00	0.00	6.79	9.63	0.60	3.09	98.25	27.34	72.66
70569	band 1 middle	56.31	0.00	22.23	0.04	0.02	0.00	6.54	9.77	0.53	3.23	98.67	26.42	73.58
70569	band 1 middle	57.33	0.01	21.53	0.05	0.00	0.00	5.55	10.24	0.59	3.46	98.77	22.55	77.45
70569	band 1 middle	56.58	0.03	21.96	0.02	0.00	0.00	6.54	9.85	0.50	3.27	98.76	26.33	73.67
70569	band 1 middle	55.62	0.00	21.14	0.04	0.00	0.00	6.06	9.61	0.48	3.25	96.21	25.33	74.67
70569	band 1 inner edge	55.46	0.00	21.28	0.07	0.00	0.00	6.22	9.63	0.45	3.26	96.37	25.89	74.11
70569	band 1 inner edge	55.21	0.01	21.31	0.05	0.00	0.00	5.92	9.78	0.47	3.34	96.09	24.62	75.38
70569	band 1 inner edge	57.02	0.00	21.82	0.03	0.00	0.00	5.90	7.94	0.55	3.42	96.68	28.26	71.74
70569	band 1 inner edge	55.94	0.03	22.08	0.05	0.04	0.00	6.58	9.48	0.49	3.19	97.88	27.23	72.77
70569	band 1 inner edge	55.43	0.00	22.26	0.07	0.02	0.00	7.04	9.48	0.47	3.10	97.87	28.60	71.40
70569	band 1 inner edge	56.84	0.00	21.85	0.01	0.02	0.00	5.91	9.87	0.73	3.44	98.68	24.01	75.99
70569	band 1 inner edge	56.70	0.00	21.84	0.07	0.00	0.00	6.08	9.85	0.54	3.34	98.42	24.93	75.07
70569	band 1 inner edge	56.08	0.00	21.88	0.06	0.01	0.00	6.92	9.68	0.50	3.17	98.30	27.77	72.23
70569	band 1 inner edge	56.57	0.00	22.02	0.04	0.00	0.00	6.30	9.96	0.55	3.31	98.75	25.32	74.68
70569	band 2 outer edge	55.54	0.03	21.38	0.03	0.01	0.00	5.85	9.60	0.59	3.37	96.39	24.59	75.41
70569	band 2 outer edge	55.39	0.00	21.48	0.03	0.00	0.00	6.19	9.56	0.53	3.34	96.52	25.75	74.25
70569	band 2 outer edge	55.07	0.00	21.92	0.04	0.00	0.00	6.88	9.32	0.60	3.25	97.09	28.23	71.77
70569	band 2 outer edge	54.61	0.00	21.92	0.02	0.02	0.00	7.02	9.44	0.46	3.17	96.66	28.53	71.47
70569	band 2 outer edge	55.05	0.00	21.77	0.04	0.03	0.00	6.65	9.58	0.48	3.31	96.91	27.17	72.83
70569	band 2 outer edge	55.44	0.00	21.59	0.04	0.03	0.00	6.33	9.87	0.46	3.24	97.00	25.69	74.31
70569	band 2 outer edge	56.30	0.00	21.12	0.04	0.00	0.00	5.68	10.04	0.55	3.49	97.23	23.28	76.72
70569	band 2 outer edge	55.58	0.01	21.54	0.00	0.02	0.00	5.82	9.85	1.21	3.46	97.48	23.20	76.80
70569	band 2 outer edge	55.81	0.02	21.44	0.00	0.00	0.00	5.84	9.67	1.01	3.44	97.23	23.84	76.16

JCU #	Sample #	SiO_2	TiO_2	Al_2O_3	FeO	MnO	MgO	CaO	Na_2O	K_2O	Cl	TOTAL	Meionite	Marialite
Slab - metaevaporite-related scapolite													(Atomic %)	
70569	band 2 outer edge	55.58	0.00	21.68	0.02	0.00	0.00	6.61	9.30	0.77	3.19	97.15	27.18	72.82
70569	band 2 inner edge	55.41	0.00	21.57	0.05	0.01	0.00	6.27	9.40	0.48	3.18	96.37	26.40	73.60
70569	band 2 inner edge	55.73	0.01	21.67	0.05	0.02	0.00	6.42	9.53	0.47	3.28	97.18	26.63	73.37
70569	band 2 inner edge	55.64	0.00	21.80	0.00	0.02	0.00	6.50	9.51	0.52	3.31	97.30	26.72	73.28
70569	band 2 inner edge	56.13	0.00	21.54	0.02	0.00	0.00	5.98	9.75	0.49	3.29	97.20	24.75	75.25
70569	band 2 inner edge	56.37	0.00	21.20	0.06	0.00	0.00	5.84	10.21	0.53	3.47	97.68	23.55	76.45
70569	band 2 inner edge	55.75	0.00	21.60	0.00	0.00	0.00	6.57	9.75	0.45	3.23	97.35	26.55	73.45
70569	band 2 inner edge	56.53	0.00	21.42	0.02	0.03	0.00	5.76	9.85	0.47	3.38	97.46	23.89	76.11
70569	band 2 inner edge	55.02	0.00	22.28	0.00	0.01	0.00	7.04	9.39	0.55	3.21	97.51	28.52	71.48
70569	band 2 inner edge	56.52	0.00	21.41	0.04	0.04	0.00	5.62	9.90	0.69	3.40	97.62	23.18	76.82
70569	band 2 inner edge	56.64	0.00	21.68	0.02	0.04	0.00	5.94	10.01	0.58	3.37	98.29	24.05	75.95
70569	band 3 outer edge	56.18	0.00	21.85	0.00	0.00	0.00	6.50	9.65	0.51	3.24	97.93	26.45	73.55
70569	band 3 outer edge	56.16	0.04	21.71	0.05	0.00	0.00	6.01	10.08	0.57	3.41	98.03	24.30	75.70
70569	band 3 outer edge	56.19	0.00	21.92	0.03	0.04	0.00	6.55	9.74	0.46	3.28	98.20	26.56	73.44
70569	band 3 outer edge	56.15	0.00	21.68	0.04	0.00	0.00	6.40	9.82	0.49	3.22	97.80	25.93	74.07
70569	band 3 outer edge	55.86	0.00	22.12	0.06	0.02	0.00	6.98	9.49	0.48	3.15	98.16	28.38	71.62
70569	band 3 outer edge	56.81	0.00	21.34	0.08	0.01	0.00	6.06	10.17	0.53	3.35	98.35	24.35	75.65
70569	band 3 outer edge	56.95	0.01	21.80	0.01	0.00	0.00	6.04	10.09	0.52	3.37	98.80	24.29	75.71
70569	band 3 outer edge	55.88	0.02	22.22	0.07	0.03	0.01	6.86	9.63	0.54	3.23	98.49	27.82	72.18
70569	band 3 outer edge	56.17	0.00	22.09	0.06	0.00	0.00	6.70	9.69	0.48	3.23	98.42	27.14	72.86
70569	band 3 inner edge	56.47	0.00	21.70	0.02	0.00	0.00	6.26	9.75	0.55	3.31	98.07	25.54	74.46
70569	band 3 inner edge	56.69	0.00	21.96	0.07	0.00	0.00	6.30	9.78	0.56	3.30	98.66	25.71	74.29
70569	band 3 inner edge	56.93	0.01	21.75	0.02	0.03	0.00	5.97	9.99	0.58	3.35	98.62	24.18	75.82
70569	band 3 inner edge	55.53	0.00	22.54	0.03	0.00	0.00	7.13	9.46	0.55	3.16	98.41	28.70	71.30
70569	band 3 inner edge	57.05	0.02	21.59	0.06	0.00	0.00	5.87	10.24	0.65	3.49	98.97	23.50	76.50
70569	band 3 inner edge	57.73	0.00	21.42	0.02	0.02	0.00	5.34	9.96	0.68	3.55	98.72	22.12	77.88
70569	band 3 inner edge	57.50	0.02	21.42	0.01	0.01	0.00	5.61	10.23	0.70	3.43	98.92	22.55	77.45
70569	band 3 inner edge	56.29	0.01	22.00	0.08	0.04	0.00	6.86	9.79	0.53	3.14	98.73	27.38	72.62
	Average	56.08	0.01	21.78	0.04	0.01	0.00	6.34	9.43	0.56	3.29	97.77	25.98	74.02
	Maximum	57.73	0.04	22.54	0.09	0.04	0.01	7.13	10.24	1.21	3.55	98.97	30.44	77.88
	Minimum	54.61	0.00	21.12	0.00	0.00	0.00	5.34	1.60	0.44	2.90	96.09	22.12	69.56

JCU #	Sample #	SiO_2	TiO_2	Al_2O_3	FeO	MnO	MgO	CaO	Na_2O	K_2O	Cl	TOTAL
Slab - metaevaporite-related biotite												
70287	SB94-4-79.6-1 biot 1	39.93	1.48	14.73	14.18	0.43	14.59	0.37	0.00	10.12	0.46	96.30
70287	SB94-4-79.6-1 biot 2	37.95	1.33	14.76	12.97	0.11	14.40	0.15	0.08	10.00	0.62	92.37
70287	SB94-4-79.6-1 biot 3	39.27	1.53	14.79	13.95	0.17	14.14	0.24	0.00	10.37	0.55	95.02
70219	SB94-1-57.43 circle 1 biot 1	39.66	2.44	13.23	13.43	0.07	14.20	0.14	0.00	10.24	0.72	94.13
70219	SB94-1-57.43 circle 1 biot 2	39.65	1.98	13.55	13.31	0.04	14.50	0.00	0.06	10.47	0.57	94.15
70219	SB94-1-57.43 circle 1 biot 3	40.64	2.35	13.83	14.41	0.28	14.22	0.23	0.61	10.32	0.61	97.49
70219	SB94-1-57.43 circle 1 biot 3	38.68	2.04	14.48	14.90	0.04	13.04	0.31	0.00	10.40	0.56	94.44
70219	SB94-1-57.43 circle 2 biot 1	37.27	1.96	13.29	14.94	0.33	12.76	0.04	0.04	9.96	0.61	91.21
70219	SB94-1-57.43 circle 2 biot 2	37.50	2.57	13.64	15.53	0.22	12.81	0.13	0.00	10.17	0.63	93.21
70219	SB94-1-57.43 circle 2 biot 3	38.63	2.35	13.68	15.21	0.20	12.86	0.05	0.00	10.63	0.56	94.17
	Maximum	40.64	2.57	14.79	15.53	0.43	14.59	0.37	0.61	10.63	0.72	97.49
	Minimum	37.27	1.33	13.23	12.97	0.04	12.76	0.00	0.00	9.96	0.46	91.21
	Average	38.92	2.00	14.00	14.28	0.19	13.75	0.17	0.08	10.27	0.59	94.25

JCU #	Sample #	Si	Ti	Al	Fe	Mn	Mg	Ca	Na	K	CL	Na/Al	Ca+Na+K	Albite	Kspar	Anorthite
ALBITE																
Igor																
70922	JH02-8-6 circle 1 albite 1	6.06	0.00	2.58	0.00	0.00	0.00	0.02	7.60	0.04	0.00	2.94	7.66	0.99	0.01	0.00
70922	JH02-8-6 circle 1 feldspar 1	6.01	0.00	2.63	0.05	0.00	0.10	0.07	7.28	0.00	0.00	2.77	7.36	0.99	0.00	0.01
70922	JH02-8-6 circle 1 feldspar 2	6.10	0.00	2.50	0.00	0.00	0.00	0.00	7.84	0.00	0.02	3.14	7.84	1.00	0.00	0.00
70922	JH02-8-6 circle 1 feldspar 3	6.07	0.03	2.50	0.03	0.00	0.00	0.06	7.39	0.03	0.04	2.95	7.49	0.99	0.00	0.01
70922	JH02-8-6 circle 1 feldspar 4	6.11	0.00	2.49	0.02	0.00	0.00	0.02	7.52	0.03	0.01	3.02	7.57	0.99	0.00	0.00
70922	JH02-8-6 circle 1 Kspar 4	6.06	0.00	2.58	0.00	0.00	0.00	0.02	7.60	0.04	0.00	2.94	7.66	0.99	0.01	0.00
70922	JH02-8-6 circle 2 albite 1	6.04	0.01	2.54	0.02	0.01	0.07	0.06	7.69	0.01	0.02	3.03	7.77	0.99	0.00	0.01
70922	JH02-8-6 circle 2 albite 2	6.11	0.00	2.56	0.05	0.02	0.00	0.04	6.73	0.05	0.03	2.63	6.82	0.99	0.01	0.01
Slab																
70233	SB94-1-128.6 circle 1 albite 1	6.12	0.01	2.50	0.04	0.03	0.06	0.06	6.47	0.01	0.00	2.58	6.54	0.99	0.00	0.01
70233	SB94-1-128.6 circle 1 albite 2	6.04	0.01	2.41	0.00	0.00	0.13	0.55	6.70	0.03	0.02	2.78	7.28	0.92	0.00	0.08
70247	SB94-1-190.90 circle 1 albite 1	6.04	0.00	2.61	0.03	0.00	0.00	0.03	7.58	0.01	0.02	2.90	7.62	0.99	0.00	0.00
70247	SB94-1-190.90 circle 2 albite 1	2.24	0.00	1.01	0.01	0.01	0.00	0.03	2.76	0.00	0.00	2.73	2.80	0.99	0.00	0.01
70247	SB94-1-190.90 circle 2 albite 1	5.98	0.00	2.70	0.03	0.04	0.00	0.07	7.37	0.01	0.00	2.73	7.45	0.99	0.00	0.01
70247	SB94-1-190.90 circle 2 albite 2	6.05	0.01	2.62	0.00	0.00	0.03	0.03	7.23	0.00	0.00	2.76	7.26	1.00	0.00	0.00
70247	SB94-1-190.90 circle 2 albite 3	6.09	0.00	2.60	0.00	0.00	0.00	0.03	7.02	0.00	0.00	2.70	7.05	1.00	0.00	0.00
70247	SB94-1-190.90 circle 2 albite 4	6.05	0.00	2.63	0.00	0.02	0.00	0.07	7.10	0.01	0.00	2.69	7.18	0.99	0.00	0.01
70255	SB94-1-332.5 circle 2 albite 1	6.00	0.00	2.69	0.02	0.00	0.05	0.06	7.25	0.02	0.00	2.69	7.33	0.99	0.00	0.01
70255	SB94-1-332.5 circle 2 albite 2	6.06	0.00	2.64	0.00	0.00	0.02	0.05	6.80	0.05	0.00	2.58	6.91	0.99	0.01	0.01
70255	SB94-1-332.5 circle 2 albite 3	6.02	0.00	2.65	0.00	0.00	0.00	0.09	7.39	0.03	0.00	2.79	7.51	0.98	0.00	0.01
70257	SB94-1-345.1 circle 1 albite 1	6.03	0.00	2.63	0.04	0.00	0.00	0.13	7.08	0.04	0.00	2.70	7.25	0.98	0.01	0.02
70257	SB94-1-345.1 circle 1 albite 2	6.01	0.00	2.69	0.00	0.00	0.00	0.05	7.45	0.02	0.00	2.77	7.53	0.99	0.00	0.01
70257	SB94-1-345.1 circle 2 albite `	5.92	0.00	2.77	0.00	0.05	0.11	0.09	7.29	0.02	0.02	2.64	7.40	0.98	0.00	0.01
70257	SB94-1-345.1 circle 1 albite 4 2nd try	6.00	0.00	2.66	0.00	0.02	0.09	0.09	7.31	0.03	0.01	2.75	7.43	0.98	0.00	0.01
70257	SB94-1-345.1 circle 1 albite 5 2nd try	6.00	0.00	2.67	0.03	0.00	0.07	0.07	7.14	0.03	0.00	2.68	7.24	0.99	0.00	0.01
70257	SB94-1-345.1 circle 1 albite 6 2nd try	6.03	0.00	2.63	0.02	0.03	0.00	0.11	7.21	0.02	0.03	2.75	7.35	0.98	0.00	0.02
70257	SB94-1-345.1 circle 2 albite 1	6.05	0.00	2.53	0.00	0.00	0.02	0.01	8.16	0.03	0.00	3.22	8.20	1.00	0.00	0.00
70257	SB94-1-345.1 circle 2 albite 3 2nd try	6.01	0.00	2.67	0.00	0.00	0.05	0.08	7.28	0.03	0.00	2.73	7.40	0.98	0.00	0.01
70221	SB94-1-59.5 circle 1 albite 1	6.03	0.00	2.62	0.00	0.01	0.00	0.07	7.49	0.03	0.01	2.85	7.58	0.99	0.00	0.01

JCU #	Sample #	Si	Ti	Al	Fe	Mn	Mg	Ca	Na	K	CL	Na/Al	Ca+Na+K	Albite	Kspar	Anorthite
70221	SB94-1-59.5 circle 1 albite 2	6.00	0.00	2.68	0.00	0.00	0.05	0.06	7.49	0.01	0.00	2.80	7.57	0.99	0.00	0.01
70221	SB94-1-59.5 circle 1 albite 3	6.36	0.01	2.16	0.02	0.01	0.10	0.03	6.12	0.00	0.02	2.84	6.15	1.00	0.00	0.00
70287	SB94-4-79.6 circle 4 albite 2	6.05	0.00	2.64	0.01	0.00	0.00	0.12	6.93	0.00	0.00	2.63	7.05	0.98	0.00	0.02
70287	SB94-4-79.6 circle 4 albite 3	5.99	0.00	2.68	0.00	0.03	0.16	0.03	7.14	0.02	0.03	2.67	7.19	0.99	0.00	0.00
70287	SB94-4-79.6 circle 4 albite1	6.01	0.00	2.64	0.00	0.03	0.04	0.09	7.40	0.00	0.00	2.80	7.49	0.99	0.00	0.01
70378	SB97-10-19.4 circle 1 albite 1	6.07	0.00	2.60	0.03	0.00	0.04	0.04	6.91	0.02	0.05	2.66	6.98	0.99	0.00	0.01
70378	SB97-10-19.4 circle 1 albite 2	5.97	0.01	2.68	0.02	0.00	0.04	0.26	6.97	0.01	0.02	2.60	7.23	0.96	0.00	0.04
70378	SB97-10-19.4 circle 1 albite 3	6.02	0.00	2.60	0.02	0.00	0.04	0.18	7.30	0.02	0.03	2.81	7.49	0.97	0.00	0.02
70378	SB97-10-19.4 circle 2 albite 1	6.00	0.01	2.61	0.00	0.00	0.01	0.24	7.33	0.03	0.02	2.80	7.60	0.97	0.00	0.03
70378	SB97-10-19.4 circle 2 albite 2	6.02	0.01	2.65	0.00	0.01	0.03	0.04	7.37	0.01	0.07	2.78	7.42	0.99	0.00	0.01
70378	SB97-10-19.4 circle 2 albite 3	6.02	0.00	2.63	0.01	0.01	0.00	0.06	7.57	0.02	0.04	2.88	7.66	0.99	0.00	0.01
70378	SB97-10-19.4 circle 3 albite 1	6.00	0.00	2.70	0.00	0.00	0.02	0.09	7.17	0.00	0.00	2.65	7.26	0.99	0.00	0.01
70378	SB97-10-19.4 circle 3 albite 2	6.03	0.00	2.63	0.05	0.00	0.03	0.03	7.33	0.01	0.04	2.78	7.37	0.99	0.00	0.00
70378	SB97-10-19.4 circle 3 albite 3	6.13	0.00	2.51	0.00	0.00	0.00	0.11	6.86	0.01	0.00	2.73	6.98	0.98	0.00	0.02
70378	SB97-10-19.4 circle 3 albite 4	5.97	0.00	2.69	0.04	0.01	0.05	0.08	7.45	0.03	0.03	2.77	7.56	0.99	0.00	0.01
70378	SB97-10-19.4 circle 5 albite 1	5.93	0.01	2.74	0.00	0.01	0.07	0.14	7.38	0.01	0.00	2.69	7.53	0.98	0.00	0.02
70378	SB97-10-19.4 circle 5 albite 2	6.12	0.00	2.51	0.03	0.00	0.00	0.15	6.75	0.00	0.02	2.69	6.90	0.98	0.00	0.02
70378	SB97-10-19.4 circle 5 albite 3	6.43	0.01	2.03	0.00	0.00	0.12	0.08	5.95	0.00	0.03	2.93	6.03	0.99	0.00	0.01
70393	SB97-19-21.45 circle 1 albite 1	6.18	0.00	2.45	0.01	0.00	0.05	0.11	6.40	0.00	0.02	2.61	6.50	0.98	0.00	0.02
70393	SB97-19-21.45 circle 1 albite 2	7.34	0.00	0.84	0.00	0.00	0.05	0.05	2.53	0.00	0.00	3.00	2.57	0.98	0.00	0.02
70393	SB97-19-21.45 circle 1 albite 3	6.00	0.00	2.65	0.02	0.00	0.08	0.09	7.37	0.02	0.01	2.78	7.49	0.98	0.00	0.01
70393	SB97-19-21.45 circle 1 albite 4	6.02	0.01	2.66	0.04	0.02	0.04	0.02	7.12	0.01	0.02	2.67	7.15	1.00	0.00	0.00
70332	SB97-9-58,65 circle 1 albite 1	6.07	0.00	2.55	0.01	0.00	0.04	0.11	7.25	0.00	0.09	2.85	7.36	0.98	0.00	0.02
70332	SB97-9-58,65 circle 1 albite 2	6.06	0.01	2.63	0.02	0.00	0.00	0.00	7.09	0.04	0.00	2.69	7.13	0.99	0.01	0.00
70332	SB97-9-58,65 circle 1 albite 3	6.06	0.00	2.61	0.03	0.00	0.03	0.00	7.31	0.00	0.02	2.80	7.31	1.00	0.00	0.00
70332	SB97-9-58,65 circle 1 albite 4	5.99	0.00	2.67	0.05	0.00	0.12	0.04	7.35	0.00	0.00	2.76	7.39	0.99	0.00	0.01
70332	SB97-9-58,65 circle 2 albite 1	6.01	0.01	2.62	0.01	0.00	0.05	0.04	7.76	0.01	0.00	2.96	7.81	0.99	0.00	0.01
70332	SB97-9-58,65 circle 2 albite 2	6.08	0.00	2.54	0.03	0.00	0.05	0.01	7.37	0.03	0.02	2.90	7.41	1.00	0.00	0.00
70332	SB97-9-58,65 circle 2 albite 3	6.03	0.00	2.60	0.02	0.03	0.08	0.00	7.48	0.01	0.02	2.88	7.50	1.00	0.00	0.00
70332	SB97-9-58,65 circle 2 albite 4	6.57	0.01	1.85	0.08	0.01	0.03	0.01	5.65	0.02	0.00	3.05	5.67	1.00	0.00	0.00
70332	SB97-9-58,65 circle 5 albite 1	6.02	0.00	2.65	0.00	0.01	0.06	0.00	7.51	0.02	0.02	2.83	7.52	1.00	0.00	0.00
70332	SB97-9-58,65 circle 5 albite 2	6.08	0.01	2.58	0.01	0.00	0.02	0.00	7.18	0.01	0.09	2.78	7.19	1.00	0.00	0.00

JCU #	Sample #	Si	Ti	Al	Fe	Mn	Mg	Ca	Na	K	CL	Na/Al	Ca+Na+K	Albite	Kspar	Anorthite
70332	SB97-9-58.65 circle 1 albite 1	6.03	0.01	2.64	0.00	0.00	0.05	0.02	7.44	0.00	0.01	2.82	7.46	1.00	0.00	0.00
70332	SB97-9-58.65 circle 1 albite 2	6.01	0.00	2.60	0.00	0.04	0.09	0.03	7.73	0.03	0.05	2.97	7.78	0.99	0.00	0.00
70332	SB97-9-58.65 circle 1 albite 3	6.00	0.00	2.66	0.01	0.00	0.02	0.04	7.70	0.02	0.00	2.90	7.76	0.99	0.00	0.00
70332	SB97-9-58.65 circle 1 albite 4	6.04	0.00	2.58	0.00	0.00	0.00	0.00	8.23	0.00	0.00	3.20	8.23	1.00	0.00	0.00
70332	SB97-9-58.65 circle 2 albite 1	6.02	0.00	2.65	0.00	0.01	0.03	0.03	7.51	0.01	0.00	2.83	7.56	0.99	0.00	0.00
70332	SB97-9-58.65 circle 2 albite 2	6.01	0.00	2.64	0.01	0.00	0.07	0.05	7.61	0.03	0.03	2.89	7.69	0.99	0.00	0.01
70332	SB97-9-58.65 circle 2 albite 2	6.01	0.00	2.64	0.01	0.00	0.07	0.05	7.61	0.03	0.03	2.89	7.69	0.99	0.00	0.01
70332	SB97-9-58.65 circle 2 albite 3	6.02	0.00	2.60	0.02	0.03	0.06	0.00	7.81	0.00	0.02	3.00	7.81	1.00	0.00	0.00
70332	SB97-9-58.65 circle 2 albite 4	6.04	0.00	2.61	0.01	0.00	0.05	0.01	7.59	0.00	0.01	2.91	7.60	1.00	0.00	0.00
70332	SB97-9-58.65 circle 5 albite 1	6.02	0.00	2.60	0.02	0.02	0.05	0.00	7.94	0.04	0.00	3.06	7.98	1.00	0.00	0.00
70332	SB97-9-58.65 circle 5 albite 2	6.02	0.00	2.64	0.03	0.00	0.12	0.02	7.22	0.00	0.02	2.73	7.24	1.00	0.00	0.00
70544	JH01-35-2 circle 1 albite 1	6.03	0.02	2.61	0.01	0.00	0.02	0.03	7.49	0.03	0.02	2.87	7.55	0.99	0.00	0.00
70544	JH01-35-2 circle 1 albite 2	6.08	0.00	2.53	0.00	0.00	0.00	0.03	7.71	0.00	0.01	3.05	7.74	1.00	0.00	0.00
70544	JH01-35-2 circle 2 albite 1	6.08	0.00	2.52	0.01	0.00	0.02	0.04	7.67	0.04	0.00	3.04	7.75	0.99	0.00	0.00
Hoover																
70686	HV94-1-695 circle 2 albite 1	6.09	0.00	2.50	0.04	0.00	0.03	0.06	7.57	0.02	0.00	3.02	7.64	0.99	0.00	0.01
70686	HV94-1-695 circle 2 albite 2	6.06	0.01	2.58	0.06	0.00	0.00	0.05	7.18	0.00	0.00	2.78	7.23	0.99	0.00	0.01
70686	HV94-1-695 circle 2 albite 3	6.05	0.00	2.61	0.00	0.00	0.00	0.06	7.44	0.01	0.01	2.85	7.50	0.99	0.00	0.01
70686	HV94-1-695 circle 3 albite 1	6.08	0.00	2.58	0.00	0.00	0.00	0.01	7.40	0.02	0.02	2.87	7.43	1.00	0.00	0.00
70686	HV94-1-695 circle 3 albite 2	6.06	0.01	2.56	0.01	0.01	0.00	0.05	7.64	0.01	0.03	2.99	7.70	0.99	0.00	0.01
70686	HV94-1-695 circle 3 albite 3	6.05	0.01	2.62	0.06	0.00	0.00	0.03	7.17	0.00	0.03	2.74	7.20	1.00	0.00	0.00
70686	HV94-1-695 circle 3 albite 4	6.07	0.01	2.58	0.04	0.00	0.08	0.03	7.03	0.00	0.03	2.73	7.06	1.00	0.00	0.00
70724	JH01-5-7A circle 2 albite 2	6.10	0.01	2.54	0.03	0.00	0.00	0.00	7.33	0.00	0.03	2.89	7.33	1.00	0.00	0.00
70727	JH01-6-1a circle 2 albite 1	5.99	0.00	2.66	0.00	0.00	0.04	0.02	7.92	0.00	0.05	2.98	7.94	1.00	0.00	0.00
70727	JH01-6-1a circle 2 albite 2	6.06	0.00	2.60	0.05	0.00	0.07	0.00	7.14	0.04	0.03	2.74	7.17	0.99	0.01	0.00
70727	JH01-6-1a circle 2 albite 3	6.08	0.00	2.61	0.00	0.01	0.02	0.02	7.00	0.00	0.08	2.68	7.02	1.00	0.00	0.00
70727	JH01-6-1a circle 3 albite 1	6.06	0.00	2.58	0.00	0.00	0.02	0.04	7.44	0.00	0.01	2.88	7.48	0.99	0.00	0.01
70727	JH01-6-1a circle 3 albite 2	6.01	0.00	2.64	0.00	0.02	0.12	0.02	7.30	0.03	0.02	2.77	7.36	0.99	0.00	0.00
70727	JH01-6-1a circle 3 albite 3	6.05	0.01	2.64	0.02	0.00	0.00	0.02	7.05	0.03	0.00	2.67	7.10	0.99	0.00	0.00
70727	JH01-6-1a circle 4 albite 1	6.00	0.00	2.67	0.00	0.02	0.09	0.00	7.58	0.03	0.01	2.84	7.61	1.00	0.00	0.00
70727	JH01-6-1a circle 4 albite 2	6.05	0.01	2.63	0.06	0.01	0.00	0.00	7.05	0.00	0.00	2.68	7.05	1.00	0.00	0.00
70727	JH01-6-1a circle 4 albite 3	6.03	0.00	2.62	0.00	0.03	0.10	0.00	7.32	0.01	0.01	2.80	7.33	1.00	0.00	0.00

JCU #	Sample #	Si	Ti	Al	Fe	Mn	Mg	Ca	Na	K	CL	Na/Al	Ca+Na+K	Albite	Kspar	Anorthite
70728	JH01-6-1b circle 1 albite 1	6.06	0.00	2.60	0.04	0.00	0.00	0.08	7.10	0.04	0.01	2.73	7.22	0.98	0.01	0.01
70728	JH01-6-1b circle 1 albite 2	6.03	0.00	2.65	0.03	0.00	0.01	0.05	7.18	0.02	0.00	2.71	7.25	0.99	0.00	0.01
70728	JH01-6-1b circle 1 albite 3	6.07	0.00	2.59	0.00	0.00	0.04	0.00	7.34	0.01	0.00	2.83	7.35	1.00	0.00	0.00
70728	JH01-6-1b circle 1 albite 3	6.07	0.00	2.59	0.00	0.00	0.04	0.00	7.34	0.01	0.00	2.83	7.35	1.00	0.00	0.00
70728	JH01-6-1b circle 1 albite 4	6.10	0.00	2.53	0.01	0.00	0.05	0.00	7.35	0.01	0.01	2.90	7.36	1.00	0.00	0.00
70728	JH01-6-1b circle 1 albite 5	6.10	0.00	2.56	0.04	0.01	0.00	0.02	7.01	0.02	0.00	2.74	7.05	0.99	0.00	0.00
70728	JH01-6-1b circle 1 albite 6	6.03	0.00	2.62	0.05	0.01	0.02	0.05	7.33	0.04	0.00	2.80	7.42	0.99	0.00	0.01
70728	JH01-6-1b circle 1 albite 7	6.02	0.00	2.66	0.00	0.00	0.04	0.07	7.26	0.01	0.00	2.73	7.34	0.99	0.00	0.01
70729	JH01-6-1c circle 1 albite 1	6.06	0.00	2.61	0.04	0.00	0.04	0.07	6.82	0.03	0.00	2.61	6.92	0.99	0.00	0.01
70729	JH01-6-1c circle 1 albite 2	6.02	0.01	2.60	0.05	0.00	0.10	0.04	7.41	0.00	0.03	2.85	7.45	0.99	0.00	0.01
70729	JH01-6-1c circle 1 albite 3	6.01	0.00	2.62	0.00	0.00	0.06	0.01	7.90	0.00	0.02	3.01	7.91	1.00	0.00	0.00
70729	JH01-6-1c circle 2 albite 1	6.05	0.00	2.62	0.03	0.00	0.03	0.05	7.15	0.00	0.03	2.73	7.20	0.99	0.00	0.01
70729	JH01-6-1c circle 2 albite 2	5.98	0.01	2.70	0.04	0.02	0.03	0.10	6.98	0.02	0.04	2.59	7.10	0.98	0.00	0.01
70729	JH01-6-1c circle 2 albite 2	5.98	0.01	2.70	0.04	0.02	0.03	0.10	6.98	0.02	0.04	2.59	7.10	0.98	0.00	0.01
70729	JH01-6-1c circle 2 albite 3	6.04	0.01	2.63	0.00	0.00	0.04	0.02	7.32	0.03	0.04	2.78	7.36	0.99	0.00	0.00
70729	JH01-6-1c circle 3 albite 1	6.02	0.00	2.64	0.01	0.02	0.00	0.07	7.43	0.00	0.00	2.81	7.50	0.99	0.00	0.01
70729	JH01-6-1c circle 3 albite 2	6.03	0.00	2.66	0.00	0.01	0.00	0.04	7.27	0.01	0.06	2.74	7.33	0.99	0.00	0.01
70729	JH01-6-1c circle 3 albite 3	6.06	0.00	2.60	0.03	0.00	0.03	0.05	7.17	0.00	0.01	2.76	7.22	0.99	0.00	0.01
70729	JH01-6-1c circle 5 albite 1	6.03	0.00	2.63	0.00	0.00	0.04	0.05	7.42	0.01	0.00	2.82	7.48	0.99	0.00	0.01
70729	JH01-6-1c circle 5 albite 2	6.12	0.00	2.58	0.00	0.00	0.00	0.01	6.87	0.00	0.01	2.66	6.88	1.00	0.00	0.00
70729	JH01-6-1c circle 5 albite 3	6.11	0.00	2.60	0.00	0.02	0.00	0.02	6.65	0.00	0.00	2.56	6.68	1.00	0.00	0.00
70734	JH01-6-3c-circle 1 albite 1	6.04	0.00	2.67	0.00	0.00	0.00	0.05	7.00	0.04	0.02	2.62	7.09	0.99	0.01	0.01
70734	JH01-6-3c-circle 1 albite 2	6.02	0.00	2.67	0.00	0.01	0.07	0.05	7.16	0.02	0.01	2.69	7.23	0.99	0.00	0.01
70734	JH01-6-3c-circle 1 albite 3	6.00	0.00	2.72	0.01	0.00	0.01	0.11	6.87	0.04	0.04	2.52	7.01	0.98	0.01	0.02
70737	JH01-6-5B-circle 1 albite 1	6.10	0.00	2.53	0.00	0.00	0.00	0.01	7.55	0.00	0.01	2.98	7.57	1.00	0.00	0.00
70737	JH01-6-5B-circle 1 albite 2	6.02	0.00	2.63	0.06	0.01	0.05	0.01	7.44	0.01	0.03	2.82	7.47	1.00	0.00	0.00
70737	JH01-6-5B-circle 1 albite 3	6.06	0.00	2.64	0.00	0.00	0.08	0.02	6.89	0.00	0.00	2.61	6.92	1.00	0.00	0.00
70748	JH01-7-13 circle 2 albite 1	6.07	0.01	2.65	0.00	0.01	0.02	0.04	6.63	0.00	0.02	2.50	6.67	0.99	0.00	0.01
70748	JH01-7-13 circle 2 albite 2	6.02	0.00	2.63	0.01	0.01	0.05	0.00	7.65	0.02	0.01	2.91	7.67	1.00	0.00	0.00
70748	JH01-7-13 circle 4 albite 1	6.02	0.01	2.64	0.01	0.00	0.08	0.03	7.29	0.00	0.00	2.76	7.33	0.99	0.00	0.00
70748	JH01-7-13 circle 4 albite 2	5.98	0.00	2.72	0.05	0.00	0.09	0.05	6.83	0.08	0.00	2.51	6.96	0.98	0.01	0.01
70748	JH01-7-13 circle 4 albite 3	6.05	0.00	2.64	0.00	0.03	0.06	0.02	7.07	0.00	0.00	2.67	7.08	1.00	0.00	0.00

JCU #	Sample #	Si	Ti	Al	Fe	Mn	Mg	Ca	Na	K	CL	Na/Al	Ca+Na+K	Albite	Kspar	Anorthite
70752	JH01-8-2 circle 1 albite 1	6.02	0.00	2.65	0.00	0.00	0.00	0.03	7.59	0.01	0.01	2.86	7.63	1.00	0.00	0.00
70752	JH01-8-2 circle 1 albite 2	6.03	0.01	2.62	0.00	0.02	0.05	0.03	7.34	0.04	0.00	2.81	7.41	0.99	0.01	0.00
70752	JH01-8-2 circle 1 albite 3	6.09	0.00	2.54	0.02	0.00	0.00	0.04	7.42	0.00	0.03	2.92	7.46	0.99	0.00	0.01
70752	JH01-8-2 circle 1 albite 4	5.98	0.01	2.66	0.01	0.00	0.00	0.00	8.16	0.00	0.00	3.06	8.16	1.00	0.00	0.00
70752	JH01-8-2 circle 1 albite 5	6.04	0.01	2.64	0.02	0.00	0.00	0.00	7.41	0.00	0.02	2.81	7.41	1.00	0.00	0.00
70766	JH01-9-11d circle 1 albite 1	6.23	0.00	2.29	0.01	0.00	0.00	0.04	7.43	0.01	0.02	3.24	7.49	0.99	0.00	0.01
70766	JH01-9-11d circle 1 albite 2	6.25	0.01	2.24	0.05	0.00	0.00	0.01	7.50	0.00	0.00	3.34	7.51	1.00	0.00	0.00
70766	JH01-9-11d circle 2 albite 1	6.14	0.00	2.45	0.02	0.00	0.00	0.00	7.63	0.00	0.01	3.11	7.63	1.00	0.00	0.00
K-FELDSPAR																
Igor																
70922	02JH-8-5 circle 1 Ksp 1	4.51	0.06	5.15	0.15	0.03	0.38	0.01	0.60	2.82	0.04	0.12	3.43	0.18	0.82	0.00
70922	02JH-8-5 circle 1 Ksp 2	4.59	0.05	5.10	0.16	0.01	0.29	0.00	0.36	2.82	0.03	0.07	3.18	0.11	0.89	0.00
70922	02JH-8-5 circle 1 Ksp 3	4.58	0.06	5.07	0.21	0.00	0.34	0.03	0.17	2.84	0.00	0.03	3.04	0.05	0.93	0.01
70922	02JH-8-5 circle 1 Ksp 4	4.60	0.03	5.14	0.15	0.01	0.29	0.01	0.26	2.79	0.03	0.05	3.06	0.09	0.91	0.00
70922	02JH-8-5 circle 1 Ksp 5	4.69	0.02	5.00	0.12	0.00	0.22	0.03	0.32	2.94	0.01	0.06	3.29	0.10	0.89	0.01
70923	JH02-8-6 circle 1 Kspar 2	6.01	0.00	2.55	0.02	0.03	0.04	0.04	0.11	4.15	0.00	0.04	4.30	0.03	0.96	0.01
70923	JH02-8-6 circle 1 Kspar 3	6.03	0.00	2.51	0.00	0.00	0.01	0.05	0.37	4.16	0.00	0.15	4.58	0.08	0.91	0.01
70923	JH02-8-6 circle 1 Kspar 4	6.02	0.02	2.51	0.01	0.00	0.00	0.03	0.53	4.09	0.01	0.21	4.64	0.11	0.88	0.01
Olympic																
71016	02JH-21-5 circle 3 fs 2 clast	5.93	0.02	2.58	0.00	0.01	0.09	0.02	0.43	4.30	0.00	0.17	4.75	0.09	0.91	0.00
71016	02JH-21-5 circle 3 fs1 clast	6.02	0.01	2.48	0.03	0.01	0.09	0.00	0.00	4.28	0.05	0.00	4.28	0.00	1.00	0.00
71019	olympic F1 circle 2 fs 1 clast	5.94	0.02	2.57	0.00	0.00	0.12	0.08	0.28	4.27	0.05	0.11	4.63	0.06	0.92	0.02
71019	olympic F1 circle 2 fs 1 v	5.94	0.04	2.56	0.04	0.01	0.14	0.00	0.15	4.22	0.02	0.06	4.37	0.03	0.97	0.00
71019	olympic F1 circle 2 fs 2 clast	5.97	0.01	2.58	0.01	0.00	0.00	0.06	0.38	4.18	0.03	0.15	4.62	0.08	0.90	0.01
71019	olympic F1 circle 2 fs 2 v	5.99	0.00	2.57	0.01	0.00	0.00	0.01	0.00	4.37	0.05	0.00	4.39	0.00	1.00	0.00
71019	olympic F1 circle 2 fs 3 clast	6.00	0.00	2.58	0.00	0.02	0.05	0.01	0.06	4.14	0.00	0.02	4.21	0.01	0.98	0.00
71019	olympic F1 circle 2 fs 3 v	5.99	0.04	2.54	0.00	0.00	0.02	0.04	0.00	4.27	0.00	0.00	4.31	0.00	0.99	0.01
71019	olympic F1 circle 2 fs 4 v	5.96	0.04	2.57	0.00	0.00	0.00	0.01	0.06	4.36	0.00	0.02	4.44	0.01	0.98	0.00
71023	Olympic F5 circle 2 Ksp 1	5.91	0.00	2.49	0.08	0.06	0.12	0.28	0.31	4.25	0.02	0.12	4.84	0.06	0.88	0.06
Slab																
70233	SB94-1-128.6 circle 1 Kspar 1	5.95	0.02	2.60	0.01	0.00	0.09	0.04	0.55	3.99	0.06	0.21	4.58	0.12	0.87	0.01
70233	SB94-1-128.6 circle 1 Kspar 2	5.98	0.01	2.63	0.01	0.02	0.06	0.00	0.04	3.97	0.00	0.01	4.01	0.01	0.99	0.00

JCU #	Sample #	Si	Ti	Al	Fe	Mn	Mg	Ca	Na	K	CL	Na/Al	Ca+Na+K	Albite	Kspar	Anorthite
70247	SB94-1-190.90 circle 1 Ksp `	2.25	0.01	0.96	0.00	0.00	0.01	0.01	0.11	1.52	0.00	0.11	1.63	0.07	0.93	0.00
70247	SB94-1-190.90 circle 1 Ksp 2	5.97	0.01	2.57	0.02	0.00	0.10	0.05	0.56	3.95	0.02	0.22	4.57	0.12	0.87	0.01
70247	SB94-1-190.90 circle 2 Ksp 1	2.26	0.00	0.95	0.00	0.00	0.00	0.03	0.08	1.54	0.00	0.09	1.65	0.05	0.93	0.02
70247	SB94-1-190.90 circle 2 Ksp 2	2.27	0.00	0.93	0.00	0.00	0.00	0.02	0.18	1.55	0.01	0.19	1.75	0.10	0.89	0.01
70247	SB94-1-190.90 circle 2 Ksp 3	2.25	0.00	0.96	0.01	0.02	0.01	0.03	0.05	1.55	0.00	0.05	1.63	0.03	0.95	0.02
70247	SB94-1-190.90 circle 2 Ksp 4	5.97	0.01	2.59	0.01	0.00	0.05	0.01	0.74	3.93	0.01	0.29	4.69	0.16	0.84	0.00
70255	SB94-1-332.5 circle 2 Ksp 1	5.97	0.01	2.61	0.00	0.00	0.05	0.07	0.31	4.05	0.06	0.12	4.43	0.07	0.92	0.02
70255	SB94-1-332.5 circle 2 Ksp 2	5.92	0.03	2.66	0.01	0.00	0.12	0.03	0.51	3.84	0.01	0.19	4.38	0.12	0.88	0.01
70257	SB94-1-345.1 circle 1 Kspar 1	6.01	0.01	2.55	0.00	0.00	0.00	0.01	0.39	4.07	0.00	0.15	4.47	0.09	0.91	0.00
70257	SB94-1-345.1 circle 1 Kspar 2	6.00	0.01	2.57	0.03	0.00	0.02	0.02	0.20	4.12	0.00	0.08	4.34	0.05	0.95	0.01
70257	SB94-1-345.1 circle 1 Kspar 3	5.98	0.01	2.57	0.00	0.00	0.08	0.07	0.17	4.10	0.01	0.07	4.33	0.04	0.95	0.02
70257	SB94-1-345.1 circle 2 Kspar 1 2nd try	5.99	0.00	2.62	0.00	0.00	0.02	0.00	0.44	4.02	0.05	0.17	4.46	0.10	0.90	0.00
70257	SB94-1-345.1 circle 2 Kspar 2 2nd try	6.00	0.00	2.55	0.00	0.02	0.04	0.05	0.48	4.07	0.01	0.19	4.60	0.10	0.88	0.01
70257	SB94-1-345.1 circle 2 Kspar 3 2nd try	6.00	0.01	2.54	0.02	0.02	0.08	0.04	0.52	3.97	0.02	0.20	4.53	0.11	0.88	0.01
70219	SB94-1-57.43 circle 3 Ksp 1	4.53	0.01	1.90	0.00	0.01	0.02	0.04	0.00	3.00	0.02	0.00	3.05	0.00	0.99	0.01
70219	SB94-1-57.43 circle 3 Ksp 1	6.03	0.02	2.53	0.00	0.02	0.02	0.05	0.00	4.01	0.03	0.00	4.06	0.00	0.99	0.01
70219	SB94-1-57.43 circle 3 Ksp 2	5.91	0.06	2.63	0.00	0.00	0.05	0.06	0.58	3.86	0.03	0.22	4.50	0.13	0.86	0.01
70219	SB94-1-57.43 circle 3 Ksp 3	5.99	0.01	2.57	0.00	0.00	0.06	0.04	0.31	4.04	0.03	0.12	4.40	0.07	0.92	0.01
70221	SB94-1-59.5 circle 2 Kspar 1	6.02	0.00	2.57	0.03	0.02	0.05	0.00	0.05	4.05	0.00	0.02	4.11	0.01	0.99	0.00
70221	SB94-1-59.5 circle 2 Kspar 2	5.99	0.00	2.55	0.01	0.00	0.09	0.06	0.39	4.09	0.03	0.15	4.54	0.09	0.90	0.01
70221	SB94-1-59.5 circle 2 Kspar 3	5.96	0.03	2.61	0.02	0.01	0.03	0.04	0.25	4.00	0.00	0.10	4.29	0.06	0.93	0.01
70286	SB94-4-69.6 circle 1 Kspar 1	5.94	0.02	2.64	0.00	0.00	0.09	0.02	0.31	3.99	0.03	0.12	4.32	0.07	0.92	0.00
70286	SB94-4-69.6 circle 1 Kspar 2	5.97	0.00	2.59	0.00	0.00	0.12	0.03	0.52	4.03	0.13	0.20	4.58	0.11	0.88	0.01
70286	SB94-4-69.6 circle 1 Kspar 3	5.97	0.01	2.61	0.00	0.00	0.08	0.01	0.31	4.05	0.01	0.12	4.37	0.07	0.93	0.00
70286	SB94-4-69.6 circle 2 Kspar 1	5.98	0.01	2.57	0.00	0.04	0.12	0.07	0.38	3.89	0.03	0.15	4.34	0.09	0.90	0.02
70286	SB94-4-69.6 circle 2 Kspar 2	5.99	0.01	2.56	0.00	0.00	0.10	0.07	0.15	4.06	0.06	0.06	4.28	0.04	0.95	0.02
70286	SB94-4-69.6 circle 2 Kspar 3	6.02	0.01	2.61	0.00	0.00	0.04	0.00	0.03	3.94	0.02	0.01	3.97	0.01	0.99	0.00
70286	SB94-4-79.6 circle 4 Ksp 3	4.66	0.06	4.70	0.46	0.01	0.63	0.03	0.06	2.84	0.01	0.01	2.93	0.02	0.97	0.01
70309	SB95-5-8.7 circle 1 Kspar 2	5.95	0.00	2.66	0.04	0.00	0.10	0.01	0.21	4.06	0.00	0.08	4.29	0.05	0.95	0.00
70378	SB97-10-19.4 circle 1 Ksp 1	4.65	0.01	4.74	0.76	0.03	0.41	0.03	0.12	2.89	0.03	0.02	3.04	0.04	0.95	0.01
70378	SB97-10-19.4 circle 1 Ksp 2	4.68	0.02	4.38	0.83	0.02	0.65	0.46	0.22	2.68	0.03	0.05	3.36	0.07	0.80	0.14
70378	SB97-10-19.4 circle 2 Ksp 1	4.67	0.01	4.58	0.88	0.00	0.60	0.04	0.28	2.79	0.00	0.06	3.11	0.09	0.90	0.01

JCU #	Sample #	Si	Ti	Al	Fe	Mn	Mg	Ca	Na	K	CL	Na/Al	Ca+Na+K	Albite	Kspar	Anorthite
70378	SB97-10-19.4 circle 2 Ksp 2	4.64	0.02	4.71	0.82	0.01	0.46	0.09	0.00	2.81	0.00	0.00	2.91	0.00	0.97	0.03
70378	SB97-10-19.4 circle 2 Ksp 3	4.64	0.00	4.84	0.75	0.01	0.26	0.01	0.37	2.86	0.00	0.08	3.24	0.11	0.88	0.00
70544	JH01-35-2 circle 2 Kspar 1	6.01	0.01	2.53	0.03	0.00	0.02	0.05	0.22	4.17	0.02	0.09	4.43	0.05	0.94	0.01
Slats-Frosty																
70772	STF95-1-16.70m circle 1 fs 1 m	6.01	0.00	2.55	0.00	0.04	0.00	0.00	0.10	4.29	0.01	0.04	4.39	0.02	0.98	0.00
70772	STF95-1-16.70m circle 1 fs 2 m	6.02	0.01	2.51	0.00	0.01	0.00	0.02	0.26	4.30	0.02	0.10	4.58	0.06	0.94	0.00
70772	STF95-1-16.70m circle 1 fs 3 m	5.99	0.01	2.53	0.00	0.01	0.03	0.06	0.22	4.27	0.03	0.09	4.55	0.05	0.94	0.01
70772	STF95-1-16.70m circle 3 fs 1 bx matrix	6.01	0.01	2.51	0.05	0.00	0.07	0.02	0.00	4.27	0.02	0.00	4.30	0.00	0.99	0.01
Hoover																
70729	JH01-6-1c circle 2 Kspar 1	4.77	0.00	4.41	0.49	0.00	1.03	0.05	0.22	2.75	0.01	0.05	3.02	0.07	0.91	0.02
70729	JH01-6-1c circle 2 Kspar 2	4.78	0.02	4.40	0.37	0.00	1.01	0.03	0.35	2.78	0.04	0.08	3.16	0.11	0.88	0.01
70743	JH01-7-6a-circle 3 Kspar 1	6.94	0.01	1.57	0.01	0.00	0.12	0.04	0.11	0.93	0.00	0.07	1.08	0.10	0.86	0.04

JCU #	Sample #	FeO	MnO	MgO	CaO	TOTAL
CARBONATE						
Igor						
70923	02JH-08-06 circle 1 carb 1	2.46	0.00	19.30	30.60	52.37
70923	02JH-08-06 circle 1 carb 2	2.60	0.08	19.63	30.30	52.61
70923	02JH-08-06 circle 1 carb 2	2.60	0.08	19.63	30.30	52.61
70923	02JH-08-06 circle 1 carb 3	2.57	0.36	18.53	30.11	51.57
70923	02JH-08-06 circle 2 carb 1	6.03	0.50	17.17	29.67	53.37
70923	02JH-08-06 circle 2 carb 2	6.84	0.27	17.60	29.61	54.31
70923	02JH-08-06 circle 2 carb 3	2.24	0.67	19.07	29.67	51.66
70923	02JH-08-06 circle 2 carb 4	12.31	1.91	5.41	35.11	54.74
70923	02JH-08-06 circle 4 fe calcite 1	9.95	0.02	1.27	44.75	56.02
70942	02JH-10-17B circle 1 carb 1 x	55.92	3.28	3.08	0.30	62.58
70942	02JH-10-17B circle1 carb 1 x	55.93	3.30	3.08	0.27	62.57
70942	02JH-10-17B circle 1 carb 2 x	56.39	2.42	4.55	0.14	63.50
70942	02JH-10-17B circle 1 carb 3 x	55.84	3.82	3.84	0.19	63.70
70942	02JH-10-17B circle 1 carb 1 m	48.77	4.55	4.60	3.85	61.76
70942	02JH-10-17B circle 1 carb 2 m	56.35	2.50	3.31	0.97	63.13
70942	02JH-10-17B circle 1 carb 3 m	58.40	2.65	1.97	0.88	63.91
70942	02JH-10-17B circle 1 carb 4 m	56.70	2.66	3.06	0.37	62.79
70942	02JH-10-17B circle 3 carb 2 v	14.88	2.52	11.10	28.59	57.08
70942	02JH-10-17B circle 3 carb 3v	14.19	2.07	11.62	28.51	56.39
70914	I80-14-500 circle 1 carb xtl 1	45.01	5.55	9.50	0.42	60.48
70914	I80-14-500 circle 1 carb xtl 2	44.35	5.53	9.45	0.64	59.98
70914	I80-14-500 circle 1 carb xtl 3	56.21	3.30	2.62	0.36	62.49
70914	I80-14-500 circle 1 carb xtl 4	54.38	3.34	3.22	0.25	61.18
70914	I80-14-500 circle 1 carb xtl 5	14.58	2.71	10.44	28.57	56.29
70914	I80-14-500 circle 2 carb v 1	42.22	3.67	11.97	0.58	58.44
70914	I80-14-500 circle 2 carb v 2	50.23	3.92	6.08	0.30	60.53
70914	I80-14-500 circle 2 carb v 3	10.69	1.11	13.46	28.41	53.67
70893	I80-10-228 circle 2 carb 1	55.64	2.89	2.77	0.09	61.38
70893	I80-10-228 circle 2 carb 2	48.57	5.72	5.92	0.40	60.60
70893	I80-10-228 circle 2 carb 3	48.84	6.43	5.90	0.26	61.43
70864	I80-10-43'10" circle 1 carbx 1	6.49	2.73	15.49	29.72	54.43
70864	I80-10-43'10" circle 1 carbx 2	6.91	3.32	15.03	28.79	54.05
70864	I80-10-43'10" circle 1 carbx 3	5.91	2.21	16.29	29.26	53.68
70864	I80-10-43'10" circle 1 carbx 4	16.52	2.62	9.46	28.23	56.83
70864	I80-10-43'10" circle 1 carbgm 1	6.32	2.68	15.90	29.21	54.10
70864	I80-10-43'10" circle 1 carbgm 2	19.84	2.04	7.83	27.21	56.93
70864	I80-10-43'10" circle 2 carbv 1	6.87	4.58	13.13	29.33	53.91
70864	I80-10-43'10" circle 2 carbv 2	6.06	2.46	14.96	29.60	53.09
70864	I80-10-43'10" circle 2 carbv 3	10.50	2.58	13.32	28.48	54.87
70864	I80-10-43'10" circle 2 carbv 4	6.29	3.97	14.76	29.24	54.27
Olympic						
71016	02JH-21-5 circle 1 carb 1	0.32	0.17	1.48	58.68	60.66
71016	02JH-21-5 circle 2 carb 1	10.02	2.91	13.18	28.62	54.74
71016	02JH-21-5 circle 2 carb 2	10.15	2.99	12.60	29.29	55.02
71016	02JH-21-5 circle 2 carb 3	7.72	2.50	11.48	33.59	55.29
71016	02JH-21-5 circle 3 carb 1 x	6.90	3.25	14.97	30.01	55.13
71016	02JH-21-5 circle 3 carb 2 x	7.74	3.83	14.56	30.20	56.32
71016	02JH-21-5 circle 3 carb 3 x	6.43	3.52	15.45	29.62	55.01
71016	02JH-21-5 circle 4 carb 1 x	4.57	2.20	17.51	30.57	54.85
71016	02JH-21-5 circle 4 carb 2 x	9.76	2.12	13.95	30.19	56.03

JCU #	Sample #	FeO	MnO	MgO	CaO	TOTAL
71016	02JH-21-5 circle 4 carb 3 x	6.11	1.70	17.47	30.35	55.64
71019	Olympic F1 circle 1 carb 1 m	2.23	1.14	19.83	31.11	54.31
71019	Olympic F1 circle 1 carb 2 m	1.99	0.87	19.63	32.21	54.70
71019	Olympic F1 circle 1 carb 3 m	2.91	1.58	19.58	31.64	55.72
71019	Olympic F1 circle 2 carb 1 m	2.81	1.26	19.57	31.88	55.51
71019	Olympic F1 circle 2 carb 2 m	3.02	1.47	18.96	31.76	55.20
71019	Olympic F1 circle 2 carb 1v m	7.15	3.02	12.31	27.37	49.85
71019	Olympic F1 circle 2 carb 2v	7.15	3.02	12.31	27.37	49.85
71019	Olympic F1 circle 3 carb 1 v	8.63	3.46	13.75	30.28	56.12
71019	Olympic F1 circle 3 carb 2 v	8.18	3.50	13.49	29.43	54.60
71019	Olympic F1 circle 3 carb 3 v	7.54	3.37	13.80	29.61	54.31
71019	Olympic F1 circle 3 carb 1 m	2.30	1.34	19.05	29.61	52.29
71019	Olympic F1 circle 3 carb 2 m	2.47	1.49	19.10	30.25	53.30
71019	Olympic F1 circle 3 carb 3 m	2.38	1.55	18.13	29.86	51.92
71023	Olympic F5 circle 1 carb 1	5.10	1.01	17.66	29.78	53.54
71023	Olympic F5 circle 1 carb 2	5.28	1.24	18.16	29.77	54.46
71023	Olympic F5 circle 1 carb 3	3.93	1.37	18.12	31.16	54.58
71023	Olympic F5 circle 2 carb 1	5.47	0.88	16.21	29.36	51.91
71023	Olympic F5 circle 2 carb 2	5.13	0.93	17.30	29.42	52.78
71023	Olympic F5 circle 2 carb 3	4.98	1.65	15.93	28.76	51.32
71023	Olympic F5 circle 2 carb 5	6.50	5.94	12.03	29.06	53.52
71023	Olympic F5 circle 2 carb 6	4.45	0.81	17.55	29.63	52.45
Slats-Frosty						
70772	STF95-1-16.70m circle 2 carb 1 v	6.02	1.87	17.32	29.50	54.70
70772	STF95-1-16.70m circle 2 carb 2 v	6.49	1.39	16.78	29.47	54.14
70772	STF95-1-16.70m circle 2 carb 3 v	4.24	2.39	17.39	29.28	53.30
70772	STF95-1-16.70m circle 2 carb 1 clast	9.76	1.78	14.38	28.71	54.63
70772	STF95-1-16.70m circle 2 carb 2 clast	9.23	1.82	14.79	28.62	54.46
70772	STF95-1-16.70m circle 2 carb 3 clast	6.59	1.01	10.23	21.90	39.73
Slab						
70445	01JH-20-3 circle 2 carb 1	0.23	1.20	0.06	60.11	61.61
70445	01JH-20-3 circle 2 carb 2	0.10	1.17	0.14	59.61	61.01
70445	01JH-20-3 circle 2 carb 3	0.27	1.05	0.06	59.92	61.30
70456	01JH-20-10C circle 1 carb XTL 1	4.32	1.15	16.43	30.04	51.93
70456	01JH-20-10C circle 1 carb XTL 2	4.60	1.14	16.61	29.68	52.03
70456	01JH-20-10C circle 1 carb XTL 3	5.04	0.66	16.99	29.63	52.32
70456	01JH-20-10C circle 1 carb GM 1	0.69	1.03	0.46	58.30	60.48
70456	01JH-20-10C circle 1 carb GM 2	2.61	1.08	4.96	48.63	57.29
70456	01JH-20-10C circle 1 carb GM 3	0.63	0.78	0.07	59.56	61.05
70456	01JH-20-10C circle 1 carb GM 4	0.47	1.24	0.41	59.53	61.66
70207	SB94-1 -1.3 circle 1 1st carb 1	0.00	0.71	0.00	59.77	60.48
70207	SB94-1 -1.3 circle 1 1st carb 2	0.02	0.63	0.00	57.46	58.10
70207	SB94-1 -1.3 circle 1 1st carb 3	0.00	0.69	0.15	56.69	57.55
70207	SB94-1 -1.3 circle 1 1st carb 4	0.00	0.51	0.00	56.44	56.94
70207	SB94-1 -1.3 circle 1 1st carb 5	0.00	0.52	0.00	57.21	57.72
70207	SB94-1-1.3 circle 2 carb 1	0.20	0.32	0.10	55.60	56.22
70207	SB94-1-1.3 circle 2 carb 2	0.02	0.55	0.06	56.75	57.38
70207	SB94-1-1.3 circle 2 carb 3	0.00	0.76	0.04	55.37	56.17
70207	SB94-1-1.3 circle 3 carb 1	0.00	0.64	0.14	56.78	57.56
70207	SB94-1-1.3 circle 3 carb 2	0.00	0.53	0.00	55.16	55.68
70207	SB94-1-1.3 circle 3 carb 3	0.31	0.66	0.00	56.15	57.13
70219	SB94-1-57.43 circle 3 carb 1	0.00	1.38	0.00	54.98	56.37
70219	SB94-1-57.43 circle 3 carb 2	0.01	1.01	0.01	55.56	56.58

JCU #	Sample #	FeO	MnO	MgO	CaO	TOTAL
70219	SB94-1-57.43 circle 3 carb 3	0.15	0.71	0.01	54.35	55.22
70219	SB94-1-57.43 circle 4 carb 1	0.05	0.72	0.08	54.44	55.29
70219	SB94-1-57.43 circle 4 carb 2	0.16	0.64	0.00	54.87	55.66
70219	SB94-1-57.43 circle 4 carb 3	0.24	0.34	0.29	57.19	58.05
70233	SB94-1-128.6 circle 1 carb 1	0.40	0.58	0.20	55.00	56.18
70233	SB94-1-128.6 circle 1 carb 2	0.16	0.47	0.05	54.26	54.93
70233	SB94-1-128.6 circle 1 carb 3	0.00	0.00	0.00	52.93	52.93
70247	SB94-1-190.90 circle 2 carb 1	0.02	0.00	0.03	52.86	52.92
70247	SB94-1-190.90 circle 5 carb 1	0.07	0.48	0.36	53.62	54.54
70247	SB94-1-190.90 circle 5 carb 2	0.00	0.54	0.00	57.75	58.29
70247	SB94-1-190.90 circle 5 carb 3	0.00	0.69	0.27	55.97	56.92
70255	SB94-1-332.5 circle 1 vein carb 1	0.18	0.61	0.46	55.34	56.59
70255	SB94-1-332.5 circle 1 vein carb 2	0.19	0.68	0.01	55.32	56.21
70255	SB94-1-332.5 circle 1 vein carb 3	0.14	0.64	0.50	57.08	58.37
70255	SB94-1-332.5 circle 1 vein carb 4	0.00	0.53	0.00	56.20	56.73
70255	SB94-1-332.5 circle 2 carb 1	0.23	0.17	0.96	51.48	52.83
70255	SB94-1-332.5 circle 2 carb 2	0.45	0.30	0.32	51.93	53.00
70255	SB94-1-332.5 circle 2 carb 3	0.44	1.32	0.82	54.95	57.53
70287	SB94-4-79.6 circle 4 carb 1	0.22	1.37	0.21	54.62	56.41
70287	SB94-4-79.6 circle 4 carb 2	0.18	1.11	0.37	54.55	56.21
70287	SB94-4-79.6 circle 4 carb 3	0.28	0.79	0.00	55.86	56.94
70287	SB94-4-79.6 circle 5 carb 1	0.00	0.67	0.13	56.15	56.96
70287	SB94-4-79.6 circle 5 carb 2	0.33	1.04	0.29	56.37	58.04
70287	SB94-4-79.6 circle 5 carb 3	0.00	1.01	0.29	56.34	57.63
70286	SB94-4-69.6 circle 2 carb 1	0.18	0.00	0.00	53.11	53.29
70286	SB94-4-69.6 circle 2 carb 2	0.00	0.09	0.00	52.42	52.51
70286	SB94-4-69.6 circle 2 carb 3	0.04	0.01	0.49	52.20	52.75
70309	SB95-5-8.7 circle 1carb 1	0.31	0.57	0.42	56.04	57.35
70309	SB95-5-8.7 circle 1carb 2	0.10	0.27	0.00	57.30	57.67
70309	SB95-5-8.7 circle 1carb 3	0.00	0.43	0.28	57.38	58.10
70332	SB97-9-58,65 circle 3 carb 1	0.71	0.78	0.46	52.15	54.10
70332	SB97-9-58,65 circle 1 carb 1	0.48	0.39	0.19	50.99	52.06
70332	SB97-9-58,65 circle 3 carb 1	0.44	0.52	0.37	50.70	52.03
70332	SB97-9-58,65 circle 3 carb 2	0.75	0.83	0.52	51.02	53.12
70332	SB97-9-58,65 circle 3 carb 3	0.45	0.69	0.14	50.65	51.93
70332	SB97-9-58,65 circle 2 carb 1	0.13	0.00	0.18	52.78	53.10
70332	SB97-9-58,65 circle 2 carb 2	0.39	0.43	0.13	51.90	52.85
70332	SB97-9-58,65 circle 2 carb 3	0.66	0.67	0.21	52.50	54.05
70332	SB97-9-58,65 circle 5 carb 1	0.96	0.19	0.21	51.82	53.17
70332	SB97-9-58,65 circle 5 carb 2	0.36	0.16	0.16	52.72	53.41
70378	SB97-10-19.4 circle 1 carb 1	1.17	0.92	0.32	48.61	51.03
70378	SB97-10-19.4 circle 2 carb 1	1.06	0.49	0.11	48.65	50.30
70378	SB97-10-19.4 circle 2 carb 2	0.92	1.00	0.00	48.60	50.53
70378	SB97-10-19.4 circle 4 carb 2	10.92	0.97	12.09	26.85	50.83
70378	SB97-10-19.4 circle 4 carb 3	11.79	1.74	10.78	27.13	51.46
70378	SB97-10-19.4 circle 4 carb 4	14.88	2.52	9.11	26.69	53.20
70378	SB97-10-19.4 circle 4 carb 5	11.52	1.40	11.65	26.43	51.01
70378	SB97-10-19.4 circle 4 carb 6	12.59	1.19	12.22	27.44	53.45
70378	SB97-10-19.4 circle 4 carb 7	12.09	1.06	11.64	27.80	52.59
70393	SB97-19-21.45 circle 2 vein carb 1	0.22	0.92	0.26	49.34	50.74
70393	SB97-19-21.45 circle 2 vein carb 2	0.01	0.45	0.22	50.77	51.45
70393	SB97-19-21.45 circle 2 vein carb 3	0.30	0.90	0.20	48.81	50.22
70393	SB97-19-21.45 circle 4 carb 1	0.51	0.64	0.63	50.34	52.12

JCU #	Sample #	FeO	MnO	MgO	CaO	TOTAL
70393	SB97-19-21.45 circle 4 carb 2	0.94	0.18	0.26	52.12	53.50
70393	SB97-19-21.45 circle 5 carb 1	0.66	0.90	0.32	50.35	52.23
70393	SB97-19-21.45 circle 5 carb 2	0.76	1.42	0.19	49.74	52.09
70393	SB97-19-21.45 circle 5 carb 3	0.92	0.92	1.68	47.32	50.84
Hoover						
70724	01JH-5-7A circle 2 carb 1	4.31	0.60	18.43	30.09	53.43
70724	01JH-5-7A circle 2 carb 2	8.39	1.07	15.38	29.36	54.20
70724	01JH-5-7A circle 3 carb 1	0.58	0.00	0.42	57.61	58.62
70724	01JH-5-7A circle 3 carb 2	0.36	0.33	0.30	58.97	59.96
70724	01JH-5-7A circle 3 carb 3	9.48	0.76	14.74	29.22	54.21
70724	01JH-5-7A circle 3 carb 4	9.58	1.01	14.52	29.30	54.41
70724	01JH-5-7A circle 3 carb 5	11.38	1.60	11.70	29.05	53.73
70727	01JH-6-1A circle 2 carb 1	0.06	1.39	0.43	54.17	56.07
70727	01JH-6-1A circle 2 carb 2	0.32	0.85	0.00	54.02	55.19
70727	01JH-6-1A circle 2 carb 3	0.29	0.91	0.07	54.66	55.92
70727	01JH-6-1A circle 2 carb 4	0.30	0.92	0.10	56.72	58.03
70727	01JH-6-1A circle 3 carb 1	0.29	1.46	0.40	57.04	59.19
70727	01JH-6-1A circle 3 carb 2	0.46	1.06	0.34	58.06	59.92
70727	01JH-6-1A circle 3 carb 3	0.50	1.42	0.02	56.00	57.94
70727	01JH-6-1A circle 3 carb 4	0.58	1.35	0.25	56.86	59.04
70727	01JH-6-1A circle 3 carb 5	0.16	0.72	0.20	56.56	57.66
70727	01JH-6-1A circle 3 carb 6	0.53	1.04	0.29	55.19	57.05
70727	01JH-6-1A circle 4 carb 1	0.45	2.05	0.39	50.82	53.72
70727	01JH-6-1A circle 4 carb 2	0.60	0.60	0.19	53.06	54.45
70727	01JH-6-1A circle 4 carb 3	0.78	1.78	0.11	53.32	55.99
70728	01JH-6-1B circle 1 carb 1	0.20	0.30	0.06	55.49	56.06
70728	01JH-6-1B circle 1 carb 2	0.30	0.54	0.50	55.24	56.58
70728	01JH-6-1B circle 1 carb 3	0.26	0.86	0.27	55.12	56.51
70729	01JH-6-1C circle 1 carb 1	0.92	1.21	0.34	53.92	56.40
70729	01JH-6-1C circle 1 carb 2	0.43	1.29	0.16	55.01	56.89
70729	01JH-6-1C circle 1 carb 3	6.04	0.70	15.54	28.27	50.55
70729	01JH-6-1C circle 1 carb 4	0.63	0.96	0.54	53.79	55.91
70729	01JH-6-1C circle 2 carb 1	0.33	2.12	0.35	54.29	57.10
70729	01JH-6-1C circle 2 carb 2	0.44	1.05	0.41	54.36	56.25
70729	01JH-6-1C circle 2 carb 3	0.04	0.00	0.00	52.89	52.93
70734	01JH-6-3C-circle 1 carb 1	0.01	0.35	0.00	53.63	54.00
70734	01JH-6-3C-circle 1 carb 2	0.79	0.34	0.24	50.51	51.88
70734	01JH-6-3C-circle 1 carb 3	0.01	0.69	0.00	53.25	53.96
70734	01JH-6-3C-circle 1 carb 4	0.09	0.68	0.00	53.21	53.98
70734	01JH-6-3C-circle 1 carb 5	0.08	0.51	0.24	52.50	53.34
70734	01JH-6-3C-circle 1 carb 6	0.50	0.61	0.09	53.06	54.27
70737	01JH-6-5B-circle 2 carb 1	0.77	0.27	0.53	56.65	58.23
70737	01JH-6-5B-circle 2 carb 2	0.51	0.35	0.68	55.01	56.55
70737	01JH-6-5B-circle 2 carb 3	0.44	0.35	0.14	55.79	56.70
70737	01JH-6-5B-circle 2 carb 3	0.00	0.36	0.30	51.54	52.20
70743	01JH-7-6A-circle 3 carb band 1	0.17	0.26	0.17	53.87	54.47
70743	01JH-7-6A-circle 3 carb band 2	0.00	0.00	0.55	54.35	54.90
70743	01JH-7-6A-circle 3 carb granular 1	0.00	0.05	0.20	55.37	55.62
70743	01JH-7-6A-circle 3 carb granular 2	0.05	0.00	0.00	56.04	56.09
70743	01JH-7-6A-circle 3 carb granular 3	0.41	0.03	0.14	55.54	56.13
70766	01JH-9-11D circle 1 carb 1	1.13	0.53	0.49	55.14	57.29
70766	01JH-9-11D circle 2 carb 2	0.99	0.20	0.13	56.85	58.18
70766	01JH-9-11D circle 2 carb 3	3.81	0.49	17.67	28.80	50.78

JCU #	Sample #	FeO	MnO	MgO	CaO	TOTAL
70766	01JH-9-11D circle 2 carb 4	4.48	0.09	17.39	29.22	51.18
70766	01JH-9-11D circle 2 carb 5	1.27	0.30	0.60	57.31	59.49
70686	HV94-1-695 circle 1 carb 1	0.57	0.95	0.71	59.20	61.43
70686	HV94-1-695 circle 1 carb 2	0.69	0.83	0.40	58.74	60.66
70686	HV94-1-695 circle 1 carb 3	0.52	1.04	0.63	56.77	58.96
70686	HV94-1-695 circle 1 carb 4	0.50	0.52	0.36	56.94	58.33
70686	HV94-1-695 circle 1 carb 5	0.42	0.56	0.29	58.36	59.63
70686	HV94-1-695 circle 1 carb 6	0.55	0.68	0.16	57.29	58.68
70686	HV94-1-695 circle 3 carb 1	0.67	1.24	0.39	61.10	63.40
70686	HV94-1-695 circle 3 carb 2	0.21	0.97	0.11	58.84	60.14
70686	HV94-1-695 circle 3 carb 3	0.04	1.11	0.24	60.16	61.55

APPENDIX II

Analytical protocols for Ar/Ar, U-Pb, Pb-Pb and Re-Os analyses

Analytical protocols for $^{40}Ar/^{39}Ar$ analyses (M. Villeneuve, written communication, 2004)

Selected samples were processed for $^{40}Ar/^{39}Ar$ analysis by standard mineral separation techniques, including hand-picking of clear, unaltered crystals in the size range 0.5 to 1 mm. Individual mineral separates were loaded into aluminum foil packets along with a single grain of Fish Canyon Tuff Sanidine (FCT-SAN) to act as flux monitor (apparent age = 28.03 ± 0.28 Ma; Renne et al., 1998). The sample packets were arranged radially inside an aluminum can. The samples were then irradiated for 12 hours at the research reactor of McMaster University in a fast neutron flux of approximately $3x10^{16}$ neutrons/cm^2 . Laser $^{40}Ar/^{39}Ar$ step-heating analysis was carried out at the Geological Survey of Canada laboratories in Ottawa, Ontario. Upon return from the reactor, samples were split into several aliquots and loaded into individual 1.5 mm-diameter holes in a copper planchet. The planchet was then placed in the extraction line and the system evacuated. Heating of individual sample aliquots in steps of increasing temperature was achieved using a Merchantek MIR10 10W CO_2 laser equipped with a 2 mm x 2 mm flat-field lens. The released Ar gas was cleaned over getters for ten minutes, and then analyzed isotopically using the secondary electron multiplier system of a VG3600 gas source mass spectrometer; details of data collection protocols can be found in Villeneuve and MacIntyre (1997) and Villeneuve *et al*. (2000). Error analysis on individual steps follows numerical error analysis routines outlined in Scaillet (2000); error analysis on grouped data follows algebraic methods of Roddick (1988). In gas release diagrams, analyses are displayed whereby the fraction of ^{39}Ar released relative to the sum total of ^{39}Ar released forms the x-axis. Thus, the apparent $^{40}Ar/^{39}Ar$ age of each heating step is plotted against the cumulative amount of ^{39}Ar released from the sample, normalized to 100% for the total ^{39}Ar released. Upon ascertaining reproducibility of individual steps in the plateau regions, data was combined by integrating plateau portions (marked by line above steps) weighted by analytical error. Alternatively, data may be presented on inverse isochron diagrams which essentially provide a graphical display of mixtures of pure atmospheric ($^{36}Ar/^{40}Ar$, marked by the y-intercept) and pure radiogenic Ar ($^{40}Ar/^{39}Ar$ marked by the x-intercept). In this case, relationship between temperature of heating and apparent age are lost, but the most radiogenic steps are considered to give the best estimate of the age.

Neutron flux gradients throughout the sample canister were evaluated by analyzing the sanidine flux monitors included with each sample packet and interpolating a linear fit against calculated J-factor and.sample position. The error on individual J-factor values is conservatively estimated at ±0.6% (2s). Because the error associated with the J-factor is systematic and not related to individual analyses, correction for this uncertainty is not applied until calculation of dates from isotopic correlation diagrams (Roddick, 1988). No evidence for excess ^{40}Ar was observed in any of the samples and, therefore, all regressions are assumed to pass through the $^{36}Ar/^{40}Ar$ value for atmospheric air (295.5). All errors are quoted at the 2σ level of uncertainty."

References

Renne P. R., Swisher C. C., Deino A. L., Karner D. B., Owens T. L., and DePaolo D. J., 1998. Intercalibration of standards, absolute ages and uncertainties in $^{40}Ar/^{39}Ar$ dating. ChemicalGeology 145:117-152.

Roddick, J.C., 1988. The assessment of errors in $^{40}Ar/^{39}Ar$ dating. In: Radiogenic Age and Isotopic Studies, Report 2. Geological Survey of Canada, Paper 88-2, pp. 7–16.

Scaillet, S., 2000. Numerical error analysis in $^{40}Ar/^{39}Ar$ dating, Chemical Geology 62: 269–298.

Villeneuve, M.E. and MacIntyre, D.G, 1997. Laser $^{40}Ar/^{39}Ar$ ages of the Babine porphyries and Newman Volcanics, Fulton Lake map area, west-central British Columbia. In: Radiogenic Age and Isotopic Studies, Report 10. Geological Survey of Canada, Current Research 1997-F, pp.131–139.

Villeneuve, M.E., Sandeman, H.A. and Davis, W.J., 2000. A method for the intercalibration of U-Th-Pb and $^{40}Ar/^{39}Ar$ ages in the Phanerozoic. Geochimica et Cosmochimica Acta 64:4017-4030.

U-Pb analytical techniques (from Friedman *et al.*, 2001)

Titanite was separated using conventional crushing, grinding and Wilfley table techniques, followed by final concentration using heavy liquids and magnetic separations. Mineral fractions were selected for analysis based on grain morphology, quality, size and magnetic susceptibility. All geochemical separations were done in the Geochronology Laboratory at The University of British Columbia following the methods outlined in Mortensen *et al.* (1995).

Titanite samples were dissolved in concentrated HF and HNO_3 in the presence of a mixed $^{233-235}U$ – ^{205}Pb isotopic tracer. Titanite fractions were dissolved in Savillex PFA beakers on a hot plate at 80 ^{o}C. HF was evaporated and fluorides were dissolved in 6.2 N HCl on a hot plate for 24 hours. This solution was evaporated to dryness, and chlorides were dissolved on the hot plate for 24 hours. Separation and purification of Pb and U from titanite fractions employed modified ion exchange column techniques (see Friedman *et al.*, 2001). Pb and U were eluted separately and loaded together on a single Re filament using a phosphoric acid – silica gel emitter. Isotopic ratios were measured using a modified single collector VG-54R thermal ionization mass spectrometer equipped with a Daly photomultiplier. U and Pb analytical blanks were in the range of 1 pg and 1-5 pg, respectively during the course of the study. U fractionation was determined directly on individual runs using the $^{233-235}U$ tracer. Pb isotopic rations were corrected for a fractionation of 0.12 %/amu and 0.35 %/amu for Faraday and Daly runs, respectively, based on replicate analyses of the NBS-981 Pb standard and the values recommended by Todt *et al.*, (1984). All analytical errors were propagated through the entire age calculation using the technique of Roddick (1987). Errors for Pb/Pb ages are quoted at the 2σ level.

References

Friedman, R.M., Diakow, L.J., Lane, R.A. and Mortensen, J.K., 2001. New U-Pb age constraints on latest Cretaceous magmatism and associated mineralization in the Fawnie Range, Nechako Plateau, central British Columbia. Canadian Journal of Earth Science 38:619-637.

Mortensen, J.K., Gosh, D. and Ferri, F., 1995. U-Pb age constraints of intrusive rocks associated with copper-gold porphyry deposits in the Canadian Cordillera. In: Schroeter, T.G. (ed.) Porphyry deposits of the northwestern Cordillera of North America. Canadian Institute of Mining and Metallurgy, Special volume 46:142-158.

Roddick, J.C., 1987. Generalized numerical error analysis with application to geochronology and thermodynamics. Geochimica et Cosmochimica Acta 51: 2129-2135.

Todt, W., Cliff, R., Hanser, A. and Hofman, A.W.,1984. 202Pb + 205Pb double spike for lead isotopic analyses. Terra Cognita 4:209.

Pb-Pb analytical techniques (from Woodhead and Hergt, 1997)

Carbonate samples were first crushed to coarse sand-sized fragments using a steel press and then washed repeatedly in ultrapure water to remove adhered rock powder. After drying, fresh fragments, free from any obvious signs of alteration and veining, were hand-picked under a stereo dynascope. Approximately 300 mg of this material were weighed into an acid-cleaned polymethylpentate (PMP) beaker. Beakers were discarded after a single use.

Samples were first washed in ultrapure water with ultrasonic agitation for 30 minutes. After repeated rinsing, 2 ml of ultrapure water was added to each sample and 6 N HCl added dropwise to maintain a slow but steady effervescence (dolomite samples were gently warmed if necessary to promote this reaction). After complete reaction (no more effervescence when HCl was added) the samples were centrifuged and the supernatant dried down in a 6 ml Teflon vessel. Residues were weighed in order to determine the total carbonate content of each sample – information used to optimise spiking. Once dry, samples were taken up in HBr and processed using a standard Pb extraction procedure incorporating a double pass through anion exchange microcolumns, Pb being eluted in 6 N HCl. Samples were split for spiking prior to mass spectrometry, with the ^{207}Pb – ^{204}Pb double spike added to the smaller aliquot. Full details of the spiking procedure are in Woodhead *et al.* (1995). Spiked and unspiked samples were loaded using the conventional silica gel-phosphoric acid method on single Re filaments and run on a Finnigan MAT 262 mass spectrometer, operated in static multicollector mode.

References

Woodhead, J.D. and Hergt, J.M., 1997. Application of the "double spike" technique to Pb-isotope geochronology. Chemical Geology (Isotope Geoscience) 138:311-321.

Woodhead, J.D., Volker, F.and McCulloch, M.T., 1995. Routine lead isotope determinations using a ^{207}Pb – ^{204}Pb double spike: a long-term assessment of analytical precision and accuracy. Analyst 120: 35-39.

Re-Os analytical techniques (from Selby and Creaser, 2001)

Sample preparation

The Re and Os contents of molybdenite were determined by isotope dilution mass spectrometry at the University of Alberta Radiogenic Isotope Facility. Molybdenite seperates were obtained by scraping the mineral surface of by crushing the sample in a porcelain disk mill, with molybdenite separated by heavy liquid techniques or by flotation using high-purity water. The samples were handpicked under a microscope to remove any impurities.

Re-Os methodology

Molybdenite is naturally Re enriched and contains insignificant nonradiogenic Os (Morgan *et al.* 1986; Markey *et al.* 1998), meaning that effectively all ^{187}Os is derived from the decay of ^{187}Re (*cf.* Faure, 1986). The abundance of ^{187}Re and ^{187}Os in the molybdenite samples was measured by isotope dilution, using mixed tracer solutions that contained isotopically enriched ^{185}Re together with isotopically normal Os, in the form of a gravimetric and isotopic Os standard. The ^{185}Re abundance in the tracer solution is calibrated directly against a gravimetric Re standard solution made from 99.9999 % Re metal. By using an isotopically normal Os solution, the abundance of ^{187}Os in molybdenite is calculated by measuring the ^{187}Os abundance after equilibrating ^{187}Os in molybdenite and common Os in the tracer solution (*cf.* Suzuki *et al.* 1992). In this way, the isotopic analysis of Os can be correlated for instrumental fractionation during analysis (*cf.* Markey *et al.* 1998). Ammonium hexachloro-osmate (Johnson and Mtthey, 99.999 % metal basis purity) was used as the source of Os in the tracer solutions. This salt was reduced to metallic Os in 98 % N_2 and 2 % H_2 gas at ~500 ^{o}C for ~ 2 hours in order to obtain the metallic Os weight fraction. This determination was used together with the measured isotopic composition of the salt to determine the ^{187}Os abundance in molybdenite.

The Carius tube method was used for the dissolution of molybdenite and equilibration of sample and tracer Re and Os (*cf.* Creaser *et al.,* 1993; Shirey and Walker, 1995; Shen *et al.,* 1996). Molybdenite samples of 1 to 8 mg were dissolved and equilibrated with a known amount of tracer in reverse aqua regia (2:1 16*N* HNO_3 and 12*N* HCl, 3 ml) at 240 ^{o}C for 24 hours then cooled and refrigerated prior to Os and Re separation.

Extraction of OsO_4 from the acid sample mix was achieved by using modified solvent extraction and microdistillation techniques (Cohen and Waters, 1996; Birck *et al.*, 1997). The Carius tube contents were frozen using liquid nitrogen, the tube opened, and carbon tetrachloride (CCl_4, 3.5 ml) added. After thawing, the contents were place in a 50-ml centrifuge tube in a water bath of ~ 25 ^oC for ~ 15 minutes. The mixture was agitated for 1 minute, centrifuged, and the Os-bearing CCl_4 removed to a PFA Teflon vial containing 9*N* HBr (3 ml). This procedure was completed 3 times. Back extraction of Os from CCl_4 was achieved by heating the CCl_4-HBr mix at ~60 ^oC for ~12 hours under a heat lamp. The CCl_4 was removed and the Os-bearing HBr evaporated to dryness at ~60 ^oC in HEPA filtered air. This Os fraction was then purified by microdistillation. The Os fraction dissolved in 9*N* HBr (30 µl) was dried onto the lid of a conical Teflon vial, oxidized using CrO_3 at ~80 ^oC for 3 hours, with the OsO_4 reduced by 9*N* HBr (20 µl) held in the tip of the conical Teflon vial. The Os-bearing HBr was then evaporated to dryness under nitrogen gas at ~60 ^oC.

Mo was removed by solvent extraction from the acid sample mixture after Os separation. The aqua regia residuum was evaporated at ~60 ^oC and converted to a chloride form using 6*N* HCl (5 ml), heated for ~2 hours at ~ 60 ^oC, placed in a centrifuge tube with Amyl acetate (5 ml), and agitated ~ 1 minute. The Mo-bearing Amyl acetate was then removed to waste. This procedure is repeated, and the sample solution (Re-bearing HCl) was evaporated to dryness at ~ 60 ^oC, converted to nitric form using 0.2*N* HNO_3 (3 ml), and heated at ~ 60 ^oC for ~ 2 hours. Re was then purified by HNO_3-HCl based anion exchange chromatography using standard techniques (Morgan *et al.*, 1991).

The purified Os fraction was loaded onto a Pt filament in 9*N* HBr (0.5 µl) drying in air at 0.8 A, with a $Ba(OH)_2$/NaOH solution (0.2 µl) added to the dried solution. The purified Re fraction was loaded onto a Pt filament in 16*N* HNO_3 (0.3 µl) with an equal amount of $Ba(NO_3)_2$ solution drying in air at 0.8 A. The Re and Os isotope compositions were measured using negative thermal ionization mass spectrometry (Creaser *et al.*, 1991; Volkening *et al.*, 1991) on a Micromass Sector 54 mass spectrometer. All Re and Os fractions were measured using the Faraday collector.

References

Birck, J.L., Roy Barman, M. and Capmas, F., 1997. Re-Os isotopic measurements at the femtomole level in natural samples. Geostandards Newsletter – Journal of Geostandards and Geoanalysis 20:19-27.

Cohen, A.S. and Waters, F.G., 1996. Separation of osmium from geological materials by solvent extraction for analysis by thermal ionization mass spectrometry. Analytica Chimica Acta 332:269-275.

Creaser, R.A., Papanastassiou, D.A. and Wasserburg, G.J., 1991. Negative thermal ion mass spectrometry of osmium, rhenium and iridium. Geochimica et Cosmochimica Acta 55:397-401.

Creaser, R.A., Papanastassiou, D.A. and Wasserburg, G.J., 1993. Rhenium-osmium isotope systematics of group IIA and group IVA iron meteorites. Lunar and planetary science conference, 24th, 1993, Houston, TX, Abstracts, pp. 339-340.

Faure, G., 1986. Principles of isotope geology. New York, John Wiley and Sons, 589p.

Markey, R., Stein, H. and Morgan, J., 1998. Highly precise Re-Os dating for molybdenite using alkaline fusion and NTIMS. Talanta 45:935-946.

Morgan, J.W., Lovering, J.F. and Ford, R.J., 1986. Rhenium and non-radiogenic osmium in australian molybdenites and other sulphide minerals by neutron activation analysis. Journal of the Geological Society of Australia 15:189-194.

Morgan, J.W., Golightly, D.W. and Dorrzapf, A.F., 1991. Methods for the separation of rhenium, osmium and molybdenum applicable to isotope geochemistry. Talanta 38: 259-265.

Selby, D. and Creaser, R.A., 2001. Re-Os Geochronology and systematics in molybdenite from the Endako porphyry molybdenum deposit, British Columbia, Canada. Economic Geology 96:1:197-204.

Shen, J.J., Papanastassiou, D.A. and Wasserburg, G.J., 1996. Precise Re-Os determinations and systematics of iron meteorites. Geochimica et Cosmochimica Acta 60:2887-2900.

Shirey, S.B. and Walker, R.J., 1995. Carius tube digestion for low blank Re-Os analysis. Analytical Chemistry 67:2136-2141.

Suzuki, K., Li, Q., Shimizu, H. and Masuda, A., 1992. Determination of osmium abundance in molybdenite mineral by using isotope dilution mass spectrometry with microwave digestion using potassium dichromate as oxidizing agent. Analyst 117: 1151-1156.

Völkening, J., Walczyk, T. and Heumann, K.G., 1991. Osmium isotope ration determinations by negative thermal ion mass spectrometry. International Journal of mass spectrometry Ion Processes 105: 147-159.

APPENDIX III

Fluid inclusion thermometric data

WERNECKE PROJECT FLUID INCLUSION RESULTS

Sample #	Phases	generation	Ti	Tmice	Tmhh	Thv	Ths	Th	Wt % NaCl	Wt % $CaCl_2$	NaCl eq wt %	Na:Ca ratio (Wt %)	moles of NaCl	moles of $CaCl_2$
Slab - quartz crystal from Wernecke Breccia matrix														
slab SW qz	L+V+H	p	-83.1	-50.4	na	158.3	226	226	22.3	17.5	40.7	1.3	3.82	1.58
slab SW qz	L+V+H	p	-90.3	-44.4	na	175	236.6	236.6	23.6	17.1	41.6	1.4	4.04	1.54
slab SW qz	L+V+H	p	-91.6	-50.1	na	168.5	236	236	23.5	17.0	41.4	1.4	4.02	1.53
slab SW qz	L+V+H	p	na	na	na	172	233.8	233.8	na	na	na	na		
slab SW qz	L+V+H	p	-88.5	-45.3	na	171	229	229	22.7	17.1	40.7	1.3	3.88	1.54
slab SW qz	L+V+H	p	-83.7	-49.3	na	168.7	236	236	23.5	17.0	41.4	1.4	4.02	1.53
slab SW qz	L+V+H	p	-84.3	-50.3	na	166	232.8	232.8	23.0	16.9	40.8	1.4	3.94	1.52
slab SW qz	L+V+H	p	na	na	na	167	na	na	na	na	na	na		
slab SW qz	L+V+H	p	-89.1	-36.3	na	154.2	245	245	24.2	17.3	42.4	1.4	4.14	1.56
slab SW qz	L+V+H	p	-89	-48.8	na	157.8	244.6	244.6	24.2	17.3	42.4	1.4	4.14	1.56
Hoover - quartz from a clast within Wernecke Breccia														
01JH-5-7A (B)	L+V+H	s	-64	-29.6	na	165	188	188	20.0	17.0	37.9	1.2	3.42	1.53
01JH-5-7A (B)	L+V	s	-67	-35	na	172	na	172	32.0	na	32.0			
01JH-5-7A (B)	L+V	s	-68	-29	na	166	na	166	28.0	na	28.0			
01JH-5-7A (B)	L+V	s	-67	-30	0.9	165	na	165	12.2	16.8	29.9	0.7	2.09	1.51
01JH-5-7A (B)	L+V	s	-74	-25	na	167	na	167	25.6	na	25.6			
01JH-5-7A (B)	L+V	s	-76	-34	-1	168	na	168	8.5	21.1	30.7	0.4	1.45	1.90
01JH-5-7A (B)	L+V	s	-74	-30	na	163	na	163	28.7	na	28.7			
01JH-5-7A (B)	L+V	s	-78	-34	na	153	na	153	31.3	na	31.3			
Slats - fluorite-ferroan dolomite-pyrite-chalcopyrite vein that cuts hematite-altered metasiltstone														
stf95-1-20.30	L+V	ps	-72.3	-28.1	-12.5	112.1	na	112.1	12.3	15.0	28.1	0.8	2.10	1.35
stf95-1-20.30	L+V	ps	-75	-27.1	-8.3	> 158.6	na	> 158.6	14.2	13.4	28.3	1.1	2.43	1.21
stf95-1-20.30	L+V	ps	-90.8	-23.1	na	111.9	na	111.9	24.4	na	24.4			
stf95-1-20.30	L+V	ps	-76	-24.9	na	>160	na	>160	25.5	na	25.5			
stf95-1-20.30	L+V	ps	-77.8	-23.3	na	116.3	na	116.3	24.5	na	24.5			
stf95-1-20.30	L+V	ps	-77.4	-23.6	na	121.8	na	121.8	24.7	na	24.7			
stf95-1-20.30	L+V+H	ps	-76.6	-25.7	1.5	113	na	>113	17.3	10.8	28.7	1.6	2.96	0.97
stf95-1-20.30	L+V+H	ps	-77	-22.9	na	89	na	>89	24.3	na	24.3			
stf95-1-20.30	L+V+H	ps	-75.4	-23.6	na	>160	na	>160	24.7	na	24.7			
stf95-1-20.30	L+V+H	ps	-75.6	-28.0	3.0	101.1	na	>101	14.5	14.3	29.6	1.0	2.48	1.29
stf95-1-20.30	L+V+H	ps	-89.2	-26.6	-0.1	141.8	na	>142	16.3	12.3	29.3	1.3	2.79	1.11
stf95-1-20.30	L+V+H	ps	-85	-27.5	-3.7	134.9	na	>135	14.4	13.8	28.9	1.0	2.46	1.24

Sample #	Phases	generation	Ti	Tmice	Tmhh	Thv	Ths	Th	Wt % NaCl	Wt % $CaCl_2$	NaCl eq wt %	Na:Ca ratio (Wt %)	moles of NaCl	moles of $CaCl_2$
stf95-1-20.30	L+V+Op	ps	-90.5	-26.5	-22.1	124.4	na	>124	13.0	13.0	26.7	1.0	2.22	1.17
stf95-1-20.30	L+V+Op	ps	-103.1	-25.8	0	125	na	>125	17.2	11.0	28.8	1.6	2.94	0.99
stf95-1-20.30	L+V+Op	ps	-82.7	-27.6	-6.5	129.5	na	>130	13.9	14.1	28.7	1.0	2.38	1.27
stf95-1-20.30	L+V+Op	ps	-77.4	-34.6	na	68	na	>68	31.7	na	31.7			
stf95-1-20.30	L+V+H+Op	ps	-76.6	-27.8	-7.1	123.8	na	>124	13.5	14.4	28.7	0.9	2.31	1.30
Igor -barite from Wernecke Breccia matrix at the edge of massive pyrite-hematite-chalcopyrite ± magnetite mineralization														
02JH-10-17B (A)	L+V	p	na	-54		250	na	250	54.9	na	54.9			
02JH-10-17B (A)	L+V	p	-77	-50	-26	250	na	250	2.2	30.1	33.9	0.1	0.38	2.71
02JH-10-17B (A)	L+V	p	no changes seen on reheating			220	na	220	na	na	na			
Olympic - quartz crystal in Wernecke Breccia matrix (fluid inclusions in the outermost growth zone)														
02JH-21-5 A	L+V	p	-60	-28	na	168	na	168	27.4	na	27.4			
02JH-21-5 A	L+V	p	na	-26	na	158	na	158	26.2	na	26.2			
02JH-21-5 A	L+V	p	na	-29	na	160	na	160	28.0	na	28.0			
02JH-21-5 A	L+V	p	-67	-27	na	170	na	170	26.8	na	26.8			
02JH-21-5 A	L+V	p	na	na	na	165	na	165	na	na	na			
02JH-21-5 A	L+V	p	na	na	na	167	na	167	na	na	na			
02JH-21-5 A	L+V	p	na	na	na	162	na	162	na	na	na			
Olympic - ferroan dolomite-quartz-chalcopyrite ± pyrite vein cutting Wernecke Breccia														
OY94-3-24.70m	L+V	p	-64	-25	na	212	na	212	25.6	na	25.6			
OY94-3-24.70m	L+V	p	na	-29.6	na	188	na	188	28.4	na	28.4			
OY94-3-24.70m	L+V	p	na	-56	-13	205	na	205	2.6	31.0	35.2	0.1	0.44	2.79
OY94-3-24.70m	L+V	p	na	na	na	212	na	212	na	na	na			
OY94-3-24.70m	L+V	p	na	na	na	213	na	213	na	na	na			
OY94-3-24.70m	L+V	p	na	na	na	214	na	214	na	na	na			
OY94-3-24.70m	L+V	p	na	na	na	215	na	215	na	na	na			
OY94-3-24.70m	L+V	p	na	na	na	223	na	223	na	na	na			
OY94-3-24.70m	L+V	p	na	na	na	216	na	216	na	na	na			
OY94-3-24.70m	L+V	p	na	na	na	194	na	194	na	na	na			
OY94-3-24.70m	L+V	p	na	na	na	218	na	218	na	na	na			

L = liquid, V = vapour, S = solid, Ox = oxide, p = primary, ps = pseudosecondary, s = secondary

Ti = initial melting; Tmice = final melting temperature of ice; Tmhh = final melting temperature of hydrohalite

Thv = temperature of vapour bubble disappearance;

Ths = temperature of halite dissolution; Th = final homogenisation temperature

(eq) Wt % = (equivalent) weight percent;

APPENDIX IV

Results of stable isotope analyses

WERNECKE PROJECT STABLE ISOTOPE RESULTS												
Sample ID	$\delta^{13}C$ carbonate (V-PDB)	$\delta^{18}O$ carbonate (V-SMOW)	$\delta^{13}C$ shale (V-PDB)	$\delta^{34}S$ pyrite (CDT)	$\delta^{34}S$ chalcopyrite (CDT)	$\delta^{34}S$ barite (CDT)	$\delta^{18}O$ muscovite (V-SMOW)	$\delta^{18}O$ biotite (V-SMOW)	$\delta^{18}O$ actinolite (V-SMOW)	δ D muscovite (V-SMOW)	δ D biotite (V-SMOW)	δ D actinolite (V-SMOW)
Wernecke Breccia related samples												
HOOVER												
01JH-05-05B			-26.70									
01JH-07-01A				-7.99								
01JH-07-11A	-6.76	12.21										
01JH-07-11B				13.39								
01JH-07-12 (breccia)	-4.52	12.03										
01JH-07-12 (vein)	-5.45	9.40										
01JH-08-02							11.13			na		
01JH-08-07A	-3.82	13.46										
01JH-09-5A			-20.80									
01JH-09-11A				4.55								
01JH-09-11E					8.78							
HV94-01-036'				-5.53								
HV94-01-120.5'	-3.87	11.15										
HV94-01-507.3'	-2.41	11.23		-12.41								
HV94-01-599.6'				-6.99								
HV94-01-642.5'	-2.30	11.92										
HV94-01-650'	-2.39	12.08										
HV94-01-695'								7.77			-119	
HV94-01-936.4'				-1.56								
SLAB												
01JH-13-08A					3.78							
01JH-15-10	-0.10	12.35										
01JH-19-01								6.7			-141	
01JH-19-02D	-0.01	12.16										
01JH-19-02E	0.17	6.72										

Sample ID	δ ^{13}C carbonate	δ ^{18}O carbonate	δ ^{13}C shale	δ ^{34}S pyrite	δ ^{34}S chalcopyrite	δ ^{34}S barite	δ ^{18}O muscovite	δ ^{18}O biotite	δ ^{18}O actinolite	δ D muscovite	δ D biotite	δ D actinolite
	(V-PDB)	(V-SMOW)	(V-PDB)	(CDT)	(CDT)	(CDT)	(V-SMOW)	(V-SMOW)	(V-SMOW)	(V-SMOW)	(V-SMOW)	(V-SMOW)
01JH-20-02								9.5			-84	
01JH-20-03							10.63			-45		
01JH-20-06A								8.25			-115	
01JH-20-06F	0.14	12.60										
01JH-20-08	-0.70	14.60										
01JH-20-10C								8.14	10.96		-23	-22; -18
01JH-27-03D				-5.40								
01JH-29-02B	1.24	14.06										
01JH-29-02C	1.48	15.32										
01JH-29-05C	-1.08	2.73										
01JH-29-15D					-3.97							
01JH-30-04B	-1.61	13.99										
01JH-30-07A	-0.56	12.78										
01JH-32-04C				-2.41								
01JH-32-04D	-1.23	14.78										
01JH-32-04F			-24.90									
01JH-32-06B	-3.69	7.18										
01JH-32-07A	-2.74	10.13										
01JH-32-07D					-10.99							
01JH-34-11C	-3.18	13.67										
01JH-34-11D (dark brown)	-3.16	13.78										
01JH-34-11D (medium brown)	-3.32	10.94										
01JH-34-11E	-2.61	-2.11										
01JH-35-01B	-3.24	13.01										
01JH-35-01C	-3.71	12.67										
01JH-35-02	-1.51	3.04						8.74			-34	

Sample ID	δ ^{13}C carbonate	δ ^{18}O carbonate	δ ^{13}C shale	δ ^{34}S pyrite	δ ^{34}S chalcopyrite	δ ^{34}S barite	δ ^{18}O muscovite	δ ^{18}O biotite	δ ^{18}O actinolite	δ D muscovite	δ D biotite	δ D actinolite
	(V-PDB)	(V-SMOW)	(V-PDB)	(CDT)	(CDT)	(CDT)	(V-SMOW)	(V-SMOW)	(V-SMOW)	(V-SMOW)	(V-SMOW)	(V-SMOW)
01JH-35-03B					2.40							
01JH-35-05B	-2.75	14.03										
02JH-14-01A2							11.13			-54		
02JH-14-01B					-11.48							
02JH-20-02								9.46			-84	
SB94-01-009.90m	-1.08	14.75										
SB94-01-033.70m	-0.23	14.09					11.61			-21		
SB94-01-128.60m				-3.29								
SB94-01-198.60m				-1.51	-2.69							
SB94-01-345.10m							11.47			na		
SB94-01-358.30m				-1.05								
SB94-04-177.60m				-0.66	-0.76							
SB95-05-107.30m				6.49								
SB97-09-051.50m	-3.00	14.27		7.09								
SB97-09-119.90m (beige)	-2.84	14.08										
SB97-09-119.90m (vein)	-2.77	13.04			-4.05							
SB97-09-166.10m				-5.76								
SB97-09-166.10m (pink)	-3.41	9.03										
SB97-09-166.10m (tan)	-2.61	13.55										
SB97-09-200.10m (brown)	-2.14	12.53										
SB97-09-200.30m (tan)	-2.41	13.03										
SB97-09-200.30m (white)	-2.62	6.69										
SB97-10-043.70m					-7.35							
SB97-19-070.10m	-2.29	4.25					10.09			na		
SLAB FL1				-3.24	-2.95							
SLATS												
02JH-04-01A				4.21								

Sample ID	δ ^{13}C carbonate	δ ^{18}O carbonate	δ ^{13}C shale	δ ^{34}S pyrite	δ ^{34}S chalcopyrite	δ ^{34}S barite	δ ^{18}O muscovite	δ ^{18}O biotite	δ ^{18}O actinolite	δ D muscovite	δ D biotite	δ D actinolite
	(V-PDB)	(V-SMOW)	(V-PDB)	(CDT)	(CDT)	(CDT)	(V-SMOW)	(V-SMOW)	(V-SMOW)	(V-SMOW)	(V-SMOW)	(V-SMOW)
02JH-04-01B	-4.37	15.35										
02JH-04-01G	-2.92	15.61										
02JH-05-01 (brown)	-7.26	15.39										
02JH-05-02	-2.21	16.78										
02JH-05-05B (vein)	-6.54	14.27										
02JH-06-03 (matrix)	-6.23	16.48										
02JH-06-04A	-10.46	14.54										
02JH-06-04C	-10.57	14.59			-1.73							
STW95-01-05.75m	-6.15	14.89										
STW95-01-11.10m tan	-5.12	15.68										
STW95-02-14.60m	-2.94	14.11			-6.78							
STW95-02-25.50m					-4.79							
STW95-03-05.20m (vein or matrix)	-4.14	16.11										
STW95-03-05.20m (vein or matrix)	-6.47	14.65										
STW95-03-41-10m				-6.23								
STF95-01-12.70m	-2.00	13.84										
STF95-01-62.50m	-0.80	13.97										
STF95-01-67.70m	-1.12	17.66										
STF95-01-110.60m (carb-hem vein)	-0.19	14.90										
STF95-01-110.60m (red carb-qz vein)	-0.45	14.14										
STF95-05-60.65m	-3.59	13.71										
STF95-05-74.90m	-4.33	20.12										
IGOR												
02JH-09-06C					-4.73							

Sample ID	δ ^{13}C carbonate	δ ^{18}O carbonate	δ ^{13}C shale	δ ^{34}S pyrite	δ ^{34}S chalcopyrite	δ ^{34}S barite	δ ^{18}O muscovite	δ ^{18}O biotite	δ ^{18}O actinolite	δ D muscovite	δ D biotite	δ D actinolite
	(V-PDB)	(V-SMOW)	(V-PDB)	(CDT)	(CDT)	(CDT)	(V-SMOW)	(V-SMOW)	(V-SMOW)	(V-SMOW)	(V-SMOW)	(V-SMOW)
02JH-10-17A				4.75								
02JH-12-01							9.92			-55		
02JH-12-05					-4.02							
02JH-12-13D					-7.86	17.12						
I80-10-045' 6	-2.95	16.70										
I80-10-113' tan	-6.14	16.42										
I80-10-115' 6"	-4.77	19.96										
I80-10-181' (tan)	-3.87	19.03										
I80-10-181' (brown)	-4.29	18.89										
I80-10-182' (white)	-2.91	17.26				11.29						
I80-10-208'	-2.59	15.45										
I80-10-210' (tan)	-1.35	15.94										
I80-10-216'	-1.85	16.55			-8.37	8.66						
I80-14-046'	-3.03	15.38										
I80-14-150'	-3.58	16.25										
I80-14-234'					-4.39							
I80-14-236'				-7.36								
I80-14-402.5' (white)	-3.12	18.56										
I80-14-441'	-2.84	17.24										
I80-14-500'	-4.61	14.62										
I80-14-539.5'				3.27		7.66						
IGOR						8.38						
OLYMPIC												
02JH-22-04A				-0.52								
OLYMPIC	-0.81	16.75										
OY94-01-021.30m	-1.46	7.97										
OY94-01-117.60m	0.08	16.69										
OY94-03-016.70m	-1.38	17.37										
OY94-03-024.70m	-5.06	16.94			5.31							

Sample ID	$\delta^{13}C$ carbonate	$\delta^{18}O$ carbonate	$\delta^{13}C$ shale	$\delta^{34}S$ pyrite	$\delta^{34}S$ chalcopyrite	$\delta^{34}S$ barite	$\delta^{18}O$ muscovite	$\delta^{18}O$ biotite	$\delta^{18}O$ actinolite	δD muscovite	δD biotite	δD actinolite
	(V-PDB)	(V-SMOW)	(V-PDB)	(CDT)	(CDT)	(CDT)	(V-SMOW)	(V-SMOW)	(V-SMOW)	(V-SMOW)	(V-SMOW)	(V-SMOW)
OY94-03-025.60m	-3.07	18.26										
OY94-03-038.60 (tan)	-2.91	16.98										
OY94-03-046.30m	-1.13	16.57										
OY94-03-063.50m (vein1)	0.41	16.61			-10.75							
OY94-03-063.50m (vein2)	-0.90	15.73										
OY94-03-132.8m	-1.10	17.12										
OY94-04-013.00m (white)	-0.61	16.70										
OY94-04-013.00m (tan)	-1.52	18.53										
OY94-04-021.90m	-1.65	14.97										
OY94-04-038.90m (tan)	-2.73	15.58										
OY94-04-038.90m (pink)	-2.79	14.76										
OY94-04-067.60m (bx matrix)	-2.15	16.79										
OY94-04-067.60m (post bx)	-2.49	16.89										
OY94-04-089.00m (white)	-1.64	18.71										
OY94-04-089.0m (carb-cp)	-1.89	16.34										
Host Wernecke Super Group samples												
Fairchild Lake Group												
DT02-9-2-1	-2.02	13.59										
01JH-09-07i	0.44	13.30										
01JH-09-07ii	0.40	13.14										
01JH-15-03	-1.41	11.80										
01JH-23-12	0.03	14.36										
01JH-29-15C	0.05	14.08										
Quartet Group												
02JH-10-12	-0.28	13.94										
02JH-12-09C	-1.68	15.44										
02JH-12-14	-1.86	15.91										
JH01 5 5B	-26.70											
JH01 9 5A	-20.80											

Sample ID	$\delta^{13}C$ carbonate	$\delta^{18}O$ carbonate	$\delta^{13}C$ shale	$\delta^{34}S$ pyrite	$\delta^{34}S$ chalcopyrite	$\delta^{34}S$ barite	$\delta^{18}O$ muscovite	$\delta^{18}O$ biotite	$\delta^{18}O$ actinolite	δD muscovite	δD biotite	δD actinolite
	(V-PDB)	(V-SMOW)	(V-PDB)	(CDT)	(CDT)	(CDT)	(V-SMOW)	(V-SMOW)	(V-SMOW)	(V-SMOW)	(V-SMOW)	(V-SMOW)
JH01 32 4F	**-24.90**											
Gillespie Lake Group												
CW92-53-01	**-1.28**	**19.23**										
DT92-51-1	**-0.16**	**24.56**										
02JH-04-02	**-1.31**	**19.55**										
02JH-04-03 (matrix)	**-1.91**	**16.39**										
02JH-04-04	**-1.81**	**19.19**										
02JH-06-01 (matrix)	**0.71**	**19.91**										
02DG-01	**1.63**	**20.28**										
02DG-02	**0.36**	**22.88**										
02JH-21-01	**0.22**	**20.03**										
02JH-21-04 (clasts)	**1.17**	**17.47**										
02JH-21-04 (matrix)	**0.32**	**16.62**										
02JH-22-03B	**-1.16**	**19.31**										
02JH-04-03 (clasts)	**-4.17**	**15.54**										

WERNECKE PROJECT STA			
Sample ID	**Paragenetic Stage**	**Mineral**	**Sample Description**
Wernecke Breccia related samples			
HOOVER			
01JH-05-05B		carbon	Quartet Group carbonaceous shale
01JH-07-01A	H2 or H3	pyrite	sulphides forming breccia matrix
01JH-07-11A	HU	calcite + kutnohorite	carbonate vein cutting black slate (Quartet Group)
01JH-07-11B	HU	pyrite	carbonate-sulphide vein cutting black slate (Quartet Group)
01JH-07-12 (breccia)	H3	calcite + ankerite + dolomite	carbonate breccia (upper breccia)
01JH-07-12 (vein)	HU	ankerite + dolomite	carbonate vein cutting carbonate breccia (upper breccia)
01JH-08-02	H3	muscovite	quartz-muscovite-malachite-hematite vein cutting siltstone (Fairchild Lake Group)
01JH-08-07A	H3	calcite	carbonate from breccia matrix
01JH-09-5A		carbon	Quartet Group carbonaceous shale
01JH-09-11A	H3	pyrite	sulphide vein at contact of upper breccia and black slate
01JH-09-11E	H2 or H3	chalcopyrite	talus sample from below breccia
HV94-01-036'	H3	pyrite	disseminated pyrite at breccia-siltstone contact
HV94-01-120.5'	H1 or H3	calcite	carbonate-magnetite vein
HV94-01-507.3'	H3	calcite + dolomite; pyrite	carbonate-pyrite vein brecciating siltstone
HV94-01-599.6'	H3 or H4	pyrite	carbonate-chlorite-pyrite-chalcopyrite vein cuts feldspar-quartz altered siltstone
HV94-01-642.5'	H3	calcite	carbonate brecciating siltstone clasts in breccia
HV94-01-650'	H3	calcite	carbonate-pyrite-chalcopyrite veinlet cutting a siltstone clast
HV94-01-695'	H3 or H4	biotite	biotite porphyroblasts in breccia matrix and clasts
HV94-01-936.4'	H3	pyrite	quartz-chlorite-pyrite vein cutting phyllitic siltstone
SLAB			
01JH-13-08A	S4	chalcopyrite	quartz-chalcopyrite vein parallel to layering in Fairchild Lake Group
01JH-15-10	S4	calcite	pink carbonate-hematite vein cutting breccia
01JH-19-01	S3	biotite	quartz-carbonate-hematite-biotite vein cutting breccia
01JH-19-02D	S4	calcite + magnesite	pink carbonate-actinolite-quartz vein cutting a siltstone clast in breccia
01JH-19-02E	S2	calcite + kutnohorite	carbonate±magnetite clast in breccia

Sample ID	Paragenetic Stage	Mineral	Sample Description
01JH-20-02		biotite	quartz-carbonate-hematite-biotite pyrite-chalcopyrite vein cutting breccia clast
01JH-20-03	S3 or S4	muscovite	muscovite from breccia matrix
01JH-20-06A	S3	biotite	biotite from breccia matrix
01JH-20-06F	S3	calcite	brown-weathering carbonate crystals in breccia matrix
01JH-20-08	S3	calcite	carbonate-quartz-pyrite vein at contact between breccia and siltstone
01JH-20-10C	S4	biotite; actinolite	carbonate-actinolite-biotite vein cutting siltstone near siltstone-breccia contact. Siltstone has been crackle brecciated by chlorite-quartz fluids - biotite may be chloritized.
01JH-27-03D	S1	pyrite	quartz-?feldspar-pyrite-chalcopyrite-molybdenite vein cutting siltstone
01JH-29-02B	S3	calcite	pink carbonate vein cutting breccia
01JH-29-02C	S3	calcite + quartz + albite	brown carbonate brecciating siltstone
01JH-29-05C	S3	calcite + ankerite + siderite + dolomite …	carbonate matrix to breccia proximal to slab volcanics
01JH-29-15D	S3 or S4	chalcopyrite	quartz-carbonate-chalcopyrite vein cutting Fairchild Lake Group siltstone
01JH-30-04B	S3	calcite + kutnohorite + azurite	brown carbonate-quartz ± chalcopyrite crackle brecciating siltstone
01JH-30-07A	S4	calcite	large carbonate crystals from calcite-muscovite/chlorite-quartz-fluorite breccia matrix
01JH-32-04C	S2	pyrite	quartz-magnetite-carbonate-garnet-pyrite-biotite vein cutting Fairchild Lake Group siltstone
01JH-32-04D	S2	calcite + dolomite	quartz-carbonate-magnetite pod in siltstone
01JH-32-04F		carbon	Quartet Group carbonaceous shale
01JH-32-06B	S3	calcite + ankerite + rhodochrosite …	carbonate-epidote crackle brecciating siltstone
01JH-32-07A	S3	calcite + huntite	pink carbonate-chlorite veins cutting breccia
01JH-32-07D	S4	chalcopyrite	chalcopyrite bleb 15x5 cm in a coarse-grained carbonate-quartz-magnetite vein cutting siltstone around bx with quartz-carbonate-magnetite-chalcopyrite matrix
01JH-34-11C	S2	ankerite	carbonate-magnetite-quartz vein cutting siltstone
01JH-34-11D (dark brown)	S2	ankerite + dolomite …	dark brown carbonate from dark brown carbonate-magnetite- medium brown carbonate vein cutting siltstone
01JH-34-11D (medium brown)	S2	calcite	medium brown carbonate from dark brown carbonate-magnetite- medium brown carbonate vein cutting siltstone
01JH-34-11E	S3	calcite + huntite + rhodochrosite	carbonate matrix from breccia that cuts above carbonate-magnetite veins
01JH-35-01B	S2	ankerite	carbonate-magnetite alteration
01JH-35-01C	S2	ankerite + dolomite + magnesite + azurite	carbonate-quartz vein (xcuts carbonate-magnetite alteration)
01JH-35-02	S3	calcite + kutnohorite + rhodochrosite; biotite	carbonate and biotite from matrix of breccia that cuts above carbonate-magnetite veins

Sample ID	Paragenetic Stage	Mineral	Sample Description
01JH-35-03B	S3	chalcopyrite	chalcopyrite from sulphide veinlet at edge of pyrite-chalcopyrite-quartz-carbonate-muscovite vein cutting
01JH-35-05B	S2	calcite + dolomite	carbonate-magnetite vein (xcuts carbonate-magnetite breccia)
02JH-14-01A2	S3	muscovite	pyrite-chalcopyrite-quartz-carbonate-muscovite vein cutting carbonate-magnetite-altered sediments.
02JH-14-01B	S3	chalcopyrite	pyrite-chalcopyrite-quartz-carbonate-muscovite vein cutting carbonate-magnetite-altered sediments.
02JH-20-02	S3	biotite	biotite from breccia matrix (rubble breccia)
SB94-01-009.90m	S3	calcite	carb-ms vein cutting biotite altered FLG siltstone
SB94-01-033.70m	S3	calcite; muscovite	carbonate-quartz-muscovite-pyrite-chalcopyrite-vein cutting feldspar altered FLG siltstone
SB94-01-128.60m	S3	pyrite	pyrite clast in breccia
SB94-01-198.60m	S3	pyrite; chalcopyrite	carbonate-chlorite-pyrite-chalcopyrite vein cuts Kfeldspar-quartz altered siltstone
SB94-01-345.10m	S3	muscovite	carbonate-quartz-muscovite/chlorite-chalcopyrite-molybdenite vein cutting biotite altered FLG siltstone
SB94-01-358.30m	S3	pyrite	massive coarse-grained pyrite with interstitial chalcopyrite overprinting purple quartz-fluorite altered siltstone
SB94-04-177.60m	S3	pyrite; chalcopyrite	chalcopyrite-pyrite from carbonate-muscovite/chlorite-chalcopyrite-pyrite-biotite vein cutting siltstone
SB95-05-107.30m	S3	pyrite	pyrite ± chalcopyrite overprinting massive magnetite-carbonate
SB97-09-051.50m	S2	dolomite; pyrite	carbonate-magnetite vein overprinted by hematite-pyrite
SB97-09-119.90m (beige)	S2	calcite + dolomite	white carbonate blebs in crackle breccia (overprinting carbonate-magnetite altered siltstone)
SB97-09-119.90m (vein)	S2	ankerite + minor dolomite; chalcopyrite	carbonate-chalcopyrite vein cutting crackle brecciated siltstone (overprinting carbonate-magnetite altered siltstone)
SB97-09-166.10m	S3	pyrite	pyrite ± chalcopyrite forming breccia matrix and overprinting massive magnetite-carbonate
SB97-09-166.10m (pink)	S3	ankerite + dolomite + huntite	tan carbonate overprinting carbonate-magnetite
SB97-09-166.10m (tan)	S2	ankerite + dolomite	pink carbonate cutting above tan carbonate
SB97-09-200.10m (brown)	S2	ankerite	brown-weathering carbonate (?part of carbonate-magnetite alteration)
SB97-09-200.30m (tan)	S2	ankerite	tan-weathering carbonate (?part of carbonate-magnetite alteration)
SB97-09-200.30m (white)	S5	calcite + albite	white carbonate vein that cuts above tan carbonate
SB97-10-043.70m	S3	chalcopyrite	chalcopyrite clast in breccia
SB97-19-070.10m	S4	ferroan dolomite; muscovite	carbonate-quartz-rutile blebs/bx cut ms-rich breccia
SLAB FL1	S3 or S4	pyrite; chalcopyrite	carbonate-pyrite-chalcopyrite forming breccia matrix
SLATS			
02JH-04-01A	FU	pyrite	hematite-pyrite-quartz veinlet cutting phyllite

Sample ID	Paragenetic Stage	Mineral	Sample Description
02JH-04-01B	FU	dolomite	quartz-carbonate-hematite vein
02JH-04-01G	FU	dolomite	2m wide massive hematite-magnetite-carbonate vein cutting phyllite
02JH-05-01 (brown)	W5	siderite	carbonate-quartz (tension) vein cutting diorite
02JH-05-02	W5	ferroan dolomite	carbonate vein cutting interlayered shale and dolomite
02JH-05-05B (vein)	W5	dolomite	carbonate-quartz vein cutting red breccia
02JH-06-03 (matrix)	W5	ferroan dolomite	Wernecke Breccia matrix
02JH-06-04A	W6	ankerite	carbonate-pyrite-chalcopyrite-fluorite vein cutting massive magnetite at contact between Wernecke breccia and Gillespie Lake Group interlayered dolomite and black shale
02JH-06-04C	W6	ankerite; chalcopyrite	carbonate-pyrite-chalcopyrite-quartz vein cutting massive magnetite at contact between Wernecke breccia and Gillespie Lake Group interlayered dolomite and black shale
STW95-01-05.75m	W5	ferroan dolomite	carbonate-chalcopyrite vein cutting Wernecke Breccia
STW95-01-11.10m tan	W5	ankerite	breccia matrix (replacing earlier ser matrix)
STW95-02-14.60m	W5	ferroan dolomite + ankerite; chalcopyrite	carbonate-chalcopyrite vein at breccia-siltstone contact
STW95-02-25.50m	W5	pyrite	albite-quartz-chlorite-chalcopyrite vein cutting hematite altered sediments in breccia zone
STW95-03-05.20m (vein or matrix)	W5	dolomite	carbonate-albite-quartz-pyrite vein cutting breccia or carbonate matrix to breccia (mix up at lab and samples were not labelled)
STW95-03-05.20m (vein or matrix)	W5	dolomite	carbonate-albite-quartz-pyrite vein cutting breccia or carbonate matrix to breccia (mix up at lab and samples were not labelled)
STW95-03-41-10m	W5	pyrite	massive pyrite vein cutting crackle-brecciated siltstone
STF95-01-12.70m	F4	ferroan dolomite	Quartz-albite-carbonate-± chalcopyrite ± hematite vein cutting K-altered siltstone
STF95-01-62.50m	F3	ferroan dolomite	Quartz-albite-carbonate-± chalcopyrite ± hematite vein cutting brecciated phyllite
STF95-01-67.70m	F3	ferroan dolomite	Quartz-albite-carbonate-± chalcopyrite vein cutting phyllite
STF95-01-110.60m (carb-hem vein)	F2	dolomite	quartz-carbonate-albite-specular hematite vein cutting sericite altered phyllite
STF95-01-110.60m (red carb-qz vein)	F3	ferroan dolomite	quartz-carbonate-red hematite vein cutting above vein
STF95-05-60.65m	F3	ferroan dolomite	carbonate-quartz vein cutting breccia
STF95-05-74.90m	F3	ankerite	carbonate vein cutting breccia
IGOR			
02JH-09-06C	I3	chalcopyrite	quartz-carbonate-pyrite-chalcopyrite vein/pod in foliated breccia

Sample ID	Paragenetic Stage	Mineral	Sample Description
02JH-10-17A	I3	pyrite	massive pyrite breccia
02JH-12-01	I4	muscovite	muscovite from breccia matrix
02JH-12-05	I3	chalcopyrite	carbonate-chalcopyrite-hematite vein cutting foliated K-chlorite-carbonate altered rock
02JH-12-13D	I4	chalcopyrite; barite	barite-chalcopyrite vein
I80-10-045' 6	I4	ferroan dolomite	carbonate-barite vein cutting breccia
I80-10-113' tan	I4	siderite	tan carbonate-red barite vein cutting breccia
I80-10-115' 6"	I3	siderite	carbonate-chalcopyrite vein cutting Wernecke Breccia and cross-cut by pyrite-chalcopyrite-magnetite vein
I80-10-181' (tan)	I4	ferroan dolomite	tan carbonate-brown carbonate-barite-pyrite-chalcopyrite vein cutting breccia
I80-10-181' (brown)	I4	siderite	tan carbonate-brown carbonate-barite-pyrite-chalcopyrite vein cutting breccia
I80-10-182' (white)	I4	ferroan dolomite; barite	carbonate-barite vein cutting breccia
I80-10-208'	I4	siderite	carbonate vein cutting semi-massive magnetite
I80-10-210' (tan)	I4	siderite	carbonate-?feldspar-barite-chalcopyrite vein cutting breccia
I80-10-216'	I4	siderite; chalcopyrite; barite	carbonate-barite-chalcopyrite-pyrite vein cutting breccia
I80-14-046'	I3	siderite	carbonate overprinting breccia
I80-14-150'	I3	siderite	carbonate vein cutting breccia
I80-14-234'	IU	chalcopyrite	quartz-chalcopyrite vein cutting breccia
I80-14-236'	I3	pyrite	massive pyrite overprinting breccia
I80-14-402.5' (white)	I3	ferroan dolomite	carbonate-feldspar-chalcopyrite-hematite vein cutting breccia
I80-14-441'	I3	ferroan dolomite	carbonate-barite-pyrite vein cutting breccia
I80-14-500'	I3	siderite	carbonate-pyrite vein cutting breccia
I80-14-539.5'	I4	pyrite; barite	barite-pyrite vein
IGOR	I4	barite	1m wide barite-magnetite vein cutting breccia
OLYMPIC			
02JH-22-04A	OU	pyrite	pyrite from diorite-breccia contact zone
OLYMPIC	O5	ferroan dolomite	brown-weathering carbonate cutting Wernecke breccia
OY94-01-021.30m	O3	calcite	carbonate vein cutting WBx
OY94-01-117.60m	O1	dolomite	dark brown-weathering carbonate veins cut breccia
OY94-03-016.70m	O3	dolomite	carbonate-quartz vein cut WBx
OY94-03-024.70m	O3	ferroan dolomite; chalcopyrite	carbonate-quartz-chalcopyrite ± pyrite vein cutting WBx

Sample ID	Paragenetic Stage	Mineral	Sample Description
OY94-03-025.60m	O2	ferroan dolomite	carbonate-quartz-chalcopyrite-pyrite-arsenopyrite vein cutting WBx
OY94-03-038.60 (tan)	O5	ferroan dolomite	carbonate-quartz vein cutting WBX and quartz-hematite-pyrite veinlets
OY94-03-046.30m	O3	ferroan dolomite	pink carbonate cutting hematite-altered WBx
OY94-03-063.50m (vein1)	O2	dolomite; chalcopyrite	carbonate-hematite-chalcopyrite-quartz vein cutting WBX
OY94-03-063.50m (vein2)	O5	dolomite	carbonate vein cutting above vein
OY94-03-132.8m	O2	dolomite	carbonate-quartz-chalcopyrite vein
OY94-04-013.00m (white)	O3	dolomite	white carbonate±chalcopyrite vein cutting siltstone
OY94-04-013.00m (tan)	O5	ferroan dolomite	tan carbonate±chalcopyrite vein cutting above vein
OY94-04-021.90m	O3	ankerite	carbonate-quartz-?feldspar vein cutting WBX
OY94-04-038.90m (tan)	O3	dolomite	tan and pink carbonate-quartz-?feldspar vein cutting WBX
OY94-04-038.90m (pink)	O3	ankerite	tan and pink carbonate-quartz-?feldspar vein cutting WBX
OY94-04-067.60m (bx matrix)	O1	dolomite	WBX matrix
OY94-04-067.60m (post bx)	O3	ferroan dolomite	carbonate-quartz vein cutting WBX
OY94-04-089.00m (white)	O2	dolomite	carbonate-quartz-hematite vein cutting fine-grained sediments
OY94-04-089.0m (carb-cp)	O3	ankerite	carbonate-quartz-chalcopyrite vein cutting above vein
Host Wernecke Super Group samp			
Fairchild Lake Group			
DT02-9-2-1		dolomite	carbonate layer
01JH-09-07i		calcite	carbonate band in sediments
01JH-09-07ii		calcite	carbonate band in sediments
01JH-15-03		calcite + rhodochrosite + kutnohorite ..	carbonate-muscovite layer in siltstone
01JH-23-12		calcite	carbonate layer in biotite-altered siltstone
01JH-29-15C		calcite	carbonate layer in siltstone
Quartet Group			
02JH-10-12		ankerite	brown-weathering carbonate layers in QG siltstone overlying foliated breccia
02JH-12-09C		ferroan dolomite	dolostone clast from breccia
02JH-12-14		ferroan dolomite + ankerite	carbonate clast in breccia
JH01 5 5B			carbonaceous shale
JH01 9 5A			carbonaceous shale

Sample ID	Paragenetic Stage	Mineral	Sample Description
JH01 32 4F			carbonaceous shale
Gillespie Lake Group			
CW92-53-01		ferroan dolomite	carbonate layer
DT92-51-1		dolomite	carbonate layer
02JH-04-02		dolomite	orange weathering, fine-grained, grey dolostone (Gillespie Lake Group)
02JH-04-03 (matrix)		dolomite	brecciated dolomite (Gillespie Lake Group)
02JH-04-04		dolomite	Orange weathering, fine-grained, grey dolostone (Gillespie Lake Group)
02JH-06-01 (matrix)		dolomite	brecciated dolomite (Gillespie Lake Group)
02DG-01		ferroan dolomite	Gillespie Lake Group dolostone
02DG-02		ferroan dolomite	Gillespie Lake Group dolostone
02JH-21-01		dolomite	Gillespie Lake Group stromatolitic dolostone
02JH-21-04 (clasts)		dolomite	brecciated dolostone
02JH-21-04 (matrix)		dolomite	brecciated dolostone
02JH-22-03B		dolomite	clast of brecciated dolostone from Wernecke Breccia
02JH-04-03 (clasts)		ankerite	brecciated dolomite (Gillespie Lake Group)

APPENDIX V

Calculations for log fO_2 versus log fS_2 plots

WERNECKE PROJECT LOG fO_2 VERSUS LOG fS_2 PLOTS

log K values were calculated using the programme "The Geochemists Workbench release 4.0.2"
using T=300oC, P=2.5kb and the following equations:

Pyrite-Magnetite: 3 FeS2 + 2 O2(g) = Fe3O4 + 3 S2(g)
Pyrite-Hematite: 4 FeS2 + 3 O2(g) = 2 Fe2O3 + 4 S2 (g)
Pyrrhotite-Magnetite: 6 FeS + 4 O2(g) = 2 Fe3O4 + 3 S2
Bornite-Chalcopyrite: Cu5FeS4 + 4 FeS2 = 5 CuFeS2 + S2
Graphite-CO2(g): C + O2(g) = CO2(g)
Calcite-gypsum: 2 CaCO3 + S2(g) + 3 O2(g) + 4 H2O = 2 CaSO4 + 2 CO2(g)
Witherite-Barite: 2 BaCO3 + S2(g) + 3O2(g) = 2 BaSO4 + 2 CO2(g)
Siderite-Pyrite: FeCO3 + S2(g) = FeS2 + CO2(g) + 0.5O2(g)
Ferrodolomite-(Calcite + Pyrite): (Ca, Fe)2CO3 + S2(g) = CaCO3 + FeS2 + CO2(g) + 0.5 O2(g)
Log K = activity of products - activity of reactants. Assume activity of solid phases = 1; Remember Log 1 = 0

	Log K	**fCO2(g)**
Pyrite-Pyrrhotite; Log fS2 = 2 Log K	-4.6	100
Pyrite-Magnetite; Log fS2 = 0.33 (Log K + 2 Log fO2); Log fO2 = 0.5 (3 Log fS2 - Log K)	33.88	0.01
Pyrite-Hematite; Log fS2 = 0.25 (Log K + 3 Log fO2); Log fO2 = 0.33 (4 Log fS2 - Log K)	55.34	
Pyrrhotite-Magnetite; Log fS2 = 0.33 (Log K + 4 Log fO2); Log fO2 = 0.25 (3 Log fS2 - Log K)	83.64	
Bornite-Chalcopyrite; Log fS2 = Log K	-6.93	
Graphite-CO2(g); Log fO2 = Log f CO2 - Log K	36.13	
Calcite-Gypsum; Log fO2 = 0.33 (2 Log fCO2 - Log fS2 - Log K); Log fS2 = 2 Log fCO2 - 3 Log fO2 - Log K	101.53	
Witherite-Barite; Log fO2 = 0.33 (2 Log fCO2 - Log fS2 - Log K); Log fS2 = 2 Log fCO2 - 3 Log fO2 - Log K	111.29	
Siderite-Pyrite; Log fO2 = 2 (Log fCO2 - Log fS2 - Log K); Log fS2 = Log fCO2 + 0.5 Log fO2 - Log K	-3.74	
Magnetite-Hematite: Log fO2 = -2 Log K	15.25	
Ferrodolomite-Calcite+pyrite: Log fS2 = Log fCO2 + 0.5 Log fO2 - Log K	-3.72	

APPENDIX VI

Calculations for log pH versus logf_{O_2} plots

WERNECKE PROJECT CALCULATION OF $\delta^{34}S_i$ VALUES FOR LOG fO_2 VERSUS pH PLOTS

Fluid Conditions

T =	300oC
P =	2500bars
pH	variable
logfO2(g)	variable
Cl-	2.539
Na	3
K	0.35
Ca	1
H2O	1 (kg)
logaH2S	-2.6
Fe++	0.5

*Estimates of log fO2 and logS2 were made from mineral stability fields on a log fO2 vs log fS2 plot using the mineral assemblage at Slab. Na & Ca values are from Slab fluid inclusion salinity data

Ionic strength =3.2 (calculated for above fluid by GWB)

Conditions for the fluid were fixed at the following conditions in order to be in the H2S dominant field and obtain a concentration for S:
Log fS2 = -8.5
Log fO2 = -31.24 [calculated from: 0.5S2(g) + H2O = 0.5O2(g) + H2S(aq) using Log fS2 = -8.5]
LogaH2S = -2.6 (mid value calculated from range of log fO2 and log fS2 values for the Slab area
pH = 5
This gives a sulphur concentration of 0.0032 (molality) ≈ 75ppm

Examples of molality calculated in "The Geochemists Workbench" programme:

Species	Molality	Mole fraction (X)
NaSO4-	0.6985	0.497
CaSO4(aq)	0.3741	0.266
KSO4-	0.165	0.117
SO4--	0.1623	0.115
H2S(aq)	2.51E-03	0.002
HSO4-	1.54E-03	0.001

HS-	1.30E-03	0.001
NaHS(aq)	5.66E-04	0.000
KHS(aq)	1.52E-05	0.000
KHSO4(aq)	1.04E-05	0.000
S2O3--	5.82E-06	0.000
HSO3-	4.07E-06	0.000
SO2(aq)	6.66E-08	0.000
SO3--	2.54E-08	0.000
S2--	1.21E-08	0.000
Total	1.405851288	

Isotope enrichment factors from Ohmoto (1972):

$\Delta i = \delta^{34}Si - \delta^{34}SH_2S$ ‰

species	**250 oC**	**300 oC**	**350 oC**	**$\delta 34S_{\Sigma S}$ ‰**	
HS-	-1.4	-1.4	-1.3	0	magmatic
S-2	-6.2	-5.5	-4.8	23	middle Proterozoic seawater
SO-2 & other sulphates	26.5	22	19	12	
FeS, ZnS	-1.4	-1.5	-1	17	higest barite value at Igor
FeS2	-0.3	-0.6	-0.2		
PbS	-4.1	-3.8	-2.9		

Examples of δ34Si from the calculated molalities - using the method of Ohmoto (1972):

$\delta^{34}Si = \delta 34S_{\Sigma S} + \Delta i - [(\Delta HS^- * XHS^-) + (\Delta S^{-2} * XS^{-2}) + (\Delta SO4^{-2} * XSO4^{-2}) + (\Delta HSO4- * XHSO4-)$

$+ (\Delta KSO4- * XKSO4-) + (\Delta NaSO4- * XNaSO4-) + (\Delta CaSO4 * XCaSO4)]$

using 300 oC	$\delta^{34}S_{\Sigma S} = 0$‰	$\delta^{34}S_{\Sigma S} = 23$‰	$\delta^{34}S_{\Sigma S} = 12$‰	$\delta^{34}S_{\Sigma S} = 17$‰
δ^{34}Spy	-22.53	0.47	-10.53	-5.53
δ^{34}S HS-	-23.33	-0.33	-11.33	-6.33

δ^{34}S S-2	-27.43	-4.43	-15.43	-10.43
δ^{34}S SO4-2	0.07	23.07	12.07	17.07
δ^{34}S HSO4-2	0.07	23.07	12.07	17.07
δ^{34}S KSO4-	0.07	23.07	12.07	17.07
δ^{34}S NaSO4-	0.07	23.07	12.07	17.07
δ^{34}S CaSO4-	0.07	23.07	12.07	17.07

APPENDIX VII

Rock sample descriptions and locations

Abbreviations used in Appendix VII

Ab = albite
Act = actinolite
Altn = alteration
Aspy = arsenopyrite
Bar = barite
Bor = bornite
Bt = biotite
Bx = breccia
Carb = carbonate
Cbx = crackle breccia
Cc = calcite
Ck = creek
Cl = chlorite
Cpy = chalcopyrite
Dec = decrease
Diss = disseminated
Dt = dolomite
Ep = epidote
Feldspar = feldspar
FG = fine-grained
Fracs = fractures
Ft = fluorite
CG = coarse-grained
Gt = garnet
Hb = hornblende
Ht = hematite
Inc = increase
Ksp = potassium feldspar
Moly = molybdenite
Musc = muscovite
Mt = magnetite
Mtn = mountain
OP = overprint(s) or overprinting
Py = pyrite
Po = pyrrhotite
Qz = quartz
Repl = replaced
Ser = sericite
Slc = siliceous
ss = sandstone
sst = siltstone
Tour = tourmaline
Vlts = veinlets
XC = cross-cutting

JCU #	Sample # or Drill Hole	Depth (m)	Depth (feet)	Location	NTS map sheet	Datum (NAD)	Easting	Northing	Thin Section	Isotopes				Fluid Inclusions	Geochron
										O	C	S	D		
SLAB PROPERTY: DRILL CORE SAMPLES															
70207	SB94-1	1.30	-	Slab Mtn	D/16	27	0545727	7208459	**Y**						
70208	SB94-1	4.29	-	Slab Mtn	D/16	27	0545727	7208459	**Y**						
70209	SB94-1	5.80	-	Slab Mtn	D/16	27	0545727	7208459							
70210	SB94-1	6.90	-	Slab Mtn	D/16	27	0545727	7208459	**Y**						**U-Pb**
70211	SB94-1	9.90	-	Slab Mtn	D/16	27	0545727	7208459		**Y**	**Y**				
70212	SB94-1	10.80	-	Slab Mtn	D/16	27	0545727	7208459							
70213	SB94-1	15.40	-	Slab Mtn	D/16	27	0545727	7208459							
70214	SB94-1	29.10	-	Slab Mtn	D/16	27	0545727	7208459							
70215	SB94-1	31.50	-	Slab Mtn	D/16	27	0545727	7208459							
70216	SB94-1	33.70	-	Slab Mtn	D/16	27	0545727	7208459	**Y**	**Y**	**Y**		**Y**		
70217	SB94-1	41.40	-	Slab Mtn	D/16	27	0545727	7208459							
70218	SB94-1	51.40	-	Slab Mtn	D/16	27	0545727	7208459							
70219	SB94-1	57.43	-	Slab Mtn	D/16	27	0545727	7208459	**Y**						
70220	SB94-1	58.30	-	Slab Mtn	D/16	27	0545727	7208459							
70221	SB94-1	59.50	-	Slab Mtn	D/16	27	0545727	7208459	**Y**						
70222	SB94-1	63.00	-	Slab Mtn	D/16	27	0545727	7208459							
70223	SB94-1	64.90	-	Slab Mtn	D/16	27	0545727	7208459							
70224	SB94-1	70.40	-	Slab Mtn	D/16	27	0545727	7208459							
70225	SB94-1	71.40	-	Slab Mtn	D/16	27	0545727	7208459							
70226	SB94-1	75.80	-	Slab Mtn	D/16	27	0545727	7208459							
70227	SB94-1	77.10	-	Slab Mtn	D/16	27	0545727	7208459							
70228	SB94-1	79.85	-	Slab Mtn	D/16	27	0545727	7208459							
70229	SB94-1	90.50	-	Slab Mtn	D/16	27	0545727	7208459							
70230	SB94-1	91.80	-	Slab Mtn	D/16	27	0545727	7208459							
70231	SB94-1	94.50	-	Slab Mtn	D/16	27	0545727	7208459							
70232	SB94-1	100.00	-	Slab Mtn	D/16	27	0545727	7208459							
70233	SB94-1	128.60	-	Slab Mtn	D/16	27	0545727	7208459	**Y**			**Y**			
70234	SB94-1	129.10	-	Slab Mtn	D/16	27	0545727	7208459							
70235	SB94-1	130.60	-	Slab Mtn	D/16	27	0545727	7208459							

JCU #	Sample # or Drill Hole	Depth (m)	Depth (feet)	Lithology
70207	SB94-1	1.30	-	Carb-Mt bands
70208	SB94-1	4.29	-	Fs vlts, Bt altn & grey-green altn
70209	SB94-1	5.80	-	Carb with Py & Pyrrhotite
70210	SB94-1	6.90	-	Sulphide vein
70211	SB94-1	9.90	-	Carb vein with Musc
70212	SB94-1	10.80	-	Carb-sulphide veinlet
70213	SB94-1	15.40	-	White to pink spots
70214	SB94-1	29.10	-	Aspy
70215	SB94-1	31.50	-	Carb crystals
70216	SB94-1	33.70	-	Carb-Qz-Musc-sulphide vein
70217	SB94-1	41.40	-	Multiple veins
70218	SB94-1	51.40	-	
70219	SB94-1	57.43	-	Bt Cbx
70220	SB94-1	58.30	-	Qz-Fs altn cut by bright white Qz altn & cross-cut by Qz-Fs vlts
70221	SB94-1	59.50	-	Grey slc altn repl by bright white Qz altn
70222	SB94-1	63.00	-	Bright white Qz-Ft vein
70223	SB94-1	64.90	-	Ft veinlet
70224	SB94-1	70.40	-	Carb vein
70225	SB94-1	71.40	-	Grey-green altn
70226	SB94-1	75.80	-	White spots
70227	SB94-1	77.10	-	Sulphide spots
70228	SB94-1	79.85	-	Pink Fs-Qz altn overprinting Bt, Cl-Carb-Cpy-Po, overprinting Fs-Qz, all cut by white Carb vlts
70229	SB94-1	90.50	-	Carb with Cpy & Aspy
70230	SB94-1	91.80	-	Fs altn & Carb-Ft
70231	SB94-1	94.50	-	General lithology
70232	SB94-1	100.00	-	White spots
70233	SB94-1	128.60	-	Py clast
70234	SB94-1	129.10	-	Pale brown spots
70235	SB94-1	130.60	-	Late glassy Qz veins & blebs

JCU #	Sample # or Drill Hole	Depth (m)	Depth (feet)	Location	NTS map sheet	Datum (NAD)	Easting	Northing	Thin Section	Isotopes				Fluid Inclusions	Geochron
										O	C	S	D		
70236	SB94-1	134.30	-	Slab Mtn	D/16	27	0545727	7208459							
70237	SB94-1	137.40	-	Slab Mtn	D/16	27	0545727	7208459							
70238	SB94-1	138.60	-	Slab Mtn	D/16	27	0545727	7208459							
70239	SB94-1	144.60	-	Slab Mtn	D/16	27	0545727	7208459							
70240	SB94-1	146.60	-	Slab Mtn	D/16	27	0545727	7208459							
70241	SB94-1	160.90	-	Slab Mtn	D/16	27	0545727	7208459							
70242	SB94-1	168.10	-	Slab Mtn	D/16	27	0545727	7208459							
70243	SB94-1	178.80	-	Slab Mtn	D/16	27	0545727	7208459							
70244	SB94-1	179.50	-	Slab Mtn	D/16	27	0545727	7208459							
70245	SB94-1	179.70	-	Slab Mtn	D/16	27	0545727	7208459							
70246	SB94-1	186.00	-	Slab Mtn	D/16	27	0545727	7208459							
70247	SB94-1	190.90	-	Slab Mtn	D/16	27	0545727	7208459	**Y**						
70248	SB94-1	198.60	-	Slab Mtn	D/16	27	0545727	7208459	**Y**			**Y**			
70249	SB94-1	202.40	-	Slab Mtn	D/16	27	0545727	7208459							
70250	SB94-1	227.65	-	Slab Mtn	D/16	27	0545727	7208459							
70251	SB94-1	264.50	-	Slab Mtn	D/16	27	0545727	7208459							
70252	SB94-1	270.95	-	Slab Mtn	D/16	27	0545727	7208459							
70253	SB94-1	285.90	-	Slab Mtn	D/16	27	0545727	7208459							
70254	SB94-1	319.00	-	Slab Mtn	D/16	27	0545727	7208459							
70255	SB94-1	332.50	-	Slab Mtn	D/16	27	0545727	7208459	**Y**						
70256	SB94-1	335.60	-	Slab Mtn	D/16	27	0545727	7208459							
70257	SB94-1	345.10	-	Slab Mtn	D/16	27	0545727	7208459	**Y**				**Y**		**Re-Os, Ar-Ar**
70258	SB94-1	345.80	-	Slab Mtn	D/16	27	0545727	7208459							
70259	SB94-1	357.00	-	Slab Mtn	D/16	27	0545727	7208459							
70260	SB94-1	358.10	-	Slab Mtn	D/16	27	0545727	7208459							
70261	SB94-1	358.30	-	Slab Mtn	D/16	27	0545727	7208459	**Y**			**Y**			
70262	SB94-1	364.00	-	Slab Mtn	D/16	27	0545727	7208459							
70263	SB94-1	368.85	-	Slab Mtn	D/16	27	0545727	7208459							
70264	SB94-2	15.90		Slab Mtn	D/16	27	0544765	7208465							
70265	SB94-2	205.10	-	Slab Mtn	D/16	27	0544765	7208465							

JCU #	Sample # or Drill Hole	Depth (m)	Depth (feet)	Lithology
70236	SB94-1	134.30	-	Qz-Fs vein with Moly
70237	SB94-1	137.40	-	Glassy Qz in centre of white Carb vein
70238	SB94-1	138.60	-	Vug lined with Carb crystals + Py + Cpy
70239	SB94-1	144.60	-	Cl spots & vlts
70240	SB94-1	146.60	-	Fs-Qz-Cl-sulphide
70241	SB94-1	160.90	-	Moly in Carb-Cl altn with Py & Cpy
70242	SB94-1	168.10	-	Massive Bt altered rock
70243	SB94-1	178.80	-	Cpy
70244	SB94-1	179.50	-	Mt-Py-Ep
70245	SB94-1	179.70	-	Cpy
70246	SB94-1	186.00	-	Cl-Carb altn replacing Bt
70247	SB94-1	190.90	-	Bright white Qz-Ft vein with Diss Moly & Py
70248	SB94-1	198.60	-	Carb overprinting
70249	SB94-1	202.40	-	Cl-Fs ?-scapolite?-Ep vein cut by white Qz ? Vein with Moly
70250	SB94-1	227.65	-	Qz-Fs-Cpy-Py veins cut by Carb-Qz-Fs ?-Cpy-Py veins +/- Ft
70251	SB94-1	264.50	-	Bt in Carb + veins
70252	SB94-1	270.95	-	Gt??
70253	SB94-1	285.90	-	Bt overprinted by bright white to purple Qz-Ft ?veins with Diss Cpy-Py, cut by chalky white vlts
70254	SB94-1	319.00	-	Typical Bt altn
70255	SB94-1	332.50	-	Bxted sst
70256	SB94-1	335.60	-	Moly in Slc rock
70257	SB94-1	345.10	-	Moly in Carb altn
70258	SB94-1	345.80	-	CG Bt vein
70259	SB94-1	357.00	-	Qz-Ft veins overprinted by Carb-Cl altn & Cpy-Py
70260	SB94-1	358.10	-	Brannerite??
70261	SB94-1	358.30	-	Py
70262	SB94-1	364.00	-	Large Carb crystals in Bt altn
70263	SB94-1	368.85	-	Py overgrowing Carb + altn (wormy texture)
70264	SB94-2	15.90		Bt-Cl altered sst & Fs-Qz altn cross cut by Carb vein
70265	SB94-2	205.10	-	Bt altered sst

JCU #	Sample # or Drill Hole	Depth (m)	Depth (feet)	Location	NTS map sheet	Datum (NAD)	Easting	Northing	Thin Section	Isotopes				Fluid Inclusions	Geochron
										O	C	S	D		
70266	SB94-3	126.85		Slab Mtn	D/16	27	0545784	7208084							
70267	SB94-3	240.75	-	Slab Mtn	D/16	27	0545784	7208084							
70268	SB94-3	283.25	-	Slab Mtn	D/16	27	0545784	7208084							
70269	SB94-4	4.30		Slab Mtn	D/16	27	0545397	7208280							
70270	SB94-4	17.00	-	Slab Mtn	D/16	27	0545397	7208280							
70271	SB94-4	23.70	-	Slab Mtn	D/16	27	0545397	7208280							
70272	SB94-4	32.50	-	Slab Mtn	D/16	27	0545397	7208280							
70273	SB94-4	40.30	-	Slab Mtn	D/16	27	0545397	7208280							
70274	SB94-4	44.00	-	Slab Mtn	D/16	27	0545397	7208280							
70275	SB94-4	45.30	-	Slab Mtn	D/16	27	0545397	7208280							
70276	SB94-4	47.60	-	Slab Mtn	D/16	27	0545397	7208280							
70277	SB94-4	48.40	-	Slab Mtn	D/16	27	0545397	7208280							
70278	SB94-4	53.70	-	Slab Mtn	D/16	27	0545397	7208280							
70279	SB94-4	55.80	-	Slab Mtn	D/16	27	0545397	7208280							
70280	SB94-4	58.50	-	Slab Mtn	D/16	27	0545397	7208280							
70281	SB94-4	62.30	-	Slab Mtn	D/16	27	0545397	7208280							
70282	SB94-4	61.70	-	Slab Mtn	D/16	27	0545397	7208280							
70283	SB94-4	63.70	-	Slab Mtn	D/16	27	0545397	7208280							
70284	SB94-4	63.20	-	Slab Mtn	D/16	27	0545397	7208280							
70285	SB94-4	67.60	-	Slab Mtn	D/16	27	0545397	7208280							
70286	SB94-4	69.60	-	Slab Mtn	D/16	27	0545397	7208280	**Y**						
70287	SB94-4	79.60	-	Slab Mtn	D/16	27	0545397	7208280	**Y**						
70288	SB94-4	108.00	-	Slab Mtn	D/16	27	0545397	7208280							
70289	SB94-4	109.50	-	Slab Mtn	D/16	27	0545397	7208280							
70290	SB94-4	115.40	-	Slab Mtn	D/16	27	0545397	7208280							
70291	SB94-4	125.00	-	Slab Mtn	D/16	27	0545397	7208280							
70292	SB94-4	152.70	-	Slab Mtn	D/16	27	0545397	7208280							
70293	SB94-4	177.60	-	Slab Mtn	D/16	27	0545397	7208280				**Y**			
70294	SB94-4	180.60	-	Slab Mtn	D/16	27	0545397	7208280							
70295	SB94-4	186.80	-	Slab Mtn	D/16	27	0545397	7208280							
70296	SB94-4	187.30	-	Slab Mtn	D/16	27	0545397	7208280							

JCU #	Sample # or Drill Hole	Depth (m)	Depth (feet)	Lithology
70266	SB94-3	126.85		Friable, bleached Bx
70267	SB94-3	240.75	-	Scapolite-bearing calc-silicate
70268	SB94-3	283.25	-	Scapolite-bearing calc-silicate
70269	SB94-4	4.30		Multiple altn stages
70270	SB94-4	17.00	-	Retrograde Cl
70271	SB94-4	23.70	-	White spots overprinting Bt altn, cut by blue-white vlts
70272	SB94-4	32.50	-	Yellow Carb & tan Carb
70273	SB94-4	40.30	-	Yellow Carb altn overprints typical white Carb altn & is overprinted by pale pink Carb
70274	SB94-4	44.00	-	XC veins
70275	SB94-4	45.30	-	Faults
70276	SB94-4	47.60	-	Fs-Cl-Carb veins offset by fractures
70277	SB94-4	48.40	-	White Carb-Qz-Cl overprinting yellow Carb
70278	SB94-4	53.70	-	Bt altn cut by Qz-Bt veins with CG black Bt, overprinted by Py
70279	SB94-4	55.80	-	Grey-purple Qz veins cross cut by white Carb + altn
70280	SB94-4	58.50	-	Grey-purple Qz veins cross cut by bright white Qz-scapolite? Veins
70281	SB94-4	62.30	-	Pervasive Cl
70282	SB94-4	61.70	-	White vlts in fractures offset layers in sst
70283	SB94-4	63.70	-	Sst cut by Qz-Bt veins
70284	SB94-4	63.20	-	CG Bt layers with red Gt? & Ht; also Gt? in or overprinting Qz +/- Bt vlts
70285	SB94-4	67.60	-	Red uranium mineral?
70286	SB94-4	69.60	-	Tension fractures filled with black (Bt?)-Py
70287	SB94-4	79.60	-	White Carb-Qz -Cl -Py cutting bright white Qz/scapolite? veins
70288	SB94-4	108.00	-	CG vuggy Carb-Qz-Cl-Py vein + Gt? + martite?
70289	SB94-4	109.50	-	Fracture with white mineral; fracture with Py & red coating
70290	SB94-4	115.40	-	Bleached section cut by Qz-Fs-Ft veins
70291	SB94-4	125.00	-	Pervasive Bt Altn
70292	SB94-4	152.70	-	Yellow-brown weathering CG Carb vein cuts Carb-Musc-Qz-Cpy altn
70293	SB94-4	177.60	-	CG Carb-Qz-Musc/Cl -Cpy-Py-Bt vein
70294	SB94-4	180.60	-	Anastamosing bright white veins & XC Carb + altn with Cpy
70295	SB94-4	186.80	-	Bleached Cbx
70296	SB94-4	187.30	-	Qz-Bt/Cl flooding

JCU #	Sample # or Drill Hole	Depth (m)	Depth (feet)	Location	NTS map sheet	Datum (NAD)	Easting	Northing	Thin Section	Isotopes				Fluid Inclusions	Geochron
										O	C	S	D		
70297	SB94-4	188.00	-	Slab Mtn	D/16	27	0545397	7208280							
70298	SB94-4	204.60	-	Slab Mtn	D/16	27	0545397	7208280							
70299	SB94-4	217.90	-	Slab Mtn	D/16	27	0545397	7208280							
70300	SB94-4	234.40	-	Slab Mtn	D/16	27	0545397	7208280							
70301	SB94-4	238.10	-	Slab Mtn	D/16	27	0545397	7208280							
70302	SB94-4	243.00	-	Slab Mtn	D/16	27	0545397	7208280							
70303	SB94-4	251.00	-	Slab Mtn	D/16	27	0545397	7208280							
70304	SB94-4	254.70	-	Slab Mtn	D/16	27	0545397	7208280	**Y**						
70305	SB94-4	264.30	-	Slab Mtn	D/16	27	0545397	7208280							
70306	SB94-4	269.00	-	Slab Mtn	D/16	27	0545397	7208280							
70307	SB94-4	273.50	-	Slab Mtn	D/16	27	0545397	7208280							
70308	SB94-4	343.50	-	Slab Mtn	D/16	27	0545397	7208280							
70309	SB95-5	8.70		Slab ck	E/1	27	0544990	7209488	**Y**						
70310	SB95-5	18.70	-	Slab ck	E/1	27	0544990	7209488							
70311	SB95-5	64.60	-	Slab ck	E/1	27	0544990	7209488	**Y**						
70312	SB95-5	72.70	-	Slab ck	E/1	27	0544990	7209488	**Y**						
70313	SB95-5	74.90	-	Slab ck	E/1	27	0544990	7209488	**Y**						
70314	SB95-5	75.10	-	Slab ck	E/1	27	0544990	7209488							
70315	SB95-5	88.30	-	Slab ck	E/1	27	0544990	7209488							
70316	SB95-5	93.65	-	Slab ck	E/1	27	0544990	7209488	**Y**						
70317	SB95-5	107.30	-	Slab ck	E/1	27	0544990	7209488				**Y**			
70318	SB97-9	8.43		Slab ck	E/1	27	0545500	7209490							
70319	SB97-9	8.93	-	Slab ck	E/1	27	0545500	7209490							
70320	SB97-9	13.60	-	Slab ck	E/1	27	0545500	7209490							
70321	SB97-9	18.00	-	Slab ck	E/1	27	0545500	7209490							
70322	SB97-9	23.77	-	Slab ck	E/1	27	0545500	7209490							
70323	SB97-9	24.55	-	Slab ck	E/1	27	0545500	7209490							
70324	SB97-9	25.36	-	Slab ck	E/1	27	0545500	7209490							
70325	SB97-9	25.85	-	Slab ck	E/1	27	0545500	7209490							
70326	SB97-9	26.90	-	Slab ck	E/1	27	0545500	7209490							
70327	SB97-9	30.20	-	Slab ck	E/1	27	0545500	7209490							

JCU #	Sample # or Drill Hole	Depth (m)	Depth (feet)	Lithology
70297	SB94-4	188.00	-	Cpy & Qz crystals in a Qz vein; drusy Qz lining vugs
70298	SB94-4	204.60	-	Bleached rock veined & crackled Bxted by white to cream coloured Fs?
70299	SB94-4	217.90	-	Pale pink Fs? Veins with Cl XC grey-purple Qz & cross cut by Carb-Cl altn
70300	SB94-4	234.40	-	Bx
70301	SB94-4	238.10	-	Bx
70302	SB94-4	243.00	-	Bx
70303	SB94-4	251.00	-	Bx
70304	SB94-4	254.70	-	Bx
70305	SB94-4	264.30	-	Bx
70306	SB94-4	269.00	-	Bx
70307	SB94-4	273.50	-	Bx
70308	SB94-4	343.50	-	Bx
70309	SB95-5	8.70		Carb-Ep altn of sst (beginnings of Cbxtion)
70310	SB95-5	18.70	-	Bt altered sst
70311	SB95-5	64.60	-	Carb-Mt altered Bx
70312	SB95-5	72.70	-	Green rubble Bx with Carb-Mt clasts
70313	SB95-5	74.90	-	Dark matrix Bx with clasts of massive Mt
70314	SB95-5	75.10	-	Dark Bx/Bxted phyllite contact
70315	SB95-5	88.30	-	Cbxted sst with Carb matrix; cut by green Ft
70316	SB95-5	93.65	-	Green rubble Bx with Bt crystals
70317	SB95-5	107.30	-	Massive Mt-Carb overprinted by Py +/- Cpy (in phyllite)
70318	SB97-9	8.43		XC veins
70319	SB97-9	8.93	-	Cpy with Ht
70320	SB97-9	13.60	-	Cpy + Py
70321	SB97-9	18.00	-	XC relationships & Py-Cpy blebs
70322	SB97-9	23.77	-	Slc repl Bt
70323	SB97-9	24.55	-	Ht vein Bxting slc
70324	SB97-9	25.36	-	Slc sst cut by Carb vein
70325	SB97-9	25.85	-	XC Carbs
70326	SB97-9	26.90	-	Carb with Ser
70327	SB97-9	30.20	-	Carb-Mt with rare Cpy

JCU #	Sample # or Drill Hole	Depth (m)	Depth (feet)	Location	NTS map sheet	Datum (NAD)	Easting	Northing	Thin Section	Isotopes				Fluid Inclusions	Geochron
										O	C	S	D		
70328	SB97-9	35.00	-	Slab ck	E/1	27	0545500	7209490							
70329	SB97-9	36.80	-	Slab ck	E/1	27	0545500	7209490							
70330	SB97-9	38.50	-	Slab ck	E/1	27	0545500	7209490							
70331	SB97-9	51.50	-	Slab ck	E/1	27	0545500	7209490	**Y**	**Y**	**Y**	**Y**			
70332	SB97-9	58.65	-	Slab ck	E/1	27	0545500	7209490	**Y**						
70333	SB97-9	61.50	-	Slab ck	E/1	27	0545500	7209490							
70334	SB97-9	65.80	-	Slab ck	E/1	27	0545500	7209490							
70335	SB97-9	73.70	-	Slab ck	E/1	27	0545500	7209490							
70336	SB97-9	81.70	-	Slab ck	E/1	27	0545500	7209490							
70337	SB97-9	86.70	-	Slab ck	E/1	27	0545500	7209490							
70338	SB97-9	93.70	-	Slab ck	E/1	27	0545500	7209490							
70339	SB97-9	94.20	-	Slab ck	E/1	27	0545500	7209490							
70340	SB97-9	94.55	-	Slab ck	E/1	27	0545500	7209490							
70341	SB97-9	98.50	-	Slab ck	E/1	27	0545500	7209490							
70342	SB97-9	99.43	-	Slab ck	E/1	27	0545500	7209490							
70343	SB97-9	99.85	-	Slab ck	E/1	27	0545500	7209490							
70344	SB97-9	107.35	-	Slab ck	E/1	27	0545500	7209490							
70345	SB97-9	111.70	-	Slab ck	E/1	27	0545500	7209490	**Y**						
70346	SB97-9	115.50	-	Slab ck	E/1	27	0545500	7209490							
70347	SB97-9	119.90	-	Slab ck	E/1	27	0545500	7209490		**Y**	**Y**	**Y**			
70348	SB97-9	121.50	-	Slab ck	E/1	27	0545500	7209490							
70349	SB97-9	123.50	-	Slab ck	E/1	27	0545500	7209490							
70350	SB97-9	129.00	-	Slab ck	E/1	27	0545500	7209490							
70351	SB97-9	132.30	-	Slab ck	E/1	27	0545500	7209490							
70352	SB97-9	135.50	-	Slab ck	E/1	27	0545500	7209490							
70353	SB97-9	136.45	-	Slab ck	E/1	27	0545500	7209490							
70354	SB97-9	139.20	-	Slab ck	E/1	27	0545500	7209490							
70355	SB97-9	140.00	-	Slab ck	E/1	27	0545500	7209490	**Y**						
70356	SB97-9	146.50	-	Slab ck	E/1	27	0545500	7209490							
70357	SB97-9	150.80	-	Slab ck	E/1	27	0545500	7209490							

JCU #	Sample # or Drill Hole	Depth (m)	Depth (feet)	Lithology
70328	SB97-9	35.00	-	Ht vein Bxting
70329	SB97-9	36.80	-	XC Carbs
70330	SB97-9	38.50	-	Bt altered sst with Diss Mt xcut by Carb fracs
70331	SB97-9	51.50	-	Bt & slc altered sst cut by Carb-Mt veins. Ht replc Mt & then OP by Py. Trace Diss Cpy intergrown with Py. XC by white Carb veins
70332	SB97-9	58.65	-	CG Carb with Cpy (may not belong here)
70333	SB97-9	61.50	-	Sst with Cpy & CG Carb
70334	SB97-9	65.80	-	Bx & cbx with Ht/Mt matrix
70335	SB97-9	73.70	-	Carb-Mt cut by Ht veins
70336	SB97-9	81.70	-	Sst cut by Qz-Mt veins
70337	SB97-9	86.70	-	Py crystals
70338	SB97-9	93.70	-	Slc sst cbx (tectonic?) with Qz-Mt matrix xcut by Qz-Fs vlts
70339	SB97-9	94.20	-	Bx
70340	SB97-9	94.55	-	Bx-sst lower contact
70341	SB97-9	98.50	-	Cpy & Qz cutting Carb-Mt
70342	SB97-9	99.43	-	"vague" Bx
70343	SB97-9	99.85	-	Ht cutting white Carb & Carb-Mt
70344	SB97-9	107.35	-	Slc Carb-Mt Bxted by Ht
70345	SB97-9	111.70	-	Ht Bx with Cpy & Py
70346	SB97-9	115.50	-	Cpy & Py are intergrown & op Mt.
70347	SB97-9	119.90	-	Ht Bxtion of Carb-Mt altered slc sst. Cpy bleb surrounded by Mt in Carb vein. Cpy blebs in Bx matrix
70348	SB97-9	121.50	-	Ht Bxtion of Carb-Mt altered slc sst. Cpy bleb surrounded by Mt in Carb vein. Cpy blebs in Bx matrix
70349	SB97-9	123.50	-	Pinkish Carb
70350	SB97-9	129.00	-	Dark green Ft
70351	SB97-9	132.30	-	Carb vein
70352	SB97-9	135.50	-	Py-Cpy-Ht vlts
70353	SB97-9	136.45	-	Carb-Mt & Carb-Qz altn
70354	SB97-9	139.20	-	Carb-Mt & Carb-Qz altn
70355	SB97-9	140.00	-	Py + Cpy in fracs, vlts & blebs op Carb-mg
70356	SB97-9	146.50	-	Carb Cbx
70357	SB97-9	150.80	-	Laminated sst xcut by Qz veins

JCU #	Sample # or Drill Hole	Depth (m)	Depth (feet)	Location	NTS map sheet	Datum (NAD)	Easting	Northing	Thin Section	Isotopes				Fluid Inclusions	Geochron
										O	C	S	D		
70358	SB97-9	152.70	-	Slab ck	E/1	27	0545500	7209490							
70359	SB97-9	156.50	-	Slab ck	E/1	27	0545500	7209490	Y						
70360	SB97-9	158.40	-	Slab ck	E/1	27	0545500	7209490							
70361	SB97-9	164.70	-	Slab ck	E/1	27	0545500	7209490							
70362	SB97-9	165.20	-	Slab ck	E/1	27	0545500	7209490							Re-Os
70363	SB97-9	166.10	-	Slab ck	E/1	27	0545500	7209490		Y	Y	Y			
70364	SB97-9	173.20	-	Slab ck	E/1	27	0545500	7209490							
70365	SB97-9	175.25	-	Slab ck	E/1	27	0545500	7209490	Y						
70366	SB97-9	177.55	-	Slab ck	E/1	27	0545500	7209490							
70367	SB97-9	183.80	-	Slab ck	E/1	27	0545500	7209490							
70368	SB97-9	188.10	-	Slab ck	E/1	27	0545500	7209490							
70369	SB97-9	197.12	-	Slab ck	E/1	27	0545500	7209490							
70370	SB97-9	200.10	-	Slab ck	E/1	27	0545500	7209490		Y	Y				
70371	SB97-9	200.30	-	Slab ck	E/1	27	0545500	7209490		Y	Y				
70372	SB97-9	206.00	-	Slab ck	E/1	27	0545500	7209490							
70373	SB97-9	206.50	-	Slab ck	E/1	27	0545500	7209490							
70374	SB97-9	208.50	-	Slab ck	E/1	27	0545500	7209490							
70375	SB97-9	210.00	-	Slab ck	E/1	27	0545500	7209490							
70376	SB97-9	210.10	-	Slab ck	E/1	27	0545500	7209490							
70377	SB97-9	211.10	-	Slab ck	E/1	27	0545500	7209490							
70378	SB97-10	19.40		Slab ck	E/1	27	0544470	7209760	Y						
70379	SB97-10	37.00	-	Slab ck	E/1	27	0544470	7209760							
70380	SB97-10	43.70	-	Slab ck	E/1	27	0544470	7209760				Y			
70381	SB97-11	10.55		Slab ck	E/1	27	0545255	7209490							
70382	SB97-12	23.97		Slab ck	E/1	27	0545560	7209410							
70383	SB97-12	38.35	-	Slab ck	E/1	27	0545560	7209410							
70384	SB97-12	39.50	-	Slab ck	E/1	27	0545560	7209410	Y						
70385	SB97-12	58.30	-	Slab ck	E/1	27	0545560	7209410							
70386	SB97-14	46.20		Slab ck	E/1	27	0545350	7209365	Y						
70387	SB97-14	53.70	-	Slab ck	E/1	27	0545350	7209365	Y						
70388	SB97-16	46.45		Slab ck	E/1	27	0547540	7209860							

JCU #	Sample # or Drill Hole	Depth (m)	Depth (feet)	Lithology
70358	SB97-9	152.70	-	Cl altn
70359	SB97-9	156.50	-	Carb-Cpy vein bxting sst
70360	SB97-9	158.40	-	Vuggy Carb vein with minor Cpy
70361	SB97-9	164.70	-	Sulphide network
70362	SB97-9	165.20	-	Py-Cpy-Mt vein
70363	SB97-9	166.10	-	Massive Mt-Carb op by Py +/- Cpy
70364	SB97-9	173.20	-	Bleached sst
70365	SB97-9	175.25	-	Slc sst op by Carb
70366	SB97-9	177.55	-	Py vein cutting sst
70367	SB97-9	183.80	-	Cpy + Py
70368	SB97-9	188.10	-	Massive white Fs-Carb vein
70369	SB97-9	197.12	-	Py + Cpy
70370	SB97-9	200.10	-	Carb-Mt bxting laminated sst
70371	SB97-9	200.30	-	Tan Carb cut by white Carb vein
70372	SB97-9	206.00	-	Pink & white altn & sulphides
70373	SB97-9	206.50	-	Sulphides in fracs in Slc altn
70374	SB97-9	208.50	-	Laminated sst xcut by Qz+/- Carb veins. Op by tan Carb. Minor sulphide vlts & net texture.
70375	SB97-9	210.00	-	Laminated sst cut by Carb-Mt & white Carb veins
70376	SB97-9	210.10	-	Py & Cpy op Carb-Mt & is xcut by white Carb?
70377	SB97-9	211.10	-	Mt altered to ???
70378	SB97-10	19.40		Bx
70379	SB97-10	37.00	-	Bx
70380	SB97-10	43.70	-	Bx
70381	SB97-11	10.55		Bt altered sst clast in green matrix Bx - "flow texture" in matrix
70382	SB97-12	23.97		Bx
70383	SB97-12	38.35	-	Bx
70384	SB97-12	39.50	-	Bx
70385	SB97-12	58.30	-	Bx
70386	SB97-14	46.20		Friable green Bx
70387	SB97-14	53.70	-	Cbxted sst with Carb matrix
70388	SB97-16	46.45		Bx

JCU #	Sample # or Drill Hole	Depth (m)	Depth (feet)	Location	NTS map sheet	Datum (NAD)	Easting	Northing	Thin Section	Isotopes				Fluid Inclusions	Geochron
										O	C	S	D		
70389	SB97-16	51.40	-	Slab ck	E/1	27	0547540	7209860	Y						
70390	SB97-17	37.00		Slab ck	E/1	27	0545070	7209290							
70391	SB97-19	14.53		Slab ck	E/1	27	0545915	7209110							
70392	SB97-19	17.20	-	Slab ck	E/1	27	0545915	7209110							
70393	SB97-19	21.45	-	Slab ck	E/1	27	0545915	7209110	Y						
70394	SB97-19	25.45	-	Slab ck	E/1	27	0545915	7209110	Y						
70395	SB97-19	27.20	-	Slab ck	E/1	27	0545915	7209110							
70396	SB97-19	27.35	-	Slab ck	E/1	27	0545915	7209110							
70397	SB97-19	30.20	-	Slab ck	E/1	27	0545915	7209110							
70398	SB97-19	30.60	-	Slab ck	E/1	27	0545915	7209110	Y						
70399	SB97-19	34.30	-	Slab ck	E/1	27	0545915	7209110	Y						
70400	SB97-19	37.00	-	Slab ck	E/1	27	0545915	7209110							
70401	SB97-19	44.25	-	Slab ck	E/1	27	0545915	7209110							
70402	SB97-19	46.60	-	Slab ck	E/1	27	0545915	7209110							
70403	SB97-19	62.30	-	Slab ck	E/1	27	0545915	7209110	Y						
70404	SB97-19	65.90	-	Slab ck	E/1	27	0545915	7209110							
70405	SB97-19	68.00	-	Slab ck	E/1	27	0545915	7209110							
70406	SB97-19	70.10	-	Slab ck	E/1	27	0545915	7209110	Y	Y	Y		Y		
SLAB PROPERTY: OUTCROP SAMPLES															
70407	JH01-3-1	-	-	Slab ck	E/1	27	0545915	7209110							
70408	JH01-4-2	-	-	Top Slab Mtn	D/16	27	0545146	7208902							
70409	JH01-4-3	-	-	Slab Mtn	D/16	27	0545146	7208902							
70410	JH01-13-6A	-	-	west end Slab Mtn	D/16	27	0545212	7208361							
70411	JH01-13-7A	-	-	west end Slab Mtn	D/16	27	0545279	7208459							
70412	JH01-13-7B	-	-	west end Slab Mtn	D/16	27	0545343	7208486							
70413	JH01-13-8A	-	-	west end Slab Mtn	D/16	27	0545467	7208412				S			
70414	JH01-13-8B	-	-	west end Slab Mtn	D/16	27	0545467	7208412							
70415	JH01-13-8C	-	-	west end Slab Mtn	D/16	27	0545467	7208412							
70416	JH01-13-8D	-	-	west end Slab Mtn	D/16	27	0545467	7208412							
70417	JH01-13-8E	-	-	west end Slab Mtn	D/16	27	0545467	7208412							
70418	JH01-13-9A	-	-	west end Slab Mtn	D/16	27	0545510	7208412							

JCU #	Sample # or Drill Hole	Depth (m)	Depth (feet)	Lithology
70389	SB97-16	51.40	-	Bx
70390	SB97-17	37.00		Intensely Cl altered? Bx
70391	SB97-19	14.53		Green Bx with varicoloured sst clasts; Mt & Musc in Carb matrix
70392	SB97-19	17.20	-	Sst Cbxted by green Bx matrix
70393	SB97-19	21.45	-	Green Bx similar to 14.53 but less Carb in the matrix
70394	SB97-19	25.45	-	Cl altered clast with pink splotches
70395	SB97-19	27.20	-	Diorite clast ??
70396	SB97-19	27.35	-	Brown matrix in the Bx at the contact with diorite
70397	SB97-19	30.20	-	Diorite?
70398	SB97-19	30.60	-	Ht altered Bx with phyllite clasts
70399	SB97-19	34.30	-	Green Bx cutting Ht altered Bx (may be Ht altn of green Bx) at HW contact of a 3m thick rubble zone
70400	SB97-19	37.00	-	Slc bleached Bx in footwall of rubble zone
70401	SB97-19	44.25	-	Chloritic sst?? Cut by bright white/purple scapolite? veins
70402	SB97-19	46.60	-	Dark green siliceous Bx (dark Bx??)
70403	SB97-19	62.30	-	Bx (Bxtion of massive Mt)
70404	SB97-19	65.90	-	Two phases of Bx
70405	SB97-19	68.00	-	Bx - Carb matrix with lots of Musc (footwall to above Bx)
70406	SB97-19	70.10	-	Rutile (or titanite) in Carb-Qz blebs - possible age of younger Bx phase
70407	JH01-3-1	-	-	White mica from a Carb-Mt vein
70408	JH01-4-2	-	-	Qz-Musc-Ft vein
70409	JH01-4-3	-	-	Bx with Fs & Mt crystals in the matrix
70410	JH01-13-6A	-	-	CG Qz crystals in Qz vein with malachite
70411	JH01-13-7A	-	-	Boudinaged Qz-Py-Cpy vein
70412	JH01-13-7B	-	-	Qz-Carb-Ft-Py vein cutting sst
70413	JH01-13-8A	-	-	Qz-sulphide vein
70414	JH01-13-8B	-	-	Hornfelsed' sst with white spots
70415	JH01-13-8C	-	-	Qz-Carb-sulphide vein with large Qz crystals
70416	JH01-13-8D	-	-	Qz flooding
70417	JH01-13-8E	-	-	Qz-sulphide vein
70418	JH01-13-9A	-	-	Qz-Carb-Py-Cpy-malachite vein

JCU #	Sample # or Drill Hole	Depth (m)	Depth (feet)	Location	NTS map sheet	Datum (NAD)	Easting	Northing	Thin Section	Isotopes				Fluid Inclusions	Geochron
										O	C	S	D		
70419	JH01-13-9B	-	-	west end Slab Mtn	D/16	27	0545510	7208412							
70420	JH01-13-9C	-	-	west end Slab Mtn	D/16	27	0545510	7208412							
70421	JH01-13-9D	-	-	west end Slab Mtn	D/16	27	0545510	7208412							
70422	JH01-13-9E	-	-	west end Slab Mtn	D/16	27	0545510	7208412							
70423	JH01-13-10	-	-	west end Slab Mtn	D/16	27	0545372	7208365	Y						
70424	JH01-15-3	-	-	Slab Ridge	C/13	27	0548802	7207740		Y	Y				
70425	JH01-15-8A	-	-	Slab Ridge	C/13	27	0547731	7208040	Y						
70426	JH01-15-8B	-	-	Slab Ridge	C/13	27	0547731	7208040							
70427	JH01-15-9	-	-	Slab Ridge	C/13	27	0547635	7208141							
70428	JH01-15-10A	-	-	Slab Ridge	C/13	27	0547616	7208166		Y	Y				
70429	JH01-15-10B	-	-	Slab Ridge	C/13	27	0547616	7208166	Y						
70430	JH01-15-10C	-	-	Slab Ridge	C/13	27	0547616	7208166							
70431	JH01-18-1A	-	-	east end Slab ck	D/16	27	0547943	7210043	Y						
70432	JH01-18-1B	-	-	east end Slab ck	D/16	27	0547943	7210043							
70433	JH01-18-1C	-	-	east end Slab ck	D/16	27	0547943	7210043							
70434	JH01-18-2	-	-	south saddle	D/16	27	0546451	7208204	Y						
70435	JH01-19-1	-	-	east end Slab Mtn	D/16	27	0545880	7207549	Y				Y		
70436	JH01-19-2A	-	-	east end Slab Mtn	D/16	27	0545994	7207645	Y						
70437	JH01-19-2B	-	-	east end Slab Mtn	D/16	27	0545994	7207645	Y						
70438	JH01-19-2C	-	-	east end Slab Mtn	D/16	27	0545994	7207645							
70439	JH01-19-2D	-	-	east end Slab Mtn	D/16	27	0545994	7207645		Y	Y				
70440	JH01-19-2E	-	-	east end Slab Mtn	D/16	27	0545994	7207645		Y	Y				
70441	JH01-19-3	-	-	east end Slab Mtn	D/16	27	0545985	7207931							
70442	JH01-19-5A	-	-	east end Slab Mtn	D/16	27	0546239	7207942	Y						
70443	JH01-19-5B	-	-	east end Slab Mtn	D/16	27	0546239	7207942	Y						
70444	JH01-20-2	-	-	west front Slab Mtn	D/16	27	0544747	7208098							
70445	JH01-20-3	-	-	west front Slab Mtn	D/16	27	0544768	7208086	Y				Y		
70446	JH01-20-6A	-	-	west front Slab Mtn	D/16	27	0545007	7208248	Y				Y		
70447	JH01-20-6B	-	-	west front Slab Mtn	D/16	27	0545007	7208248	Y						
70448	JH01-20-6C	-	-	west front Slab Mtn	D/16	27	0545007	7208248							
70449	JH01-20-6D	-	-	west front Slab Mtn	D/16	27	0545007	7208248							

JCU #	Sample # or Drill Hole	Depth (m)	Depth (feet)	Lithology
70419	JH01-13-9B	-	-	Qz-Carb-Py-Cpy vein
70420	JH01-13-9C	-	-	Hornfelsed & Qz flooding
70421	JH01-13-9D	-	-	Qz-Fs-sulphide vein
70422	JH01-13-9E	-	-	Qz-sulphide vein
70423	JH01-13-10	-	-	Rusty weathering sst
70424	JH01-15-3	-	-	Sst with Carb-Musc interbeds
70425	JH01-15-8A	-	-	Bx
70426	JH01-15-8B	-	-	Qz vein clast
70427	JH01-15-9	-	-	Bx with rounded clasts
70428	JH01-15-10A	-	-	Pink Carb vein with Ht blebs
70429	JH01-15-10B	-	-	Piece of large sst clast from contact with pink Carb vein
70430	JH01-15-10C	-	-	Bx from contact with pink Carb vein
70431	JH01-18-1A	-	-	Phyllite
70432	JH01-18-1B	-	-	Sulphide layer
70433	JH01-18-1C	-	-	Qz vein
70434	JH01-18-2	-	-	Bx with phyllite clasts
70435	JH01-19-1	-	-	Qz-Carb-Ht-Bt vein cutting sst clast in Bx
70436	JH01-19-2A	-	-	Qz-Fs altn
70437	JH01-19-2B	-	-	Bx
70438	JH01-19-2C	-	-	Carb clast
70439	JH01-19-2D	-	-	Carb veins in sst clast
70440	JH01-19-2E	-	-	Carb clast
70441	JH01-19-3	-	-	Carb-Qz-Ht vein cutting Bx matrix
70442	JH01-19-5A	-	-	Slc Bx-volcanic contact
70443	JH01-19-5B	-	-	Amygdaloidal Slab Volcanics
70444	JH01-20-2	-	-	Qz-Carb-Ht vein cutting sst clast
70445	JH01-20-3	-	-	Crystalline Qz coating fractures in Bx
70446	JH01-20-6A	-	-	Bx
70447	JH01-20-6B	-	-	Bx
70448	JH01-20-6C	-	-	Bx
70449	JH01-20-6D	-	-	Bx with Carb crystals

JCU #	Sample # or Drill Hole	Depth (m)	Depth (feet)	Location	NTS map sheet	Datum (NAD)	Easting	Northing	Thin Section	Isotopes				Fluid Inclusions	Geochron
										O	C	S	D		
70450	JH01-20-6E	-	-	west front Slab Mtn	D/16	27	0545007	7208248							
70451	JH01-20-6F	-	-	west front Slab Mtn	D/16	27	0545007	7208248		Y	Y				
70452	JH01-20-8	-	-	west front Slab Mtn	D/16	27	0545117	7208209		Y	Y				
70453	JH01-20-9	-	-	west front Slab Mtn	D/16	27	0545201	7208182							
70454	JH01-20-10A	-	-	west front Slab Mtn	D/16	27	0545230	7208182	Y						
70455	JH01-20-10B	-	-	west front Slab Mtn	D/16	27	0545230	7208182							
70456	JH01-20-10C	-	-	west front Slab Mtn	D/16	27	0545230	7208182	Y				Y		
70457	JH01-23-6	-	-	west end Slab Mtn	D/16	27	0544941	7208307							
70458	JH01-23-10A	-	-	west end Slab Mtn	D/16	27	0545103	7208419							
70459	JH01-23-10B	-	-	west end Slab Mtn	D/16	27	0545103	7208419							
70460	JH01-23-10C	-	-	west end Slab Mtn	D/16	27	0545103	7208419							
70461	JH01-23-10D	-	-	west end Slab Mtn	D/16	27	0545103	7208419							
70462	JH01-23-10E	-	-	west end Slab Mtn	D/16	27	0545103	7208419							
70463	JH01-23-10F	-	-	west end Slab Mtn	D/16	27	0545103	7208419							
70464	JH01-23-11A	-	-	west end Slab Mtn	D/16	27	0545173	7208431							
70465	JH01-23-11B	-	-	west end Slab Mtn	D/16	27	0545173	7208431							
70466	JH01-23-11C	-	-	west end Slab Mtn	D/16	27	0545173	7208431							
70467	JH01-23-11D	-	-	west end Slab Mtn	D/16	27	0545173	7208431							
70468	JH01-23-12	-	-	west end Slab Mtn	D/16	27	0545172	7208515		Y	Y				
70469	JH01-23-13	-	-	west end Slab Mtn	D/16	27	0545212	7208598							
70470	JH01-27-1	-	-	centre front Slab Mtn	D/16	27	0545543	7207957	Y						
70471	JH01-27-2A	-	-	centre front Slab Mtn	D/16	27	0545578	7208023							
70472	JH01-27-2B	-	-	centre front Slab Mtn	D/16	27	0545578	7208023	Y						
70473	JH01-27-3A	-	-	centre front Slab Mtn	D/16	27	0545639	7208014							
70474	JH01-27-3B	-	-	centre front Slab Mtn	D/16	27	0545639	7208014							
70475	JH01-27-3C	-	-	centre front Slab Mtn	D/16	27	0545639	7208014							
70476	JH01-27-3D	-	-	centre front Slab Mtn	D/16	27	0545639	7208014				Y			Re-Os, Ar-
70477	JH01-29-1	-	-	Slab Ridge	C/13	27	0547188	7208877							
70478	JH01-29-2A	-	-	Slab Ridge	C/13	27	0547148	7208790							
70479	JH01-29-2B	-	-	Slab Ridge	C/13	27	0547148	7208790		Y	Y				
70480	JH01-29-2C	-	-	Slab Ridge	C/13	27	0547148	7208790		Y	Y				

JCU #	Sample # or Drill Hole	Depth (m)	Depth (feet)	Lithology
70450	JH01-20-6E	-	-	Carb crystals
70451	JH01-20-6F	-	-	Brown weathering Carb crystals
70452	JH01-20-8	-	-	Carb-Qz-Py vein
70453	JH01-20-9	-	-	Bleached & Slc sst at Bx contact
70454	JH01-20-10A	-	-	Slc & rusty sst
70455	JH01-20-10B	-	-	Bleached & chalky sst
70456	JH01-20-10C	-	-	Carb vein with Act & Bt
70457	JH01-23-6	-	-	Bx with silty Dt clasts
70458	JH01-23-10A	-	-	White Carb vein
70459	JH01-23-10B	-	-	Pink Carb crystals
70460	JH01-23-10C	-	-	Qz crystals
70461	JH01-23-10D	-	-	Carb & Qz crystals
70462	JH01-23-10E	-	-	Sst & Carb blebs
70463	JH01-23-10F	-	-	Sst with Py fractures
70464	JH01-23-11A	-	-	Carb-Act Qz vein
70465	JH01-23-11B	-	-	Qz vein
70466	JH01-23-11C	-	-	Sulphide & Slc sst
70467	JH01-23-11D	-	-	Qz crystals
70468	JH01-23-12	-	-	Carb
70469	JH01-23-13	-	-	Sst with white spots
70470	JH01-27-1	-	-	Sst
70471	JH01-27-2A	-	-	Carb layer in sst
70472	JH01-27-2B	-	-	Carb-Tour vein cutting sst
70473	JH01-27-3A	-	-	Sst
70474	JH01-27-3B	-	-	Carb-Cl veins
70475	JH01-27-3C	-	-	Float sample of multiply folded rock
70476	JH01-27-3D	-	-	Qz-Moly-Musc vein
70477	JH01-29-1	-	-	Bx
70478	JH01-29-2A	-	-	Carb-Qz pod
70479	JH01-29-2B	-	-	Carb vein
70480	JH01-29-2C	-	-	Carb Bx

JCU #	Sample # or Drill Hole	Depth (m)	Depth (feet)	Location	NTS map sheet	Datum (NAD)	Easting	Northing	Thin Section	Isotopes				Fluid Inclusions	Geochron
										O	C	S	D		
70481	JH01-29-4	-	-	Slab Ridge	C/13	27	0546973	7208856							
70482	JH01-29-5A	-	-	Slab Ridge	C/13	27	0546912	7208804							
70483	JH01-29-5B	-	-	Slab Ridge	C/13	27	0546912	7208804							
70484	JH01-29-5C	-	-	Slab Ridge	C/13	27	0546912	7208804		**Y**	**Y**				
70485	JH01-29-5D	-	-	Slab Ridge	C/13	27	0546912	7208804							
70486	JH01-29-5E	-	-	Slab Ridge	C/13	27	0546912	7208804							
70487	JH01-29-5F	-	-	Slab Ridge	C/13	27	0546912	7208804							
70488	JH01-29-8A	-	-	Slab Ridge	C/13	27	0546494	7208754							
70489	JH01-29-8B	-	-	Slab Ridge	C/13	27	0546494	7208754							
70490	JH01-29-8C	-	-	Slab Ridge	C/13	27	0546494	7208754							
70490	JH01-29-10	-	-	north side of saddle	D/16	27	0546270	7208710							
70491	JH01-29-12	-	-	north side of saddle	D/16	27	0546013	7208562							
70492	JH01-29-14	-	-	south side of saddle	D/16	27	0545717	7208344							
70493	JH01-29-15A	-	-	Top Slab Mtn	D/16	27	0545830	7208279							
70494	JH01-29-15B	-	-	Top Slab Mtn	D/16	27	0545830	7208279							
70495	JH01-29-15C	-	-	Top Slab Mtn	D/16	27	0545830	7208279		**Y**	**Y**				
70496	JH01-29-15D	-	-	Top Slab Mtn	D/16	27	0545830	7208279				**Y**			
70497	JH01-30-1A	-	-	Saddle south end	D/16	27	0546085	7208185							
70498	JH01-30-1B	-	-	Saddle south end	D/16	27	0546085	7208185							
70499	JH01-30-2A	-	-	Saddle south end	D/16	27	0546049	7208275							
70500	JH01-30-2B	-	-	Saddle south end	D/16	27	0546049	7208275							
70501	JH01-30-2C	-	-	Saddle south end	D/16	27	0546049	7208275							
70502	JH01-30-2D	-	-	Saddle south end	D/16	27	0546049	7208275							
70503	JH01-30-2E	-	-	Saddle south end	D/16	27	0546049	7208275	**Y**						
70504	JH01-30-2F	-	-	Saddle south end	D/16	27	0546049	7208275							
70505	JH01-30-2G	-	-	Saddle south end	D/16	27	0546049	7208275							
70506	JH01-30-4A	-	-	Top Slab Mtn	D/16	27	0545973	7208257							
70507	JH01-30-4B	-	-	Top Slab Mtn	D/16	27	0545973	7208257		**Y**	**Y**				
70508	JH01-30-7A	-	-	Top Slab Mtn	D/16	27	0545980	7208230		**Y**	**Y**				
70509	JH01-30-7B	-	-	Top Slab Mtn	D/16	27	0545980	7208230	**Y**						
70510	JH01-30-7C	-	-	Top Slab Mtn	D/16	27	0545980	7208230							

JCU #	Sample # or Drill Hole	Depth (m)	Depth (feet)	Lithology
70481	JH01-29-4	-	-	White CG Carb vein
70482	JH01-29-5A	-	-	Amygdaloidal Slab Volcanics
70483	JH01-29-5B	-	-	Bxted Slab Volcanics
70484	JH01-29-5C	-	-	Sst Bx with rusty Carb matrix & large Carb crystals
70485	JH01-29-5D	-	-	Vesicular rock
70486	JH01-29-5E	-	-	Diorite?
70487	JH01-29-5F	-	-	Amygdaloidal Slab Volcanics
70488	JH01-29-8A	-	-	Carb-Act-Qz vein
70489	JH01-29-8B	-	-	Carb-Qz
70490	JH01-29-8C	-	-	Altered sst at edge of vein
70490	JH01-29-10	-	-	Kink banded phyllite
70491	JH01-29-12	-	-	Phyllite with blebs & veins of massive white Qz-Cl
70492	JH01-29-14	-	-	Sst
70493	JH01-29-15A	-	-	Qz-Carb-Cpy-Py veins in sst
70494	JH01-29-15B	-	-	Carb-Ft veins in sst
70495	JH01-29-15C	-	-	Carb layer in sst
70496	JH01-29-15D	-	-	Grab sample of Qz-Carb-Cpy veining
70497	JH01-30-1A	-	-	Bx
70498	JH01-30-1B	-	-	Carb in fractures & tension gashes cutting Bx
70499	JH01-30-2A	-	-	Bx
70500	JH01-30-2B	-	-	Original white Qz layer in phyllite - pre Bx
70501	JH01-30-2C	-	-	Pink Qz-Carb vein phyllite
70502	JH01-30-2D	-	-	Qz-Carb-Cl-Musc-Mt vein cutting phyllite
70503	JH01-30-2E	-	-	Altered phyllite with veins
70504	JH01-30-2F	-	-	Highly altered phyllite
70505	JH01-30-2G	-	-	White Fs-Qz vein
70506	JH01-30-4A	-	-	Bleached Bx
70507	JH01-30-4B	-	-	Brown weathering Carb in sst
70508	JH01-30-7A	-	-	Carb, Ft & Qz crystals from Bx matrix
70509	JH01-30-7B	-	-	Bx 20 cm from contact with sst
70510	JH01-30-7C	-	-	Sst-Bx contact

JCU #	Sample # or Drill Hole	Depth (m)	Depth (feet)	Location	NTS map sheet	Datum (NAD)	Easting	Northing	Thin Section	Isotopes				Fluid Inclusions	Geochron
										O	C	S	D		
70511	JH01-30-10	-	-	Slab Mtn north side	D/16	27	0545576	7208588							
70512	JH01-31-1	-	-	Slab Mtn centre front	D/16	27	0545818	7208021							
70513	JH01-31-2	-	-	Slab Mtn centre front	D/16	27	0545914	7207957							
70514	JH01-32-1	-	-	Slab ck west end	E/1	27	0544397	7209415	**Y**						
70515	JH01-32-3	-	-	Slab ck west end	E/1	27	0544522	7209444	**Y**						
70516	JH01-32-4A	-	-	Slab ck west end	E/1	27	0544581	7209481							
70517	JH01-32-4B	-	-	Slab ck west end	E/1	27	0544581	7209481							
70518	JH01-32-4C	-	-	Slab ck west end	E/1	27	0544581	7209481				**Y**			
70519	JH01-32-4D	-	-	Slab ck west end	E/1	27	0544581	7209481		**Y**	**Y**				
70520	JH01-32-4E	-	-	Slab ck west end	E/1	27	0544581	7209481							
70521	JH01-32-4F	-	-	Slab ck west end	E/1	27	0544581	7209481			**Y**				
70522	JH01-32-5A	-	-	Slab ck west end	E/1	27	0544775	7209464	**Y**						
70523	JH01-32-5B	-	-	Slab ck west end	E/1	27	0544775	7209464							
70524	JH01-32-6A	-	-	Slab ck Hindoit zone	E/1	27	0544923	7209504							
70525	JH01-32-6B	-	-	Slab ck Hindoit zone	E/1	27	0544923	7209504		**Y**	**Y**				
70526	JH01-32-7A	-	-	Slab ck Hindoit zone	E/1	27	0545001	7209549		**Y**	**Y**				
70527	JH01-32-7B	-	-	Slab ck Hindoit zone	E/1	27	0545001	7209549							
70528	JH01-32-7C	-	-	Slab ck Hindoit zone	E/1	27	0545001	7209549	**Y**						
70529	JH01-32-7D	-	-	Slab ck Hindoit zone	E/1	27	0545001	7209549				**Y**			
70530	JH01-32-7E	-	-	Slab ck Hindoit zone	E/1	27	0545001	7209549	**Y**						
70531	JH01-34-3	-	-	Slab ck Canyon zone	E/1	27	0545192	7209582	**Y**						
70532	JH01-34-7	-	-	Slab ck Canyon zone	E/1	27	0545446	7209612							
70533	JH01-34-8	-	-	Slab ck Canyon zone	E/1	27	0545411	7209605	**Y**						
70534	JH01-34-10	-	-	Slab ck Canyon zone	E/1	27	0545460	7209631	**Y**						
70535	JH01-34-11A	-	-	Slab ck Canyon zone	E/1	27	0545498	7209644							
70536	JH01-34-11B	-	-	Slab ck Canyon zone	E/1	27	0545498	7209644							
70537	JH01-34-11C	-	-	Slab ck Canyon zone	E/1	27	0545498	7209644		**Y**	**Y**				
70538	JH01-34-11D	-	-	Slab ck Canyon zone	E/1	27	0545498	7209644		**Y**	**Y**				
70539	JH01-34-11E	-	-	Slab ck Canyon zone	E/1	27	0545498	7209644		**Y**	**Y**				
70540	JH01-35-1A	-	-	Slab ck Canyon zone	E/1	27	0545599	7209664							
70541	JH01-35-1B	-	-	Slab ck Canyon zone	E/1	27	0545599	7209664		**Y**	**Y**				

JCU #	Sample # or Drill Hole	Depth (m)	Depth (feet)	Lithology
70511	JH01-30-10	-	-	Bx
70512	JH01-31-1	-	-	Bx
70513	JH01-31-2	-	-	Bx
70514	JH01-32-1	-	-	Unaltered banded grey sst
70515	JH01-32-3	-	-	Banded sst
70516	JH01-32-4A	-	-	Banded sst 70 cm away from Qz-Mt + vein
70517	JH01-32-4B	-	-	Sst 10 cm away from vein contact
70518	JH01-32-4C	-	-	Qz-Carb-Mt-Gt-Py-Bt vein
70519	JH01-32-4D	-	-	Carb-Mt pod
70520	JH01-32-4E	-	-	Sst 1 m below vein
70521	JH01-32-4F	-	-	Sst 20 m upstream
70522	JH01-32-5A	-	-	Brown-grey sst (Bt altered?)
70523	JH01-32-5B	-	-	Float sample of Cbxted folded sst with Carb matrix (like Slab Ridge)
70524	JH01-32-6A	-	-	Dark & light grey sst
70525	JH01-32-6B	-	-	Cbxted sst
70526	JH01-32-7A	-	-	Sst with pink Carb-Cl veins
70527	JH01-32-7B	-	-	Bx
70528	JH01-32-7C	-	-	Micro Bx
70529	JH01-32-7D	-	-	Carb vein
70530	JH01-32-7E	-	-	Carb-Mt Bx
70531	JH01-34-3	-	-	Sst cut by Qz-Cl veins, Mt pophyroblasts
70532	JH01-34-7	-	-	Bx with white Carb matrix
70533	JH01-34-8	-	-	Diorite? or Slab Volcanics?
70534	JH01-34-10	-	-	Sericitized, phyllitic sst with 10% Diss, CG Mt
70535	JH01-34-11A	-	-	Carb-Mt vein
70536	JH01-34-11B	-	-	Sst cut by siliceous veins
70537	JH01-34-11C	-	-	Ser altered sst cut by Qz vein
70538	JH01-34-11D	-	-	Carb vein with two types of Carb
70539	JH01-34-11E	-	-	Bx
70540	JH01-35-1A	-	-	Mt
70541	JH01-35-1B	-	-	Carb from Carb-Mt altn

JCU #	Sample # or Drill Hole	Depth (m)	Depth (feet)	Location	NTS map sheet	Datum (NAD)	Easting	Northing	Thin Section	Isotopes				Fluid Inclusions	Geochron
										O	C	S	D		
70542	JH01-35-1C	-	-	Slab ck Canyon zone	E/1	27	0545599	7209664		Y	Y				
70543	JH01-35-1D	-	-	Slab ck Canyon zone	E/1	27	0545599	7209664							
70544	JH01-35-2	-	-	Slab ck Canyon zone	E/1	27	0545599	7209670	Y	Y	Y		Y		
70545	JH01-35-3A	-	-	Slab ck Canyon zone	E/1	83	0545492	7209860							
70546	JH01-35-3B	-	-	Slab ck Canyon zone	E/1	83	0545492	7209860				Y			
70547	JH01-35-3C	-	-	Slab ck Canyon zone	E/1	83	0545492	7209860							
70548	JH01-35-3D	-	-	Slab ck Canyon zone	E/1	83	0545492	7209860							
70549	JH01-35-4	-	-	Slab ck Canyon zone	E/1	27	0545636	7209684							
70550	JH01-35-5A	-	-	Slab ck Canyon zone	E/1	27	0545636	7209684							
70551	JH01-35-5B	-	-	Slab ck Canyon zone	E/1	27	0545636	7209684		Y	Y				
70552	JH01-35-5C	-	-	Slab ck Canyon zone	E/1	27	0545636	7209684							
70553	JH01-35-5D	-	-	Slab ck Canyon zone	E/1	27	0545636	7209684							
70554	JH01-35-9	-	-	Slab ck Canyon zone	E/1	27	0545755	7209600							
70555	JH01-35-10	-	-	Slab ck Canyon zone	E/1	27	0545692	7209649							
70556	JH01-36-20	-	-	Slab ck Canyon zone	E/1	27	0545631	7209710							
70557	JH01-37-2?	-	-	north side of saddle	D/16	27	0545587	7208979							
70558	JH01-37-3	-	-	north side of saddle	D/16	27	0545514	7209205							
70559	JH01-37-12	-	-	Slab ck Canyon zone	E/1	27	0545860	7209769							
70560	02JH-13-001	-	-	ck between Slab Mtn and Slab ridge	D/16	27	0544746	7208319							
70561	02JH-14-001A	-	-	Slab ck Canyon zone	E/1	27	0545610	7209676	Y				Y		**Ar-Ar**
70562	02JH-14-001B	-	-	Slab ck Canyon zone	E/1	27	0545610	7209676	Y			Y			
70563	02JH-20-002	-	-	Slab ck Canyon zone	E/1		0545610	7209676	Y				Y		**Ar-Ar**
70564	Slab SW	-	-	Slab Mtn	D/16	27	0545372	7208365						Y	
70565	Slab float 1	-	-	Slab	D/16		-	-				Y			
70566	Slab float 2	-	-	Slab	D/16		-	-							
70567	Slab float 3	-	-	Slab	D/16		-	-							
70568	Slab float 4	-	-	Slab	D/16		-	-							
70569	SLAB CREEK 1	-	-	Slab ck	E/1		0545610	7209676	Y						
70570	Marble Breccia	-	-	Slab ck	E/1	27	0545610	7209676	Y						
70571	quartz xtls	-	-	Slab ck Canyon zone	E/1	27	0545610	7209676							

JCU #	Sample # or Drill Hole	Depth (m)	Depth (feet)	Lithology
70542	JH01-35-1C	-	-	Carb-Qz vein cutting Carb-Mt altn
70543	JH01-35-1D	-	-	Cl on fractures & replacing sst (2 pieces)
70544	JH01-35-2	-	-	Bt from rubble Bx matrix. Rubble Bx cuts Carb-Mt altn
70545	JH01-35-3A	-	-	Sulphide vein on fracture cutting sst & Carb-Mt altn. Qz-Musc on vein selvages
70546	JH01-35-3B	-	-	Sulphide veinlet in sst at edge of vein
70547	JH01-35-3C	-	-	Brown banded sst at Bx contact
70548	JH01-35-3D	-	-	Bx cutting Carb-Mt altn & containing Mt clasts
70549	JH01-35-4	-	-	Pink Carb vein cutting Carb-Mt altered siltstone
70550	JH01-35-5A	-	-	Carb-sulphide vein at sst-Bx contact
70551	JH01-35-5B	-	-	Dark Bx cut by Carb-Mt vein
70552	JH01-35-5C	-	-	Bx
70553	JH01-35-5D	-	-	Bx with Mt clast
70554	JH01-35-9	-	-	Contact - pale green Bx cuts dark Bx
70555	JH01-35-10	-	-	Sulphide clast from pale green Bx
70556	JH01-36-20	-	-	Fs-Musc veins cutting Qz-Tour veins in sst
70557	JH01-37-2?	-	-	Phyllite
70558	JH01-37-3	-	-	Bx (2 pieces)
70559	JH01-37-12	-	-	Sst cut by Carb-Mt veins & altn
70560	02JH-13-001	-	-	Float of Bx with sst clasts in a white Carb matrix
70561	02JH-14-001A	-	-	Musc from selvage of Py-Cpy-Qz-Carb-Musc vein cutting Carb-Mt altered seds.
70562	02JH-14-001B	-	-	Py-Cpy-Qz-Carb-Musc vein cutting Carb-Mt altered seds
70563	02JH-20-002	-	-	Bx with abundant Bt in matrix
70564	Slab SW	-	-	Qz crystals used for fluid inclusions (+ calcite xtls + Ft xtls)
70565	Slab float 1	-	-	Bx with Carb matrix & abundant Cpy (fallen from top of slab mtn)
70566	Slab float 2	-	-	Pervasively Bt altered sediments op by scapolite
70567	Slab float 3	-	-	FG sediments with minor sulphides & minor scapolite altn
70568	Slab float 4	-	-	Ab/scapolite altd FG sediments, minor Cpy in Ab-?Qz vein
70569	SLAB CREEK 1	-	-	Scapolite in calc-silicate layers
70570	Marble Breccia	-	-	Deformed sst clasts in Carb matrix = solution bx?
70571	quartz xtls	-	-	Qz crystals

JCU #	Sample # or Drill Hole	Depth (m)	Depth (feet)	Location	NTS map sheet	Datum (NAD)	Easting	Northing	Thin Section	Isotopes				Fluid Inclusions	Geochron
										O	C	S	D		
70572	MBJH01-01-7a	-	-	Slab Mtn north end	E/1	27	0545372	7208365							
70573	MBJH01-03-1b	-	-	Slab Mtn north end	E/1	27	0545372	7208365							
70574	MBJH01-03-9a	-	-	Slab Mtn north end	E/1	27	0545372	7208365							
70575	MBJH01-03-13c	-	-	Slab Mtn north end	E/1	27	0545372	7208365							
70576	MBJH01-04-9a	-	-	Slab Mtn north end	E/1	27	0545372	7208365							
70577	MBJH01-04-10a	-	-	Slab Mtn north end	E/1	27	0545372	7208365							
70578	MBJH01-04-11a	-	-	Slab Mtn north end	E/1	27	0545372	7208365							
HOOVER PROPERTY: DRILL CORE SAMPLES															
70579	HV94-1	2.42	8	Hoover lower slope	E/1	27	0535191.53	7217860							
70580	HV94-1	5.24	17.3	Hoover lower slope	E/1	27	0535191.53	7217860							
70581	HV94-1	6.67	22	Hoover lower slope	E/1	27	0535191.53	7217860							
70582	HV94-1	9.55	31.5	Hoover lower slope	E/1	27	0535191.53	7217860							
70583	HV94-1	10.00	33	Hoover lower slope	E/1	27	0535191.53	7217860							
70584	HV94-1	10.45	34.5	Hoover lower slope	E/1	27	0535191.53	7217860							
70585	HV94-1	10.91	36	Hoover lower slope	E/1	27	0535191.53	7217860				Y			
70586	HV94-1	13.79	45.5	Hoover lower slope	E/1	27	0535191.53	7217860							
70587	HV94-1	13.94	46	Hoover lower slope	E/1	27	0535191.53	7217860							
70588	HV94-1	15.53	51.25	Hoover lower slope	E/1	27	0535191.53	7217860							
70589	HV94-1	16.36	54	Hoover lower slope	E/1	27	0535191.53	7217860							
70590	HV94-1	16.52	54.5	Hoover lower slope	E/1	27	0535191.53	7217860							
70591	HV94-1	16.67	55	Hoover lower slope	E/1	27	0535191.53	7217860							
70592	HV94-1	16.97	56	Hoover lower slope	E/1	27	0535191.53	7217860							
70593	HV94-1	17.27	57	Hoover lower slope	E/1	27	0535191.53	7217860							
70594	HV94-1	19.55	64.5	Hoover lower slope	E/1	27	0535191.53	7217860							
70595	HV94-1	22.42	74	Hoover lower slope	E/1	27	0535191.53	7217860							
70596	HV94-1	22.73	75	Hoover lower slope	E/1	27	0535191.53	7217860							
70597	HV94-1	26.97	89	Hoover lower slope	E/1	27	0535191.53	7217860							
70598	HV94-1	31.52	104	Hoover lower slope	E/1	27	0535191.53	7217860							
70599	HV94-1	31.82	105	Hoover lower slope	E/1	27	0535191.53	7217860							
70600	HV94-1	32.73	108	Hoover lower slope	E/1	27	0535191.53	7217860							
70601	HV94-1	34.55	114	Hoover lower slope	E/1	27	0535191.53	7217860							

JCU #	Sample # or Drill Hole	Depth (m)	Depth (feet)	Lithology
70572	MBJH01-01-7a	-	-	Bx with phyllite clasts & Bt in matrix
70573	MBJH01-03-1b	-	-	Qz-Musc vein
70574	MBJH01-03-9a	-	-	Cl altd seds
70575	MBJH01-03-13c	-	-	Phyllite
70576	MBJH01-04-9a	-	-	Qz xtls
70577	MBJH01-04-10a	-	-	Pink Carb-Act vein
70578	MBJH01-04-11a	-	-	White Carb-Act vein
70579	HV94-1	2.42	8	Qz-Cl vein
70580	HV94-1	5.24	17.3	Sst
70581	HV94-1	6.67	22	Qz vein cutting Qz-Cl vein
70582	HV94-1	9.55	31.5	Chloritic sst with Fs-Qz replacement & cut by Qz-Cl+/-Ht vein
70583	HV94-1	10.00	33	Chloritic sst & Bx with Fs-Qz replacement; Diss Ht in the Bx
70584	HV94-1	10.45	34.5	Bx
70585	HV94-1	10.91	36	Fs-Qz altn along a Bx-sst contact; Py porphyroblasts
70586	HV94-1	13.79	45.5	Fs-Qz flooding & bands of Mt-Carb
70587	HV94-1	13.94	46	Fs-Qz altn?
70588	HV94-1	15.53	51.25	Sst Cbx
70589	HV94-1	16.36	54	Fs-Qz altered sst being replaced by Cl-Qz
70590	HV94-1	16.52	54.5	Contact with Cbx
70591	HV94-1	16.67	55	Bleached contact with Mt
70592	HV94-1	16.97	56	Fs-Qz altered rock with Ht replacing? Mt
70593	HV94-1	17.27	57	Bx cut by Ht & ? vein
70594	HV94-1	19.55	64.5	Gt? + Mt-Cl
70595	HV94-1	22.42	74	Mt porphyroblasts
70596	HV94-1	22.73	75	Phyllite
70597	HV94-1	26.97	89	Carb veinlet cut by Cl veinlet then Cl porphyroblasts
70598	HV94-1	31.52	104	Bx & Qz-Fs altn
70599	HV94-1	31.82	105	Qz-Mt-Ht vein in chloritic sst at contact with Bx
70600	HV94-1	32.73	108	Sst
70601	HV94-1	34.55	114	Qz vein cutting Mt band

JCU #	Sample # or Drill Hole	Depth (m)	Depth (feet)	Location	NTS map sheet	Datum (NAD)	Easting	Northing	Thin Section	Isotopes				Fluid Inclusions	Geochron
										O	C	S	D		
70602	HV94-1	35.15	116	Hoover lower slope	E/1	27	0535191.53	7217860							
70603	HV94-1	36.52	120.5	Hoover lower slope	E/1	27	0535191.53	7217860		**Y**	**Y**				
70604	HV94-1	39.70	131	Hoover lower slope	E/1	27	0535191.53	7217860							
70605	HV94-1	41.21	136	Hoover lower slope	E/1	27	0535191.53	7217860							
70606	HV94-1	43.48	143.5	Hoover lower slope	E/1	27	0535191.53	7217860							
70607	HV94-1	43.64	144	Hoover lower slope	E/1	27	0535191.53	7217860							
70608	HV94-1	43.94	145	Hoover lower slope	E/1	27	0535191.53	7217860							
70609	HV94-1	44.55	147	Hoover lower slope	E/1	27	0535191.53	7217860							
70610	HV94-1	44.70	147.5	Hoover lower slope	E/1	27	0535191.53	7217860							
70611	HV94-1	45.76	151	Hoover lower slope	E/1	27	0535191.53	7217860							
70612	HV94-1	46.36	153	Hoover lower slope	E/1	27	0535191.53	7217860							
70613	HV94-1	46.36	153	Hoover lower slope	E/1	27	0535191.53	7217860							
70614	HV94-1	48.48	160	Hoover lower slope	E/1	27	0535191.53	7217860							
70615	HV94-1	50.00	165	Hoover lower slope	E/1	27	0535191.53	7217860							
70616	HV94-1	55.45	183	Hoover lower slope	E/1	27	0535191.53	7217860							
70617	HV94-1	59.09	195	Hoover lower slope	E/1	27	0535191.53	7217860							
70618	HV94-1	68.79	227	Hoover lower slope	E/1	27	0535191.53	7217860							
70619	HV94-1	70.15	231.5	Hoover lower slope	E/1	27	0535191.53	7217860							
70620	HV94-1	74.24	245	Hoover lower slope	E/1	27	0535191.53	7217860							
70621	HV94-1	75.76	250	Hoover lower slope	E/1	27	0535191.53	7217860							
70622	HV94-1	78.64	259.5	Hoover lower slope	E/1	27	0535191.53	7217860							
70623	HV94-1	80.30	265	Hoover lower slope	E/1	27	0535191.53	7217860							
70624	HV94-1	80.76	266.5	Hoover lower slope	E/1	27	0535191.53	7217860							
70625	HV94-1	81.21	268	Hoover lower slope	E/1	27	0535191.53	7217860							
70626	HV94-1	81.82	270	Hoover lower slope	E/1	27	0535191.53	7217860							
70627	HV94-1	85.15	281	Hoover lower slope	E/1	27	0535191.53	7217860							
70628	HV94-1	85.76	283	Hoover lower slope	E/1	27	0535191.53	7217860							
70629	HV94-1	87.76	289.6	Hoover lower slope	E/1	27	0535191.53	7217860							
70630	HV94-1	87.88	290	Hoover lower slope	E/1	27	0535191.53	7217860							
70631	HV94-1	90.61	299	Hoover lower slope	E/1	27	0535191.53	7217860							
70632	HV94-1	90.91	300	Hoover lower slope	E/1	27	0535191.53	7217860							

JCU #	Sample # or Drill Hole	Depth (m)	Depth (feet)	Lithology
70602	HV94-1	35.15	116	Qz-Cl vein cutting folded sst
70603	HV94-1	36.52	120.5	Carb-Mt vein
70604	HV94-1	39.70	131	Fs-Qz vein cutting Carb veins that cut Cl-Mt altn
70605	HV94-1	41.21	136	Altered sst
70606	HV94-1	43.48	143.5	Sst Cbx
70607	HV94-1	43.64	144	Carb vein
70608	HV94-1	43.94	145	Carb-Cl vlts cutting Fs-Qz altered Cbxted sst with Ht
70609	HV94-1	44.55	147	Cl-Mt Carb altn replaced by Fs-Qz altn
70610	HV94-1	44.70	147.5	Pink staining
70611	HV94-1	45.76	151	Cl-Mt-Carb altn cut by Carb vein
70612	HV94-1	46.36	153	Chloritic phyllite
70613	HV94-1	46.36	153	Cl-Mt-Carb altn
70614	HV94-1	48.48	160	Cl-Mt altn cut by sulphide veinlet
70615	HV94-1	50.00	165	Cl replacing sst clasts
70616	HV94-1	55.45	183	Folded sst with flattened Mt porphyroblasts
70617	HV94-1	59.09	195	Qz-Fs vlts in sst
70618	HV94-1	68.79	227	Sst Cbx
70619	HV94-1	70.15	231.5	Fs-Qz altn?
70620	HV94-1	74.24	245	Banded sst
70621	HV94-1	75.76	250	Christmas tree altn around Qz-Fs veins
70622	HV94-1	78.64	259.5	Folded sst
70623	HV94-1	80.30	265	Cbx
70624	HV94-1	80.76	266.5	Pink spots
70625	HV94-1	81.21	268	Carb vein
70626	HV94-1	81.82	270	Mt veins & blebs
70627	HV94-1	85.15	281	Mt needles in Carb vein
70628	HV94-1	85.76	283	Bx clasts; Ht
70629	HV94-1	87.76	289.6	Bx
70630	HV94-1	87.88	290	Sst with Diss Ht being replaced by Fs-Qz altn
70631	HV94-1	90.61	299	Sst with Fs-Qz altn cut by Qz-Cl veins & Cl-Qz+/-malachite fractures
70632	HV94-1	90.91	300	Qz-Carb lined vugs

JCU #	Sample # or Drill Hole	Depth (m)	Depth (feet)	Location	NTS map sheet	Datum (NAD)	Easting	Northing	Thin Section	Isotopes				Fluid Inclusions	Geochron
										O	C	S	D		
70633	HV94-1	92.12	304	Hoover lower slope	E/1	27	0535191.53	7217860							
70634	HV94-1	93.03	307	Hoover lower slope	E/1	27	0535191.53	7217860							
70635	HV94-1	95.52	315.2	Hoover lower slope	E/1	27	0535191.53	7217860							
70636	HV94-1	96.36	318	Hoover lower slope	E/1	27	0535191.53	7217860							
70637	HV94-1	96.97	320	Hoover lower slope	E/1	27	0535191.53	7217860							
70638	HV94-1	98.79	326	Hoover lower slope	E/1	27	0535191.53	7217860							
70639	HV94-1	101.82	336	Hoover lower slope	E/1	27	0535191.53	7217860							
70640	HV94-1	106.67	352	Hoover lower slope	E/1	27	0535191.53	7217860							
70641	HV94-1	108.64	358.5	Hoover lower slope	E/1	27	0535191.53	7217860							
70642	HV94-1	110.85	365.8	Hoover lower slope	E/1	27	0535191.53	7217860							
70643	HV94-1	122.79	405.2	Hoover lower slope	E/1	27	0535191.53	7217860							
70644	HV94-1	124.55	411	Hoover lower slope	E/1	27	0535191.53	7217860							
70645	HV94-1	126.36	417	Hoover lower slope	E/1	27	0535191.53	7217860							
70646	HV94-1	129.09	426	Hoover lower slope	E/1	27	0535191.53	7217860							
70647	HV94-1	131.21	433	Hoover lower slope	E/1	27	0535191.53	7217860							
70648	HV94-1	134.55	444	Hoover lower slope	E/1	27	0535191.53	7217860							
70649	HV94-1	141.52	467	Hoover lower slope	E/1	27	0535191.53	7217860							
70650	HV94-1	142.73	471	Hoover lower slope	E/1	27	0535191.53	7217860							
70651	HV94-1	146.67	484	Hoover lower slope	E/1	27	0535191.53	7217860							
70652	HV94-1	148.18	489	Hoover lower slope	E/1	27	0535191.53	7217860							
70653	HV94-1	149.85	494.5	Hoover lower slope	E/1	27	0535191.53	7217860							
70654	HV94-1	152.42	503	Hoover lower slope	E/1	27	0535191.53	7217860							
70655	HV94-1	153.73	507.3	Hoover lower slope	E/1	27	0535191.53	7217860		**Y**	**Y**	**Y**			
70656	HV94-1	155.30	512.5	Hoover lower slope	E/1	27	0535191.53	7217860							
70657	HV94-1	156.36	516	Hoover lower slope	E/1	27	0535191.53	7217860							
70658	HV94-1	157.58	520	Hoover lower slope	E/1	27	0535191.53	7217860							
70659	HV94-1	158.33	522.5	Hoover lower slope	E/1	27	0535191.53	7217860							
70660	HV94-1	160.61	530	Hoover lower slope	E/1	27	0535191.53	7217860							
70661	HV94-1	163.03	538	Hoover lower slope	E/1	27	0535191.53	7217860							
70662	HV94-1	165.61	546.5	Hoover lower slope	E/1	27	0535191.53	7217860							
70663	HV94-1	168.18	555	Hoover lower slope	E/1	27	0535191.53	7217860							

JCU #	Sample # or Drill Hole	Depth (m)	Depth (feet)	Lithology
70633	HV94-1	92.12	304	Sst
70634	HV94-1	93.03	307	Bt? overprinting Fs-Qz altn & Qz-Cl veins
70635	HV94-1	95.52	315.2	Qz-Ft? vein cutting Fs-Qz altn
70636	HV94-1	96.36	318	Vug with Qz-sulphide; malachite
70637	HV94-1	96.97	320	Bx intruding chloritic phyllite; Fs-Qz altn
70638	HV94-1	98.79	326	Christmas tree altn around Qz-Fs veins
70639	HV94-1	101.82	336	Qz-Cl+/-Carb veins cutting chloritic phyllite
70640	HV94-1	106.67	352	Chloritic phyllite
70641	HV94-1	108.64	358.5	Qz+/-Ft? Vein cutting folded Qz-Cl vein
70642	HV94-1	110.85	365.8	Mt blebs; Qz vug
70643	HV94-1	122.79	405.2	Mt porphyroblasts in chloritic phyllite
70644	HV94-1	124.55	411	Vuggy Qz-Fs-Carb vein +/- cpy, po, py
70645	HV94-1	126.36	417	Vuggy Qz-Ht vein
70646	HV94-1	129.09	426	Qz-Ht vein cutting phyllite with Mt porphyroblasts
70647	HV94-1	131.21	433	Early Qz-Mt-Cl vein
70648	HV94-1	134.55	444	Phyllite with Mt porphyroblasts overprinted by Cl-Mt altn & cut by Qz-Carb vein
70649	HV94-1	141.52	467	Qz-Carb tension veins
70650	HV94-1	142.73	471	Qz-Mt vein
70651	HV94-1	146.67	484	Qz-Ht veins cut by Carb veins
70652	HV94-1	148.18	489	Mt blebs parallel to foliation, Qz-Carb veins, tan spots
70653	HV94-1	149.85	494.5	Carb vein cutting sst
70654	HV94-1	152.42	503	Slc rock cut by Carb vein
70655	HV94-1	153.73	507.3	Bxted & bleached sst cut by Carb vein & Py bleb
70656	HV94-1	155.30	512.5	30 cm thick Carb vein
70657	HV94-1	156.36	516	Slc Carb veined sst
70658	HV94-1	157.58	520	Carb vein & siliceous rock
70659	HV94-1	158.33	522.5	Orange & black sst & Qz-Ht-Cu vein
70660	HV94-1	160.61	530	Qz veins following crenulation axes
70661	HV94-1	163.03	538	Cbx
70662	HV94-1	165.61	546.5	Musc-Cl replacing sst clasts
70663	HV94-1	168.18	555	XC Qz-Py-Cpy fractures & blebs

JCU #	Sample # or Drill Hole	Depth (m)	Depth (feet)	Location	NTS map sheet	Datum (NAD)	Easting	Northing	Thin Section	Isotopes				Fluid Inclusions	Geochron
										O	C	S	D		
70664	HV94-1	169.70	560	Hoover lower slope	E/1	27	0535191.53	7217860							
70665	HV94-1	171.52	566	Hoover lower slope	E/1	27	0535191.53	7217860							
70666	HV94-1	174.09	574.5	Hoover lower slope	E/1	27	0535191.53	7217860							
70667	HV94-1	175.15	578	Hoover lower slope	E/1	27	0535191.53	7217860							
70668	HV94-1	177.12	584.5	Hoover lower slope	E/1	27	0535191.53	7217860							
70669	HV94-1	180.45	595.5	Hoover lower slope	E/1	27	0535191.53	7217860							
70670	HV94-1	181.36	598.5	Hoover lower slope	E/1	27	0535191.53	7217860							
70671	HV94-1	181.70	599.6	Hoover lower slope	E/1	27	0535191.53	7217860				**Y**			
70672	HV94-1	182.27	601.5	Hoover lower slope	E/1	27	0535191.53	7217860							
70673	HV94-1	183.42	605.3	Hoover lower slope	E/1	27	0535191.53	7217860							
70674	HV94-1	185.61	612.5	Hoover lower slope	E/1	27	0535191.53	7217860							
70675	HV94-1	190.30	628	Hoover lower slope	E/1	27	0535191.53	7217860							
70676	HV94-1	190.76	629.5	Hoover lower slope	E/1	27	0535191.53	7217860							
70677	HV94-1	194.70	642.5	Hoover lower slope	E/1	27	0535191.53	7217860		**Y**	**Y**				
70678	HV94-1	196.21	647.5	Hoover lower slope	E/1	27	0535191.53	7217860							
70679	HV94-1	196.67	649	Hoover lower slope	E/1	27	0535191.53	7217860							
70680	HV94-1	196.97	650	Hoover lower slope	E/1	27	0535191.53	7217860		**Y**	**Y**				
70681	HV94-1	198.55	655.2	Hoover lower slope	E/1	27	0535191.53	7217860							
70682	HV94-1	199.09	657	Hoover lower slope	E/1	27	0535191.53	7217860							
70683	HV94-1	199.39	658	Hoover lower slope	E/1	27	0535191.53	7217860							
70684	HV94-1	202.12	667	Hoover lower slope	E/1	27	0535191.53	7217860							
70685	HV94-1	209.45	691.2	Hoover lower slope	E/1	27	0535191.53	7217860							
70686	HV94-1	210.61	695	Hoover lower slope	E/1	27	0535191.53	7217860	**Y**				**Y**		
70687	HV94-1	213.18	703.5	Hoover lower slope	E/1	27	0535191.53	7217860							
70688	HV94-1	216.97	716	Hoover lower slope	E/1	27	0535191.53	7217860							
70689	HV94-1	217.88	719	Hoover lower slope	E/1	27	0535191.53	7217860							
70690	HV94-1	222.52	734.3	Hoover lower slope	E/1	27	0535191.53	7217860							
70691	HV94-1	222.58	734.5	Hoover lower slope	E/1	27	0535191.53	7217860							
70692	HV94-1	226.52	747.5	Hoover lower slope	E/1	27	0535191.53	7217860							
70693	HV94-1	230.00	759	Hoover lower slope	E/1	27	0535191.53	7217860							
70694	HV94-1	241.36	796.5	Hoover lower slope	E/1	27	0535191.53	7217860							

JCU #	Sample # or Drill Hole	Depth (m)	Depth (feet)	Lithology
70664	HV94-1	169.70	560	Fs-Cl altered Bx
70665	HV94-1	171.52	566	Carb-Mt altered Bx
70666	HV94-1	174.09	574.5	Cbx
70667	HV94-1	175.15	578	Fs-Mt altered Bx
70668	HV94-1	177.12	584.5	Fs-Qz altered Bx cut by Carb fractures
70669	HV94-1	180.45	595.5	Bx
70670	HV94-1	181.36	598.5	Carb-Mt +/- Py vein
70671	HV94-1	181.70	599.6	Carb-Cl-Py-Cpy vein
70672	HV94-1	182.27	601.5	Patchy silicification
70673	HV94-1	183.42	605.3	Carb-Mt altn
70674	HV94-1	185.61	612.5	Ht-Carb flooding
70675	HV94-1	190.30	628	Sst-Bx contact
70676	HV94-1	190.76	629.5	Sst clasts with Carb pophyroblasts
70677	HV94-1	194.70	642.5	Carb Bxting sst clasts
70678	HV94-1	196.21	647.5	Bxtion process
70679	HV94-1	196.67	649	Bxtion process
70680	HV94-1	196.97	650	Carb-Cpy veinlet cutting sst clast & offsetting layers
70681	HV94-1	198.55	655.2	Py blebs
70682	HV94-1	199.09	657	Cpy blebs
70683	HV94-1	199.39	658	Sst clast
70684	HV94-1	202.12	667	Overprinting relationships
70685	HV94-1	209.45	691.2	Fs-Qz overprinted by Cl & Mt-Carb
70686	HV94-1	210.61	695	Bt porphyroblasts
70687	HV94-1	213.18	703.5	Fs-Qz & Ser altn
70688	HV94-1	216.97	716	Qz-py-Carb-Mt vein
70689	HV94-1	217.88	719	Diorite contact with Qz-Fs altered phyllite
70690	HV94-1	222.52	734.3	Carb-sulphide vlts
70691	HV94-1	222.58	734.5	Qz-cl vein cut by Mt veinlet
70692	HV94-1	226.52	747.5	Patches of Mt (+/- Ht)- Cpy-Qz
70693	HV94-1	230.00	759	Mt porphyroblasts & Cl-Py-Mt vlts
70694	HV94-1	241.36	796.5	Fs-Mt +/-Ht-Py-Carb

JCU #	Sample # or Drill Hole	Depth (m)	Depth (feet)	Location	NTS map sheet	Datum (NAD)	Easting	Northing	Thin Section	Isotopes				Fluid Inclusions	Geochron
										O	C	S	D		
70695	HV94-1	244.70	807.5	Hoover lower slope	E/1	27	0535191.53	7217860							
70696	HV94-1	260.00	858	Hoover lower slope	E/1	27	0535191.53	7217860							
70697	HV94-1	261.82	864	Hoover lower slope	E/1	27	0535191.53	7217860							
70698	HV94-1	266.67	880	Hoover lower slope	E/1	27	0535191.53	7217860							
70699	HV94-1	283.76	936.4	Hoover lower slope	E/1	27	0535191.53	7217860				**Y**			
70700	HV94-1	299.39	988	Hoover lower slope	E/1	27	0535191.53	7217860							
70701	HV94-1	304.55	1005	Hoover lower slope	E/1	27	0535191.53	7217860							
70702	HV94-1	315.15	1040	Hoover lower slope	E/1	27	0535191.53	7217860							
70703	HV94-1	317.88	1049	Hoover lower slope	E/1	27	0535191.53	7217860							
70704	HV94-1	325.91	1075.5	Hoover lower slope	E/1	27	0535191.53	7217860							
70705	HV94-3	1.82 m		Hoover lower slope	E/1	27	0535552.78	7216989							
70706	HV94-3	2.6 m	-	Hoover lower slope	E/1	27	0535552.78	7216989							
70707	HV94-3	6.4 m	-	Hoover lower slope	E/1	27	0535552.78	7216989							
70708	HV94-3	13.85	-	Hoover lower slope	E/1	27	0535552.78	7216989							
70709	HV94-3	29.30	-	Hoover lower slope	E/1	27	0535552.78	7216989							
70710	HV94-3	35.60	-	Hoover lower slope	E/1	27	0535552.78	7216989							
70711	HV94-3	61.00	-	Hoover lower slope	E/1	27	0535552.78	7216989							
70712	HV94-3	64.10	-	Hoover lower slope	E/1	27	0535552.78	7216989							
70713	HV94-3	69.60	-	Hoover lower slope	E/1	27	0535552.78	7216989							
70714	HV94-3	101.50	-	Hoover lower slope	E/1	27	0535552.78	7216989							
70715	HV94-3	104.80	-	Hoover lower slope	E/1	27	0535552.78	7216989							
70716	HV94-3	124.80	-	Hoover lower slope	E/1	27	0535552.78	7216989							
70717	HV94-3	143.25	-	Hoover lower slope	E/1	27	0535552.78	7216989							
70718	HV94-3	154.80	-	Hoover lower slope	E/1	27	0535552.78	7216989							
70719	HV94-3	176.70	-	Hoover lower slope	E/1	27	0535552.78	7216989							
70720	HV94-3	177.10	-	Hoover lower slope	E/1	27	0535552.78	7216989							
70721	HV94-3	201.60	-	Hoover lower slope	E/1	27	0535552.78	7216989							
HOOVER AREA: OUTCROP SAMPLES															
70722	JH01-5-5A	-	-	Top of Radio ck	E/1	27	0535567	7220398	**Y**						
70723	JH01-5-5B	-	-	Top of Radio ck	E/1	27	0535567	7220398			**Y**				
70724	JH01-5-7A	-	-	Top of Radio ck	E/1	27	0536396	7218147						**Y**	

JCU #	Sample # or Drill Hole	Depth (m)	Depth (feet)	Lithology
70695	HV94-1	244.70	807.5	General lithology
70696	HV94-1	260.00	858	White porphyroblasts
70697	HV94-1	261.82	864	Qz-Cl-Fs-Bt vein
70698	HV94-1	266.67	880	Boudinaged Qz-Cl-Py-Cpy vein
70699	HV94-1	283.76	936.4	White spots & Qz-Cl vein
70700	HV94-1	299.39	988	White spots & Cl porphyroblasts
70701	HV94-1	304.55	1005	Cl-Aspy-Cpy vlt
70702	HV94-1	315.15	1040	Bt? Porphyroblasts
70703	HV94-1	317.88	1049	Chloritic sst Bxted by pink & white Fs-Qz veins +/- Py
70704	HV94-1	325.91	1075.5	General lithology
70705	HV94-3	1.82 m		Cl altered sst + tan Carb veins + Mt-Carb-Bt altn + sulphide's
70706	HV94-3	2.6 m	-	Carb-Mt veins cut by pink Fs-Qz veins
70707	HV94-3	6.4 m	-	Tan Carb vein with large Qz xtls
70708	HV94-3	13.85	-	Sulphide's op Mt & Fs-Qz veins; sulphide's in Mt grains
70709	HV94-3	29.30	-	Gt porphyroblasts op Mt & cut by white Carb vein
70710	HV94-3	35.60	-	Gt porphyroblasts
70711	HV94-3	61.00	-	Sulphide's replacing Mt
70712	HV94-3	64.10	-	Gt + Bt + Qz in Carb
70713	HV94-3	69.60	-	Sulphide's replacing Ht replacing Mt
70714	HV94-3	101.50	-	Altered marble Bx
70715	HV94-3	104.80	-	Po & Aspy with sulphide's; Musc? with Carb-Cl altn
70716	HV94-3	124.80	-	Clear pink Ft? cutting white Carb-Cl veins & sulphide's
70717	HV94-3	143.25	-	Ht needles overprinting sulphide's
70718	HV94-3	154.80	-	Sulphide's in fracture network; white Carb-Cl & XC pink Ft
70719	HV94-3	176.70	-	Bt altn causing Bxtion of sst; Bt matrix replaced by white Carb
70720	HV94-3	177.10	-	Sulphide's op white Carb in matrix
70721	HV94-3	201.60	-	White Carb vein with Cpy, Py, Ser, Gt
70722	JH01-5-5A	-	-	Sst
70723	JH01-5-5B	-	-	Slate
70724	JH01-5-7A	-	-	Bx

JCU #	Sample # or Drill Hole	Depth (m)	Depth (feet)	Location	NTS map sheet	Datum (NAD)	Easting	Northing	Thin Section	Isotopes				Fluid Inclusions	Geochron
										O	C	S	D		
70725	JH01-5-7B	-	-	Top of Radio ck	E/1	27	0536396	7218147							
70726	JH01-5-7C	-	-	Top of Radio ck	E/1	27	0536396	7218147	Y						
70727	JH01-6-1A	-	-	old workings	E/1	27	0535032	7217710	Y						
70728	JH01-6-1B	-	-	old workings	E/1	27	0535032	7217710	Y						
70729	JH01-6-1C	-	-	old workings	E/1	27	0535032	7217710	Y						
70730	JH01-6-1D	-	-	old workings	E/1	27	0535032	7217710							
70731	JH01-6-1E	-	-	old workings	E/1	27	0535032	7217710							
70732	JH01-6-3A	-	-	lower slope	E/1	27	0535307	7217620							
70733	JH01-6-3B	-	-	lower slope	E/1	27	0535307	7217620	Y						
70734	JH01-6-3C	-	-	lower slope	E/1	27	0535307	7217620	Y						
70735	JH01-6-4A	-	-	lower slope	E/1	27	0535354	7217602							
70736	JH01-6-5A	-	-	old workings	E/1	27	0535032	7217710							
70737	JH01-6-5B	-	-	old workings	E/1	27	0535032	7217710	Y						
70738	JH01-6-5C	-	-	old workings	E/1	27	0535032	7217710							
70739	JH01-7-1A	-	-	lower slope	E/1	27	0535054	7217625				Y			
70740	JH01-7-1B	-	-	lower slope	E/1	27	0535054	7217625							
70741	JH01-7-1C	-	-	lower slope	E/1	27	0535054	7217625	Y						
70742	JH01-7-5A	-	-	middle slope	E/1	27	0535583	7217672							
70743	JH01-7-6A	-	-	middle slope	E/1	27	0535629	7217687	Y						
70744	JH01-7-11A	-	-	upper slope	E/1	27	0535946	7218158		Y	Y				
70745	JH01-7-11B	-	-	upper slope	E/1	27	0535946	7218158				Y			
70746	JH01-7-11C	-	-	upper slope	E/1	27	0535946	7218158							
70747	JH01-7-12A	-	-	upper slope	E/1	27	0535999	7218235		Y	Y				
70748	JH01-7-13A	-	-	upper slope	E/1	27	0536025	7218296	Y						
70749	JH01-7-16	-	-	middle slope	E/1	27	0535242	7218235							
70750	JH01-8-1A	-	-	lower slope	E/1	27	0535093	7217505	Y						
70751	JH01-8-1B	-	-	lower slope	E/1	27	0535093	7217505							
70752	JH01-8-2	-	-	lower slope	E/1	27	0535140	7217436	Y				Y		
70753	JH01-8-3A	-	-	lower slope	E/1	27	0535171	7217429							
70754	JH01-8-6A	-	-	lower slope	E/1	27	0535315	7217346							
70755	JH01-8-7A	-	-	lower slope	E/1	27	0535401	7217428		Y	Y				

JCU #	Sample # or Drill Hole	Depth (m)	Depth (feet)	Lithology
70725	JH01-5-7B	-	-	Cbxted sst
70726	JH01-5-7C	-	-	Slate with spots
70727	JH01-6-1A	-	-	Clast supported Bx
70728	JH01-6-1B	-	-	Sulphides in Cl altn
70729	JH01-6-1C	-	-	Black sulphide clast
70730	JH01-6-1D	-	-	Clast of black sulphide in Bx
70731	JH01-6-1E	-	-	Mt crystals in Carb vein
70732	JH01-6-3A	-	-	Diorite at contact with Bx
70733	JH01-6-3B	-	-	Diorite 4 m from contact with Bx
70734	JH01-6-3C	-	-	Bx at diorite contact
70735	JH01-6-4A	-	-	Qz vein cutting Qz-Fs altered sst
70736	JH01-6-5A	-	-	Float of coarsely crystalline Carb vein cutting Bx
70737	JH01-6-5B	-	-	Float of coarsely crystalline Carb vein with pods of sulphide
70738	JH01-6-5C	-	-	Float of white Qz vein with blebs of sulphide, Tour?
70739	JH01-7-1A	-	-	Qz-Fs-Carb veins at contact between a large sst clast & Bx. Later Cpy, malachite & Ht in pods in the vein
70740	JH01-7-1B	-	-	Qz-Fs veins within a sst clast
70741	JH01-7-1C	-	-	Muscovite
70742	JH01-7-5A	-	-	Qz-Carb-Cl-Ht vein parallel to layering in black slate (boudinaged)
70743	JH01-7-6A	-	-	10 m thick Carb band - marker horizon
70744	JH01-7-11A	-	-	Carb vein cutting black slate
70745	JH01-7-11B	-	-	Carb vein with sulphides
70746	JH01-7-11C	-	-	Large crystals in Carb layers in slate
70747	JH01-7-12A	-	-	Carb vein in Carb Bx at contact between slate & overlying sst
70748	JH01-7-13A	-	-	2 m thick banded brown & white Fs-Qz-Bt layer in sst
70749	JH01-7-16	-	-	Banded rust & tan weathering Carb cut by Carb vlts
70750	JH01-8-1A	-	-	Qz-Fs-Cl-Musc vein cutting sst
70751	JH01-8-1B	-	-	Qz-Cl-Bt vein cutting sst
70752	JH01-8-2	-	-	Qz-Musc-malachite-Ht vein about 0.5 m thick cutting sst (2 pieces)
70753	JH01-8-3A	-	-	Ksp vein cutting sst
70754	JH01-8-6A	-	-	Sst with white spots & Fs-Qz-Cl veins
70755	JH01-8-7A	-	-	Carb matrix from Bx

JCU #	Sample # or Drill Hole	Depth (m)	Depth (feet)	Location	NTS map sheet	Datum (NAD)	Easting	Northing	Thin Section	Isotopes				Fluid Inclusions	Geochron
										O	C	S	D		
70756	JH01-8-8A	-	-	lower slope	E/1	27	0535487	7217444	**Y**						
70757	JH01-8-8B	-	-	lower slope	E/1	27	0535487	7217444							
70758	JH01-8-8C	-	-	lower slope	E/1	27	0535487	7217444							
70759	JH01-8-11	-	-	lower slope	E/1	27	0535508	7217269							
70760	JH01-9-1B	-	-	lower slope	E/1	27	0534946	7217718							
70761	JH01-9-5A	-	-	middle slope	E/1	27	0535178	7217922	**Y**		**Y**				
70762	JH01-9-7A	-	-	middle slope	E/1	27	0535367	7218127		**Y**	**Y**				
70763	JH01-9-11A	-	-	upper slope	E/1	27	0535942	7218416				**Y**			
70764	JH01-9-11B	-	-	upper slope	E/1	27	0535942	7218416	**Y**						
70765	JH01-9-11C	-	-	upper slope	E/1	27	0535942	7218416							
70766	JH01-9-11D	-	-	upper slope	E/1	27	0535942	7218416	**Y**						
70767	JH01-9-11E	-	-	upper slope	E/1	27	0535942	7218416				**Y**			

JCU #	Sample # or Drill Hole	Depth (m)	Depth (feet)	Lithology
70756	JH01-8-8A	-	-	Phyllite with Mt
70757	JH01-8-8B	-	-	Bx from contact
70758	JH01-8-8C	-	-	Mt veinlet
70759	JH01-8-11	-	-	Qz vein float
70760	JH01-9-1B	-	-	Sst
70761	JH01-9-5A	-	-	Bt on foliation planes in slate (2 pieces)
70762	JH01-9-7A	-	-	Carb band
70763	JH01-9-11A	-	-	Sulphide vein at contact of Fs-Qz layer & Cbxted slate
70764	JH01-9-11B	-	-	Bx
70765	JH01-9-11C	-	-	Bx
70766	JH01-9-11D	-	-	Bx
70767	JH01-9-11E	-	-	Talus of mineralization

JCU #	Sample # or Drill Hole	Depth (m)	Location	NTS map sheet (106)	Datum (NAD)	Easting	Northing	Thin Section	Isotopes				Fluid Inclusions	Geochron
									O	C	S	D		
SLATS - FROSTY PROPERTY: DRILL CORE SAMPLES														
70768	STF95-1	4.90	Slats - F	E/1	27	0527784	7208640	**Y**						
70769	STF95-1	5.80	Slats - F	E/1	27	0527784	7208640							
70770	STF95-1	6.10	Slats - F	E/1	27	0527784	7208640							
70771	STF95-1	12.70	Slats - F	E/1	27	0527784	7208640		**Y**	**Y**				
70772	STF95-1	16.70	Slats - F	E/1	27	0527784	7208640	**Y**						
70773	STF95-1	18.20	Slats - F	E/1	27	0527784	7208640							
70774	STF95-1	20.30	Slats - F	E/1	27	0527784	7208640						**Y**	
70775	STF95-1	36.30	Slats - F	E/1	27	0527784	7208640							
70776	STF95-1	41.20	Slats - F	E/1	27	0527784	7208640							
70777	STF95-1	42.70	Slats - F	E/1	27	0527784	7208640							
70778	STF95-1	45.50	Slats - F	E/1	27	0527784	7208640		**Y**	**Y**				
70779	STF95-1	48.20	Slats - F	E/1	27	0527784	7208640		**Y**	**Y**				
70780	STF95-1	50.30	Slats - F	E/1	27	0527784	7208640							
70781	STF95-1	52.30	Slats - F	E/1	27	0527784	7208640							
70782	STF95-1	52.35	Slats - F	E/1	27	0527784	7208640							
70783	STF95-1	54.50	Slats - F	E/1	27	0527784	7208640	**Y**						
70784	STF95-1	62.50	Slats - F	E/1	27	0527784	7208640		**Y**	**Y**				
70785	STF95-1	67.70	Slats - F	E/1	27	0527784	7208640		**Y**	**Y**				
70786	STF95-1	70.90	Slats - F	E/1	27	0527784	7208640							
70787	STF95-1	78.10	Slats - F	E/1	27	0527784	7208640							
70788	STF95-1	79.10	Slats - F	E/1	27	0527784	7208640							
70789	STF95-1	90.70	Slats - F	E/1	27	0527784	7208640	**Y**						
70790	STF95-1	110.60	Slats - F	E/1	27	0527784	7208640		**Y**	**Y**				
70791	STF95-5	5.58	Slats - F	E/1	27	0527297	7208372							
70792	STF95-5	8.70	Slats - F	E/1	27	0527297	7208372							
70793	STF95-5	10.40	Slats - F	E/1	27	0527297	7208372	**Y**						
70794	STF95-5	20.20	Slats - F	E/1	27	0527297	7208372							
70795	STF95-5	22.40	Slats - F	E/1	27	0527297	7208372							

JCU #	Sample # or Drill Hole	Depth (m)	Lithology
70768	STF95-1	4.90	Qz-Ab-Carb-Cpy vein cutting K-altered laminated sediments
70769	STF95-1	5.80	Red haloes around Cpy blebs
70770	STF95-1	6.10	XC veins & K-altered sediments
70771	STF95-1	12.70	Qz-Ab-Carb vein cutting K-altered sediments
70772	STF95-1	16.70	CG K-altered layer in sediments
70773	STF95-1	18.20	Fault Bx
70774	STF95-1	20.30	Purple Ft in vein
70775	STF95-1	36.30	FG dark purple sediments with grey blebs xcut by Qz-Ab-Carb-Cpy vein
70776	STF95-1	41.20	Bx at contact with sediments
70777	STF95-1	42.70	Bx with clast of Qz vein with Ht needles
70778	STF95-1	45.50	Carb-Qz vein cutting Bx clasts & matrix
70779	STF95-1	48.20	Clast in Bx with Qz-Ab-Carb vein
70780	STF95-1	50.30	Bxtion process
70781	STF95-1	52.30	Bx with Carb replacing/forming matrix
70782	STF95-1	52.35	Py fracture XC Bx & Qz-Carb matrix
70783	STF95-1	54.50	Wispy grey clasts in Bx
70784	STF95-1	62.50	Bx with chloritic matrix cut by Qz-Ab-Carb-Ht vein
70785	STF95-1	67.70	Phyllite xcut by Qz-Ab-Carb veins & blebs
70786	STF95-1	70.90	Phyllite/Sst xcut by Carb-Qz veins
70787	STF95-1	78.10	Py vein XC Bx
70788	STF95-1	79.10	Bx with abundant Carb-Qz in matrix, xcut by Py vein
70789	STF95-1	90.70	Red stained Bx
70790	STF95-1	110.60	Ser-altered phyllite xcut by Qz-Carb-Ab-Ht veins
70791	STF95-5	5.58	Bx
70792	STF95-5	8.70	Early clasts
70793	STF95-5	10.40	Carb replaced K-altered clasts
70794	STF95-5	20.20	Black mineral
70795	STF95-5	22.40	Ht clast in Bx

JCU #	Sample # or Drill Hole	Depth (m)	Location	NTS map sheet (106)	Datum (NAD)	Easting	Northing	Thin Section	Isotopes				Fluid Inclusions	Geochron
									O	C	S	D		
70796	STF95-5	60.65	Slats - F	E/1	27	0527297	7208372		Y	Y				
70797	STF95-5	74.90	Slats - F	E/1	27	0527297	7208372	Y	Y	Y				
70798	STF95-5	80.30	Slats - F	E/1	27	0527297	7208372							
70799	STF95-5	94.00	Slats - F	E/1	27	0527297	7208372							
70800	STF95-5	104.90	Slats - F	E/1	27	0527297	7208372							
SLATS - FROSTY PROPERTY: OUTCROP SAMPLES														
70801	02JH-3-005 (2)	-	Slats - F	E/1	27	0527142	7208991	Y						
70802	02JH-3-007	-	Slats - F	E/1	27	0527223	7208996	Y						
70803	02JH-4-001A	-	Slats - F	E/1	27	0528457	7209628	Y			Y			
70804	02JH-4-001B	-	Slats - F	E/1	27	0528457	7209628		Y	Y				
70805	02JH-4-001C	-	Slats - F	E/1	27	0528457	7209628	Y						
70806	02JH-4-001D	-	Slats - F	E/1	27	0528457	7209628							
70807	02JH-4-001E	-	Slats - F	E/1	27	0528457	7209628							
70808	02JH-4-001F	-	Slats - F	E/1	27	0528457	7209628							
70809	02JH-4-001G	-	Slats - F	E/1	27	0528457	7209628		Y	Y				
70810	02JH-4-001extra	-	Slats - F	E/1	27	0528457	7209628							
SLATS-WALLBANGER PROPERTY: DRILL CORE SAMPLES														
70811	STW95-1	5.75	Slats - W	D/16	27	0529502	7203323		Y	Y				
70812	STW95-1	9.60	Slats - W	D/16	27	0529502	7203323							
70813	STW95-1	11.10	Slats - W	D/16	27	0529502	7203323		Y	Y				
70814	STW95-1	12.30	Slats - W	D/16	27	0529502	7203323	Y						
70815	STW95-1	12.80	Slats - W	D/16	27	0529502	7203323							
70816	STW95-2	8.20	Slats - W	D/16	27	0529717	7203294							
70817	STW95-2	14.60	Slats - W	D/16	27	0529717	7203294		Y	Y	Y			
70818	STW95-2	15.94	Slats - W	D/16	27	0529717	7203294							
70819	STW95-2	16.64	Slats - W	D/16	27	0529717	7203294							
70820	STW95-2	19.55	Slats - W	D/16	27	0529717	7203294							
70821	STW95-2	23.16	Slats - W	D/16	27	0529717	7203294							
70822	STW95-2	25.50	Slats - W	D/16	27	0529717	7203294	Y			Y			
70823	STW95-2	33.90	Slats - W	D/16	27	0529717	7203294							

JCU #	Sample # or Drill Hole	Depth (m)	Lithology
70796	STF95-5	60.65	Ser replacing Ksp
70797	STF95-5	74.90	Bx with massive recrystallised Ht matrix xcut by Carb veins
70798	STF95-5	80.30	Ser Altn?
70799	STF95-5	94.00	Bx with Cl matrix
70800	STF95-5	104.90	Diorite
70801	02JH-3-005 (2)	-	Diorite (BPRI?)
70802	02JH-3-007	-	Massive specular Ht
70803	02JH-4-001A	-	Ht-Py-Qz fracture vein
70804	02JH-4-001B	-	Qz-Carb-Ht vein
70805	02JH-4-001C	-	Massive Mt-specular Ht
70806	02JH-4-001D	-	Bx ted phyllite
70807	02JH-4-001E	-	Phyllite
70808	02JH-4-001F	-	Ht-Qz-Cl veins/fractures
70809	02JH-4-001G	-	Carb
70810	02JH-4-001extra	-	CG crystalline Ht
70811	STW95-1	5.75	Carb-Qz-Cpy veins cut Bx
70812	STW95-1	9.60	Carb veins cutting Bx
70813	STW95-1	11.10	Bx with Carb matrix (Carb is replacing Ser)
70814	STW95-1	12.30	Bx
70815	STW95-1	12.80	Shale clasts with CG Ser
70816	STW95-2	8.20	Sediments
70817	STW95-2	14.60	Carb veins in sediments at Bx contacts
70818	STW95-2	15.94	Bx with Cl-Mt matrix, Qz-Ht veins, pink clasts replaced by white
70819	STW95-2	16.64	Ht-Cl-altered sediments?
70820	STW95-2	19.55	Cl-altered sediments
70821	STW95-2	23.16	CBx (white replacing red?)
70822	STW95-2	25.50	Bx (purple Ht & Ab-Qz-Cl-Cpy vein)
70823	STW95-2	33.90	Cl-altered sediments cut by Qz-Ab-Ht vein

JCU #	Sample # or Drill Hole	Depth (m)	Location	NTS map sheet (106)	Datum (NAD)	Easting	Northing	Thin Section	Isotopes				Fluid Inclusions	Geochron
									O	C	S	D		
70824	STW95-2	40.95	Slats - W	D/16	27	0529717	7203294							
70825	STW95-2	44.30	Slats - W	D/16	27	0529717	7203294	Y						
70826	STW95-2	45.30	Slats - W	D/16	27	0529717	7203294							
70827	STW95-2	67.10	Slats - W	D/16	27	0529717	7203294							
70828	STW95-2	103.00	Slats - W	D/16	27	0529717	7203294							
70829	STW95-2	110.90	Slats - W	D/16	27	0529717	7203294							
70830	STW95-2	114.00	Slats - W	D/16	27	0529717	7203294							
70831	STW95-3	7.40	Slats - W	D/16	27	0529501	7203259	Y						
70832	STW95-3	5.20	Slats - W	D/16	27	0529501	7203259		Y	Y				
70833	STW95-3	18.10	Slats - W	D/16	27	0529501	7203259							
70834	STW95-3	20.25	Slats - W	D/16	27	0529501	7203259							
70835	STW95-3	38.50	Slats - W	D/16	27	0529501	7203259							
70836	STW95-3	41.10	Slats - W	D/16	27	0529501	7203259				Y			
70837	STW95-3	72.50	Slats - W	D/16	27	0529501	7203259	Y	Y	Y				
70838	STW95-3	74.40	Slats - W	D/16	27	0529501	7203259							
70839	STW95-3	100.20	Slats - W	D/16	27	0529501	7203259							
70840	STW95-3	118.70	Slats - W	D/16	27	0529501	7203259							
70841	STW95-3	132.20	Slats - W	D/16	27	0529501	7203259							
70842	STW95-3	144.20	Slats - W	D/16	27	0529501	7203259							
70843	STW95-3	154.85	Slats - W	D/16	27	0529501	7203259							
70844	STW95-3	168.20	Slats - W	D/16	27	0529501	7203259							
SLATS-WALLBANGER PROPERTY: OUTCROP SAMPLES														
70845	02JH-4-002		Slats - W	D/16	27	0529941	7202007		Y	Y				
70846	02JH-4-003	-	Slats - W	D/16	27	0529888	7202133		Y	Y				
70847	02JH-4-004	-	Slats - W	D/16	27	0529883	7202313		Y	Y				
70848	02JH-4-006	-	Slats - W	D/16	27	0529877	7202644	Y						
70849	02JH-4-011	-	Slats - W	D/16	27	0529567	7203452							
70850	02JH-5-001	-	Slats - W	D/16	27	0529441	7203224		Y	Y				
70851	02JH-5-002	-	Slats - W	D/16	27	0529360	7203312		Y	Y				
70852	02JH-5-005A	-	Slats - W	D/16	27	0528793	7204105							

JCU #	Sample # or Drill Hole	Depth (m)	Lithology
70824	STW95-2	40.95	Banded sediments with white porphyroblasts & XC Qz-Ab vein
70825	STW95-2	44.30	Bx - red Ht outlining lams in sediments
70826	STW95-2	45.30	Meta sandstone - meta?tuff contact
70827	STW95-2	67.10	Volcanic or diorite
70828	STW95-2	103.00	Ab??
70829	STW95-2	110.90	Dark purple xcut by Qz-earthy Ht-Py vein with bleached selvage
70830	STW95-2	114.00	Tuff?
70831	STW95-3	7.40	Fault Bx contact with FG sediments
70832	STW95-3	5.20	XC Carb s in fault Bx
70833	STW95-3	18.10	Pink blebs
70834	STW95-3	20.25	Purple fault Bx
70835	STW95-3	38.50	Sediments with Ab Altn xcut by Ab-Qz vein
70836	STW95-3	41.10	Py veins in fault Bx
70837	STW95-3	72.50	Ab-altered Bx ted shale xcut by Ab-Qz that is xcut by Carb-Qz vein
70838	STW95-3	74.40	Bx ted shale with Cl matrix
70839	STW95-3	100.20	Diorite
70840	STW95-3	118.70	Fault Bx with Cl matrix & H stained Clasts
70841	STW95-3	132.20	Cl matrix Bx with red clasts & Bt repl Cl
70842	STW95-3	144.20	Diorite
70843	STW95-3	154.85	Intense red & Ht & silicification
70844	STW95-3	168.20	Cl matrix Bx
70845	02JH-4-002		GLG dolostone - regional sample
70846	02JH-4-003	-	Bx ted dolomite
70847	02JH-4-004	-	GLG dolostone - regional sample
70848	02JH-4-006	-	Diorite?
70849	02JH-4-011	-	Bx
70850	02JH-5-001	-	Diorite cut by brown-weathering Carb-white Qz vein
70851	02JH-5-002	-	Black shale cut by brown-weathering Carb vein
70852	02JH-5-005A	-	Grey Bx - hard to see clasts on fresh surface

JCU #	Sample # or Drill Hole	Depth (m)	Location	NTS map sheet (106)	Datum (NAD)	Easting	Northing	Thin Section	Isotopes				Fluid Inclusions	Geochron
									O	C	S	D		
70853	02JH-5-005B	-	Slats - W	D/16	27	0528793	7204105		Y	Y				
70854	02JH-5-006	-	Slats - W	D/16	27	0528782	7204050							
70855	02JH-6-001	-	Slats - W	D/16	27	0529591	7202664		Y	Y				
70856	02JH-6-003	-	Slats - W	D/16	27	0529852	7202526		Y	Y				
70857	02JH-6-004A	-	Slats - W	D/16	27	0529877	7202526		Y	Y				
70858	02JH-6-004B	-	Slats - W	D/16	27	0529877	7202526							
70859	02JH-6-004C	-	Slats - W	D/16	27	0529877	7202526		Y	Y	Y			
70860	02JH-6-004D	-	Slats - W	D/16	27	0529877	7202526	Y						
70861	02DG-01	-	Slats - W	D/16	27	0528958	7203032		Y	Y				
70862	02DG-02	-	Slats - W	D/16	27	0528973	7203069		Y	Y				
IGOR PROPERTY: DRILL CORE SAMPLES														
70863	I80-010	44'	Igor	E/2	83	?0517492.72	?7213531.36							
70864	I80-010	43' 10"	Igor	E/2	83	?0517492.72	?7213531.36	Y						
70865	I80-010	45' 6"	Igor	E/2	83	?0517492.72	?7213531.36		Y	Y				
70866	I80-010	83'	Igor	E/2	83	?0517492.72	?7213531.36		Y	Y				
70867	I80-010	108' 2"	Igor	E/2	83	?0517492.72	?7213531.36							
70868	I80-010	113'	Igor	E/2	83	?0517492.72	?7213531.36		Y	Y				
70869	I80-010	115' 6"	Igor	E/2	83	?0517492.72	?7213531.36		Y	Y				
70870	I80-010	118' 6"	Igor	E/2	83	?0517492.72	?7213531.36							
70871	I80-010	129' 8"	Igor	E/2	83	?0517492.72	?7213531.36							
70872	I80-010	126'	Igor	E/2	83	?0517492.72	?7213531.36							
70873	I80-010	131'	Igor	E/2	83	?0517492.72	?7213531.36							
70874	I80-010	133' 6"	Igor	E/2	83	?0517492.72	?7213531.36							
70875	I80-010	141'	Igor	E/2	83	?0517492.72	?7213531.36							
70876	I80-010	143'	Igor	E/2	83	?0517492.72	?7213531.36	Y						
70877	I80-010	143' 4"	Igor	E/2	83	?0517492.72	?7213531.36							
70878	I80-010	144'	Igor	E/2	83	?0517492.72	?7213531.36							
70879	I80-010	144' 6"	Igor	E/2	83	?0517492.72	?7213531.36							
70880	I80-010	145'	Igor	E/2	83	?0517492.72	?7213531.36							
70881	I80-010	150'	Igor	E/2	83	?0517492.72	?7213531.36							

JCU #	Sample # or Drill Hole	Depth (m)	Lithology
70853	02JH-5-005B	-	Bx with Ht matrix cut by brown-weathering Carb-Qz veins
70854	02JH-5-006	-	K-altered sediments cut by Carb-Qz vein & Mt
70855	02JH-6-001	-	Bx ted dolomite
70856	02JH-6-003	-	Bx with Carb matrix
70857	02JH-6-004A	-	Massive Mt cut by brown Carb-Cpy-Bar vein
70858	02JH-6-004B	-	Massive Mt with disseminated Py, Ft, Cpy & Bor
70859	02JH-6-004C	-	Massive Mt cut by brown Carb-Py-Qz veins
70860	02JH-6-004D	-	Massive Mt cut by Qz-Cpy-Ft-brown weathering Carb veinlets & Ft veinlets
70861	02DG-01	-	Dolostone
70862	02DG-02	-	Dolostone
70863	I80-010	44'	Cambrian Bx ted dolostone xcut by cream Carb veins xcut by dark brown veinlets
70864	I80-010	43' 10"	Dolostone CBx ' d by Ht
70865	I80-010	45' 6"	CBx ' d dolostone xcut by Carb-Bar vein
70866	I80-010	83'	CBx ' d dolostone xcut by Carb-Bar vein
70867	I80-010	108' 2"	Bxted dolostone
70868	I80-010	113'	Bxted dolostone xcut by cream Carb-pink Carb vein
70869	I80-010	115' 6"	Bxted dolostone xcut by Carb-Cpy vein & xcut by Py-Cpy-Mt vein & Mt porphyroblasts
70870	I80-010	118' 6"	mineralisation xcut by pink Bar vein
70871	I80-010	129' 8"	Foliated CBx ' d dolostone + Mt porphyroblasts
70872	I80-010	126'	Dolostone Bx ' d by mineralisation
70873	I80-010	131'	Bx
70874	I80-010	133' 6"	Bx xcut by Bar vein
70875	I80-010	141'	Mt-Py-Cpy-Ht mineralisation
70876	I80-010	143'	Mt-Py-Cpy-Ht mineralisation
70877	I80-010	143' 4"	Mt-Py-Cpy-Ht mineralisation
70878	I80-010	144'	Mt-Py-Cpy-Ht mineralisation
70879	I80-010	144' 6"	Mt-Py-Cpy-Ht mineralisation
70880	I80-010	145'	Mt-Py-Cpy-Ht mineralisation
70881	I80-010	150'	Mt-Py-Cpy-Ht mineralisation

JCU #	Sample # or Drill Hole	Depth (m)	Location	NTS map sheet (106)	Datum (NAD)	Easting	Northing	Thin Section	Isotopes				Fluid Inclusions	Geochron
									O	C	S	D		
70882	I80-010	152.8'	Igor	E/2	83	?0517492.72	?7213531.36							
70883	I80-010	159'	Igor	E/2	83	?0517492.72	?7213531.36	Y						
70884	I80-010	161'	Igor	E/2	83	?0517492.72	?7213531.36							
70885	I80-010	173' 6"	Igor	E/2	83	?0517492.72	?7213531.36							
70886	I80-010	181'	Igor	E/2	83	?0517492.72	?7213531.36		Y	Y				
70887	I80-010	181' 8"	Igor	E/2	83	?0517492.72	?7213531.36							
70888	I80-010	182' 2"	Igor	E/2	83	?0517492.72	?7213531.36		Y	Y	Y			
70889	I80-010	194'	Igor	E/2	83	?0517492.72	?7213531.36							
70890	I80-010	208'	Igor	E/2	83	?0517492.72	?7213531.36		Y	Y				
70891	I80-010	210'	Igor	E/2	83	?0517492.72	?7213531.36		Y	Y				
70892	I80-010	216'	Igor	E/2	83	?0517492.72	?7213531.36		Y	Y	Y			
70893	I80-010	228'	Igor	E/2	83	?0517492.72	?7213531.36	Y						
70894	I80-010	263'	Igor	E/2	83	?0517492.72	?7213531.36							
70895	I80-010	264'	Igor	E/2	83	?0517492.72	?7213531.36							
70896	I80-010	291' 4"	Igor	E/2	83	?0517492.72	?7213531.36							
70897	I80-010	343' 6"	Igor	E/2	83	?0517492.72	?7213531.36							
70898	I80-014	21'	Igor	E/2	83	517387.03	7213898.96							
70899	I80-014	46'	Igor	E/2	83	517387.03	7213898.96		Y	Y				
70900	I80-014	30.5'	Igor	E/2	83	517387.03	7213898.96							
70901	I80-014	76'	Igor	E/2	83	517387.03	7213898.96							
70902	I80-014	95.5'	Igor	E/2	83	517387.03	7213898.96							
70903	I80-014	119.5'	Igor	E/2	83	517387.03	7213898.96							
70904	I80-014	150'	Igor	E/2	83	517387.03	7213898.96		Y	Y				
70905	I80-014	189'	Igor	E/2	83	517387.03	7213898.96							
70906	I80-014	234'	Igor	E/2	83	517387.03	7213898.96				Y			
70907	I80-014	236'	Igor	E/2	83	517387.03	7213898.96				Y			
70908	I80-014	291.5'	Igor	E/2	83	517387.03	7213898.96							
70909	I80-014	402.5'	Igor	E/2	83	517387.03	7213898.96		Y	Y				
70910	I80-014	441'	Igor	E/2	83	517387.03	7213898.96		Y	Y				
70911	I80-014	539.5'	Igor	E/2	83	517387.03	7213898.96				Y			

JCU #	Sample # or Drill Hole	Depth (m)	Lithology
70882	I80-010	152.8'	Mt-Py-Cpy-Ht mineralisation
70883	I80-010	159'	Mt-Py-Cpy-Ht mineralisation
70884	I80-010	161'	Mt-Py-Cpy-Ht mineralisation
70885	I80-010	173' 6"	Bx
70886	I80-010	181'	Dark matrix Bx xcut by Carb-pink Bar-Py-Cpy vein
70887	I80-010	181' 8"	Dark matrix Bx xcut by pink Bar veins
70888	I80-010	182' 2"	Dark matrix Bx xcut by pink Bar veins
70889	I80-010	194'	Dark matrix Bx xcut by cream Carb vein
70890	I80-010	208'	Semi-massive Mt xcut by Carb vein
70891	I80-010	210'	Dark matrix Bx xcut by Carb-Cpy vein
70892	I80-010	216'	Dark matrix Bx xcut by Carb-Cpy-Py vein
70893	I80-010	228'	Mt-Py-Cpy-Ht mineralisation
70894	I80-010	263'	Bx ted dolostone xcut by Ht + Ht clast
70895	I80-010	264'	Bx ted dolostone xcut/replaced by Ht
70896	I80-010	291' 4"	Red stained sediments
70897	I80-010	343' 6"	Ht-stained Bx
70898	I80-014	21'	Green matrix cutting pink clasts
70899	I80-014	46'	Carb porphyroblasts overprinting Bx
70900	I80-014	30.5'	Green matrix, pink clasts, overprinted by Py porphyroblasts, Carb porphyroblasts & Mt
70901	I80-014	76'	Euhedral Mt op Ht?
70902	I80-014	95.5'	Green Bxting pink Sst
70903	I80-014	119.5'	Bar vein XC green matrix Bx & euhedral Mt vein
70904	I80-014	150'	Chloritic Bx xcut by Carb vein
70905	I80-014	189'	Foliated Bx
70906	I80-014	234'	Qz-Cpy vein XC Bx
70907	I80-014	236'	Massive Py op Bx
70908	I80-014	291.5'	Euhedral Mt op fabric
70909	I80-014	402.5'	Carb-Qz-Cpy-Ht vein xcuts green matrix Bx & euhedral Mt
70910	I80-014	441'	Carb-Py-Bar vein xcuts green matrix Bx
70911	I80-014	539.5'	Pink Bar-Py vein

JCU #	Sample # or Drill Hole	Depth (m)	Location	NTS map sheet (106)	Datum (NAD)	Easting	Northing	Thin Section	Isotopes				Fluid Inclusions	Geochron
									O	C	S	D		
70912	I80-014	551.3'	Igor	E/2	83	517387.03	7213898.96							
70913	I80-014	546'	Igor	E/2	83	517387.03	7213898.96							
70914	I80-014	500'	Igor	E/2	83	517387.03	7213898.96	**Y**	**Y**	**Y**				
IGOR PROPERTY: OUTCROP SAMPLES														
70915	02JH-7-002	-	Igor	E/2	27	0516409	7211671							
70916	02JH-7-003A	-	Igor	E/2	27	0516608	7211637							
70917	02JH-7-003B	-	Igor	E/2	27	0516608	7211637							
70918	02JH-7-004A	-	Igor	E/2	27	0516740	7211724							
70919	02JH-7-004B	-	Igor	E/2	27	0516740	7211724							
70920	02JH-7-007A (2)	-	Igor	E/2	27	0517375	7212985							
	02JH-7-007B	-	Igor	E/2	27	0517375	7212985						**y - DG**	
	02JH-7-007C	-	Igor	E/2	27	0517375	7212985						**y - DG**	
	02JH-7-007D	-	Igor	E/2	27	0517375	7212985						**y - DG**	
	02JH-7-008	-	Igor	E/2	27	0517586	7213309						**y - DG**	
70921	02JH-8-002	-	Igor	E/2	83	0516705	7212896							
	02JH-8-003	-	Igor	E/2	83	0516638	7212994						**y - DG**	
70922	02JH-8-005A	-	Igor	E/2	83	0516615	7213076	**Y**						
	02JH-8-005B	-	Igor	E/2	83	0516615	7213076						**y - DG**	
70923	02JH-8-006A	-	Igor	E/2	83	0516715	7213092	**Y**						
70924	02JH-8-006B	-	Igor	E/2	83	0516715	7213092							
70925	02JH-8-007A	-	Igor	E/2	83	0516812	7213123							
	02JH-8-007B	-	Igor	E/2	83	0516812	7213123						**y - DG**	
	02JH-8-007C (2)	-	Igor	E/2	83	0516812	7213123						**y - DG**	
	02JH-8-009A	-	Igor	E/2	83	0516891	7213086						**y - DG**	
70926	02JH-8-009B	-	Igor	E/2	83	0516891	7213086							**Ar-Ar**
	02JH-8-009C (2)	-	Igor	E/2	83	0516891	7213086						**y - DG**	
70927	02JH-8-017	-	Igor	E/2	83	0516808	7213875							
	02JH-9-002	-	Igor	E/2	83	0517227	7213148						**y - DG**	
	02JH-9-005	-	Igor	E/2	83	0517162	7213290						**y - DG**	

JCU #	Sample # or Drill Hole	Depth (m)	Lithology
70912	I80-014	551.3'	Py
70913	I80-014	546'	Py
70914	I80-014	500'	Carb vein xcuts green matrix Bx + Mt + Py
70915	02JH-7-002	-	Cambrian Carb
70916	02JH-7-003A	-	Cambrian Carb cut by Carb veins
70917	02JH-7-003B	-	Cambrian Carb
70918	02JH-7-004A	-	Carb veins in Cambrian Carb close to contact with Iltyd
70919	02JH-7-004B	-	Vuggy Qz veins in Cambrian Carb
70920	02JH-7-007A (2)	-	Euhedral Mt in foliated Bx
	02JH-7-007B	-	Carb-Mt vein
	02JH-7-007C	-	Carb-Mt-Qz-Py vein
	02JH-7-007D	-	Carb-Mt-Qz-Py bleb in Bx
	02JH-7-008	-	Massive specular Ht + Mt + Cpy with Qz-Carb vein
70921	02JH-8-002	-	Conglomerate cut by Carb-Qz veins
	02JH-8-003	-	Qz matrix Bx
70922	02JH-8-005A	-	Cl-Ht Bx with Ser-altered clasts
	02JH-8-005B	-	Qz-Ht vein
70923	02JH-8-006A	-	Cl-Ht Bx with pink Fs-altered clasts & Ht in the matrix
70924	02JH-8-006B	-	Syn-Bx Fs-Ep vein
70925	02JH-8-007A	-	Similar Bx to 6A with inc Cl, dec Ksp, dec Ht
	02JH-8-007B	-	Syn-Bx Qz-Ht veins
	02JH-8-007C (2)	-	Syn-Bx Carb-Qz-Ht veins
	02JH-8-009A	-	Syn-Bx Qz-Carb-Ht-Ksp veins
70926	02JH-8-009B	-	Bx with Ser-Ksp-Ht
	02JH-8-009C (2)	-	Syn-Bx Qz-Carb-Ht-Cpy vein
70927	02JH-8-017	-	Ht Bx with pink Fs-altered clasts + others
	02JH-9-002	-	Qz-Ht vein XC sediments
	02JH-9-005	-	Bar-Carb-Py-Ser vein

JCU #	Sample # or Drill Hole	Depth (m)	Location	NTS map sheet (106)	Datum (NAD)	Easting	Northing	Thin Section	Isotopes				Fluid Inclusions	Geochron
									O	C	S	D		
70928	02JH-9-006A	-	Igor	E/2	83	0517136	7213308							
70929	02JH-9-006B	-	Igor	E/2	83	0517136	7213308							
70930	02JH-9-006C sulphides	-	Igor	E/2	83	0517136	7213308				**Y**			
70930	02JH-9-006C vein	-	Igor	E/2	83	0517136	7213308						**y - DG**	
	02JH-9-012 (2)	-	Igor	E/2	83	0517400	7214034						**y - DG**	**Re-Os**
	02JH-9-013 (2)	-	Igor	E/2	83	0517492	7214115						**y - DG**	
	02JH-9-016	-	Igor	E/2	83	0517815	7214109						**y - DG**	
	02JH-9-017	-	Igor	E/2	83	0517817	7214083						**y - DG**	
70931	02JH-10-001A	-	Igor	E/2	83	0517406	7213117							
	02JH-10-001B	-	Igor	E/2	83	0517406	7213117						**y - DG**	
70932	02JH-10-004	-	Igor	E/2	83	0517470	7212994							
	02JH-10-008	-	Igor	E/2	83	0517503	7213344						**y - DG**	
70933	02JH-10-011	-	Igor	E/2	83	0517587	7213739							
70934	02JH-10-012	-	Igor	E/2	83	0517566	7213743		**Y**	**Y**				
70935	02JH-10-015	-	Igor	E/2	83	0517539	7213861							
70936	02JH-10-016-1	-	Igor	E/2	83	0517497	7213833							
70937	02JH-10-016-2	-	Igor	E/2	83	0517497	7213833							
70938	02JH-10-016-3	-	Igor	E/2	83	0517497	7213833	**Y**						
70939	02JH-10-016-4	-	Igor	E/2	83	0517497	7213833							
	02JH-10-016-5	-	Igor	E/2	83	0517497	7213833						**y - DG**	
70940	02JH-10-016-6	-	Igor	E/2	83	0517497	7213833							
70941	02JH-10-017-1A	-	Igor	E/2	83	0517459	7213830				**Y**			
70942	02JH-10-017-1B	-	Igor	E/2	83	0517459	7213830						**Y**	
70943	02JH-10-018A	-	Igor	E/2	83	0517427	7213804							
70944	02JH-10-018B	-	Igor	E/2	83	0517427	7213804							
	02JH-10-018C	-	Igor	E/2	83	0517427	7213804						**y - DG**	
	02JH-10-020A	-	Igor	E/2	83	0517514	7213627						**y - DG**	
70945	02JH-10-020B	-	Igor	E/2	83	0517514	7213627							
70946	02JH-10-020C	-	Igor	E/2	83	0517514	7213627							
70947	02JH-10-021	-	Igor	E/2	83	0517493	7213551							

JCU #	Sample # or Drill Hole	Depth (m)	Lithology
70928	02JH-9-006A	-	Foliated Mt Bx
70929	02JH-9-006B	-	Foliated Mt Bx
70930	02JH-9-006C sulphides	-	Brown-weathering Carb-white Qz-Py pod
70930	02JH-9-006C vein	-	Brown-weathering Carb-white Qz-Py pod
	02JH-9-012 (2)	-	Massive Mt-Py-Ht-Cpy-Carb
	02JH-9-013 (2)	-	Massive Qz-Ht-Py cut by Qz-Cpy-Carb , Qz-Ht-Carb , Qz-Py-Carb veins
	02JH-9-016	-	Qz-Carb veins cutting sediments (away from mineralisation)
	02JH-9-017	-	Qz-Py vein (away from mineralisation)
70931	02JH-10-001A	-	Ser-Ksp-altered Bx
	02JH-10-001B	-	Carb-Ht-Qz-Cpy vein
70932	02JH-10-004	-	Quartzite
	02JH-10-008	-	Quartzite cut by Qz veins
70933	02JH-10-011	-	Foliated Mt Bx
70934	02JH-10-012	-	Dolostone
70935	02JH-10-015	-	Pink Bar
70936	02JH-10-016-1	-	Foliated Mt Bx
70937	02JH-10-016-2	-	Edge of massive Mt-Ht
70938	02JH-10-016-3	-	Middle of massive Mt-Ht
70939	02JH-10-016-4	-	Top edge of foliated Bx with euhedral Mt
	02JH-10-016-5	-	Carb-Qz vein
70940	02JH-10-016-6	-	Bx
70941	02JH-10-017-1A	-	Py Bx (massive Py-Ht-Cpy-Mt)
70942	02JH-10-017-1B	-	Ser-Cl-altered rock from edge of massive Py+
70943	02JH-10-018A	-	Bx
70944	02JH-10-018B	-	Bar vein
	02JH-10-018C	-	Carb-Qz-Bar-Py vein
	02JH-10-020A	-	Qz-Cpy vein in Bx
70945	02JH-10-020B	-	Carb vein
70946	02JH-10-020C	-	Cl-Ksp-Ht Bx
70947	02JH-10-021	-	Cl-Ht-brown Carb Bx

JCU #	Sample # or Drill Hole	Depth (m)	Location	NTS map sheet (106)	Datum (NAD)	Easting	Northing	Thin Section	Isotopes				Fluid Inclusions	Geochron
									O	C	S	D		
70948	02JH-11-002	-	Igor	E/2	83	0517782	7212074							
70949	02JH-11-003	-	Igor	E/2	83	0517808	7212094							
70950	02JH-11-006	-	Igor	E/2	83	0517528	7212487							
70951	02JH-12-001	-	Igor	E/2	83	0517196	7213545	**Y**				**Y**		**Ar-Ar**
70952	02JH-12-003	-	Igor	E/2	83	0517475	7214054							
70953	02JH-12-004	-	Igor	E/2	83	0517617	7213904							
70954	02JH-12-005	-	Igor	E/2	83	0517522	7213884				**Y**			
70955	02JH-12-006	-	Igor	E/2	83	0517390	7213811							
70956	02JH-12-009A	-	Igor	E/2	83	0517300	7213550							
70957	02JH-12-009B	-	Igor	E/2	83	0517300	7213550							
70958	02JH-12-009C	-	Igor	E/2	83	0517300	7213550		**Y**	**Y**				
70959	02JH-12-009D	-	Igor	E/2	83	0517300	7213550							
70960	02JH-12-009E	-	Igor	E/2	83	0517300	7213550							
70961	02JH-12-012A	-	Igor	E/2	83	0517367	7213631							
	02JH-12-012B	-	Igor	E/2	83	0517367	7213631						**y - DG**	
70962	02JH-12-013A	-	Igor	E/2	83	0517375	7213591							
70963	02JH-12-013B	-	Igor	E/2	83	0517375	7213591							
	02JH-12-013C	-	Igor	E/2	83	0517375	7213591						**y - DG**	
70964	02JH-12-013D	-	Igor	E/2	83	0517375	7213591				**Y**			
70965	02JH-12-014	-	Igor	E/2	83	0517353	7213515		**Y**	**Y**				
70966	02JH-12-015	-	Igor	E/2	83	0517390	7213454							
70967	02JH-12-018	-	Igor	E/2	83	0517495	7213582							
70968	C conglomerate	-	Igor	E/2	-	Float	-							
70969	C conglomerate	-	Igor	E/2	-	Float	-							
70970	C seds	-	Igor	E/2	-	Float	-							
70971	C conglomerate	-	Igor	E/2	-	Float	-							
70972	barite	-	Igor	E/2	-	Float	-				**Y**			
OLYMPIC PROPERTY: DRILL CORE SAMPLES														
70973	OY94-1	6.00	Olympic	C/13	27	0553768	7192316							
70974	OY94-1	21.30	Olympic	C/13	27	0553768	7192315	**Y**	**Y**	**Y**				

JCU #	Sample # or Drill Hole	Depth (m)	Lithology
70948	02JH-11-002	-	Iltyd silty dolomite
70949	02JH-11-003	-	Iltyd silty dolomite with "burrows"
70950	02JH-11-006	-	Dolostone with Cc Altn (labelled 005 by mistake)
70951	02JH-12-001	-	Bx with Musc
70952	02JH-12-003	-	Foliated Bx
70953	02JH-12-004	-	Ser-altered mylonitized Sst (oriented sample)
70954	02JH-12-005	-	Ksp-Cl-Carb-altered rock with Cpy-Ht-Carb veins (within foliated zone)
70955	02JH-12-006	-	Massive Ht with fabric
70956	02JH-12-009A	-	Bx 2 - sst clasts in Carb-Qz matrix
70957	02JH-12-009B	-	Bx with Carb matrix
70958	02JH-12-009C	-	Bx with dol clasts
70959	02JH-12-009D	-	Bx with abundant Carb in matrix
70960	02JH-12-009E	-	Bx 2 with intense Cl & Carb Altn
70961	02JH-12-012A	-	Bx 2 cut by pink Carb veins
	02JH-12-012B	-	Bx with large Bar vein
70962	02JH-12-013A	-	Massive Ht
70963	02JH-12-013B	-	Massive Ht + Py
	02JH-12-013C	-	Bar crystals within massive Ht-Mt
70964	02JH-12-013D	-	Cpy in Bar
70965	02JH-12-014	-	Bx replaced by Ht, Carb clasts
70966	02JH-12-015	-	Qz framework to massive Ht-Mt
70967	02JH-12-018	-	Bx
70968	C conglomerate	-	Conglomerate
70969	C conglomerate	-	Conglomerate
70970	C seds	-	Sediments
70971	C conglomerate	-	Conglomerate
70972	barite	-	Bar
70973	OY94-1	6.00	Bx
70974	OY94-1	21.30	Carb vein cutting Bx

JCU #	Sample # or Drill Hole	Depth (m)	Location	NTS map sheet (106)	Datum (NAD)	Easting	Northing	Thin Section	Isotopes				Fluid Inclusions	Geochron
									O	C	S	D		
70975	OY94-1	29.40	Olympic	C/13	27	0553768	7192315							
70976	OY94-1	60.20	Olympic	C/13	27	0553768	7192315							
70977	OY94-1	70.50	Olympic	C/13	27	0553768	7192315							
70978	OY94-1	71.60	Olympic	C/13	27	0553768	7192315							
70979	OY94-1	117.60	Olympic	C/13	27	0553768	7192315		Y	Y				
70980	OY94-1	139.10	Olympic	C/13	27	0553768	7192315							
70981	OY94-3	14.00	Olympic	C/13	27	0553502	7192334							
70982	OY94-3	16.70	Olympic	C/13	27	0553502	7192334	Y	Y	Y				
70983	OY94-3	19.50	Olympic	C/13	27	0553502	7192334							
70984	OY94-3	24.70	Olympic	C/13	27	0553502	7192334		Y	Y	Y		Y	
70985	OY94-3	25.60	Olympic	C/13	27	0553502	7192334		Y	Y				
70986	OY94-3	38.60	Olympic	C/13	27	0553502	7192334		Y	Y				
70987	OY94-3	37.90	Olympic	C/13	27	0553502	7192334							
70988	OY94-3	46.30	Olympic	C/13	27	0553502	7192334		Y	Y				
70989	OY94-3	46.60	Olympic	C/13	27	0553502	7192334							
70990	OY94-3	50.00	Olympic	C/13	27	0553502	7192334							
70991	OY94-3	63.50	Olympic	C/13	27	0553502	7192334		Y	Y	Y			
70992	OY94-3	11.90	Olympic	C/13	27	0553502	7192334							
70993	OY94-3	132.80	Olympic	C/13	27	0553502	7192334		Y	Y				
70994	OY94-3	142.30	Olympic	C/13	27	0553502	7192334	Y						
70995	OY94-3	155.90	Olympic	C/13	27	0553502	7192334							
70996	OY94-3	204.70	Olympic	C/13	27	0553502	7192334							
70997	OY94-4	13.00	Olympic	C/13	27	553066	7193609		Y	Y				
70998	OY94-4	21.90	Olympic	C/13	27	553066	7193609		Y	Y				
70999	OY94-4	27.70	Olympic	C/13	27	553066	7193609							
71000	OY94-4	33.80	Olympic	C/13	27	553066	7193609							
71001	OY94-4	36.40	Olympic	C/13	27	553066	7193609							
71002	OY94-4	38.90	Olympic	C/13	27	553066	7193609		Y	Y				
71003	OY94-4	53.70	Olympic	C/13	27	553066	7193609							
71004	OY94-4	55.00	Olympic	C/13	27	553066	7193609							

JCU #	Sample # or Drill Hole	Depth (m)	Lithology
70975	OY94-1	29.40	Qz-Fs-Cpy-Ht vein cutting Bx
70976	OY94-1	60.20	CG Qz-Fs vein
70977	OY94-1	70.50	Blebs of Qz replacing matrix xcut by white Qz-Fs veins
70978	OY94-1	71.60	Py porphyroblasts rimmed by Cpy
70979	OY94-1	117.60	Qz-Fs vein xcuts brown Carb veins
70980	OY94-1	139.10	XC veins
70981	OY94-3	14.00	Stylolites
70982	OY94-3	16.70	Carb-Qz vein xcuts stylolites
70983	OY94-3	19.50	Slc rock
70984	OY94-3	24.70	Carb-Qz-Cpy-Py vein
70985	OY94-3	25.60	Carb-Qz-Cpy-Py-Aspy vein
70986	OY94-3	38.60	Tan Carb-brown Carb-Qz vein
70987	OY94-3	37.90	Qz-Ht-Py-Cpy op Bx
70988	OY94-3	46.30	Pink Carb op Bx with Ht Altn
70989	OY94-3	46.60	Cpy in Bx
70990	OY94-3	50.00	Carb-Qz-vein
70991	OY94-3	63.50	Ht-Cpy-Qz vein overprints Bx & is xcut by tan Carb-white Carb vein
70992	OY94-3	11.90	White Carb-brown Carb-Cpy vein xcuts Bx
70993	OY94-3	132.80	Altn at edge of Carb-Qz-Cpy vein
70994	OY94-3	142.30	Bx
70995	OY94-3	155.90	CBx
70996	OY94-3	204.70	Pink zone
70997	OY94-4	13.00	XC veins
70998	OY94-4	21.90	Bx ted dolostone xcut by Carb-Qz-Fs veins
70999	OY94-4	27.70	Purple rock
71000	OY94-4	33.80	Bx + red clast
71001	OY94-4	36.40	Bx dyke
71002	OY94-4	38.90	Carb-Qz-Fs vein xcuts Bx
71003	OY94-4	53.70	Carb-Cpy vein with pink selvages
71004	OY94-4	55.00	Bx xcut by Carb vein & pink Altn

JCU	Sample #	Depth	Location	NTS map sheet (106)	Datum (NAD)	Easting	Northing	Thin Section	Isotopes				Fluid Inclusions	Geochron
#	or Drill Hole	(m)							O	C	S	D		
71005	OY94-4	67.60	Olympic	C/13	27	553066	7193609		**Y**	**Y**				
71006	OY94-4	75.20	Olympic	C/13	27	553066	7193609							
71007	OY94-4	89.00	Olympic	C/13	27	553066	7193609		**Y**	**Y**				
71008	OY94-4	99.80	Olympic	C/13	27	553066	7193609							
71009	OY94-4	112.20	Olympic	C/13	27	553066	7193609	**Y**						
71010	OY94-4	123.70	Olympic	C/13	27	553066	7193609							
OLYMPIC PROPERTY: OUTCROP SAMPLES														
71011	OLYMPIC	-	Olympic	C/13	-	Float	-		**Y**	**Y**				
71012	02JH-21-001	-	Olympic	C/13	83	0555311	7195674		**Y**	**Y**				
71013	02JH-21-002	-	Olympic	C/13	83	0555233	7195612							
71014	02JH-21-003	-	Olympic	C/13	83	0555196	7195542							
71015	02JH-21-004	-	Olympic	C/13	83	0555023	7195171		**Y**	**Y**				
71016	02JH-21-005	-	Olympic	C/13	83	0554971	7195103						**Y**	
71017	02JH-21-006	-	Olympic	C/13	83	0554937	7195055							
71018	547457	-	Olympic	C/13	83	0555322	7195801							
71019	float 1	-	Olympic	C/13	83	0555322	7195801	**Y**						
71020	float 2	-	Olympic	C/13	83	0555322	7195801							
71021	float 3	-	Olympic	C/13	83	0555322	7195801							
71022	float 4	-	Olympic	C/13	83	0555322	7195801							
71023	float 5	-	Olympic	C/13	83	0555322	7195801	**Y**						
71024	float 6	-	Olympic	C/13	83	0555322	7195801	**Y**						
71025	float 7	-	Olympic	C/13	83	0555322	7195801							
71026	float 8	-	Olympic	C/13	83	0555322	7195801							
71027	float 9	-	Olympic	C/13	83	0555322	7195801							
71028	02JH-22-001A	-	Olympic	C/13	83	0554832	7195344							
71029	02JH-22-001B	-	Olympic	C/13	83	0554832	7195344							
71030	02JH-22-002	-	Olympic	C/13	83	0554825	7195266							
71031	02JH-22-003A (2)	-	Olympic	C/13	83	0554542	7194914	**Y**						
71032	02JH-22-003B	-	Olympic	C/13	83	0554542	7194914		**Y**	**Y**				
71033	02JH-22-004A	-	Olympic	C/13	83	0554847	7195043				**Y**			

JCU #	Sample # or Drill Hole	Depth (m)	Lithology
71005	OY94-4	67.60	Bx xcut by Carb-Qz-Ht xcut by Carb-Qz veins
71006	OY94-4	75.20	Contact between purple sediments & bleached sediments
71007	OY94-4	89.00	Sediments xcut by Carb-Qz-Ht, xcut by Carb-Qz-Cpy vein
71008	OY94-4	99.80	Gritty sedimentary clasts
71009	OY94-4	112.20	Bx with CG sedimentary clast repl by Ht
71010	OY94-4	123.70	Sst
71011	OLYMPIC	-	Brown Carb vein that cross-cuts Bx
71012	02JH-21-001	-	GLG stromatolitic dolostone
71013	02JH-21-002	-	Bx
71014	02JH-21-003	-	Bx
71015	02JH-21-004	-	Bx ted dolostone
71016	02JH-21-005	-	Bx
71017	02JH-21-006	-	Bx ted dolostone
71018	547457	-	Mineralized sample
71019	float 1	-	Bx
71020	float 2	-	Bx
71021	float 3	-	Bx
71022	float 4	-	Bx
71023	float 5	-	Bx
71024	float 6	-	Bx
71025	float 7	-	Bx
71026	float 8	-	Bx
71027	float 9	-	Bx
71028	02JH-22-001A	-	Wernecke Bx with clast of CBx ted Sst
71029	02JH-22-001B	-	Carb-Qz vein cutting Sst
71030	02JH-22-002	-	Sst with CG SH+Py+Cpy
71031	02JH-22-003A (2)	-	Bx with anorthosite clasts
71032	02JH-22-003B	-	Bx with Bx ted dolostone clast
71033	02JH-22-004A	-	Diorite

JCU #	Sample # or Drill Hole	Depth (m)	Location	NTS map sheet (106)	Datum (NAD)	Easting	Northing	Thin Section	Isotopes				Fluid Inclusions	Geochron
									O	C	S	D		
71034	02JH-22-004B	-	Olympic	C/13	83	0554847	7195043	**Y**						
71035	02JH-22-004C	-	Olympic	C/13	83	0554847	7195043							
71036	02JH-22-004D	-	Olympic	C/13	83	0554847	7195043							
OUTCROP SAMPLES FROM OTHER LOCATIONS														
71037	DT02-9-2-1	-	Quartet Mt	E/11	83	0523962	7231873		**Y**	**Y**				
71038	DT92-51-1	-	Slats Ck	D/16	27	0527600	7205200		**Y**	**Y**				
71039	CW92-53-01	-	Bear River	D/16	27	0555200	7196050		**Y**	**Y**				
71038a	CW93-5-2	-	Olympic	D/16	27	0555200	7196050							

JCU #	Sample # or Drill Hole	Depth (m)	Lithology
71034	02JH-22-004B	-	Diorite
71035	02JH-22-004C	-	Diorite
71036	02JH-22-004D	-	Diorite
71037	DT02-9-2-1	-	Lower FLG Carb
71038	DT92-51-1	-	Carb
71039	CW92-53-01	-	Carb
71038a	CW93-5-2	-	Carb